HOKKAIDO UNIVERSITY

Title	A study of geomagnetic and gravity anomalies in central eastern margin of Japan sea
Author(s)	Shiobara-Morijiri, Rie; 塩原(森尻), 理恵
Degree Grantor	北海道大学
Degree Name	博士(理学)
Dissertation Number	乙第5278号
Issue Date	1998-03-25
DOI	https://doi.org/10.11501/3137241
Doc URL	https://hdl.handle.net/2115/51486
Type	doctoral thesis
File Information	000000322431.pdf

Hokkaido University Collection of Scholarly and Academic Papers : HUSCAP

A study of geomagnetic and gravity anomalies in the central eastern margin of Japan Sea

Rie SHIOBARA-MORIJIRI

A study of geomagnetic and gravity anomalies in the central eastern margin of Japan Sea

Rie SHIOBARA-MORIJIRI

Geological Survey of Japan

CONTENTS

Acknowledgement

1.Introduction

1.1. The program of "Geological investigation of the continental shelf in central eastern margin of Japan Sea" p.1

1.1.1.History of Geological/Geophysical surveys in this area p.1

1.1.2.Recent Surveys by G.S.J. p.3

1.2. Gravity and magnetic data for this study p.4

1.3. Advantages of gravity and magnetic data for crustal structural modeling p.6

2. Geological Background

2.1. Outlines of Bathymetry p.8

2.2. Geology of Sado Ridge, Dewa Bank Chain, Mogami Trough, Okushiri Ridge and their vicinities p.12

2.2.1.Basin Inversion p.12

2.2.2.Tectonic History of Northeast Japan p.12

2.2.3.Okushiri Ridge p.16

2.3. Neocene Basins: Eastern Japan Sea Rift System p.17

2.4. Models of Japan Sea Opening p.20

2.5. A nascent subduction zone? p.21

3. Outline of Survey

3.1. Surveys on R/V Hakurei-maru p.22

3.2. Survey systems on R/V Hakurei-maru p.24

3.3. On board processing p.27

4. Gravity study

4.1. Noise Reduction p.31

4.2. Bouguer Reduction p.33

4.3. Feature of gravity anomaly p.37

4.4. 2.5-dimensional structure from gravity anomaly p.39

4.4.1.method p.39

4.4.2.models p.41

4.4.3.results p.42

4.5. 3-dimensional structure of Sado Ridge, Dewa Bank Chain, and Okushiri Ridge p.44

4.5.1.method p.44

4.5.2.Sado Ridge p.45

4.5.3.Dewa Bank Chain p.48

4.5.4.Okushiri Ridge p.49

4.6. Conclusion p.52

5. Geomagnetic study

5.1. Data processing for magnetic anomaly maps p.53

5.1.1. Cross-point magnetic control p.53

5.1.2. Survey design and structural models p.57

5.2. Approximating edges of source bodies from total force p.58

5.3. Data processing for Shipbord Three Component Magnetometer p.62

5.3.1.Shipbord Three Component Magnetometer p.62

5.3.2.Present situation of measurement on the R/V Hakurei-maru p.64

5.3.3.Differences between total intensities by P.P.M. and S.T.C.M. p.70

5.4. Approximating edges of source bodies from vector anomaly p.75

5.5. Estimation of magnetic intensity distribution, 2.5-dimensional modeling p.77

5.5.1.method p.77

5.5.2.models p.80

5.6. Estimation of magnetic intensity distribution, 3-dimensional modeling p.83

5.6.1.method p.83

5.6.2.Northern part of the Sado Ridge p.85

5.6.3.North of Sado Island p.89

5.6.4.Northern part of Mogami Trough p.90

5.7. Discussions p.91

5.7.1.direction of magnetization p.91

5.7.2.magnetic structure p.92

5.8. Conclusion p.96

6.Discussion

6.1. Basin Inversion p.97

6.2. Structural boundaries p.100

7.Conclusion p.102

References

Acknowledgement

I would like to express my sincere thanks to Professor Hideki Shimamura of Hokkaido University for his critical reading of manuscript, instructive comments and encouragements. And I also thank to Professor Yasunori Nishida of Hokkaido University for his valuable suggestions, advice, critical reading of manuscript and encouragements.My sincere thanks are extended to Professor Yoichi Sasai of the University of Tokyo and Professor Teruo Watanabe of Hokkaido University for critical reading of manuscript, instructive comments and encouragements.

I thank Dr.Nakatsuka, Dr.Okuma, Dr.Makino*, and Dr.Komazawa of Geophysics Department(*now at Environmental Geology Dept.) of Geological Survey of Japan. They always give valuable advices and discussions for potential studies. And I also thank Dr.Okamura, Dr.Yamazaki, Mr.Joshima, and Dr.Ishihara of Marine Geology Department of Geological Survey of Japan for their help for this study.
Acknowledgements are due to the captains, officers, crew and scientists of R/V Hakurei-maru for kind help throughout the surveys. This work was financially supported by the Agency of Industrial Science and Technology special research program on geological investigation of the continental shelf in central eastern margin of Japan Sea by Geological Survey of Japan.

1. Introduction

1.1. *The program of "Geological investigation of the continental shelf in central eastern margin of Japan Sea"*

1.1.1. History of Geological/Geophysical surveys in this area

The central eastern margin of Japan Sea area (Fig.1-1-1) has two important tectonic subjects. One is "Japan Sea Opening during Miocene", and another is "compressional field in Quaternary". Many investigations have been carried out in this area. Until 1950s, bathymetry and sediment sampling were mainly investigated (e.g. Mogi and Sato, 1957). In 1965, the Hydrographic Department of Japan Maritime Safety Agency carried out a seismic reflection survey with an air gun in the continental shelf area from Wakasa Bay to Oga Peninsula and Yamato Basin (Hotta, 1967). Furthermore, Iwabuchi (1968) showed the topographic features of continental shelf area in the Japan Sea based on the result of the investigation. Iwabuchi (1968) also argued about tectonics due to erosional surface of the Sado Ridge and tilting of continental shelf.

Moreover, the Hydrographic Department of Japan Maritime Safety Agency carried out detailed bathymetry, seismic reflection, and magnetic surveys in the northeastern margin of the Japan Sea during 1967 to 1969. They observed at intervals of about 2 nautical miles. It was an epoch-making dense survey in those days (Sato, 1971). After that, Geological Survey of Japan published the 1:1,000,000 Marine Geology Map based on the result of the investigation over the Japan Sea during 1976 to 1977(Tamaki et al., 1981). Furthermore, Tamaki (1988) summed up tectonics of the Japan Sea.

Isezaki (1986a) compiled a magnetic anomaly map of the

Japan Sea. It was compiled with data by Yasui et al. (1967), Isezaki and Uyeda (1973), Oshima et al. (1975,1980), and Tamaki et al. (1981). After this, Seama and Isezaki (1990) carried out magnetic survey around Japan Basin area. Unfortunately, many studies focused on the opening of Japan Sea, then there were few surveys and reports about gravity and magnetic study in the continental shelf area.

On the other hand, multi channel seismic reflection surveys for petroleum resources were carried out since 1970's around coast area of Japan Sea. Especially in off Akita, Yamagata, Niigata Prefectures as being a few oil fields in Japan, many investigations were carried out by Japan National Oil Company and other private oil companies. However, their investigations were covered mainly coast areas. They have high possibility to produce petroleum and natural gas because of thick sedimentary layers. However, almost all their seismic reflection and drilling data have been unpublished yet. Only some structural maps or interpretation charts of continental shelf area were published.

Suzuki (1989) summed up their data (obtained by Idemitsu Co.) and interpreted about the East Japan Sea Tectonic Line (Fig.1-1-2).

Nakamura (1983) proposed the nascent subduction hypothesis for eastern margin of the Japan Sea (Fig.1-1-3). In addition, it was becoming to be supported and accepted, because of focal mechanism and aftershock distribution of 1983 Nihonkai-Chubu earthquake, and 1993 Hokkaido Nansei-oki earthquake. Then, many investigations focused on the continental shelf area and Japan Basin or Yamato Basin area were started (e.g. Kato et al., 1986, Asada et al., 1989, Nishizawa et al., 1996).

1.1.2. Recent Surveys by G.S.J.

From 1989 to 1993, geological Survey of Japan carried out detailed survey around the central eastern margin of Japan Sea; the survey track was designed as grid. The survey lines were designed at intervals of 1.6 nautical miles (about 3km) in WNW-ESE direction and 3.3 nautical miles (about 6km) in NE-SW direction. The outlines of these surveys will be explained in Chapter 3. This program purposed (1) to get detailed geological/geophysical data around the continental shelf area because of the lack of available data, (2) to reveal of subsurface structures and geology. These data were analyzed by each category (geological structure, sedimentation, gravity and magnetic study, and others). We published four areas of marine geology maps (Fig.1-1-4). They were included 1:200,000 Marine Geology Map series.

Free-air gravity, Bouguer gravity and total force magnetic anomaly data were also published as additional maps of Marine Geological Maps (Okamura, et al., 1994,1995a, 1996a, and 1996b). And cruise data files (Joshima et al., 1990a, 1990b; Joshima and Kikawa, 1991a, 1991b; Morijiri and Yamazaki, 1992a, 1992b; Joshima and Ishihara, 1993a, 1993b) were supplied to the Japan Oceanography Data Center of the Hydrographic Department of the Maritime Safety Agency.

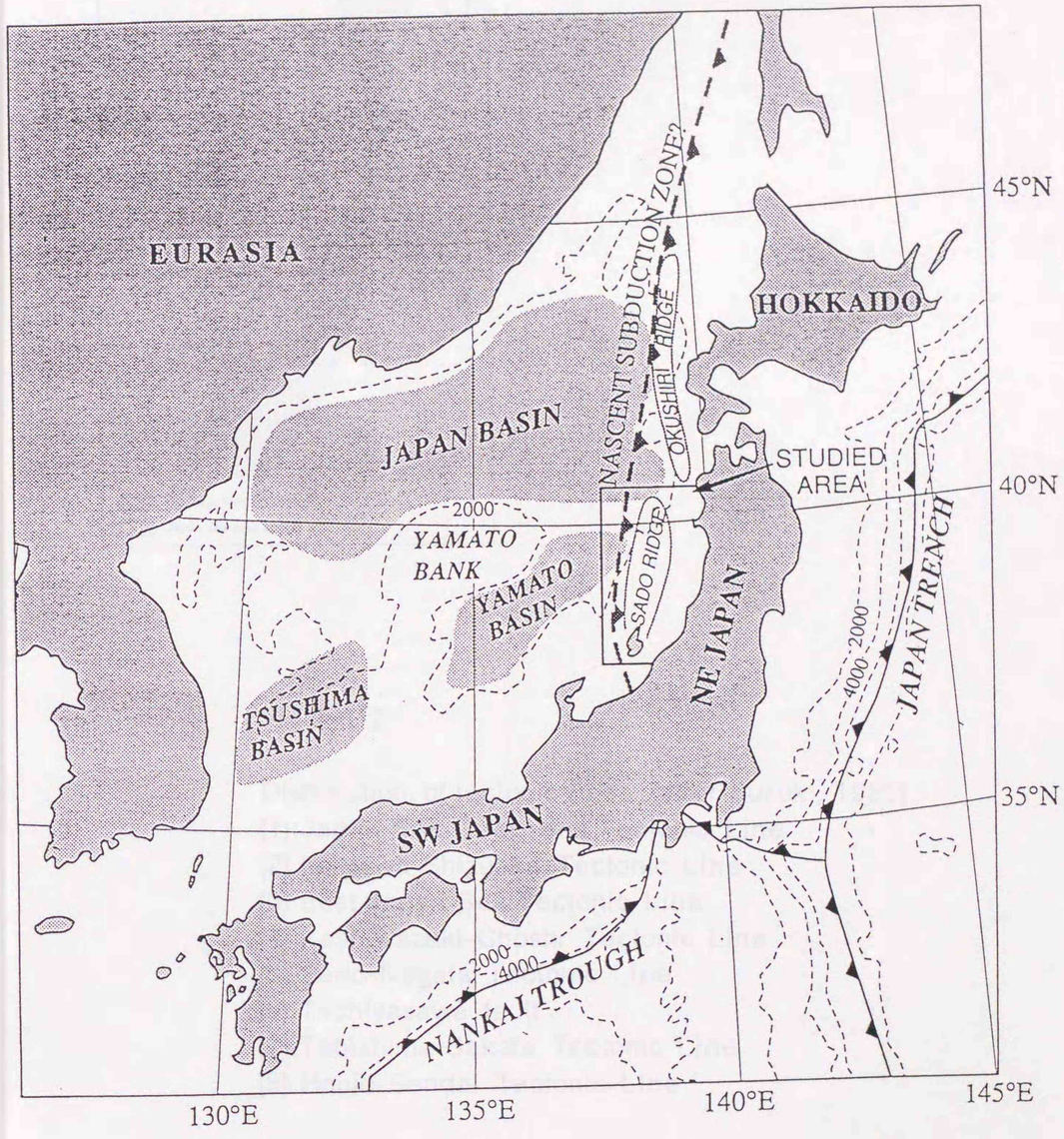

Fig.1-1-1

Index map of the Japan Sea and studied area.

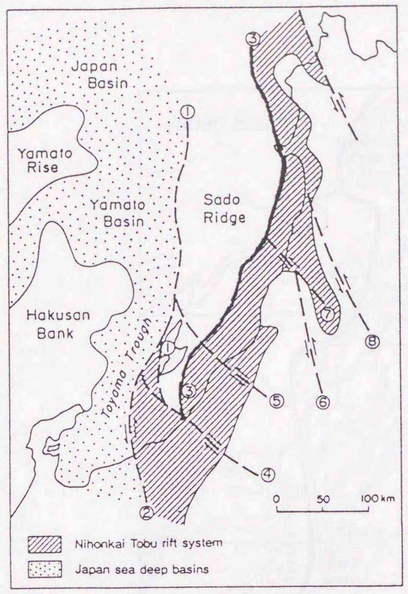

Fig.1-1-2

Distribution of tectonic lines. (after Suzuki, 1989)
(1) Japan Sea Deep Sea Tectonic Line
(2) Itoigawa-Shizuoka Tectonic Line
(3) East Japan Sea Tectonic Line
(4) Kashiwazaki-Choshi Tectonic Line
(5) Sado-Niigata Tectonic Line
(6) Tachiyasawa fault
(7) Tobishima-Sakata Tectonic Line
(8) Honjo-Sendai Tectonic Line

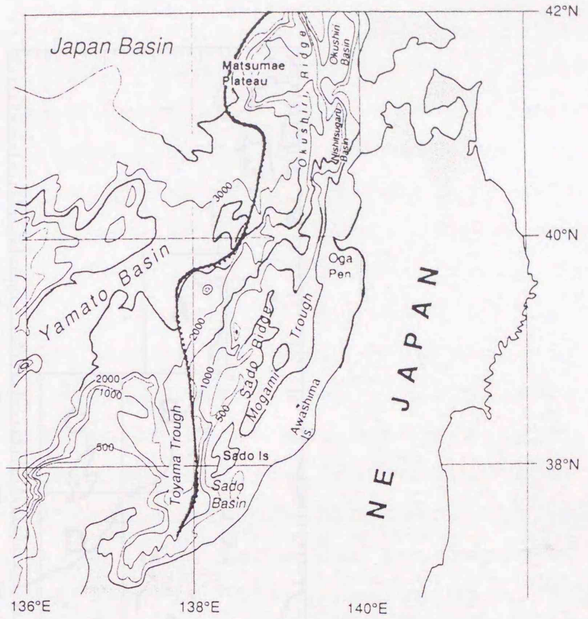

Fig.1-1-3

An incipient subduction zone in the eastern margin of the Japan Sea proposed by Nakamura(1983).

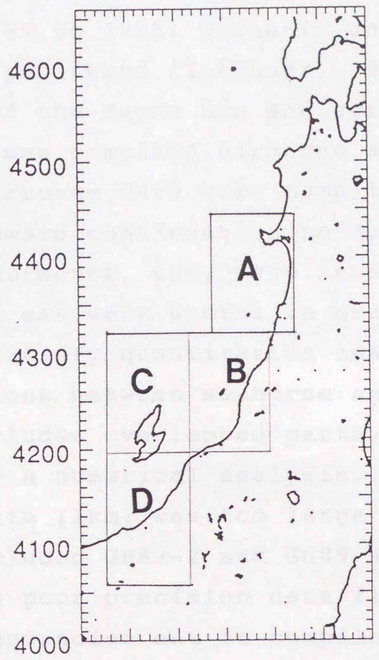

Fig.1-1-4

Index of published Marine Geology Maps.
A; West of Akita, B; Vicinity of Awashima
C; North of Sado Island, D; South of Sado Island

1.2. *Gravity and magnetic data for this study*

All of data used in this study were obtained from R/V Hakurei-maru cruises by Geological Survey of Japan (GSJ) since 1989 to 1992. Magnetic anomaly map of East Asia was already published (Ishihara, 1994). Around the eastern margin of the Japan Sea and surroundings was shown in Fig.1-2-1. It was compiled airborne and seaborne magnetic anomaly data. Airborne data were compiled by Makino et al. (1992) using upward continuation to 3,200m altitude above sea level. Moreover, they were interpolated to 2km mesh data. This map was very useful to grasp magnetic features, but it didn't satisfy quantitative analysis because of no level corrections between seaborne and airborne data. This study area includes overlapped parts. Therefore, they were not good for a numerical analysis. Moreover, the mesh size of these data (2km) was too large for our purpose. The data file included GH89-2 and GH89-4 cruise data. However, if it includes poor precision data files, they should be filtered high frequencies out to compile with poor data.

In generally, gravity and magnetic field data show anomalies of space distribution. Data often suffered from positioning and/or measuring errors. Therefore, high frequency anomalies were difficult to judge whether they were caused by small-scale crustal structures or measurement errors. Unfortunately, previous positioning resolution was worse than recent systems. Then, if we try to compile them with our data, we have to attenuate local anomalies in our data. Our data were measured with almost the same systems, although the positioning system was replaced in 1990 from LORAN-C to single-GPS. Our new magnetic anomaly maps were published at contour intervals of 25nT, and our gravity anomaly maps were published at contour intervals of 5mgal. Finally, only our new data were used to reveal small-scale

structures around the continental shelf area. The crustal structural models were calculated from detailed geomagnetic and gravity anomalies shown in these maps. Therefore, high-resolution observations and careful data processing were very important. Discussions of tectonics should be supported by piles of such researches.

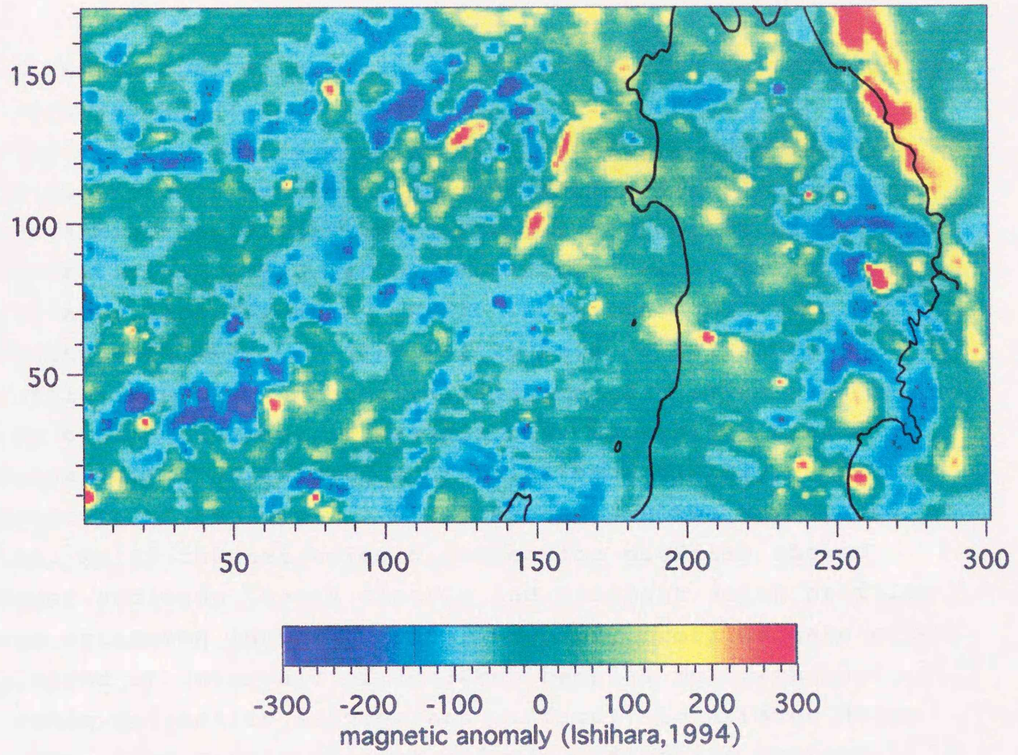

Fig.1-2-1

Magnetic anomaly map around the northeast Japan.
After Ishihara (1994).

1.3. *Advantages of gravity and magnetic data for crustal structural modeling*

Our results of the program of "Geological investigation of the continental shelf in central eastern margin of Japan Sea" are not only publishing the Marine Geology Map series. Okamura et al. (1992,1995b) showed that many small ridges in this area were formed by "Basin Inversion". However, their results were obtained from mainly seismic reflection profiles and other geological studies. The seismic profiles didn't show basement layers clearly. Generally, single channel seismic reflection profiles show clearly geologic structure of the upper 1.0-2.0 seconds in two way travel time. Multi channel seismic reflection profiles showed deeper sediment layers clearly and basement depth profiles were estimated (Suzuki, 1989). However, profiles were often obtained at intervals of 20-30km, because multi-channel seismic reflection surveys are difficult to arrange dense surveys like single-channel seismic reflection systems. Therefore, these results didn't show horizontally detail structures.

On the other hand, gravity and magnetic anomalies are possible to be obtained from dense surveys. Moreover, the advantages of these data are calculation of 3-dimensional crustal structural models and estimation of physical properties, i.e., density, magnetized intensity, and so on. Of course, modeling due to potential data always suffered from problems of the uniqueness of solution. However, if gravity, magnetic anomaly, and seismic reflection data are obtained on the same lines, we can get some kinds of constraint conditions for the crustal structural modeling.

Results of gravity and magnetic studies estimate a present shape of basement and physical properties. It is very important to know basement structure and physical properties

for discussion of the tectonics based on the geological studies. In this study, a basement structural model due to gravity and magnetic anomalies was calculated, and discussed about tectonic models proposed by Okamura et al. (1995b).

The review of geologic studies and tectonics in this area is shown in next Chapter.

2.Geological Background

This chapter outlines topographic feature, geological structure, and tectonics due to results of geologic studies by Okamura et al. (1992,1994,1995a, 1995b, 1996a, 1996b).

2.1. *Outlines of Bathymetry*

(0). Outlines

Topographic feature of the central part of eastern margin of the Japan Sea is divided into some parts (fig.2-1-1). For example, they were (1) Dewa Bank Chain, (2) Sedimentary Basins, (3) continental shelf, (4) Mogami Trough, (5) Sado Ridge, (6) Okushiri Ridge, (7) Toyama Trough, and (8) the Yamato Basin and the Japan Basin. Roughly speaking, the Mogami Trough and the Sado Ridge trend in parallel to northeastern Japan arc (in NNE direction). Otherwise, the Toyama Trough trends in N-S direction, and it crosses to the west side of the Sado Ridge.

(1) Dewa Bank Chain

The Dewa Bank Chain is located between the Tobishima Island (t in Fig.2-1-1) offshore Sakata and Oga Peninsula. The chain consists of the Tobishimatai Bank (R15), the Shinguri Bank (R11), the Ogamukouse Bank (R12), and small-scale banks between the Shinguri Bank and the Tobishimatai Bank.

(2) Sedimentary Basins

There is the Sado Basin between the Honshu Island and the Sado Island. Moreover, small-scale basins were formed between the Dewa Bank Chain and the continental shelf. They are the Tobishima Basin (B2) and the Oga Basin (B3). In addition, the Nishi-Tsugaru Basin (B4) was formed between the Tsugaru Peninsula and the Okushiri Ridge.

(3) Continental shelf

The width of the continental shelf off Tohoku district has

variety. The widest part is off Niigata and it is about 50km wide. Next is off Akita and off Noshiro, it is about 30km wide. Otherwise, the narrowest part is west of the Oga Peninsula or off Honjyo, it is less than 15km wide. It is the 15km following with west of Oga Peninsula, off Honjyo to be narrow on the other hand.

(4) Mogami Trough

The Mogami Trough trends in NNE direction from east of the Sado Island. Its trending is changed into N-S at off Akita. The length is about 250km from the Sado Island to west of the Tsugaru Peninsula. It is burying into the Japan Basin around Latitude 40 ° 30'N.

The Mogami Trough can be divided into northern(>40° N), central(39° N-40° N), and southern(<39° N) parts. The northern part of the Mogami Trough is deeper than southern part. The southern part is 600-700m deep, and 15-20km wide. Moreover, deep-sea channels on a south side slope descend to the bottom of the trough. The central part is 700-1,500m deep, and 20-40km wide. The water depth is increasing like a step forward to the north. The northern part is 2,000-3,000m deep, and 20km wide. The water depth of the north end of the trough is more than 3,000m, and the trough continues to the Japan Basin there. A discontinuous channel, which was known as the Mogami deep channel, was developed in the central and the northern parts of the trough. Sakurai and Sato (1971) divided the Mogami Trough due to the basement structure into the Gassan-area, the Torimi-area, the Tobishima-area, and the Shinguri-area from the south. The Gassan-area corresponded to the southern part, the Torimi-area and the Tobishima-area corresponded to the central part, and the Shinguri-area corresponded to the northern part, respectively.

(5) Sado Ridge

The Sado Ridge was developed and bounded the western margin of the Mogami Trough. The ridge is 200-700m high from the bottom of the trough with steep slopes. It is one of major uplift zones in this study area, and trends in NNE direction. It is more than 250km long including the Sado Island, and maximum width is 80km(Iwabuchi, 1968). The ridge consists of many small ridges trending N20-70° E direction. In addition, the ridge is divided into southern and northern parts.

The southern part of the Sado Ridge is 30-50km long, 10-20km wide, and 87-150m deep. These banks are larger and shallower than the northern part of the Sado Ridge. Some banks in the southern part are shallower than 150m deep, and their tops are erosional flat surfaces.

On the other hand, the ridges chain located north of latitude 39° N is less than 30km long, and deeper than 180m except the Kamaguri Bank(R8). Moreover, they don't have erosional surfaces. They have similar characteristic features to mountain chains of the Sado Island. The small ridges in southern part of Sado Ridge are asymmetric. Their southeast sides are steep, and the northwest sides are gentle. In addition, many erosional surface of the top of the banks incline to the northwest side (Iwabuchi, 1968).

(6) Okushiri Ridge

The Okushiri Ridge is located north of the Tsugaru Peninsula that trends in N-S direction. It is at least 400km long along the west of Hokkaido, from the Tsugaru Peninsula to latitude 44° N trended in N-S direction. In addition, the Japan Basin spreads for the west of the ridge. The Kyuroku Jima Island (k) is a volcano formed at the south end of the Okushiri Ridge. Northern part from the Kyuroku Jima Island, the Okushiri Ridge consists of two prominent anticline zones. The west one continues from 40° 30'N to 41° 05'N, it

is about 70km long, the water depth of on the axis of anticline is shallower than 1,500m. The east one trends in north increasing depth gradually from the shelf of the southeast of the Kyuroku Jima Island to around 40° 48'N where it is burying into the Nishi-Tsugaru Basin(B4). Other anticline appears in northern area from latitude 40° 54'N, getting larger toward north(Okamura and Sato,1993).

(7) Toyama Trough

The Toyama Trough trends in N-S direction between the Sado Island and Noto Peninsula. It is 200km long, and 20-50km wide. The bottom of the trough is 1,000m deep in the Toyama Bay, and 1,800m deep at north end where connected to Yamato Basin. The Toyama deep channel develops as excising 200-800m deeper for the bottom of the trough. It is bounded by steep sloped on east and west side. At the west of the Sado Island, the slope is especially steep and it is 1,500m high from the bottom. The prominent deep-sea channel was developed on the southeast steep slope (Okamura et al., 1994,1995a).

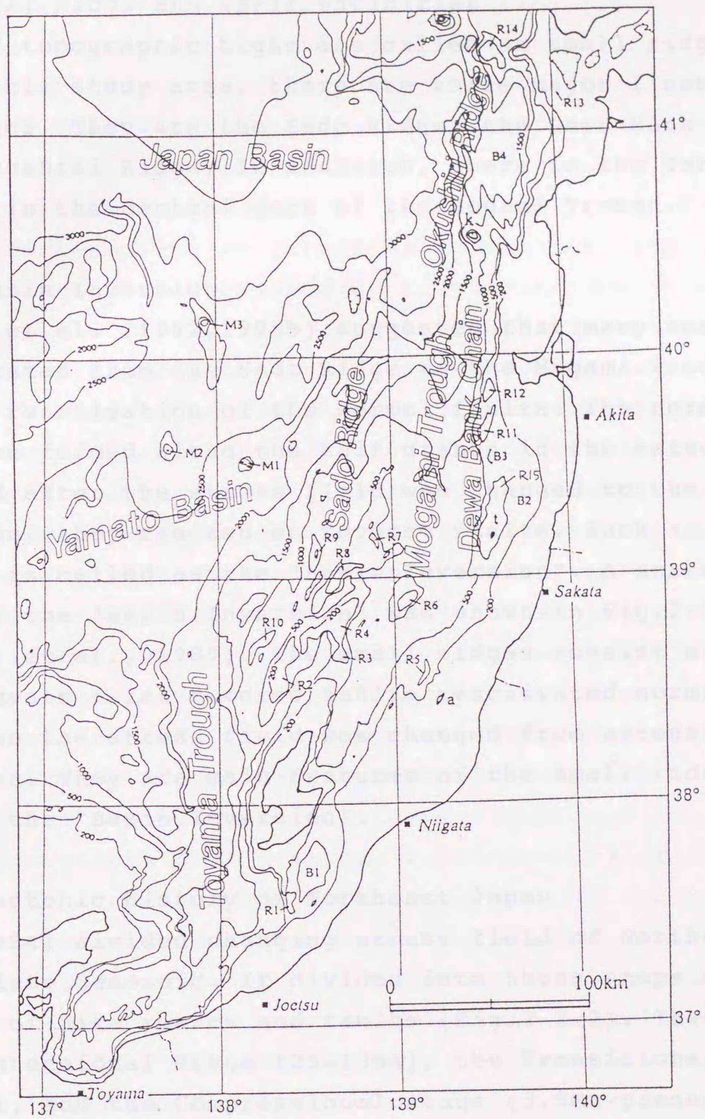

Fig.2-1-1
Bathymetric contour map of the southern part of the eastern margin of the Japan Sea.
a:Awashima Island, k:Kyurokujima Island, t:Tobishima Island,
B1:Sado Basin, B2:Tobishima Basin, B3:Oga Basin, B4:Nishi-Tsugaru Basin, M1:Matsu Seamount, M2:Maiyo No.2 Seamount, M3:Maiyo No.3 Seamount, R1:Sado Bank, R2:Hyotanguri Bank, R3:Gassanguri Bank, R4:Mukouse Bank, R5:Awashimaguri Bank, R6:Torimiguri Bank, R7:Mogamitai Bank, R8:Kamaguri Bank, R9:Yahikotai Bank, R10:Koshijisho Bank, R11:Shinguri Bank, R12:Ogamukouse Bank, R13:Nishi-Tsugarutai Bank, R14:Kojimatai Bank, R15:Tobishimatai Bank

2.2. *Geology of Sado Ridge, Dewa Bank Chain, Mogami Trough and Okushiri Ridge and their vicinities*

Isolated topographic highs are called as small ridges here. In this study area, there are three major lines of small ridges. They are the Sado Ridge, the Dewa Bank Chain, and the Okushiri Ridge. In addition, there is the Torimiguri Bank (R6) in the central part of the Mogami Trough.

2.2.1. Basin Inversion

Okamura et al. (1992,1995b) suggested that many small ridges located from the Sado Ridge to the Mogami Trough were formed by reactivation of the normal faults. The normal faults were formed along the half graben in the extensional field, and after the stress field was changed to the compression, they reacted as reverse faults. Such a tectonics is called as the "Basin Inversion". A schematic diagram of the "Basin Inversion" was shown in Fig.2-2-1 (Williams, et al., 1989). The small ridges consist of syn-rift sediments exist reverse faults reactivated normal faults when the stress field was changed from extension to compression. They are main features of the small ridges formed by the "Basin Inversion".

2.2.2. Tectonic History of Northeast Japan

Sato (1994) divided changing stress field of Northeast Japan in late Cenozoic. It divided into three steps due to direction of dike swarms and faults (Fig.2-2-2). These steps are the Extensional stage (25-13Ma), the Transitional stage (13-3.5Ma), and the Compressional stage (3.5Ma-present). Okamura et al. (1992,1995b) suggested that small ridges were formed in four major tectonic stages due to sedimentary structures. They are (1) rifting stage (an Early to Early middle Miocene), (2) post-rifting stage (middle Miocene to

late Miocene), (3) pre-inversion stage (a Late Miocene to Pliocene), and (4) inversion stage (a Late Pliocene to Quaternary).

A schematic cartoon of tectonic history of the Sado Ridge formed by "Basin Inversion" is shown in Fig.2-2-3 after Okamura et al. (1995b). In the figure, (a), (b), and (c) indicate rifting stage, (d) indicates post-rifting stage, (e) indicates pre-inversion stage, and (f) indicates inversion stage. According to these four stages, tectonics of this study area is reviewed. In addition, names of places are shown in Fig.2-1-1.

(1) Rifting stage (early Miocene to early middle Miocene)

The Japan Arc was a part of the Eurasian Continent in Oligocene. In addition, in Early Miocene, the Japan Arc started a seaward shift from the Eurasian Continent because its stress field became extension. Therefore, many rifts were formed and the detritus sedimentation was started (Kano et al., 1991; Sato, 1994). Okamura et al. (1995b) called the period as the rifting stage. During the rifting stage, small-scale half grabens were formed under the Sado Ridge, the Mogami Trough, and the Dewa Bank Chain (Okamura et al., 1995b). And the large scale rifts were formed under sedimentary basins from off Niigata over northern part of Fossamagna of Niigata Plain and from north of Tobishima Island over Akita Plain. Otherwise, half grabens whose structures were similar to under the sedimentary basins were also formed under the southern part of the Sado Ridge.

The half grabens under the southern part of the Sado Ridge were discontinued by normal faults on their east side, and the grabens were inclined to southeast. The normal faults trended in NNE-NE directions, though they were bent from N-S to ENE directions. The widths of rifts were 5-15km, and the longer rift was wider one. A few parallel intermittent

normal fault lines bounded on each large scale rifts. These normal fault lines were more than 50km long; the maximum displacement was more than 1,000m. On the other hand, the size of small rifts was only 1/5 of the large rifts. At the end of the rifts, displacement became smaller; strike was changed and diverged.

On the other hand, a small half graben whose width was 10-20km was formed between the Torimiguri Bank (R6) and the Awashima Island (a). In addition, a small half graben whose width was 5-10km was formed under the west of Dewa Bank Chain. Moreover, under the northwestern slope of the Torimiguri Bank (R6) and under the Mogami Trough, small half grabens were formed, too. Though the structural feature of this half graben was similar to that of the southern part of the Sado Ridge, their scale was much smaller. Large scale rifts trended in N-S direction. On the other hand, most of all small scale rifts trended in NE-direction.

(2) Post-rifting stage (middle Miocene to late Miocene)

The post-rifting stage was a stable time, in which rifted continental slope widely subsided. Any distinctive faults and folds were not formed in this stage. Unit III or sub-unit IIIa (see Fig.2-2-3) widely covered the rifts and the uplifted zone. This indicates the subsidence of whole the Sado Ridge, the Mogami Trough, and the lack of significant tectonic movement during the deposition of this unit. And Unit IIIa was generally thicker above the rifts than the uplifted zone, because the rift which were formed in the rifting stage were still topographic lows before the deposition of Unit III.

(3) Pre-inversion stage (late Miocene to Pliocene)

The pre-inversion stage for late Miocene to Pliocene was in slight compressional stress field and began tectonic movement caused by a gentle compression. The most

distinctive change was subsidence of the Torimiguri Bank (R6 in Fig.2-1-1) of central part of the Mogami Trough. Some subsidences similar to the Torimiguri Bank were recognized in the uplift zone of the Sado Ridge. Moreover, small-scale anticlines began to grow in the south of Awashima Island (a in Fig.2-1-1). These anticlines trend in N-S direction and reach to the Torimiguri Bank. This suggests these anticlines were relevant to the Torimiguri Bank. On the other hand, Dewa Bank Chain was almost stable in this stage.

(4) Inversion stage (Pliocene to Quaternary)

Most of distinctive folds and reverse faults were formed by reactivation of the normal faults caused by E-W compressional stress field from Pliocene to Quaternary. And upper plates of the reverse faults were uplifted on westward tilts, because the normal faults which were distributed under Sado Ridge and Dewa Bank Chain were had westward tilts. Then, anticlines that were formed on the upper plate have asymmetry sections. The strike of the normal faults and the reactivated reverse faults were in NE direction. However, the uplift zones that were located off Niigata and off Sakata were basement high areas during the rifting stage. Then uplifting during the inversion stage was not the reactivation of the normal faults, and the reverse faults must be newly formed. Though the Awashima uplift zone might be a part of the rift during the rifting stage, it was not cleared whether reverse faults were formed by reactivation of the normal faults or by new activation. The Awashimaguri Bank (R5) was anticline which had symmetric section, but there was not clear that it accompanied with reverse faults. The Torimiguri Bank (R6) accompanied with normal faults which were not reactivated.

On the other hand, during the inversion stage, direction of compression is almost E-W. Then, a whole of uplift zone

trended in N-S direction which was rectangular direction of compression, and the faults was supposed to be en echelon arrangement. It supposed that the beginning of reactivation as reverse faults was different by a place during the period (Watanabe et al., 1994, Okamura et al., 1995b). The structural map was shown in Fig.2-2-4 (Okamura et al., 1995b). The areas covered with late rift sediment (Unit II in Fig.2-2-3) were considered "Basin Inversion" structure.

2.2.3. Okushiri Ridge

The Okushiri Ridge as a structural uplift zone continues to around the Oga Peninsula, as its topographic feature of the Okushiri Ridge was described before. The uplift zones from the Oga Peninsula to the Kyuroku-Jima Island become a few anticline lines spacing out 6-9km. East side of each anticline was steep. In addition, the east dipping faults often cut the slopes. Axis of anticlines trend in N-S to SSW directions southern than 40° 20'N, but it changed to NNW in the area where its topographic feature becomes clear, from 40° 20'N to the Kyuroku-Jima Island.

A distribution of reverse faults by Okamura and Kuramoto (1996) was shown in Fig.2-2-5. The structure around the Okushiri Ridge was quite different from that of the Sado Ridge which were formed by "Basin Inversion"(Okamura and Sato, 1993).

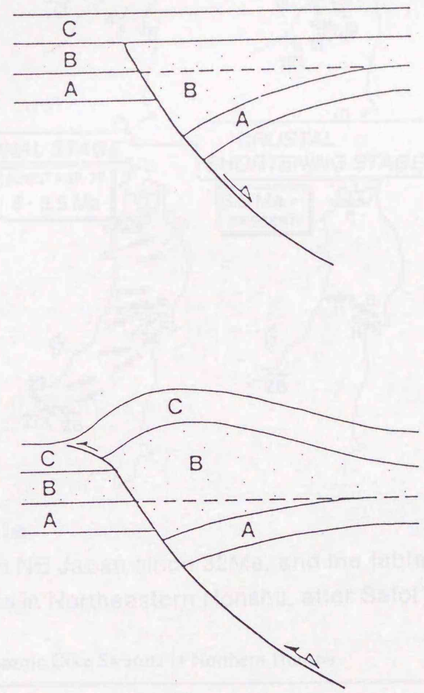

Fig.2-2-1
Schematic diagram of a classical positive inversion structure.A,B, and C are stratigraphic sequences. A:prerift, B:synrift, C:postrift sequence. after Williams et al(1989)

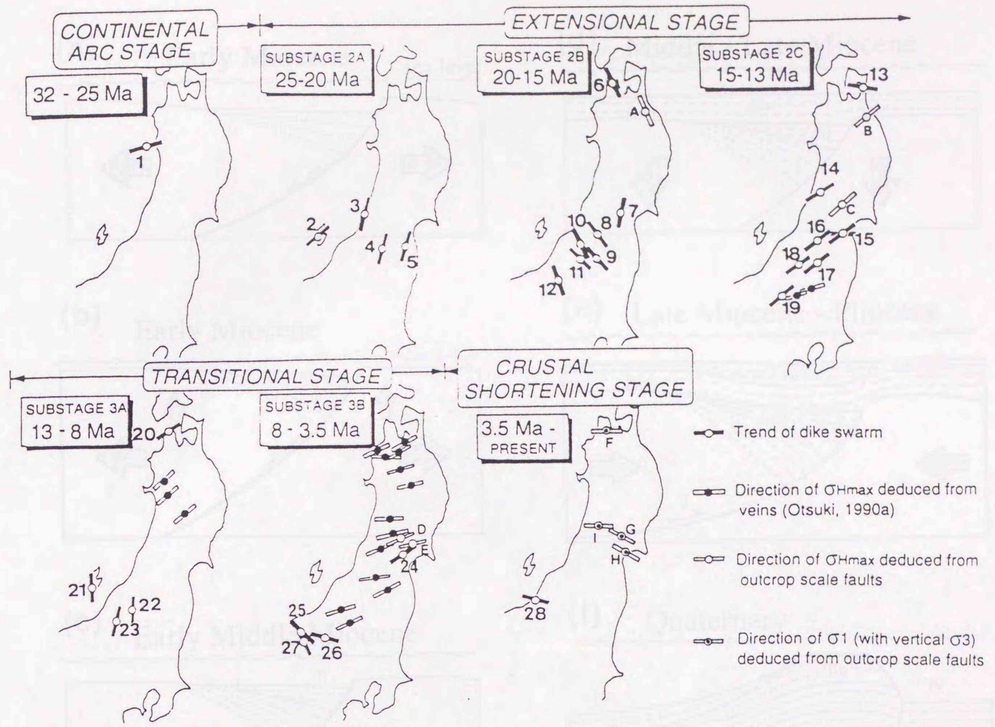

Fig.2-2-2 and Table.

Reqional stress field in NE Japan since 32Ma, and the table shows the trend of Late Cenozoic Dike swarms in Northeastern Honshu, after Sato(1994).

Table . Trend of Late Cenozoic Dike Swarms in Northern Honshu

No.	Site	σ_{Hmax}	Stage	Age, Ma	*N*	*F*	Ref.
1	Oga	ENE-WSW	1		—	—	5
2	Sado	NE-SW	2A	22.6-29	—	—	6
3	Atsumi	30	2A		32	0.66	1
4	Tohachiyama	20	2A		23	0.63	1
5	Rhyozen	20	2A	21.3, 22.1	197	0.58	1, 4
6	Tsugaru	-40	2B		17	0.40*	7
7	Kawasaki	15	2B		70	0.47	8, 9
8	Tamaniwa	-35	2B		350	—	3
9	Wakamatsu	-40	2B		75	—	3
10	Tsugawa	-30	2B		98	0.29*	10
11	Takizawagawa	NW-SE	2B		—	—	11
12	Yuzawa	-20	2B		600	—	12, 3
13	Tomari	-70-90	2C-3A		240	—	13
14	Aosawa	60	2C-3A		371	0.44*	14, 15
15	Obara	50, 85	2C		23	—	16
16	Tamaniwa	40	2C		22	0.45*	3
17	Wakamatsu	55	2C		22	0.40*	3
18	Tadami	NE-SW	2C		—	—	11
19	Minakami	50	2C		107	0.42*	17
20	Tsugaru	20-60	3A		18	—	7
21	Ogi	-5	3A	12	50	0.40	1, 2, 4
22	Tadami	5	2C-3A		57	0.56	1, 11
23	Tanigawadake	25	3A	12.0-12.3	54	0.80	1, 2, 4
24	Shimokura	45	3B	8	108	0.38*	8, 4
25	Shiragami	60	3B	5.1, 5.6	20	0.25	1, 2, 4
26	Tochiku	-20	3B		50	0.39	1
27	Kirizumi	-80	3B	6.5	—	—	2, 4
28	Yoneyama	-75	4	2.5-2.8	33	0.42	1, 2, 4

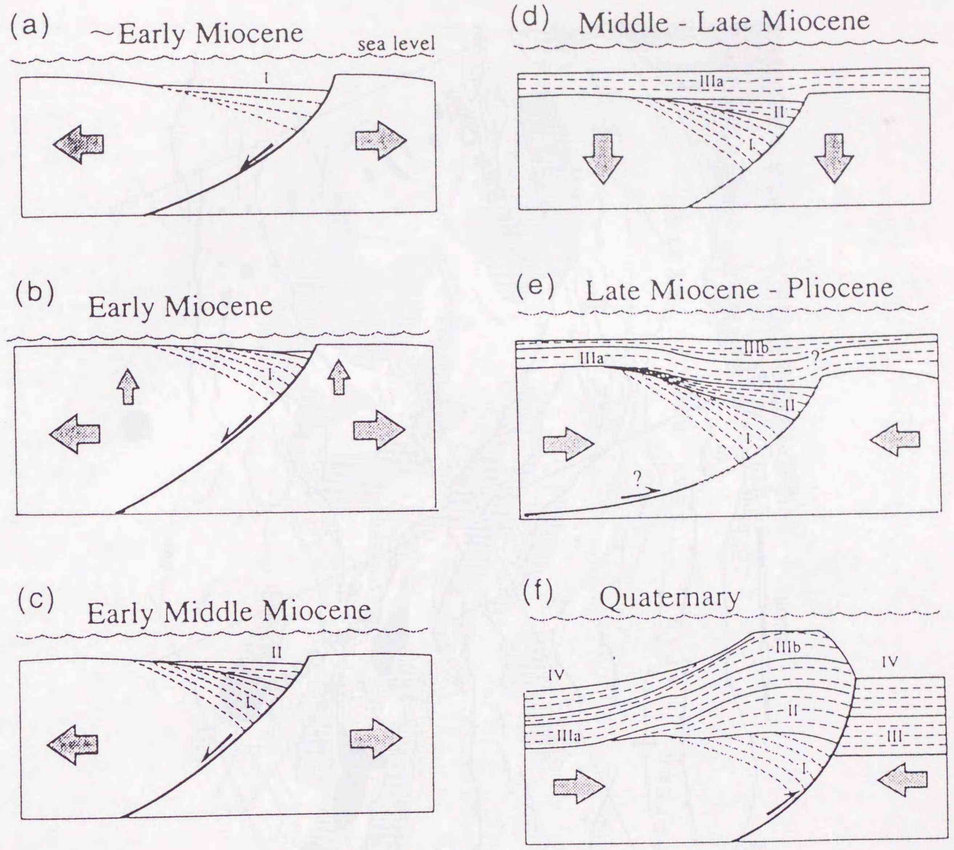

Fig.2-2-3
Schematic cartoon showing the structural evolution of a typicaltructural ridge.
(a)Rift initiation and deposition of Unit I in the Early Miocene.
(b)Uplift and erosional truncation at the end of Unit I.
(c)Deposition of Unit II by subsidence and transgression in the Early to early Middle Miocene.
(d)Post-rift subsidence and Unit III deposition in the Middle to Late Miocene.
(e)Down warp of the former rift in the Late Miocene to Pliocene.
(f)Basin inversion by reactivation of the former normal fault in the Pliocene to Quaternary.
after Okamura et al(1995b)

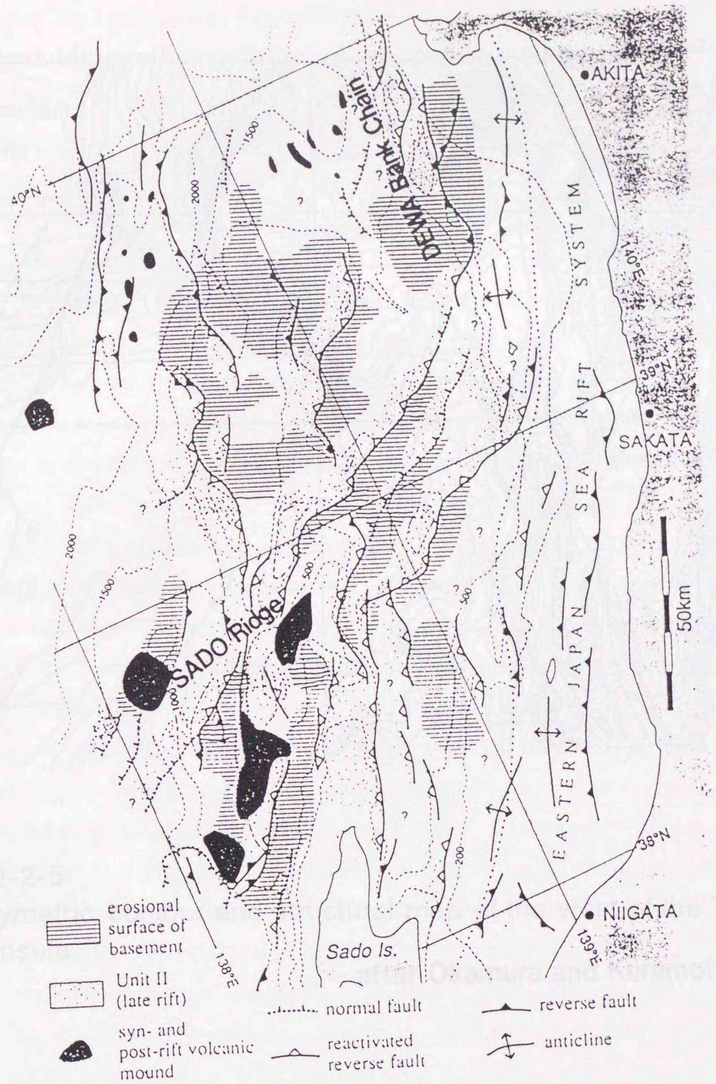

Fig.2-2-4

Structural map of the southern part of the eastern margin of the Japan Sea. Most of present ridges were rifts in the Early Miocene period and have been uplifted by the change of fault movement from normal to reverse sense. Basement structure of the shelf and shelf slope areas is not shown, because it is not clearly resolved by multiple reflections.
after Okamura et al(1995b).

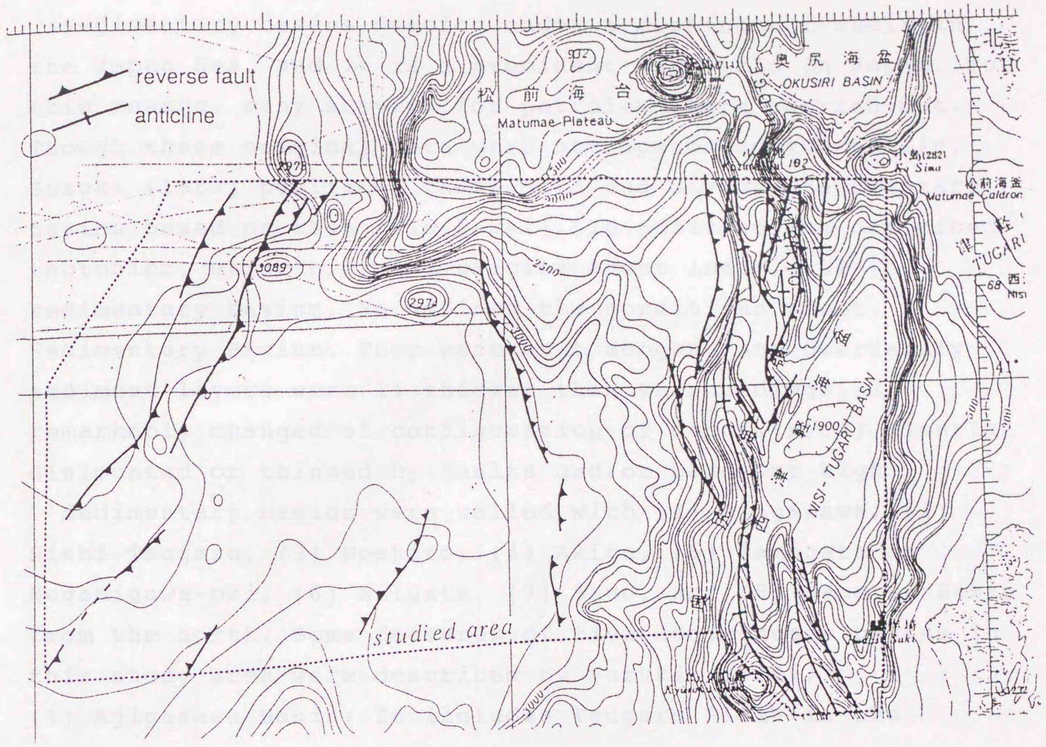

Fig.2-2-5
Bathymetric contour and structural map of the west of the Tsugaru Peninsula.

after Okamura and Kuramoto (1994)

2.3. *Neogene Basins: Eastern Japan Sea Rift System*

Sedimentary basins develop under a continental shelf in the Japan Sea, and it is a prominent oil field in Japan. For this reason, many surveys for petroleum were carried out. Though these original data were not opened to the public, Suzuki (1989) published these data and divided sedimentary basins based on them (Fig.2-3-1). In addition, he described tectonics, structure, and origins about individual sedimentary basins. He defined the conditions about Sedimentary Basins. They were that Neogene and Quartanaly sediment layers were 1) thicker than surroundings, 2) remarkably changed of configuration of deposits, 3) clearly dislocated or thinned by faults and/or basement high.

Sedimentary basins were called with (1) Ajigasawa, (2) Nishi-Tsugaru, (3) Noshiro, (4) Akita, (5) Yamagata or Mogamigawa-oki, (6) Niigata, (7) Sado, and (8) Naoetsu Basin from the north. Some features of five sedimentary basins in this study area were described by Suzuki (1989).

(1) Ajigasawa Basin: It includes Tsugaru Plain in the western part of Aomori Prefecture and it's offshore. The eastern boundary between the basin and acoustic basement is the normal fault trended in NE-SW direction. The northern, southern, and western boundaries are uplifted zones of the acoustic basement which is consists of the green-tuff. The area is 10km×50km. The sediment layer thickness is more than 1,500m, and maximum is about 3,000m. In addition, a thickness of Quartanaly sediment is 2,500m, and a young stratum is extremely thick. In generally, the sediment layer is characterized by a few sand beds and most of all consists of mudstones accumulated in sub-deep sea.

(2) Nishi-Tsugaru Basin: It locates on the west of the Ajigasawa Basin. The basement depth is estimated about 4,000m by the result of a multichannel seismic reflection

profiling. The area which thickness of deposit is more than 1,500m is 20km×70km. The maximum thickness is estimated at 2,500m.

(3) Noshiro Basin: It includes Noshiro Plain in the northern part of Akita Prefecture and offshore. The eastern boundary is the Ouu Mountains and the northern boundary is the Shirakami Mountains. Both boundaries are uplifted zones of the basement which is consists of the green-tuff. The western boundary is the north prolongation of the Dewa Bank Chain, which continues from Tobishima Island to Oga Peninsula. It bounds on normal faults. The south boundary is ambiguous, but around Oga Peninsula, it connects to the Akita Basin. The area which thickness of deposit is more than 1,500m is 40km×40km. The maximum thickness is estimated at 3,500m, and it locates close to the Noshiro coast.

(4) Akita Basin: It includes Akita Plain in the central and southern part of Akita Prefecture and offshore. It is bounded on the west by the reverse faults along the Dewa Bank Chain. The eastern boundary is the Dewa Mountains and the Ouu Mountains. In addition, it is bounded on the north by the Noshiro Basin. The south boundary is ambiguous, but it is estimated around the tie line from Tobishima Island to Mt.Chokai. The area which thickness of deposit is more than 1,500m is 45km×90km. The maximum thickness is estimated at more than 5,000m. The acoustic basement is consists of thick andesite and basaltic tuff breccia.

(5) Yamagata (Mogamigawa-oki) Basin: It locates in north of the Awashima Island area, offshore Asahi mountains. It is bounded on the Mogami Trough by Awashima uplift zone. The area which thickness of deposit is more than 1,500m is 30km ×50km. The maximum thickness is estimated at 3,000m.

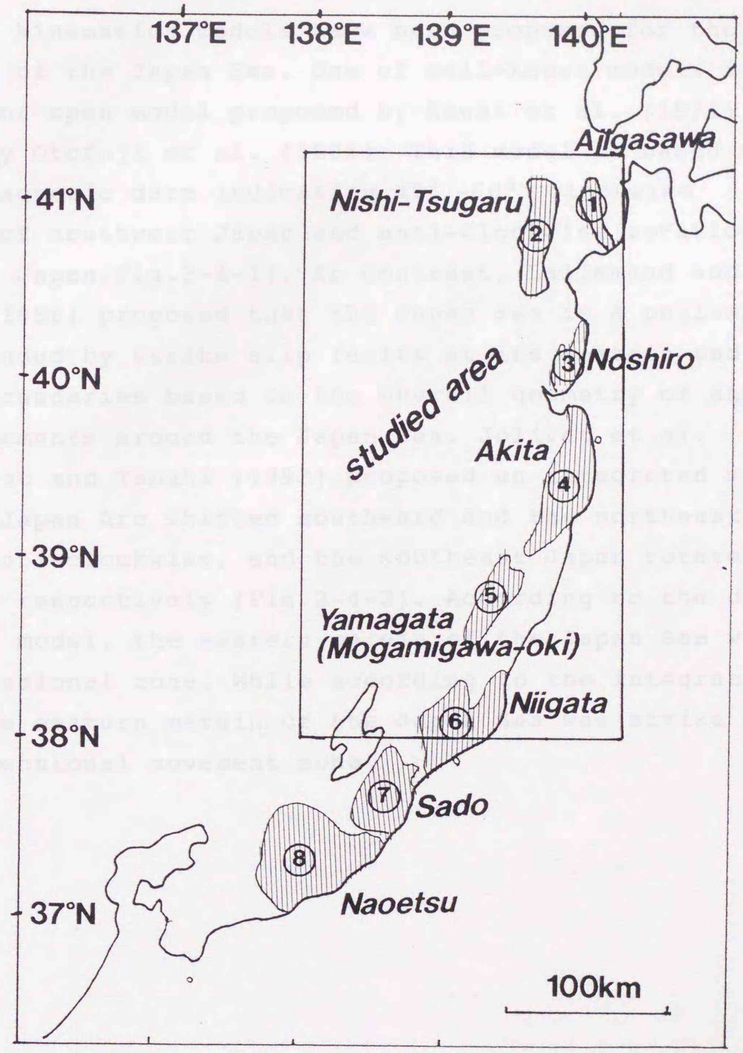

Fig.2-3-1
Sedimentary Basins of the eastern margin of the Japan Sea.
after Suzuki(1989).

2.4. *Models of Japan Sea Opening*

The Japan Sea is a back-arc basin formed by a seaward shift of the Japan Arc from the Eurasian Continent mainly in the Early to Middle Miocene (Tamaki et al., 1992). Several different kinematics models have been proposed for the spreading of the Japan Sea. One of well-known models is a double-door open model proposed by Kawai et al. (1971) and revised by Otofuji et al. (1985). This model is based mainly on paleomagnetic data indicating 45° -60° clockwise rotation of southwest Japan and anti-clockwise rotation of northeast Japan(Fig.2-4-1). In contrast, Lallemand and Jolivet (1986) proposed that the Japan Sea is a pull-apart basin bounded by strike slip faults at its eastern and western boundaries based on the overall geometry of and fault movements around the Japan Sea. Jolivet et al. (1991) and Jolivet and Tamaki (1992) proposed an integrated model that the Japan Arc shifted southward and the northeast Japan rotated anti-clockwise, and the southeast Japan rotated clockwise respectively (Fig.2-4-2). According to the double-door open model, the eastern margin of the Japan Sea was a pure extensional zone. While according to the integrated model, the eastern margin of the Japan Sea was strike slip or transtensional movement zone.

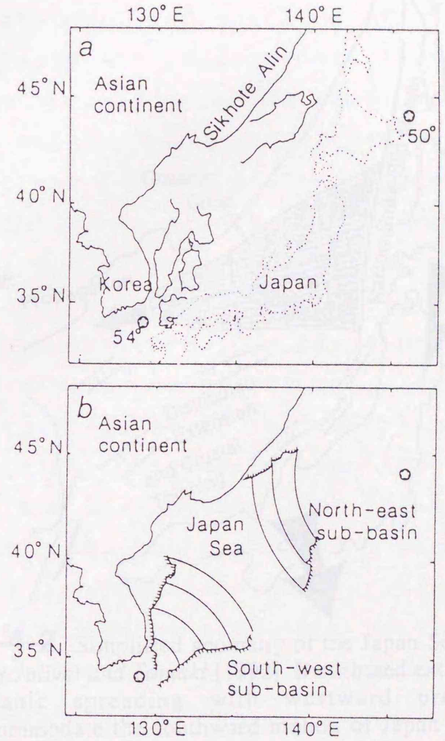

Fig.2-4-1

Double-door opening mode of the Japan Sea. *a*, Palaeoposition of the north-east Japan and south-west Japan arcs before the rotation at 21 Myr. *b*, Possible opening mode for the Japan Sea. North-east Japan rotated about a northern pivot (146° E, 44° N) through 50° and south-west Japan rotated about a southern pivot (129° E, 34° N) through 54°. Both arcs rotated concurrently between 21 and 11 Myr. The clockwise rotation of south-west Japan is attributed to a typical fan-shape opening of the south-west sub-basin, while the counter-clockwise rotation of north-east Japan is due to a sub-parallel opening (a fan shape opening with a fairly parallel mode) of the north-east sub-basin.

after Otofuji *et al.* (1985)

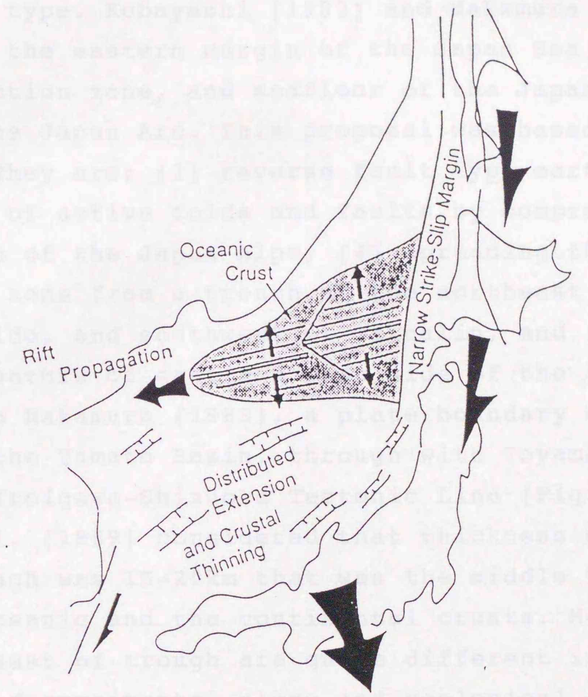

Fig.2-4-2 Simplified geometry of the Japan Sea opening after *Jolivet and Tamaki* [1992]. Distributed extension and oceanic spreading with westward propagation accommodate the southward motion of Japan along two major shear zones.

2.5. *A nascent subduction zone?*

In Quaternary, stress field of the eastern margin of the Japan Sea changed to E-W compression from extension as seen as many reverse faults, dikes, veins, and earthquakes of reverse fault type. Kobayashi (1983) and Nakamura (1983) proposed that the eastern margin of the Japan Sea was a nascent subduction zone, and seafloor of the Japan Sea underthrust the Japan Arc. This proposal was based on some occurrences. They are; (1) reverse fault type earthquakes, (2) existence of active folds and faults by compression, (3) fast rising up of the Japan Alps, (4) spreading the compressional zone from a trench at the northeast Japan, west of Hokkaido, and southwest of Sakhalin, and (5) topographic feature of east and west side of the Japan Sea.

According to Nakamura (1983), a plate boundary exists from east side of the Yamato Basin, through with Toyama Trough, and enter to Itoigawa-Shizuoka Tectonic Line (Fig.2-5-1).

Asada, et al. (1989) considered that thickness of a crust of Toyama Trough was 15-20km that was the middle value between the oceanic and the continental crusts. Moreover, the west and east of trough are quite different in bathymetry of a continental slope and geological structures. Then, even if the trough is a plate boundary or not, it is an important structural boundary.

Kato et al. (1990) carried out two profiles over Toyama Trough with a multichannel seismic reflection survey, and showed that both west-dipping and east-dipping reverse faults were growing there. It suggested that it was not simple subduction, because Toyama Trough was seemed not to be a plate boundary, or it was quite nascent.

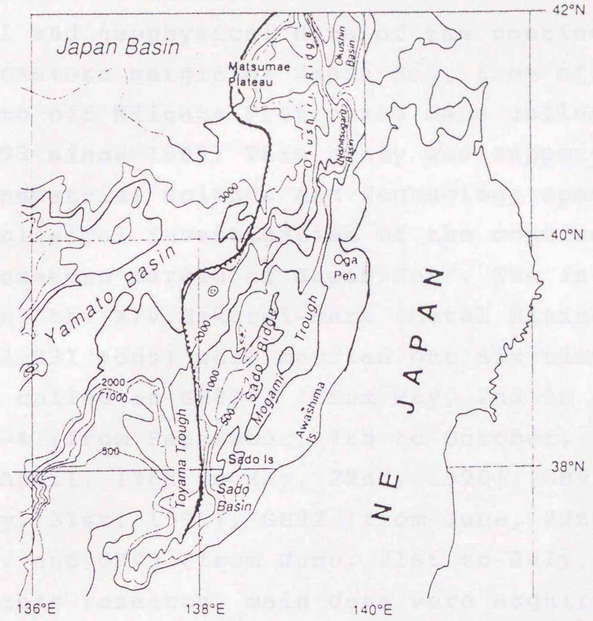

Fig.2-5-1

An incipient subduction zone in the eastern margin of the Japan Sea proposed by Nakamura(1983).

(*It is the same as Fig.1-1-3.*)

3.Outline of survey

3.1. *Surveys on R/V Hakurei-maru*

Geological and geophysical data of the continental shelf in central eastern margin of Japan Sea, from off Aomori Prefecture to off Niigata Prefecture were collected for five years by 1993 since 1989. This study was supported by the Agency of Industrial Science and Technology special research program "Geological Investigation of the continental shelf in central eastern margin of Japan Sea". The investigation cruises using the R/V Hakurei-maru (Metal Mining Company ownership, 1,831 tons) were carried out six times. These cruises are called as GH89-2 (from May, 2nd to July, 10th, 1989), GH89-4 (from September, 7th to October, 6th, 1989), GH90 (from April, 13th to May, 22nd, 1990), GH91 (from June, 23rd to July, 31st, 1991), GH92 (from June, 22nd to July, 31st, 1992), and GH93 (from June, 21st to July, 30th, 1993) cruise. In this research, main data were acquired from GH89-2 to GH92 cruises, and a supplementary investigation was done in GH93 cruise. Author participated in GH91 cruise, and acquired bathymetry, position, gravity, magnetic total force, and magnetic vector data. All of data which author used in this study were obtained from five cruises (GH89-2, GH89-4, GH90, GH91, and GH92) with R/V Hakurei-maru.

During the R/V Hakurei-maru cruises, five kinds of observations were carried out on the same survey lines. They were bathymetry with a 12kHz PDR, surface layer profiling with a 3.5 kHz SBP, single channel seismic reflection profiling using air guns as a sound source, magnetic total force measurement with a proton precession magnetometer, and gravity measurement with an on-board gravity meter. Moreover, dredging, getting core samples with a rock corer or gravity corer, and getting surface sediments with a glove sampler were carried out at many points in the study area.

Basically, sediment samplings were done in the daytime, and running observations were done in the night time.

Survey lines were obtained about 5,900miles in GH89-2, 2,900miles in GH89-4, 3,780miles in GH90, 3,830miles in GH91, and 3,080miles in GH92. Then, we got about 19,400miles in total. The distribution of survey lines is shown in Fig.3-1-1. Survey lines were designed as 3.3 nautical miles (5.9km) in parallel to the coast and 1.6 nautical miles (2.9km) in cross to the coast mesh. It is much denser than previous surveys. For example, Hydrographic Department of the Maritime Safety Agency carried the survey at intervals of 2 nautical miles for WNW-ESE or E-W direction (Sato, 1971). Our data have advantages of the accuracy of positioning, therefore we could find detail topographic features from our new data. For example, shape of banks and small basins were different from previous maps (Miyazaki and Sato, 1992). Because, the accuracy of positioning was about 1 nautical mile in 1970's(Sato, 1971). In contrast, our data was about 0.1 nautical mile (Miyazaki and Sato, 1992).

Our advantages are not only topographic features but also magnetic anomalies. Many previous surveys were not designed as mesh. Then they couldn't show detail magnetic anomaly maps. The reasons were described later chapters.

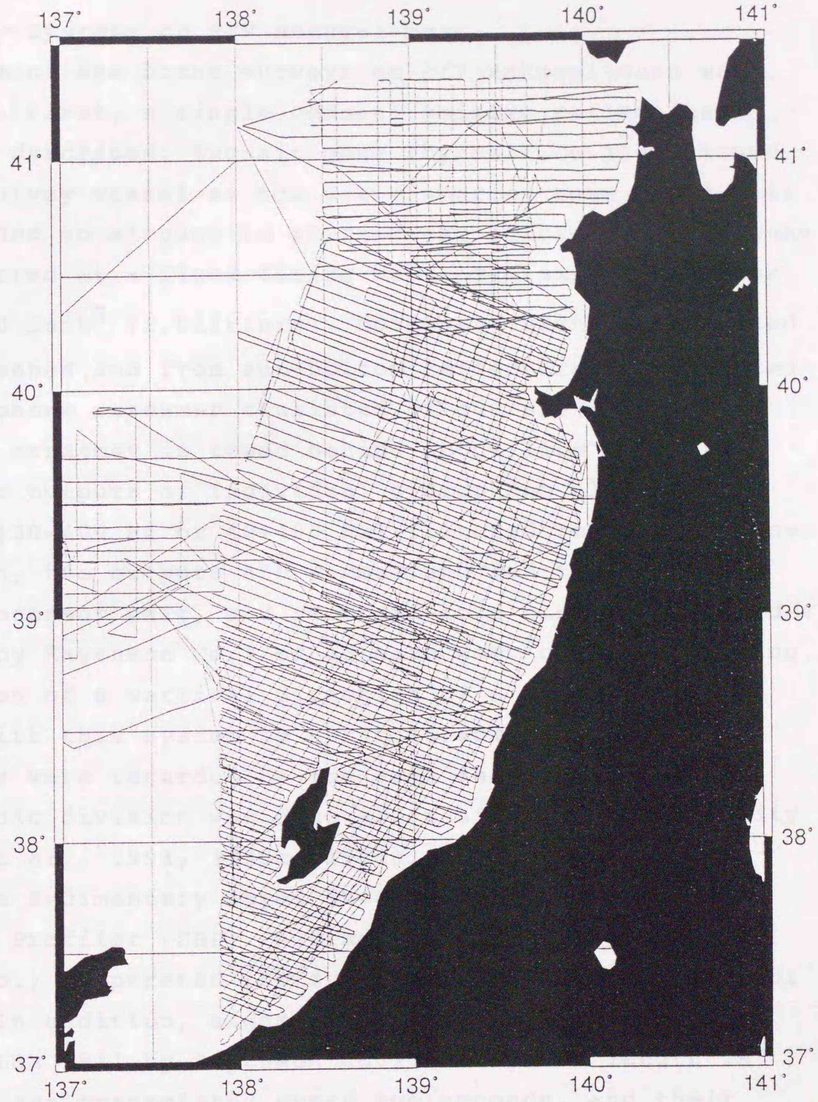

Fig.3-1-1
Seismic, Gravimetric, and Magnetic Survey lines during five R/V Hakurei-maru cruises, GH89-2, GH89-4, GH90, GH91, and GH92.

3.2. *Survey systems on R/V Hakurei-maru*

The system of sea borne surveys at R/V Hakurei-maru was introduced. First, a single channel seismic reflection system was described. Two air guns (by Bolt Co.) are towed behind a survey vessel as the sound source. Wave shape kits were attached to airguns to shorten for pulses. The air guns were triggered at a fixed firing rate. The air gun chamber size is 120 inch^3 (2.0litters). Moreover, signals reflected from the seabed and from sub-bottom reflectors are detected by a hydrophone streamer consisted of 100 elements. The hydrophone streamer is towed behind about 150m from the vessel. The outputs of individual hydrophone elements are band-pass (30-400 Hz or 40-400 Hz) filtered to reduce noise. In addition, the outputs are summed and fed to a single-channel processor unit, and recorded to a Line Scan Recorder (LSR 1811 by Raytheon Co.) of an each 4sec or 2sec scanning. A resolution of a vertical direction of a profile that is obtained with this system is about 35-60m. Similar reflections were regarded as the same sequences; a stratigraphic division was done as considering unconformity (Okamura et al., 1994, 1995a, 1996a, 1996b).

A surface sedimentary layer investigation using 3.5 kHz Sub Bottom Profiler (SBP). A transceiver PTR105B (by Raytheon Co.) cooperated the system with a signal processor CESP-III. In addition, signals are fed to a Line Scan Recorder (LSR 1811 by Raytheon Co.). The pulse length is 50ms. They are transmitted every two seconds, and their record length on the LSR is 1 second. A resolution of vertical structure of this 3.5 kHz SBP profiles is 1-2m. However, it is hardly to see submarine structures at the area covered with sandy deposits.

Gravity surveys are used an on-board gravity meter which

is a straight-line type (SL-2) by the LaCoste & Romberg company. A measurement resolution is nominally 1mgal. We are fundamentally measuring gravity during the cruise. Data are fed every 10 seconds to a complex positioning system, and recorded on magnetic tapes with positioning data, NNSS (Navy Navigation Satellite System) and LORAN-C (LOng RAnge Navigation) or GPS (Global Positioning System). This complex positioning system was replaced to Magnavox Series 5000 in 1990. Then, after 1990, R/V Hakurei-maru uses Single-GPS and NNSS for deciding its position.

Magnetic surveys are used a proton precession magnetometer (by EG&G Geometrics, type G801D in 1989, and type G866 since 1990). A magnetometer is towed behind the vessel about 250m. A measurement resolution is nominally 0.5nT. Data are fed every 10 seconds to a complex positioning system, and recorded on magnetic tapes with gravity, positioning and other data.

Since 1990, magnetic vectors were measured with the Shipboard Three Component Magnetometer (Telatechnica, SFG-1211). The magnetometer consists of magnetic sensor unit, control unit, and ship's attitude sensor unit. The magnetic sensor unit is set on the upper deck. There is a dome made by aluminum on the top of the 1.5m height pole. There are ring core type flux gate magnetometers that are set as head, starboard, and downward, and a platinum thermometer in the dome.

As a ship's attitude measurement unit, a horizontal attitude meter (Tamagawa Seiki, TA7175N2) to measure pitching and rolling of a ship is set on a floor of a research room in the ship. Yawing data are come from the gyrocompass (Yokogawa Navitec, CMZ300X) of the bridge of R/V Hakurei-maru.

A control unit has a 16bit A/D converter. Magnetic field

data(3nT/LSB), ship's attitude(yawing, 0.1° ; pitching and rolling, 0.01°), and temperature(1℃) are fed to the control unit by 8Hz sampling. Otherwise, ship's position and speed come from the complex positioning system (Magnavox Series 5000) every 10 seconds. These data are recorded on digital audiotape (DAT). Later processes use the mean value of 1-sec data (Fig.3-2-1).

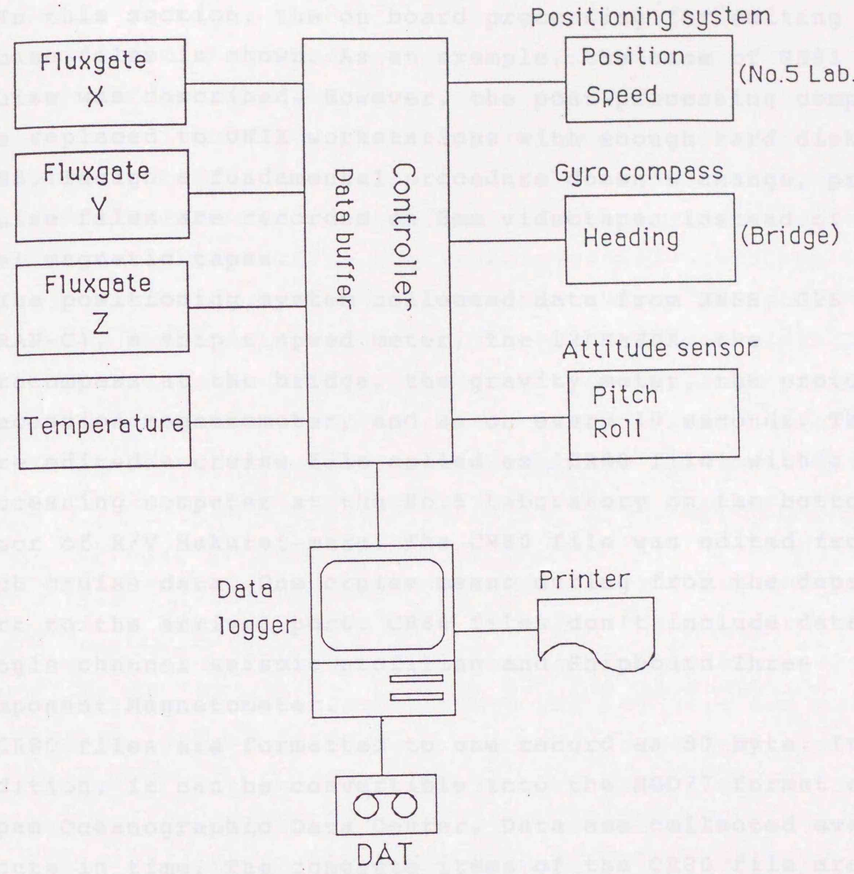

Fig.3-2-1
Block diagram of a three component magnetometer system equipped on-board the R/V Hakurei-maru.

3.3. *On board processing*

In this section, the on board processing for editing cruise files is shown. As an example, the case of GH91 cruise was described. However, the post-processing computer was replaced to UNIX workstations with enough hard disks in 1993. Though a fundamental procedure doesn't change, present cruise files are recorded on 8mm videotapes instead of open-reel magnetic tapes.

The positioning system collected data from NNSS, GPS (or LORAN-C), a ship's speed meter, the 12kHzPDR, the gyrocompass at the bridge, the gravity meter, the proton precession magnetometer, and so on every 10 seconds. These were edited a cruise file called as 'CR80 file' with a post processing computer at the No.5 Laboratory on the bottom floor of R/V Hakurei-maru. The CR80 file was edited from each cruise data. One cruise means during from the departure port to the arrival port. CR80 files don't include data of single channel seismic profiling and Shipboard Three Component Magnetometer.

CR80 files are formatted to one record as 80 byte. In addition, it can be convertible into the MGD77 format of Japan Oceanographic Data Center. Data are collected every 1-minute in time. The concrete items of the CR80 file are shown in Table 3-1-1 (after Kisimoto et al., 1984).

Experience has shown that the position data from the positioning system often suffered from many kinds of noise. Therefore, they often need to be checked and corrected for the post-processing.

In 1991, because a receiving condition of GPS signals was poor, position data were corrected for CR80 file output. They were recalculated after rejecting the data to be judged that an error is large, as checking for a receiving condition of NNSS and GPS (or LORAN-C). However, recently,

this correction isn't required so often, because a receiving condition of GPS becomes good.

As for bathymetry data, they were digitized from analog chart of LSR for 12kHzPDR. Though digital output of 12 kHz PDR were fed to the complex positioning system, there were many errors in output numerical value, where topographic inflection is strong. Therefore, bathymetric data to be edited as CR80 files were digitized with a digitizer from 12kHzPDR analog charts almost every day in the cruise.

We finally get the free-air anomalies trough on-board processes. It is necessary to correct for all variations in the Earth's gravitational field, which do not result from the differences of density in the underlying rocks. They are drift correction, Eoetvoes correction, and free-air correction.

First for drift correction, we need to know the absolute gravity value at the wharf of departure port and at the wharf of arrival port of the cruise. Usually, the gravity base was the pier for R/V Hakurei-maru at Funabashi, Chiba Prefecture. The base value was the absolute gravity. And another base value at a wharf was obtained from a relative value between the nearest station where showed an absolute gravity of IGSN 1971 system by Geographical Survey Institute of Japan, for example at a meteorological observatory. The relative gravity was measured with a portable gravity meter, LaCoste & Romberg D-type. In the GH91 cruise, gravity bases were set at Funabashi Port and Sakata Port. The absolute gravity at the wharf of Sakata Port was obtained from relative value between the wharf and Sakata meteorological observatory. Moreover, correction for instrumental drift is based on the difference in gravity readings and in absolute gravity between the Funabashi Port and the Sakata Port. Drift is assumed linear during the cruise. At that time, we

obtained 0.17mgal/day as the drift (Morijiri and Yamazaki, 1992a).

After drift correction, the absolute gravity at each observation points (gobs) was calculated from the known value of difference between each point and the base (Funabashi Port).

The Eoetvoes correction (EC) is applied to gravity measurements which taken on a moving vehicle such as a ship or an aircraft. Depending on the direction of travel, vehicular motion will generate a centripetal acceleration that either reinforces or opposes gravity. The correction required is

$$EC=7.5\emptyset 3V\sin\alpha\cos\phi+\emptyset.\emptyset\emptyset 4154V^2 \ (\text{mgal})$$

where V is the ship's speed in knots, α is the heading, and ϕ is latitude at observation points.

The free-air anomaly (FAA) is defined

$$FAA=g_{obs}-g_{\emptyset}+FAC+EC \qquad (3\text{-}3\text{-}1)$$

Where, g_0 is theoretical gravity and FAC is elevation correction. FAC is given by

$$FAC=-\emptyset.3\emptyset 86h \qquad (3\text{-}3\text{-}2)$$

Where h is the height of observation points above sea level. Then observations on the sea always give FACs as zero. The values of g_0 at each observation points were calculated from the International Gravity Formula (International Association of Geodesy 1967).

$$g_{\emptyset}=9.78\emptyset 31846(1+\emptyset.\emptyset\emptyset 53\emptyset 24\sin^2\phi-\emptyset.\emptyset\emptyset\emptyset\emptyset 058\sin^2(2\phi)) \qquad (3\text{-}3\text{-}3)$$

where ϕ is latitude at observation points.

Magnetic anomalies were deducted values of IGRF85 (International Geomagnetic Reference Field, IAGA Division I, Working Group 1,1987) from measured values. We didn't consider diurnal variation of geomagnetic total force. At

the GH91 cruise, IGRF90 (IAGA Division V, Working Group 8,1991) wasn't published yet. After the publishing, magnetic anomalies were recalculated anomalies using IGRF90 coefficients.

CR80 File (after Kisimoto et al., 1984)

HEADER Record No.1(Cruise information)

Character	Code	Description
1	1H1	Record Type-"1"
2	1H1	"1" for No.1 record
3-10	8A1	Cruise Identifer
11-12	I2	Survey Departure Year
13-15	I3	Survey Departure Day(Julian Day)
16-43	28A1	Port of Departure
44-45	I2	Survey Arrival Year
46-48	I3	Survey Arrival Day(Julian Day)
49-76	28A1	Port of arrival
77-80	4A1	Available Data Identifer "NMBG", when navigational, bathymetric, magnetic, and gravity data are in the file. "N-B-"means no bathymetric and gravity measurements in the cruise.

Table 3-1-1
Contents of CR80 Cruise file of R/V Hakurei-maru.

HEADER Record No.2(Cruise information)

Character	Code	Description
1	1H1	Record Type-"1"
2	1H1	"2" for No.2 record
3-40	38A1	Magnetic Reference Field(e.g."IGRF90")
41-49	9A1	Gravity Reference Field(e.g."IAG1967")
50-57	8A1	Gravity Reference System(e.g."IGSN71")
58-59	I2	Year at the Gravity base station
60-62	I3	Julian Day at the Gravity base station
63-69	I7	Absolute gravity value at the base station(x0.1mgal)
70-75	I6	Gravity reading by the sea gravity meter at the base station(x0.1mgal)
76-80	I5	Drift rate of the sea gravity mater(x0.01mgal)

continued-2-

HEADER Record No. 3 and No. 4

Character	Code	Description
1	1H1	Record Type-"2"
2	1H1	"1" for No. 3 record and "2" for No. 4 record
3-4	I2	Number of 10-Degree Identifers.
5	I1	Blank
6-80	I5 (I4, 1H,)	10-Degree Identifers("9999", if no more data)

DATA Record

continued-3-

DATA Record

Character	Code	Description
1	1H3	Record Type-"3"
2-3	I2	Year
4-6	I3	Julian Day
7-10	I4	Time(GMT in minute)
11	1HN	(Navigation Data)
12-19	I8	Latitude(x10^{-5} deg; - if south)
20-28	I9	Longitude(x10^{-5} deg; - if west)
29	1HV	(velocity data for Eoetvoes correction)
30-33	I4	Ship's speed(x0.01knot)
34-37	I4	Ship's course(x0.1deg; clockwise from North)
38	1HB	(Bathymetric data)
39-43	I5	uncorrected depth(m;750m/sec)
44-48	I5	corrected depth(m)
49-50	I2	Matthews Zone Code for corrected depth
51	1HM	(magnetic data)
52-56	I5	Total magnetic force(nT)
57-61	I5	Magnetic anomaly(nT)
62	1HG	(gravity data)
63-68	I6	Gravity reading(x0.1)
69-75	I7	Absoluted gravity value(x0.1mgal)
76-80	I5	Free-Air Anomaly(x0.1mgal)

continued-4-

4. Gravity study

4.1. *Noise Reduction*

Gravity is measured on the ship; it is considered that measurement on the ship is equal to on geoid (average sea surface). Then, free-air gravity anomaly($\Delta g'$) is

$$\Delta g' = g+(7.5*\cos\phi*\sin\theta+0.0042*\nu)*\nu-\gamma+0.87 \qquad (4\text{-}1\text{-}1)$$

where, latitude is ϕ, ship's speed is ν, heading is θ, Absolute gravity is g, normal gravity is γ, and the last term is Air-correction.

The value of γ gives the predicted value of gravity at sea-level at any point on the Earth's surface and is subtracted from observed gravity to correct for latitude variation. It is given as Gravity Formula 1967.

$$\gamma=978031.85*(1+0.005278895*\sin^2\phi+0.000023462*\sin^4\phi) \qquad (4\text{-}1\text{-}2)$$

We usually process data on R/V Hakurei-maru during each cruise and edit to a cruise file (Kisimoto et al., 1984).

However, frequency of free-air anomalies is higher than that of gravity meter readings. It seems to be anomalous. And frequency of ship's speed(ν) and heading(θ) were also high and anomalous. Then I judged high frequency of free-air anomaly was caused by Eoetvoes correction error. Eoetvoes correction was under the influence of positioning error, because ship's speed(ν) and heading(θ) were calculated from ship's position data. Actually, measurement values of ship's speed and heading didn't correspond to gravity variation because of waves and currents. For this processing, ship's heading and speed were regarded as constant during moving on each survey lines, and these data were smoothed by weighted running means method using each 9 data. After smoothing, Etvoes correction was recalculated using smoothed ship's speed and heading data. Smoothed

ship's speed and heading were shown in Fig.4-1-1, and gravity reading and recalculated free-air anomalies were shown in Fig.4-1-2. However, free-air anomalies were smoothed again by a weighted running means method using each nine data, because frequency of recalculated free-air anomaly was still higher and anomalous than that of gravity readings.

The weight values for running means were shown in Table.4-1-1. They were set by Savitzky and Golay (1964).

Now at every point j for 2m+1 points which were considered the point i as the center, signals y(j) were approximated as 2nd-ordered formula is:

$$y(j)=a(j-i)^2+b(j-i)+c$$

Where,

$$j= -m+i\ldots-1+i,i,1+i,,,m+i \qquad (4\text{-}1\text{-}3)$$

Then, square error between an actual measurement value x(j) and y(j) is:

$$\Sigma\{x(j)-y(j)\}^2 \qquad (4\text{-}1\text{-}4)$$

To minimize the quantity estimates coefficients a, b, and c. At that time, y(i) becomes c. Consequently, smoothed value y(i) at a center point i is calculated using weighted coefficients w(j) in Table.4-1-1 and actual measurement values x(j):

$$y(i)=1/W\{\Sigma x(i+j)w(j)\}$$

$$W=\Sigma w(j) \qquad j= -m,,,,m \qquad (4\text{-}1\text{-}5)$$

Moreover, data during changing course were regarded as No-data in this processing.

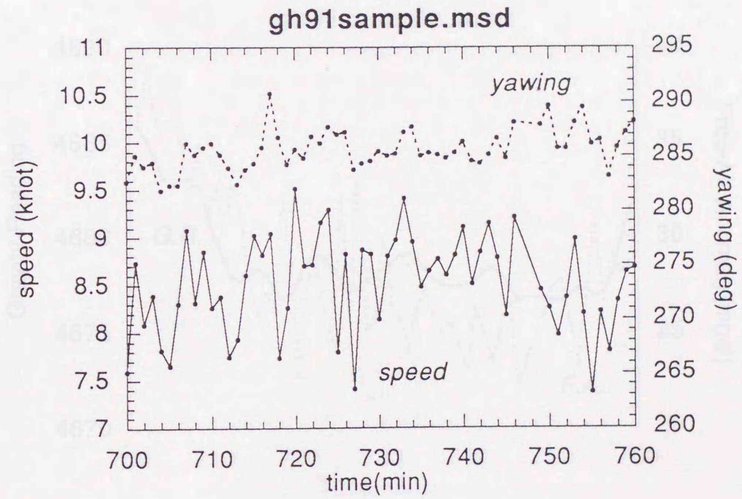

Fig.4-1-1
Sample data for ship's speed and yawing on a survey line of GH91 cruise. Horizontal axis indicates time in minute. Right vertical axis indicates yawing in degrees. Left vertical axis indicates ship's speed in knot.

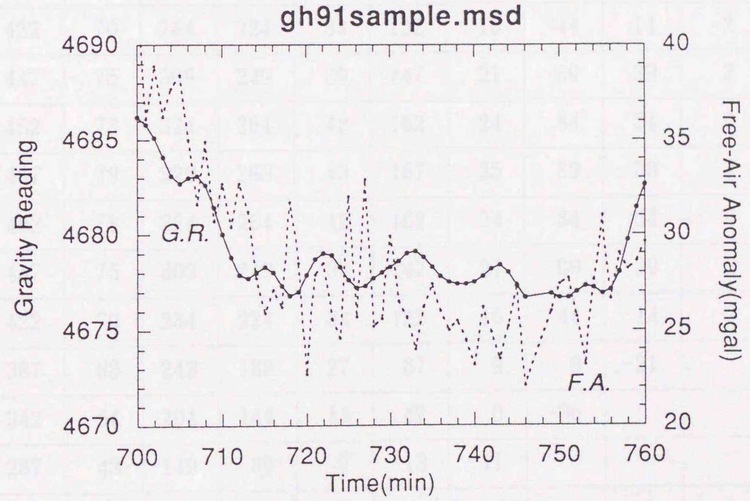

Fig.4-1-2
The same sample data shown in Fig.4-1-1 for Gravity meter readings and Freeair Gravity anomalies. Horizontal axis indicates time in minute. Right vertical axis indicates freeair gravity anomaly in mgal. Left vertical axis indicates Gravitymeter reading in mgal.

No	25	23	21	19	17	15	13	11	9	7	5
-12	-253										
-11	-138	-42									
-10	-33	-21	-171								
-09	62	-2	-76	-136							
-08	147	15	9	-51	-21						
-07	222	30	84	24	-6	-78					
-06	287	43	149	89	7	-13	-11				
-05	342	54	204	144	18	42	0	-36			
-04	387	63	249	189	27	87	9	9	-21		
-03	422	70	284	224	34	122	16	44	14	-2	
-02	447	75	309	249	39	147	21	69	39	3	-3
-01	462	78	324	264	42	162	24	84	54	6	12
00	467	79	329	269	43	167	25	89	59	7	17
01	462	78	324	264	42	162	24	84	54	6	12
02	447	75	309	249	39	147	21	69	39	3	-3
03	422	70	284	224	34	122	16	44	14	-2	
04	387	63	249	189	27	87	9	9	-21		
05	342	54	204	144	18	42	0	-36			
06	287	43	149	89	7	-13	-11				
07	222	30	84	24	-6	-78					
08	147	15	9	-51	-21						
09	62	-2	-76	-136							
10	-33	-21	-171								
11	-138	-42									
12	-253										

Table.4-1-1
Coefficient of weight for running mean smoothing.
after Savitzky and Golay(1964).

4.2. *Bouguer Reduction*

Next step was to calculate Bouguer anomalies from smoothed free-air anomalies. Bouguer anomaly $\Delta g''$ is;

$$\Delta g'' = \Delta g' - 2\pi G\rho h + \rho T \qquad (4\text{-}2\text{-}1)$$

where, $\Delta g'$ is free-air anomaly, $2\pi G\rho h$ is Bouguer correction, and ρT is terrain correction. And h is water depth at a measurement point, G is Newton's gravitational constant($=0.00667 mgal*cm^3/g*m$), ρ is density, and T is mass of topography.

Here, observed points on the survey lines were regarded as isolated measured points. Then terrain correction(ρT) suffered from crossover errors of each survey lines, because data included positioning or measurement errors. However, data were not reduced with cross-point control method, because crossover errors in this study area were within 2-3mgal and accuracy of gravity measurement was approximated at 5mgal. Terrain correction was made to account for topographic relief near the each gravity measurement points. It was applied using annular prism models (see Fig.4-2-1; Komazawa, 1988,1989). In addition, data for terrain correction were 1km mesh data that were introduced by Komazawa and Kisimoto (1995) and measured water depth in our cruises.

Usually, terrain corrections are applied using four divisions; they are 'very near' (<0.5km), 'near' (0.5-4km), 'middle' (4-16km), and 'far' (16-60km). However, 'very near' zone correction was not applied here, and 1km mesh topographic data were used for 'near' and 'middle' zone corrections, and 4km mesh data were used for 'far' zone correction. In addition, before terrain corrections, topographic data were converted to UTM coordinates system (Universal Transverse Mercator Projection), and newly 125m,

500m, and 2km mesh data files were made. In case that the center of an annular prism model was within 125m from an observed point, an observed water depth and depth values in a mesh data file were used for calculation of an annular prism depth. Therefore, depths of annular prisms were not influenced by local errors of water depth data.

A Schematic diagram of terrain corrections under the sea level was shown in Fig.4-2-2. (I) indicates that the terrain correction was made to account for topographic relief of land area near the gravity observation point. (II) indicates that terrain correction was made to account for topographic relief of water area. Terrain correction (III) was subtracted correction (I) from correction (II). The total of terrain correction values, $T(\rho)$ was;

$$T(\rho)=\rho T1+(\rho-\rho w)Tw \qquad (4\text{-}2\text{-}2)$$

Where, T1 indicated terrain correction value of (I), and Tw was terrain correction value of (III), both of their calculated density was 1.0g/cm^3. And ρ indicated density of crust, and ρw was density of water.

A Schematic diagram of relations between assumed Bouguer correction density(ρ) and Bouguer gravity anomaly was shown in Fig.4-2-3(after Komazawa, 1995). Bouguer correction density(ρ) was assumed by Gravity-Height(G-H) correlation diagram or correlation with topographical map and gravity anomaly map. A case of sea area was fundamentally similar to a land area. However, compared with a land area case, because measurement accuracy both positioning and gravity were low, strict method was improper. Therefore, Bouguer correction density was approximated at 2.3g/cm^3 compared with a bathymetry map and Bouguer gravity anomaly maps using 2.0, 2.3, 2.5, and 2.7g/cm^3. An argument of concrete density estimation was described later. When 3-dimensional analyses

of divided shallow areas were carried out; Bouguer anomalies were re-calculated using the most suitable density of each area.

Bouguer gravity anomalies on each observed points, z(xr,yr) were interpolated into mesh data by fitting on a hyperboloid. Then,

$$z(x,y) = A + Bx + Cy + Dx^2 + Ey^2 + Fxy \qquad (4\text{-}2\text{-}3)$$

These coefficients of the expression were repeatedly estimated by the least square mean method, then the values on mesh points were calculated.

Concretely,

(1) to decide a taking radius R from a distribution of observed points.

(2) to calculate a distance r between the mesh point (x_i,y_i) and each observed points (x_r,y_r).

Then,

$$r=\sqrt{(x_r-x_i)^2+(y_r-y_i)^2} \qquad (4\text{-}2\text{-}4)$$

Moreover, to calculate weight w as doing

$$w=\{1/(r^2+\varepsilon^2)-(1/(R^2+\varepsilon^2)\}^2. \qquad (4\text{-}2\text{-}5)$$

To calculate an azimuth in order to see a distribution of observed points in vicinity of the mesh point.

(3) Residual λ was described as

$$\lambda=\Sigma\, w\{z-(A+Bx+Cy+Dx^2+Ey^2+Fxy)\}^2 \qquad (4\text{-}2\text{-}6)$$

The most suitable hyperboloid makes a residual λ the minimum.

After all,

$$\partial\lambda/\partial A=0,\ \partial\lambda/\partial B=0,\ \partial\lambda/\partial C=0,\ \partial\lambda/\partial D=0,$$
$$\partial\lambda/\partial E=0,\ \text{and}\ \partial\lambda/\partial F=0 \qquad (4\text{-}2\text{-}7)$$

are satisfied.

(4) When every mesh point (x_i,y_i) always satisfy these two

conditions. One is that there are more than six observed points (x_r, y_r) within radius R, and another is that the azimuth of no observed point area is less than 120° .

$$\Sigma zw(A+Bx+Cy+Dx^2+Exy+Fy^2)=\Sigma zw(z)$$

$$\Sigma zw(Ax+Bx^2+Cxy+Dx^3+Ex^2y+Fxy^2)=\Sigma zw(xz)$$

$$\Sigma zw(Ay+Bxy+Cy^2+Dx^2y+Exy^2+Fy^3)=\Sigma zw(yz)$$

$$\Sigma zw(Ax^2+Bx^3+Cx^2y+Dx^4+Ex^3y+Fx^2y^2)=\Sigma zw(x^2z)$$

$$\Sigma zw(Axy+Bx^2y+Cxy^2+Dx^3y+Ex^2y^2+Fxy^3)=\Sigma zw(xyz)$$

$$\Sigma zw(Ay^2+Bxy^2+Cy^3+Dx^2y^2+Exy^3+Fy^4)=\Sigma zw(y^2z)$$

Where,

$$x=|x_i-x_r|,\ y=|y_i-y_r| \qquad (4\text{-}2\text{-}8)$$

Then to solve the simultaneous equation and get A, B, C, D, and F. A is given as the mesh point value at that time.

(5) To repeat the above-mentioned operation as transporting a mesh point (x_i, y_i).

Here, the radius R was considered as 20km, and made 1km mesh data. The Bouguer gravity anomaly map was shown in Fig.4-2-4 whose contour interval was 5mgal.

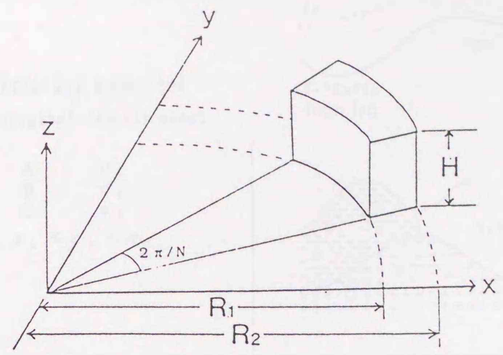

Fig.4-2-1 Annular prism model of topography. The height of annular prism is approximated from four near prisms by weighted average method

H : height difference between annular prism and station.
N : Division number of circle.
R_1: Radius of inner circle. R_2: Radius of outer circle.

after Komazawa(1988)

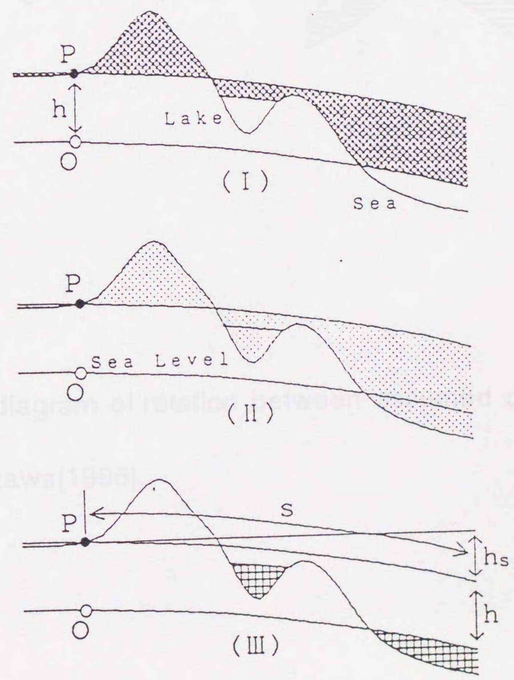

Fig.4-2-2

Terrain correction of land area and water area, and spherical effect.
P:observation point. O:observation point on the sea level.
after Komazawa(1989).

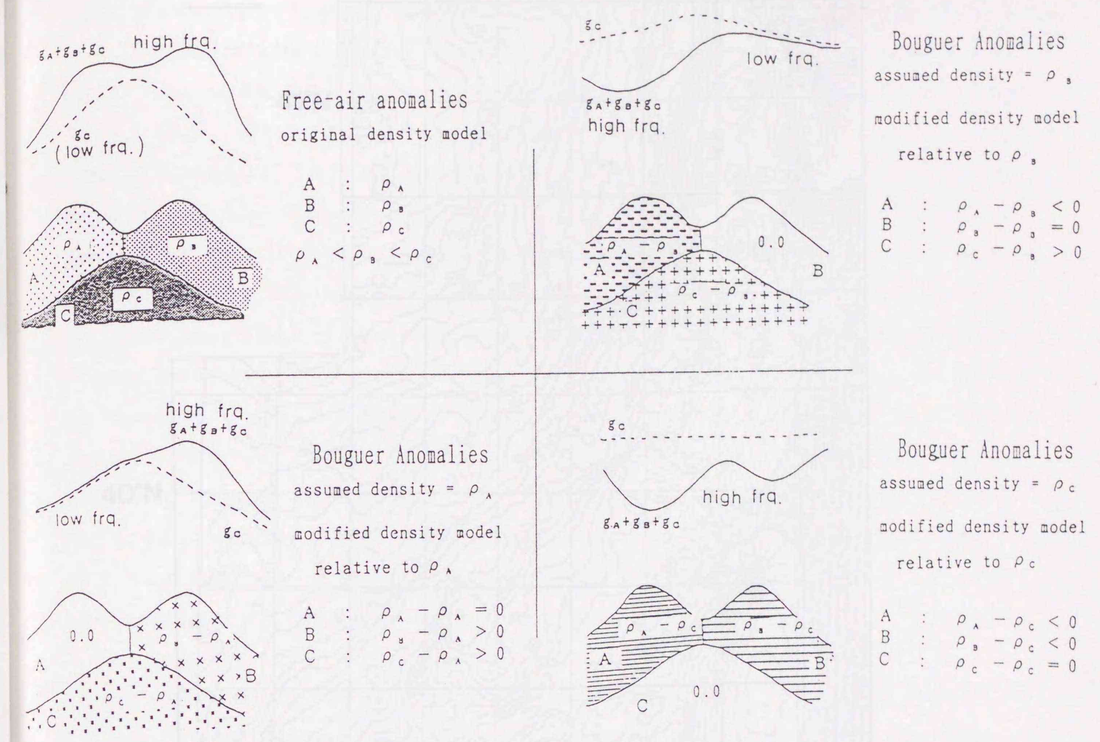

Fig.4-2-3
Schematic diagram of relation between assumed density and Bouguer anomalies.
after Komazawa(1995).

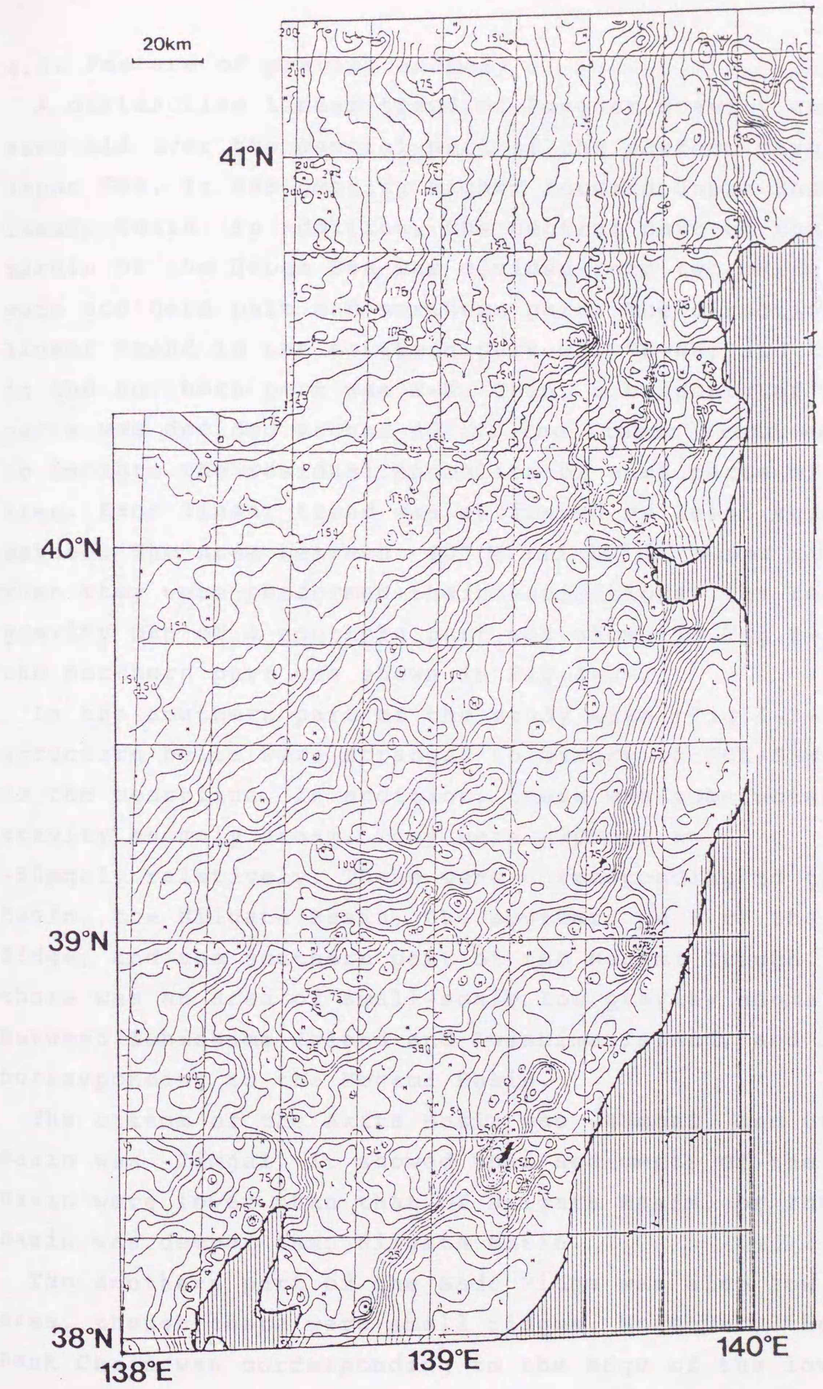

Fig.4-2-4
Bouguer gravity anomaly map of the studied area. Bouguer density is assumed to be 2.3g/cm3. Contour interval is 5mgal.

4.3. *Feature of gravity anomaly*

A distinctive linear trend of Bouguer gravity anomaly was seen all over the central part of the eastern margin of the Japan Sea. It was getting higher forward Japan Basin or Yamato Basin. In addition, the central part of the eastern margin of the Japan Sea was divided into two parts; they were southern part and northern part. The direction of the linear trend in the southern part was SE-NW, and the trend in the northern part was E-W. Then, a boundary of these two parts was decided around 40° N. The linear trend was removed to isolate the residual anomalies of each parts of the study area. Each linear trend was estimated by least square means method. The area between 40° N and 40° 20'N was overlapped when they were performed their estimations. The residual gravity map of a southern part was shown in Fig.4-3-1, and the northern part was shown in Fig.4-3-2.

In the southern part of the study area (Fig.4-3-1), structure belts were arranged to direction NNE-SSW, parallel to the coastline. In addition, there was some notable low gravity anomaly areas. They were -30mgal to -50mgal, relatively. These were corresponding to the Akita Basin, the Niigata Basin, the southern part of the Sado Ridge, and the southern part of the Mogami Trough. Moreover, there was an area of small-scale low gravity anomalies between Tobishima Island and Awashima Island, and it was corresponding to the Mogami Basin.

The bottom of the Akita Basin was -45mgal, and the Niigata Basin was -25mgal. It showed that sediments of the Akita Basin were lower than that of Niigata Basin, or the Akita Basin was deeper than Niigata Basin.

The southern part of the Sado Ridge was also low gravity area, though there were small ridges. Moreover, the Dewa Bank Chain was corresponding to the edge of the low gravity

of the Akita Basin. Then, it became high gravity anomalies.

On the other hand, in the northern part of this study area, there was a remarkable zone of low gravity anomalies that trend in N-S direction between Okushiri Ridge and Tsugaru Peninsula in Fig.4-3-2. From 40° N to 40° 15'N, the low gravity area along the coast was corresponding to the Noshiro Basin. In addition, the area of low gravity anomalies in north of Kyuroku Jima Island was divided into two parts. East part was corresponding to the Ajigasawa Basin, and another was corresponding to the Nishi-Tsugaru Basin. Residual Bouguer gravity anomaly was about -30mgal in the Ajigasawa Basin. Moreover, the high gravity anomalies corresponded to the Okushiri Ridge was not so remarkable in this map (Fig.4-3-2). It suggested that assumed density 2.3g/cm^3 was suitable to the Okushiri Ridge.



Fig.4-3-1
Residual Bouguer gravity anomaly map of the southern part of the study area. Data were obtained by removing linear trend. Broken lines indicate negative values, and solid lines indicate positive values.

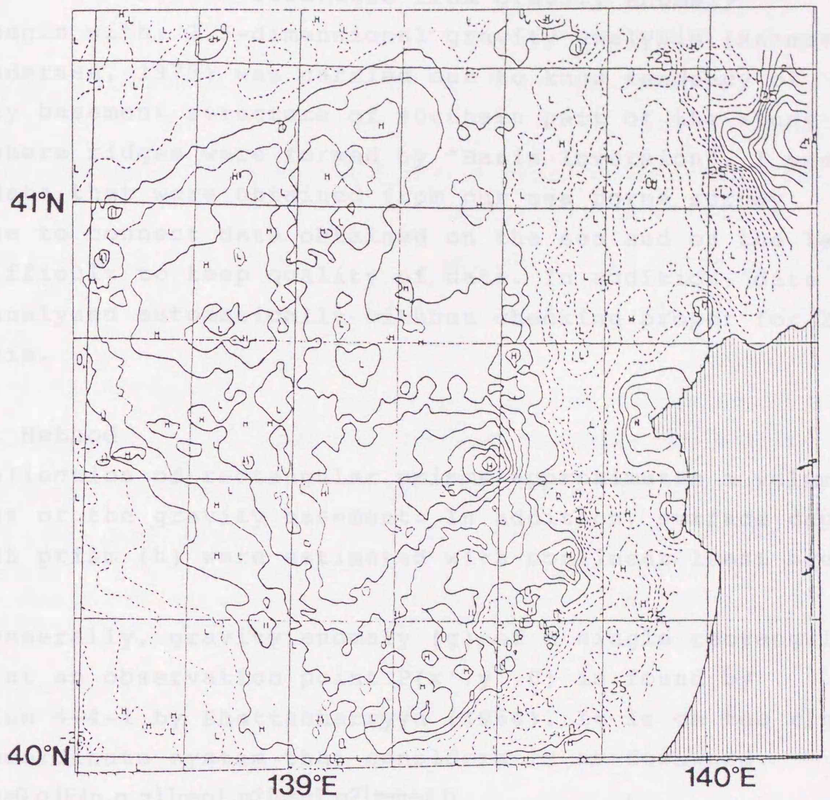

Fig.4-3-2

Residual Bouguer gravity anomaly map of the northern part of the study area. Data were obtained by removing linear trend. Broken lines indicate negative values, and solid lines indicate positive values.

4.4. *2.5-dimensional structure from gravity anomaly*

To begin with, 2.5-dimensional gravity analysis (Rasmussen and Pedersen, 1979) was carried out to know tendency of gravity basement structure of southern part of the study area where ridges were formed by "Basin Inversion". I used only data that were obtained from our sea borne survey because to connect data obtained on the sea and on the land was difficult to keep quality of data. In addition, data were analyzed automatically without checking proper for 2-D analysis.

4.4.1. Method

A collection of rectangular prisms approximates a volume of mass of the gravity basement. In addition, surface depth of each prism (h) were estimated with nonlinear least square means.

In generally, gravity anomaly (g) of a single rectangular prism at an observation point P(x',y',0) is found by equation 4-4-1 by Bhattacharryya (1964). It is on the right hand coordinate system that considers +z as downward.

$$g(x',y')=G\rho[F(p,q,z)]p=p1,p2|q=q1,q2|z=h+d,h$$

$$F(p,q,z)=p/2(\log(R-q)/(R+q))+q/2(\log(R-p)/(R+p))+z/2(\tan^{-1}(pq)/(Rz))$$

$$R=\sqrt{(p^2+q^2+z^2)} \qquad (4\text{-}4\text{-}1)$$

Where Newton's gravitational constant is G. And, surface depth as h, thickness as d, center of a prism surface as (x_0,y_0,h), a prism with uniform density ρ and with dimensions described by the limits

$-a<x<a$, $-b<y<b$, and $h<z<h+d$.

Here,

$x=x'-x_0$, $y=y'-y_0$, $p1=-x+a$, $p2=-x-a$, $q1=-y+b$, $q2=-y-b$.

Some parameters in equation 4-4-1 were calculated with Marquardt's method of nonlinear least square means.

Parameters were m (m_i, i=1,M) and observed data were f_u(u=1,N), calculated data were g(x_u,m). 'True' parameters were mt. Since observed data fu included errors ε, then

$$f_u=g(x_u,m_t)+\varepsilon \qquad (4\text{-}4\text{-}2)$$

The best parameters made minimum squares of residual between observed data and calculated data.

$$S(m)=\Sigma\{f_u-g(x_u,m)\}^2 \rightarrow \text{minimum.} \qquad (4\text{-}4\text{-}3)$$

$$S'(m)=\partial S(m)/\partial m_r=2\Sigma\{f_u-g(x_u,m)\}\{\partial g(x_u,m)/\partial m_r\}=\emptyset \quad (1\leqq r\leqq M) \qquad (4\text{-}4\text{-}4)$$

Solve these simultaneous equations.

Because g(x_u,m) was non-linear function of m, we cannot use the least-squares analysis. Then, we changed the elements of m only small amounts over a number of iterations. If the changes in m were small, g(x_u,m) became nearly a linear function. We gave initial parameters m_0, and Taylor series was applied;

$$g(x_u,m)=g(x_u,m_\emptyset)+\Sigma\{\partial g(x_u,m_i)/\partial m_i\}(m_i-m_{\emptyset i}) \qquad (4\text{-}4\text{-}5)$$

Equation (4-4-5) was substituted into equation (4-4-2) to get;

$$f_u=g(x_u,m_\emptyset)+\Sigma\{\partial g(x_u,m_i)/\partial m_i\}(m_i-m_{\emptyset i})+\varepsilon$$

$$=g_u{}^\emptyset+\Sigma[Z_{iu}{}^\emptyset\beta_i{}^\emptyset]+\varepsilon$$

$$g_u{}^\emptyset=g(x_u,m_\emptyset),\ \beta_i{}^\emptyset=m_i-m_{\emptyset i},\ Z_{iu}{}^\emptyset=\partial g(x_u,m_i)/\partial m_i \qquad (4\text{-}4\text{-}6)$$

Then, it was linearized of $\beta_i{}^0$. Equation (4-4-6) was substituted into equation (4-4-3) to get equation (4-4-7);

$$S(m)=\Sigma\{f_u-g_u{}^\emptyset-\Sigma(Z_{iu}{}^\emptyset\beta_i{}^\emptyset)\}^2 \qquad (4\text{-}4\text{-}7)$$

In addition, equation (4-4-4) became;

$$\partial S(m)/\partial m_r=2\Sigma\{f_u-g_u{}^\emptyset-\Sigma(Z_{iu}{}^\emptyset\beta_i{}^\emptyset)\}Z_{ru}{}^\emptyset=\emptyset \quad (1\leqq r\leqq M) \qquad (4\text{-}4\text{-}8)$$

$$\Sigma\Sigma(Z_{iu}{}^\emptyset\beta_i{}^\emptyset Z_{ru}{}^\emptyset)=\Sigma\{(f_u-g_u{}^\emptyset)Z_{ru}{}^\emptyset\} \qquad (4\text{-}4\text{-}9)$$

Then,

$$Z_\emptyset{}^T Z_\emptyset b_\emptyset=Z^T d$$

$$Z_\emptyset=\begin{matrix} Z_{11}{}^\emptyset & \cdots & Z_{M1}{}^\emptyset \\ \vdots & & \vdots \\ Z_{1N}{}^\emptyset & \cdots & Z_{MN}{}^\emptyset \end{matrix} \quad b=\begin{matrix}\beta_1{}^\emptyset \\ \vdots \\ \beta_M{}^\emptyset\end{matrix} \quad d=\begin{matrix}f_1-g_1{}^\emptyset \\ \vdots \\ f_N-g_N{}^\emptyset\end{matrix} \qquad (4\text{-}4\text{-}10)$$

Equation (4-4-10) was solved to get $\beta_i{}^0$, and it was iterated as revising

m_i as $m_i=m_{0i}+\beta_i{}^0$. In order to make a convergence better, λ was added to diagonal elements of Z_0;

$$(Z_\emptyset{}^T Z_\emptyset+\lambda E)b_\emptyset=Z^T d \qquad (4\text{-}4\text{-}11)$$

Every time of a calculation of inversion, 5 kinds of λs were given as average value of a diagonal element of M×M matrix ($Z_0{}^T Z_0$)

$$\{\Sigma\Sigma(Z_{iu}{}^\emptyset)^2\}/M \qquad (4\text{-}4\text{-}12)$$

multiplied 0.01, 0.1, 1, 10, 100, respectively. And the best of λ which minimized standard deviations was chosen.

4.4.2. Models

In the previous section, a case of analysis using 3-D finite prism-shaped body was described. Here, 2.5-D analysis applied least square means was described. As show in Fig.4-4-1, the centerlines of prisms were parallel to Y-axis, length of each prism for direction of X-axis was given enough long against surface depth. In addition, assumed observed points were set along the Y-axis.

E-W profiles were taken as observed lines from mesh data of residual gravity anomalies removed linear trend of

Bouguer gravity anomaly that shown in Fig.4-3-1 and Fig.4-3-2.

Parameters of prism-shaped body were as follows; to show position;x, y, h, to show size; a,b, to show density; ρ, and to show thickness; d. Here, two-layer modeling was carried out. The density contrast of layers was $0.4g/cm^3$ as constant. The length in X-direction was given as 8km, the width in Y-direction was given as 1km within the assumed survey line, the thickness was given as 4km, and the surface depth was given as variable. Rectangular prisms were arranged along Y-axis, and extra prisms whose width were 2km and 4km were set on beginning and end points of the assumed survey line to avoid influence of closing errors. The initial values of surface depth were given as water depth plus 1km for each prisms and constraint condition was given that the surface depth of prisms could not become smaller than its water depth on each data points.

Concretely, a parameter, z was considered to the surface depth, from equation (4-4-1) and equation (4-4-4);

$$\partial g/\partial z = H(p,q,h) - H(p,q,h+d)$$

$$H = \partial F(p,q,z)/\partial z$$

$$= pqz/((q^2+z^2)R) + pqz/((p^2+z^2)R)$$

$$-pqz(p^2+q^2+2z^2)/\{(p^2+q^2)(q^2+z^2)R\} + 1/2\tan^{-1}(pq/zR) \quad (4\text{-}4\text{-}13)$$

In addition, the determinant (4-4-10) was solved. Calculation was iterated 10 times.

Using required ${\beta_1}^0$, surface depth of a prism was corrected by Bouguer correction, it was;

$$h_{i+1} = h_i + {\beta_1}^{\emptyset}/2\pi G \quad (4\text{-}4\text{-}14)$$

4.4.3. Results

Gravity basement models along E-W profiles were analyzed by 2.5-D least square means method. There were 26 profiles taken every 10km from off Sado Island to northern area. The results were shown in Fig.4-4-2. In addition, difference between gravity basement depth and water depth was considered to sediment thickness, and it was shown in Fig.4-4-3. Furthermore, each profiles of basement structure were shown in the Chapter 5 with apparent magnetization intensities.

Basement depth of Niigata Basin was calculated about 5km. Moreover, basement depth of Akita Basin was calculated about 10km. Further basement depth of Noshiro Basin was calculated as more than 10km. As shown in Fig.4-4-4 (after Kearey and Brooks, 1984), generally if assumed density was the most suitable value, the gravity anomaly profile showed the least correlation with topography. Then, if assumed density was given as too low, the basement depth became too deep. Actually, densities of sediment layers were not unique. Though density contrast with basement layer probably became smaller with deeper, uniform density was given. However, even if assumed density of sediments in Akita Basin and Noshiro Basin were changed within the possible range, they became at least 5-7km deep. Mogami Basin that located between Akita Basin and Niigata Basin was much smaller than those basins and depth was calculated at most 2-3km. Rather basement depth of Mogami Trough which located the west of Mogami Basin was calculated at least 5-6km. However, as described before, basement depth was changed depends on assumed density, then the purpose of this analysis was to know a tendency of study area. Numerical values were regarded as standards.

The depth of Mogami trough became shallow with going to

north, and around North of Sado Island was the deepest.

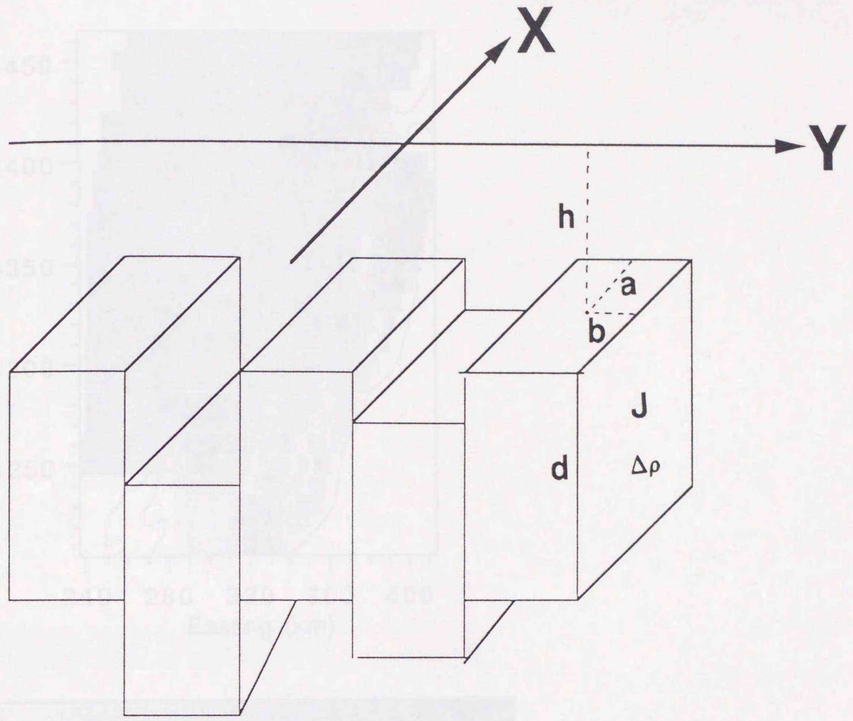

Fig.4-4-1

Prism model. Data were given along Y-axis. h:depth of surface of the prism. a:half size of the length of the prism. b:half size of the width of the prism. d:thickness of the prism. J:intensity of magnetization. $\Delta\rho$:density

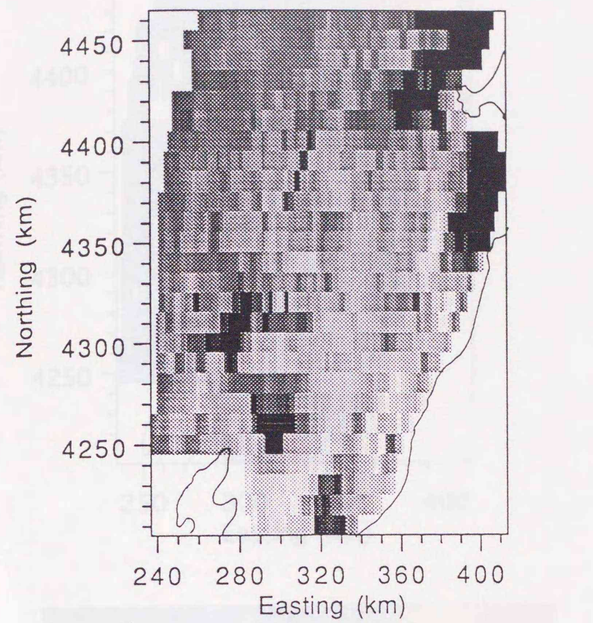

Fig.4-4-2

Results of 2-D inversion for basement depth.

Northing and Easting were UTM values origin Longitude was 141° E.

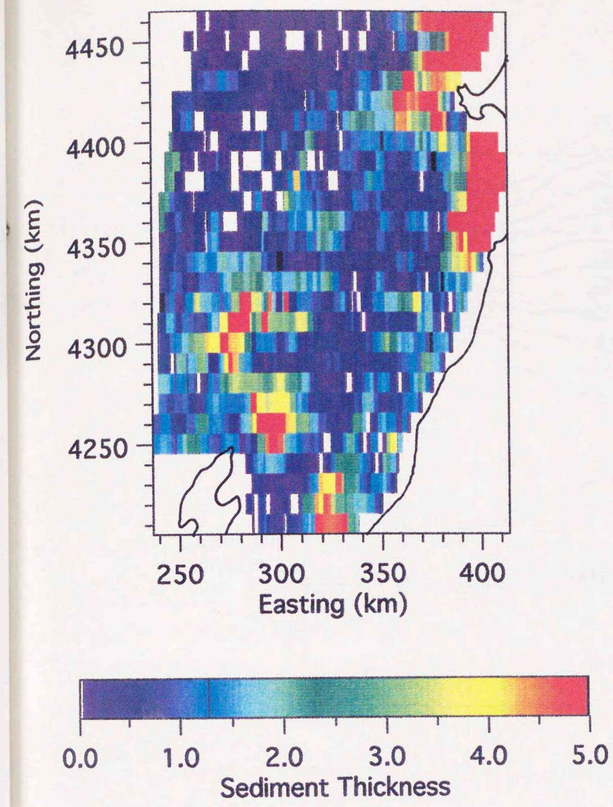

Fig.4-4-3

Sediment thickness map. Thickness is water depth minus basement depth.

Northing and Easting were UTM values origin Longitude was 141° E.

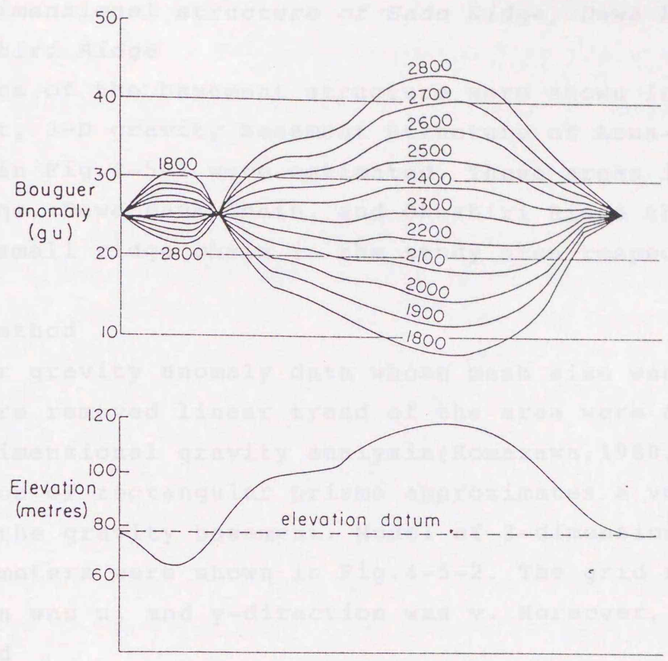

Fig.4-4-4

Nettleton's method(Nettleton,1971) of density determination over an isolated topographic feature. Gravity reductions have been performed using densities ranging from 1800 to 2800kg/m^3(1.8 to 2.8 g/cm^3) for both Bouguer and terrain corrections. The profile corresponding to a value of 2300kg/m^3 shows least correlation with topography so that this density is taken to represent the density of the feature.
after Kearey and Brooks(1984).

4.5. *3-dimensional structure of Sado Ridge, Dewa Bank Chain, and Okushiri Ridge*

Outlines of the basement structure were shown in Section 4.4. Next, 3-D gravity basement structure of Area-A, B, and C shown in Fig.4-5-1 were estimated. These areas included Sado Ridge, Dewa Bank Chain, and Okushiri Ridge that were typical small ridge chain in the study area respectively.

4.5.1. Method

Bouguer gravity anomaly data whose mesh size was 1km×1km which were removed linear trend of the area were analyzed with 3-dimensional gravity analysis(Komazawa,1980,1984). A collection of rectangular prisms approximates a volume of mass of the gravity basement. Model of 3-dimensional prism and parameters were shown in Fig.4-5-2. The grid size of x-direction was u, and y-direction was v. Moreover, grid point indicated

$$x_i = iu$$
$$y_j = jv \qquad (4\text{-}5\text{-}1)$$

Half-infinite prism indicated

$$(k-1/2)u < x \leqq (k+1/2)v$$
$$(l-1/2)u < y \leqq (l+1/2)v$$
$$-\infty < z \leqq h_{kl} \qquad (4\text{-}5\text{-}2)$$

Calculated gravity anomaly $g(z,h_{kl})$ at the point (x_i,y_j,z) were calculated as;

$$g(z,h_{kl})=G\rho\{F(+\xi,+\eta,\zeta)-F(+\xi,-\eta,\zeta)-F(-\xi,+\eta,\zeta)+F(-\xi,-\eta,\zeta)\}$$
$$|i-k| \leqq 3 \text{ and } |j-l| \leqq 3$$
$$g(z,h_{kl})=G\rho uv/\sqrt{(R^2+\zeta^2)}$$
$$|i-k|>3 \text{ or } |j-l|>3$$

Where,

$$\pm\xi = (i-k\pm 1/2)u,\quad \pm\eta=(j-l\pm 1/2)v$$

$R^2=(i-k)^2u^2+(j-l)^2v^2$

$\zeta=|z-h_{kl}|$, $F(x,y,z)=\{\{\{(zd_xd_yd_z)/(x^2+y^2+z^2)^{3/2}\}$ (4-5-3)

Surface depth of a prism, h was revised by Bouguer correction;

$h_{i+1}=h_i+(g^*-g)/2\pi G$ (4-5-4)

In order that a difference between a calculated gravity anomaly g and an observed gravity anomaly g* became small. Iteration became end when average of a difference of gravity became smaller than 1mgal. Every side was expanded as 40km in order to avoid error caused by finite area. In addition, mean depth obtained with least square means from a gradient of power spectrum was given as the initial value of basement depth. The constraint was given that basement depth could not be shallower than bathymetry.

4.5.2. Sado Ridge

First, Gravity basement structure of Area-A shown in Fig.4-5-1 was calculated. Bathymetry of Area-A was shown in Fig.4-5-3.

Okamura et al. (1995b) showed the clear seismic reflection profile along the Torimiguri Bank (Fig.4-5-4). Locations of the profile were shown in Fig.4-5-3 as T-T'.

Along the profile of Torimiguri Bank, four kinds of Bouguer gravity anomalies that were removed linear trend were shown in Fig.4-5-5. The locations of the profiles were the same as Fig.4-5-4. The Bouguer gravity anomalies were calculated using four assumed densities, i.e., 1.8g/cm^3, 2.0g/cm^3, 2.3g/cm^3, and 2.5g/cm^3. If the most suitable assumed density was used for Bouguer and terrain correction, Bouguer anomaly was scarcely correlated with the topography. Then, comparison of Bouguer gravity anomalies estimated a

difference of density of surface layer of small ridges. However, the gravity anomalies measured on the sea surface were not influenced by a local density structure and it showed average density of some range depended on water depth. In a case of Torimiguri Bank, surface density was estimated as 1.8-2.0g/cm^3. In addition, the seismic profile indicated that the basement of east side of the bank was deeper than basement of west of there.

The clear seismic reflection profile across the Yahikotai and Kamaguri Banks were also obtained by Okamura et al. (1995b; Fig.4-5-6). Location of the profile was shown in Fig.4-5-3 as Y-Y'. Similarly, Bouguer gravity anomalies of the E-W profile across from Yahikotai Bank over Kamaguri Bank. Location of the profiles was shown in Fig.4-5-3 as A-A'. They were removed linear trend were calculated using four kinds of assumed densities. These profiles were shown in Fig.4-5-7. The densities were 1.8g/cm^3, 2.0g/cm^3, 2.3g/cm^3, and 2.5g/cm^3. Surface density of Kamaguri Bank (K) was estimated as 1.8-2.0g/cm^3. In addition, that of Yahikotai Bank (Y) was 2.0-2.3g/cm^3. The seismic reflection profile along the Kamaguri and Yahikotai Banks (Fig.4-5-6) showed that basement between Yahikotai and Kamaguri Banks was deep. From the above-mentioned, Bouguer correction density of this area was assumed as 2.0g/cm^3, and obtained Bouguer gravity anomaly. Then, assumed density 2.0g/cm^3 was used for re-calculated for Bouguer anomalies.

Residual gravity anomalies that were removed linear trend from Bouguer anomalies (Fig.4-5-8) were used as observed data for 3-D analysis. Density contrast was considered 0.4g/cm^3. The gravity basement was shown in Fig.4-5-9. Color

map indicated resultant gravity basement depth and it was overlaid with bathymetric contour. The gravity basement became a quite different pattern from the bathymetry. For example, Mogami Trough trended in NNE direction both sides of Torimiguri Bank in topographic, but basement obtained from gravity anomalies were bent from NNE for NE in south side of Torimiguri Bank. Moreover, the shallow zones of gravity basement trend in NE direction. It was continued from the north of Hyotanguri Bank to Hirase Bank and north side of Torimiguri Bank. Another shallow zone of gravity basement trended in NNE direction along Awashima uplift zone.

Next, the profile of gravity basement across Torimiguri Bank was shown in Fig.4-5-10. The location of profile was indicated in Fig.4-5-4 as T-T'. However, data on this profile were taken points of 1km mesh data. Then the profile became rough. Gravity basement of under the top of bank was estimated about 2.5km deep below the sea level. Then, a sediment thickness of Torimiguri Bank became about 2.3km. In addition, gravity basement of northwest side of the bank became more than 3km deep under the small topographic high.

Similarly, the E-W profile of gravity basement from Yahikotai Bank over Kamaguri Bank was shown in Fig.4-5-11. Location of the profile was shown in Fig.4-5-9 as A-A'. Here, gravity basement under east side slope of Kamaguri Bank was depression like a wedge, and thickness of sediment layer was almost 3km. On the other hand, gravity basement under the top of Yahikotai Bank was a little shallower, but average thickness of sediment layer was about 2km. Surface density of Kamaguri Bank was estimated as 1.8-2.0g/cm^3. On the other hand, surface density of Yahikotai Bank was estimated as 2.0-2.3g/cm^3. They were decided with comparison

of profiles using four assumed densities. These surface layers deposited in contemporaneous (Okamura et al., 1995b), but assumed density indicated average of bulk. Then, it was influenced by difference of basement structures. On the other point of view, if density of surface layers were significantly different, basement depth under the Kamaguri Bank was deeper than true. Moreover, basement depth under the Yahikotai Bank was shallower and correlated with topography because assumed density was given as 2.0g/cm^3 in the case.

4.5.3. Dewa Bank Chain

Dewa Bank Chain trended in almost N-S direction and it consisted of the Tobishimatai, Shinguri, and Ogamukouse Banks. The Area-B included Dewa Bank Chain and northern part of Mogami Trough (Fig.4-5-12). Figure 4-5-13 indicated one of E-W profiles across to Oga-mukouse Bank. Location of the profile was shown in Fig.4-5-12 as B-B'. Bouguer gravity anomalies using four kinds of assumed densities (1.8g/cm^3, 2.0g/cm^3, 2.3g/cm^3, and 2.5g/cm^3) were compared to find the best suitable density. These profiles were removed each linear trends. The most suitable density around Ogamukouse Bank was suggested as 2.3-2.5g/cm^3. It was similar to density of basement rather than that of sediment layer. However, density of the sediment layer of Mogami Trough was estimated as 2.0g/cm^3. Because, for the basement of Oga-mukouse Bank, in the west side of the bank should be deeper than east side of the bank. In this case, Okamura et al. (1996b) showed the records of seismic profiling across the Ogamukouse Bank (Fig.4-5-14). It showed the basement of Ogamukouse Bank was very shallow. Then, the assumed density

was estimated as 2.0g/cm^3 to re-calculate Bouguer gravity anomaly. The residual gravity anomalies were calculated with removing linear trend from re-calculated Bouguer gravity anomalies (Fig.4-5-15). 3-D analysis was carried that density contrast of sediment and basement layers was given as 0.4g/cm^3.

A result of 3-D analysis of Area-B was shown in Fig.4-5-16. The map indicated that gravity basement correlated with bathymetric pattern and basement of Shinguri and Ogamukouse Banks were shallow. The E-W profile of gravity basement across Ogamukouse Bank was shown in Fig.4-5-17. Location of the profile was shown in Fig.4-5-16 as B-B'. The basement depth under the Ogamukouse Bank was estimated about 1.5km below the sea level. It was deeper than the seismic profiling (Fig.4-5-14). If the assumed density was smaller, basement became shallower, but the west of the bank, i.e., Mogami Trough became much deeper. Anyway, basement structure was different from banks in Area-A (e.g., Kamaguri and Yahikotai Banks of Sado Ridge).

4.5.4. Okushiri Ridge

Area-C was the surroundings of Okushiri Ridge and Nishi-Tsugaru Basin (Fig.4-5-18). The E-W profile of four kinds of Bouguer gravity anomalies is shown in Fig.4-5-19. Location of the profile was shown in Fig.4-5-18 as A-A'. The profile was across to Okushiri Ridge and Nishi-Tsugaru Basin. Four kinds of corrected densities were 2.0g/cm^3, 2.3g/cm^3, 2.5g/cm^3, and 2.7g/cm^3. They were removed linear trends. In comparison with these profiles, surface density of Okushiri Ridge was estimated as 2.3-2.5g/cm^3. In addition, it was similar to the basement density around Dewa Bank Chain and

Sado Ridge. If surface density was given as 2.0g/cm^3, gravity basement of Okushiri Ridge became almost as shallow as surface and there were no sediment layers. Gravity anomalies of Nishi-Tsugaru Basin were fluctuated due to correction densities. It was larger than that of Ajigasawa Basin. Further more, the east edge of the Nishi-Tsugaru Basin showed less than 2.5g/cm^3. Then, assumed density was given as 2.3g/cm^3 for Bouguer and terrain collections. Residual Bouguer gravity anomalies were calculated with removing linear trend. The map of residual Bouguer anomalies with bathymetric contour was shown in Fig.4-5-20.

In 3-D analysis, the residual anomalies were considered to observed gravity data, and the density contrast of sediment and basement layers was given as 0.4g/cm^3.

Gravity basement depth was shown in Fig.4-5-21. In addition, the southeast of this map was filled with interpolated data. Because terminate errors became small. A profile of gravity basement was shown in Fig.4-5-22. Location of the profile was shown in Fig.4-5-21 as A-A'. The gravity basement profile under Okushiri Ridge became almost flat. In this area, the surface density was assumed as 2.3g/cm^3, and the basement density was 2.7g/cm^3. Therefore, density of basement in this area was corresponding to granite rocks.

Gravity anomalies showed that Nishi-Tsugaru Basin and Ajigasawa Basin were clearly separated. The gravity basement of Nishi-Tsugaru Basin was 4-5km deep below sea surface, and Ajigasawa Basin was 6-7km deep below sea surface. The basement depth of Nishi-Tsugaru basin was influenced sensitively by variation of surface density more than Ajigasawa Basin. It showed that Ajigasawa Basin was much

deeper than Nishi-Tsugaru Basin, too.

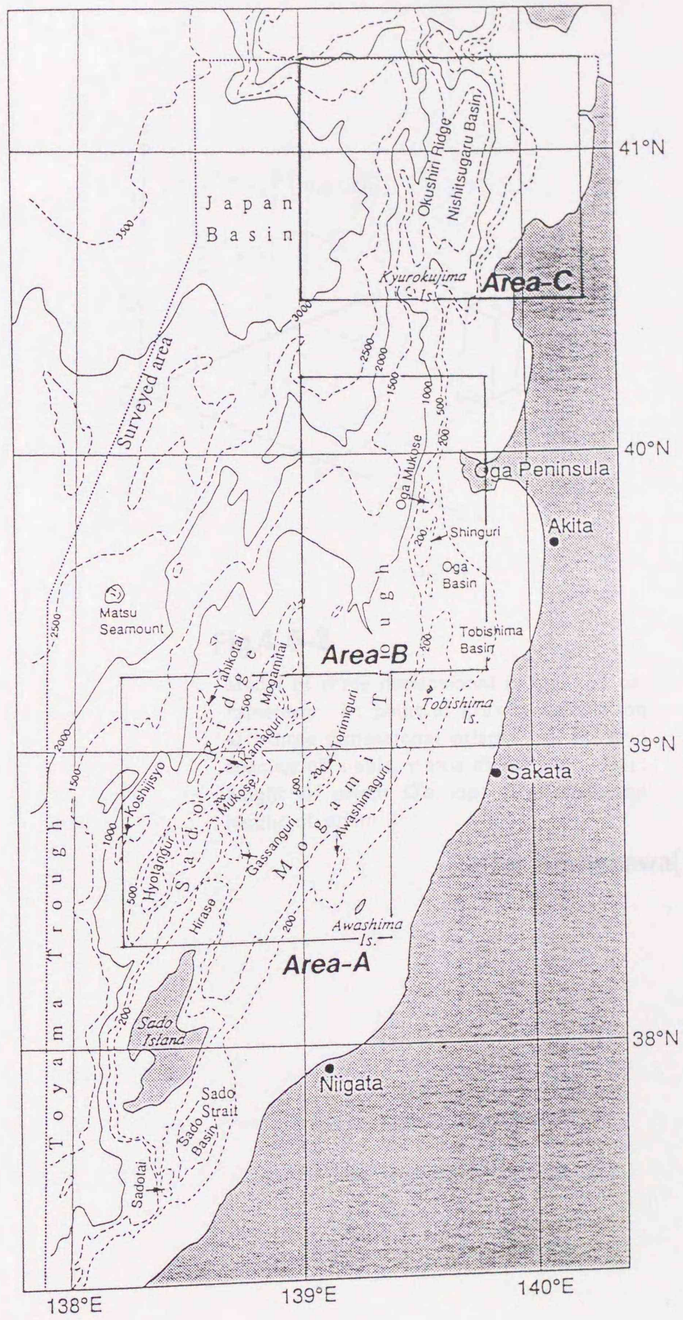

Fig.4-5-1

Index map of analyzed area-A,B, and C.

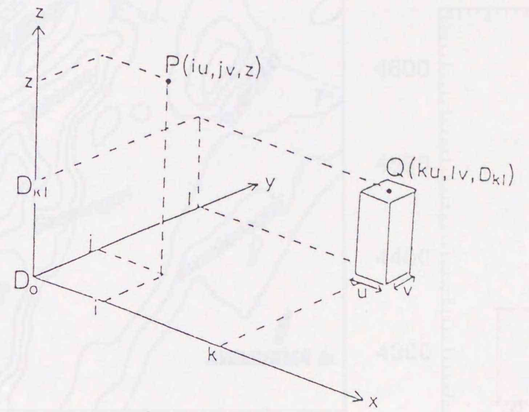

Fig.4-5-2

Model of three dimensional prism and parameters. P: point of gravity calculation Q: three dimensional prism u, v: grid spacing of x-axis, y-axis directions D_{kl}: height of prism Q's top D_o: reducing height of prism

after Komazawa(1984)

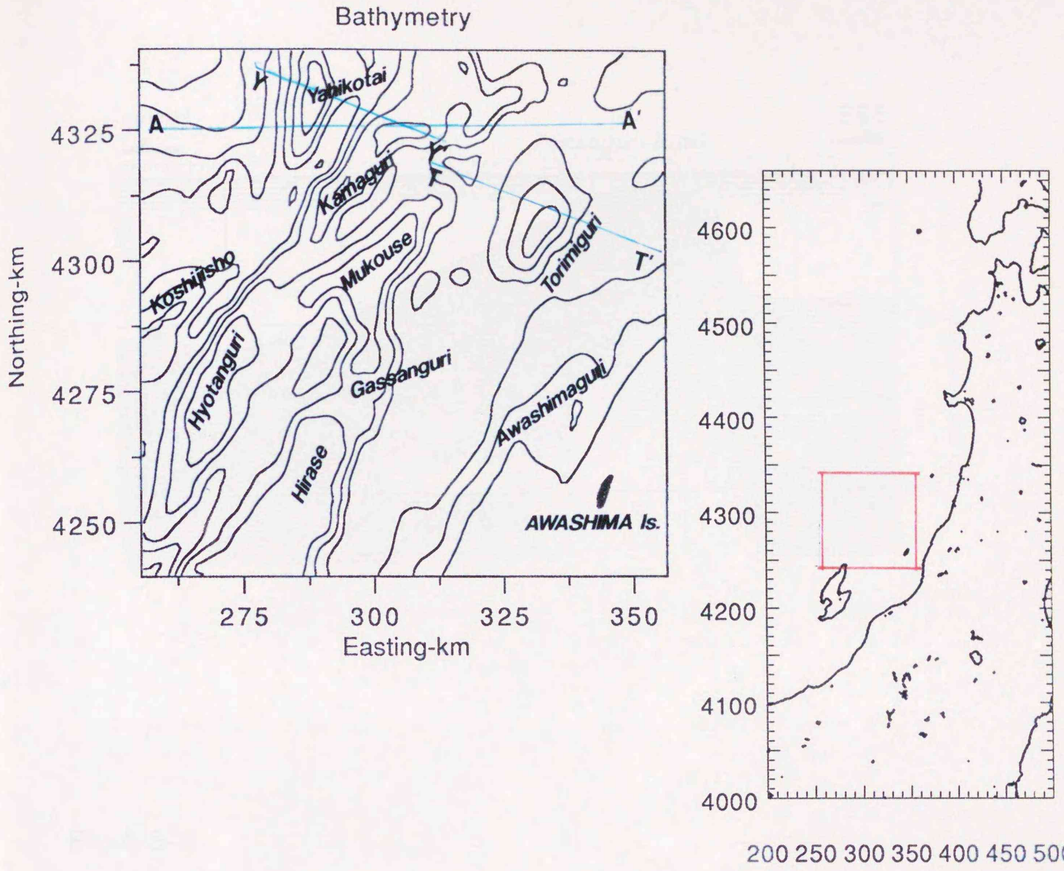

Fig.4-5-3

Bathymetry of Area-A. Line T-T' indicates the location of profiles shown in Fig.4-5-3 and Fig.4-5-4. Line Y-Y' indicates the location of a profile shown in Fig.4-5-5. Line A-A' indicates the location of profiles shown in Fig.4-5-6.

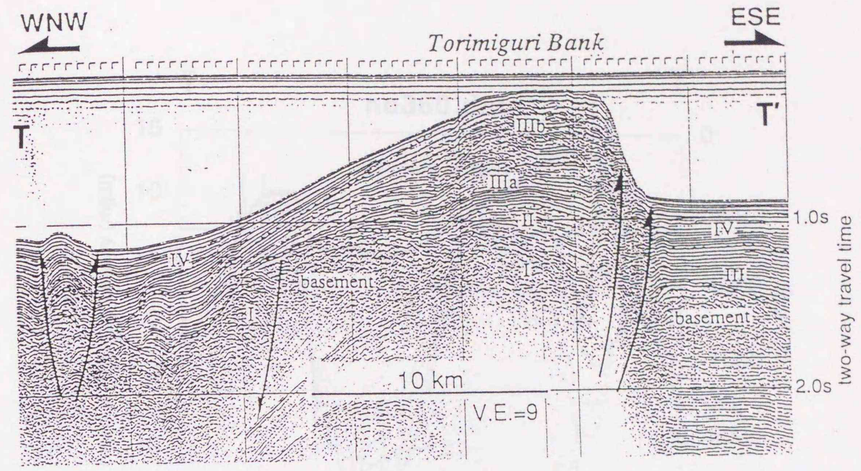

Fig.4-5-4

Seismic profile of the Torimiguri Bank showing typical basin inversion.

See Fig.4-5-3 for the location.

after Okamura et al(1995b).

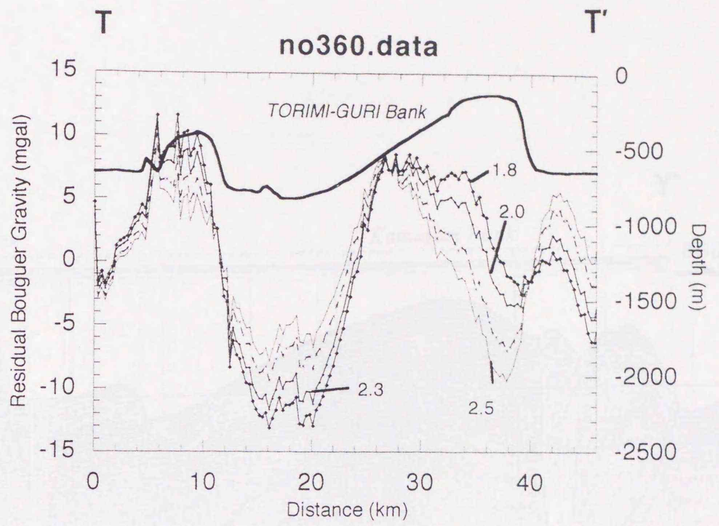

Fig.4-5-5

Relationship between assumed density and Bouguer anomalies removed the linear trend. It shows ESE-WNW profile over Torimiguri Bank. Location of the profile was shown in Fig.4-5-3 as T-T'. Gravity reductions have been performed using densities, 1.8g/cm^3, 2.0g/cm^3, 2.3g/cm^3, and 2.5g/cm^3 for Bouguer and terrain corrections.

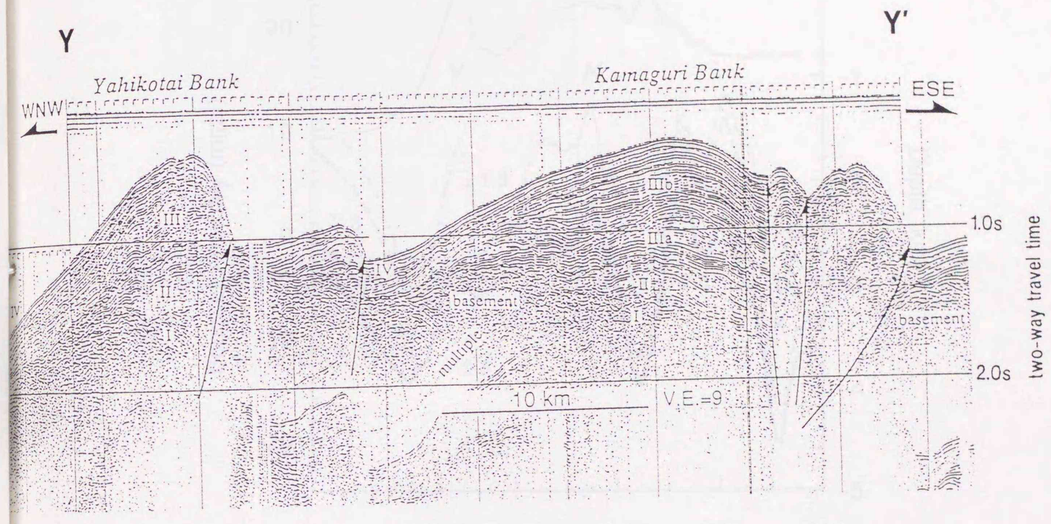

Fig.4-5-6

Seismic profile of the Kamaguri and the Yahikotai Banks. The forelimb of the Kamaguri Bank consists of two anticlines bounded by reverse faults. See Fig.4-5-3 for the location.
after Okamura et al(1995b).

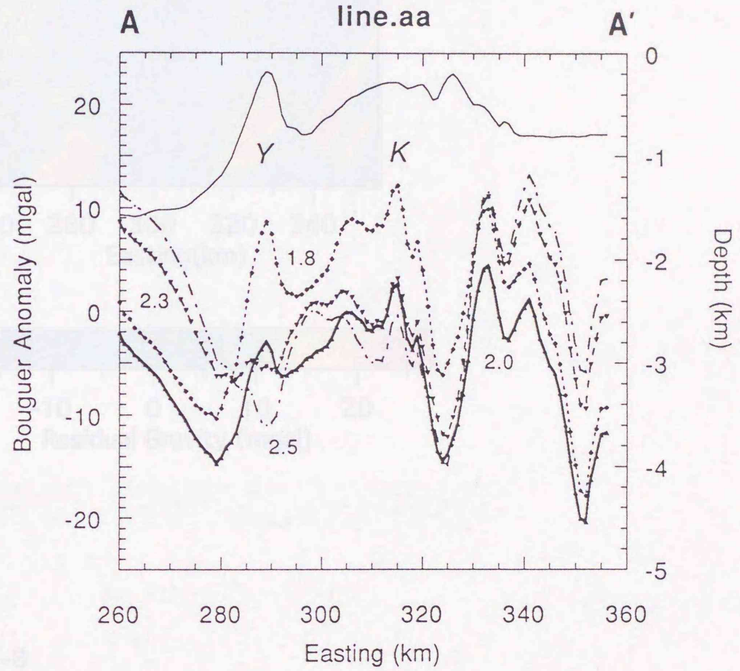

Fig.4-5-7

Relationship between assumed density and Bouguer anomalies removed the regional field. It shows E-W profile over Yahikotai and Kamaguri Bank as an isolated topographic feature. Gravity reductions have been performed using densities, 1.8g/cm^3, 2.0g/cm^3, 2.3g/cm^3, and 2.5g/cm^3 for Bouguer and terrain corrections. Easting was UTM values origin Longitude was 141° E.

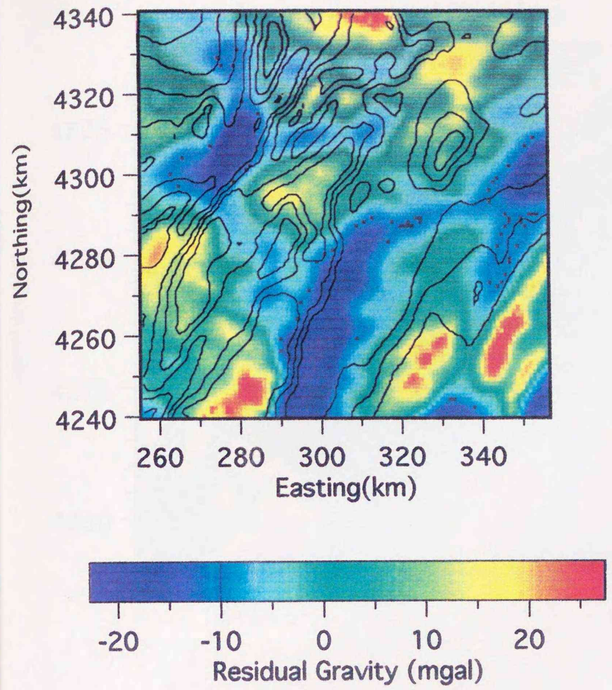

Fig.4-5-8

Residual Gravity anomalies around Sado Ridge of north of the Sado Island. Data were subtracted linear trend from Bouguer gravity anomalies which assumed density was 2.0g/cm^3. The map was overlaid with bathymetric contour. Its interval was 200 m. Northing and Easting were UTM values origin Longitude was 141° E.

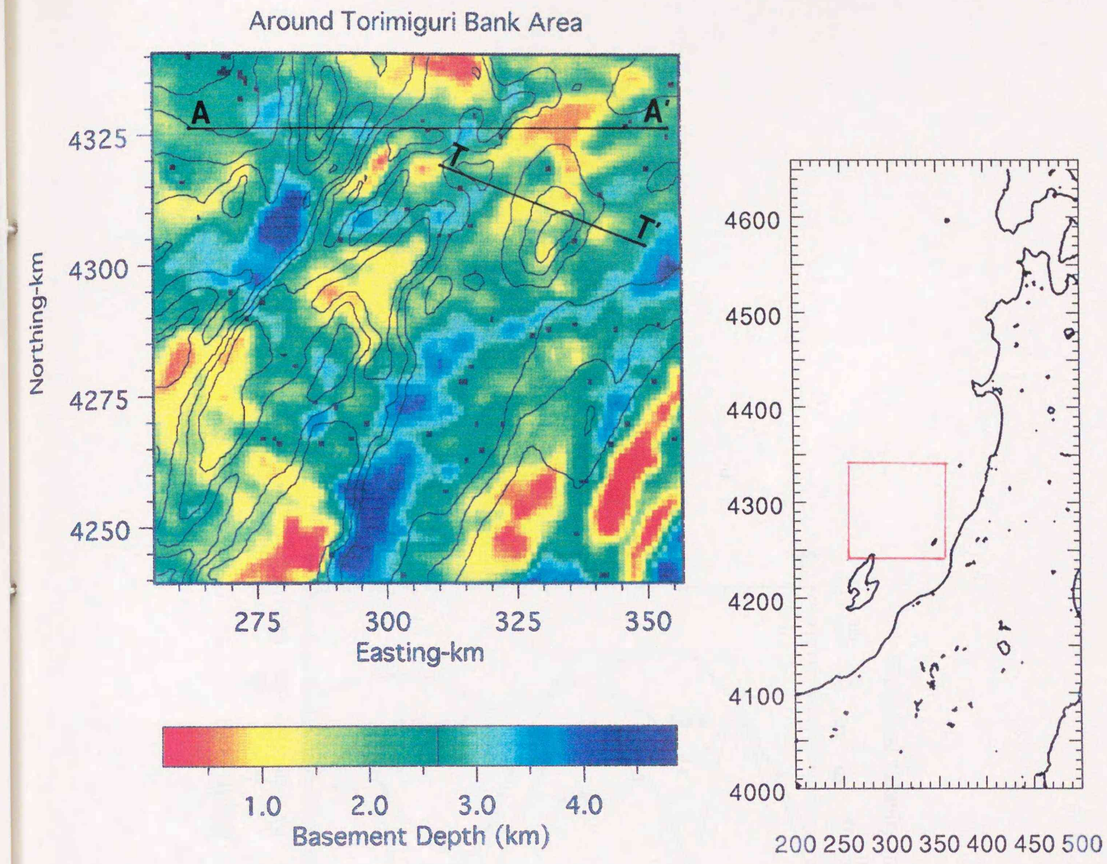

Fig.4-5-9

Gravity basement depth of Area-A. Basement depth were shown in color map. The map was overlaid with bathymetric contour which interval was 200 m. Density of sediment was assumed as 2.0 g/cm^3, and basement was assumed as 2.4 g/cm^3. Northing and Easting were UTM values origin Longitude was 141° E.

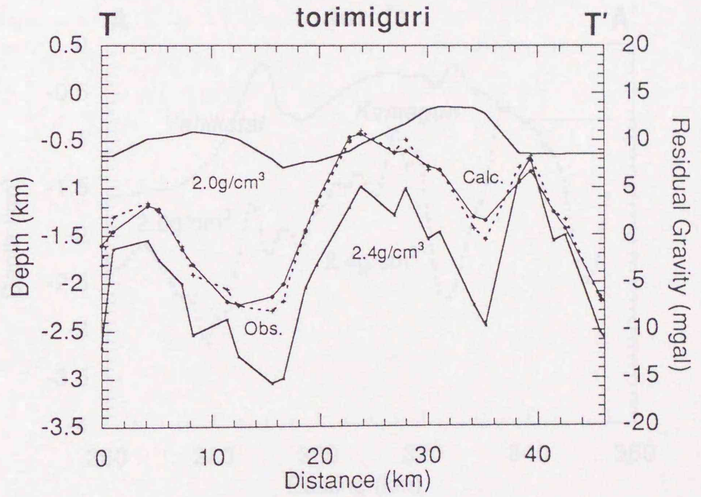

Fig.4-5-10

A profile of gravity basement model of the Torimiguri Bank. Location is shown in Fig.4-5-9 as T-T'. Obs. means the profile of residual gravity anomalies, and Calc. means the profile of calculated anomalies due to the basement depth model.

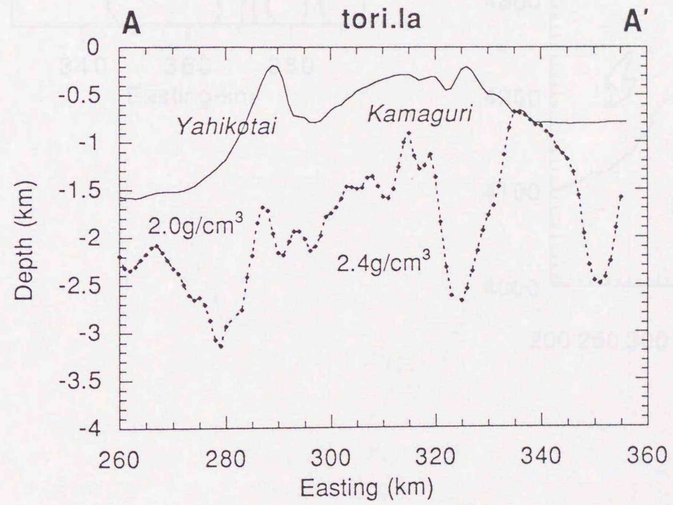

Fig.4-5-11

A E-W profile of gravity basement model of the Kamaguri and Yahikotai Banks. Location is shown in Fig.4-5-9 as A-A'. Solid line indicates bathymetry. Broken line indicates gravity basement depth. Easting was UTM values origin Longitude was 141° E.

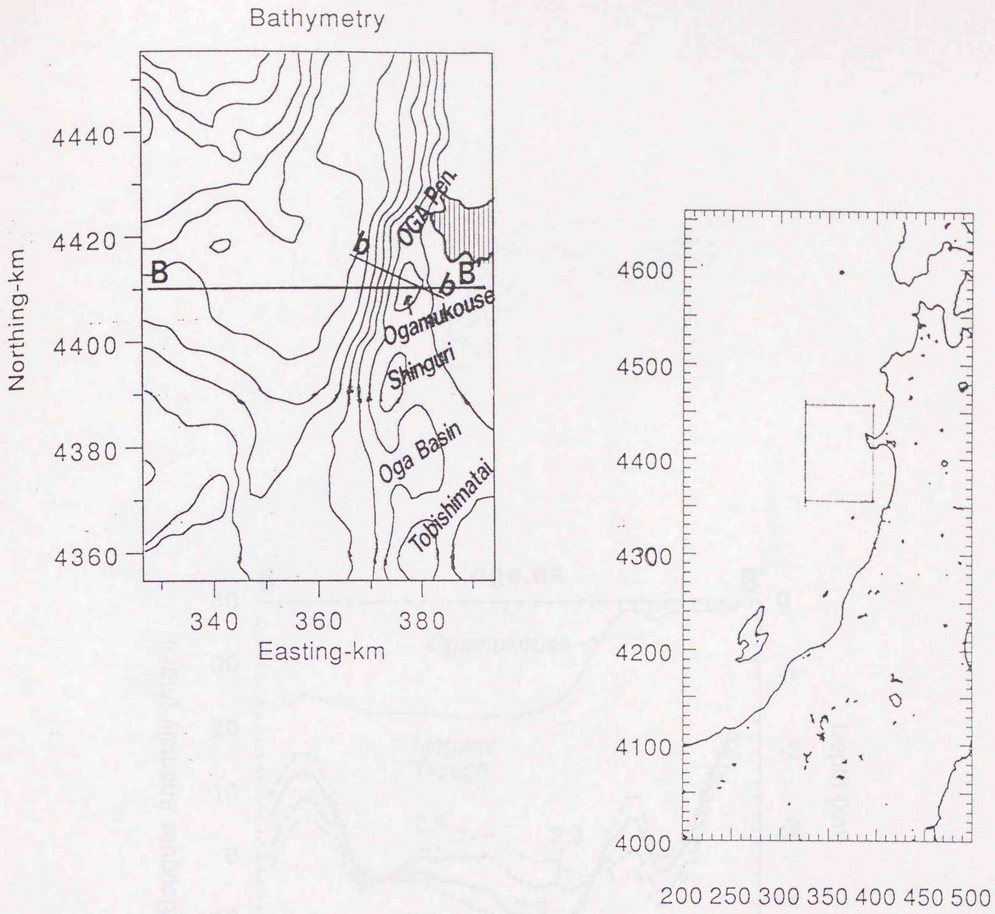

Fig.4-5-12

Bathymetry of Area-B. Line B-B' indicates the location of profiles shown in Fig.4-5-13. Line b-b' indicates the location of a profile shown in Fig.4-5-14. Contour interval was 200 m. Northing and Easting were UTM values origin Longitude was 141° E.

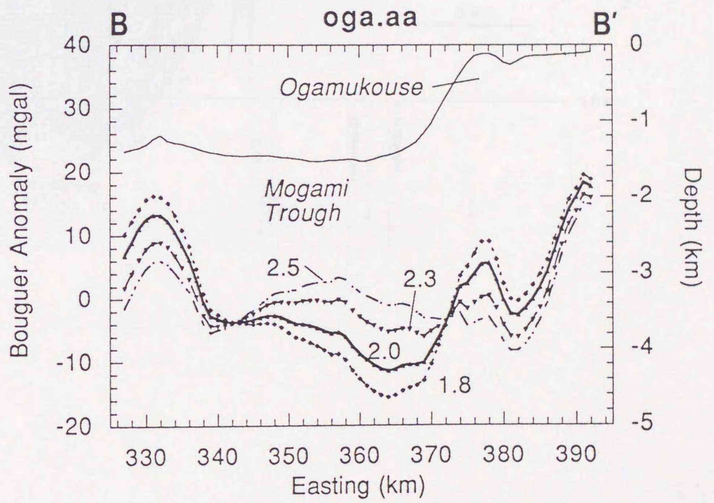

Fig.4-5-13

Relationship between assumed density and Bouguer anomalies removed the regional field. It shows E-W profile over Ogamukouse Bank and Mogami Trough. Gravity reductions have been performed using densities, 1.8g/cm^3, 2.0g/cm^3, 2.3g/cm^3, and 2.5g/cm^3 for both Bouguer and terrain corrections. Easting was UTM values origin Longitude was 141° E.

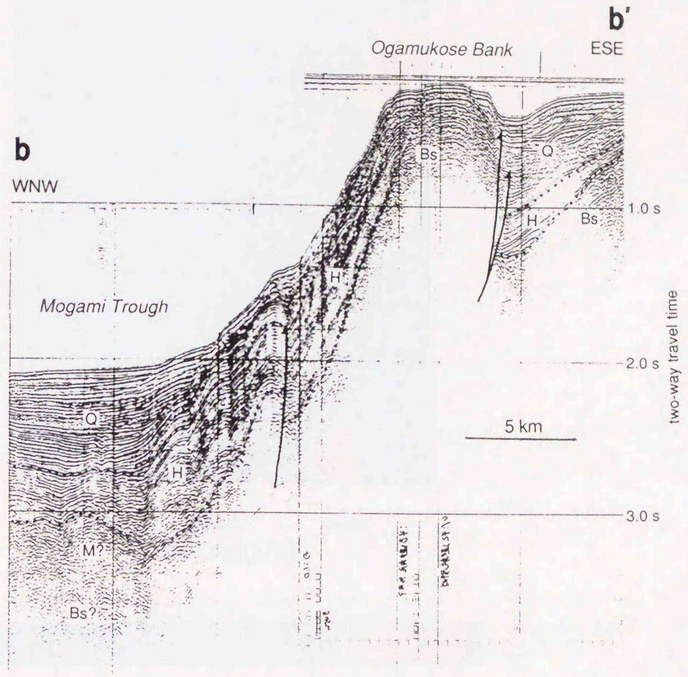

Fig.4-5-14

Seismic profile of the Ogamukose Bank. The Ogamukose Bank is an asymmetric anticline similar to the Shinguri Bank, and small-scale anticlines are developed on its western limb.

after Okamura et al.(1996).

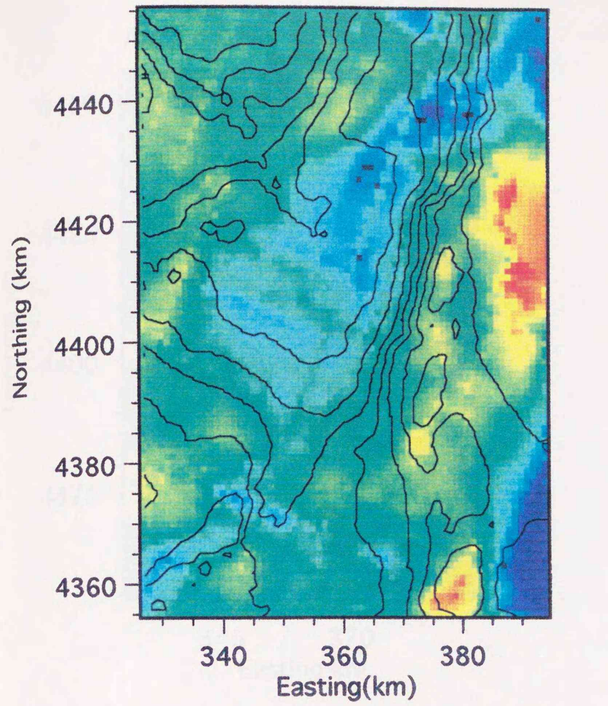

Fig.4-5-15

Residual Gravity anomalies around Dewa Bank Chain, the west of Oga Peninsula. Data were subtracted linear trend from Bouguer gravity anomalies which assumed density was 2.0g/cm^3. The map was overlaid with bathymetric contour. Its interval was 200 m. Northing and Easting were UTM values origin Longitude was 141° E.

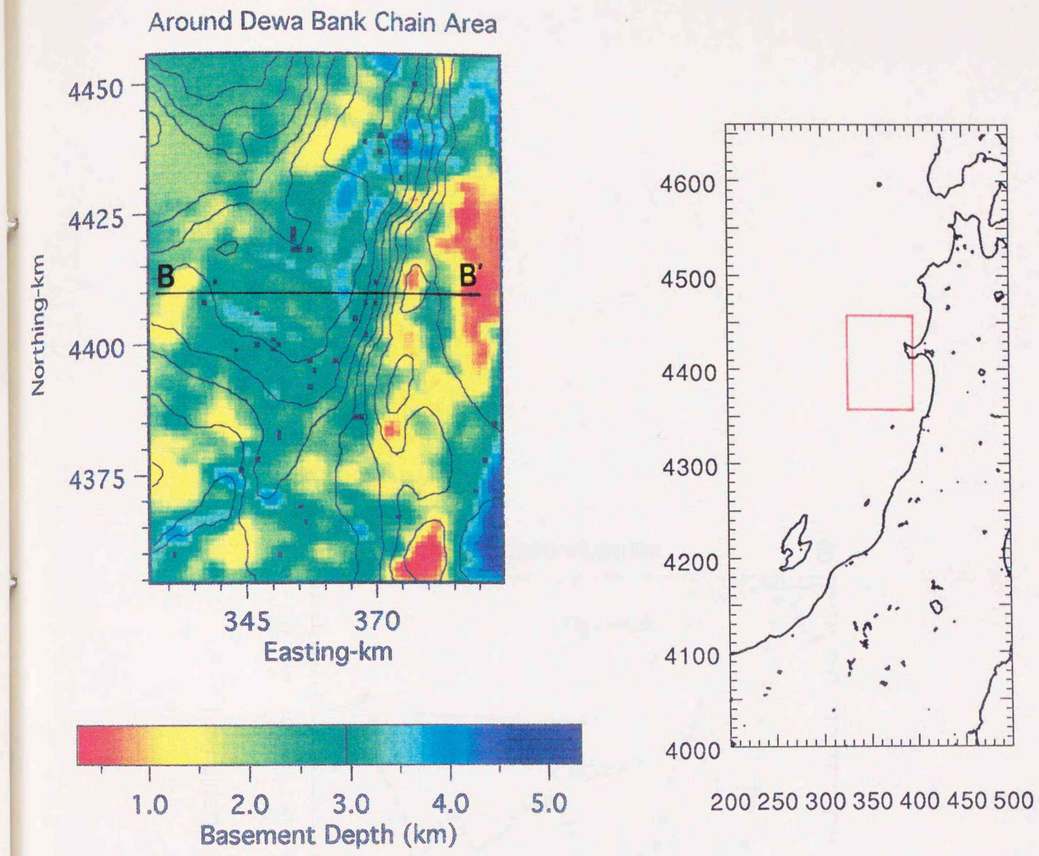

Fig.4-5-16

Gravity basement depth of Area-B. Basement depth were shown in color map. The map was overlaid with bathymetric contour which interval was 200 m. Density of sediment was assumed as 2.0 g/cm^3, and basement was assumed as 2.4 g/cm^3. Northing and Easting were UTM values origin Longitude was 141° E.

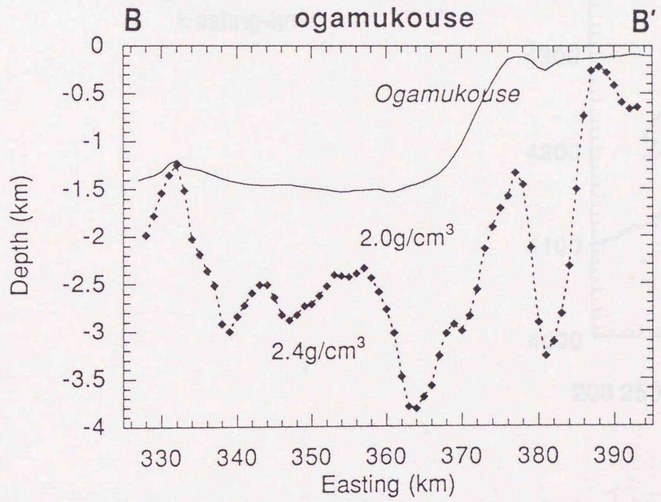

Fig.4-5-17

A E-W profile of gravity basement model over the Ogamukouse Bank and Mogami Trough. Location is shown in Fig.4-5-16 as B-B'. Solid line indicates bathymetry. Broken line indicates gravity basement depth. Easting was UTM values origin Longitude was 141° E.

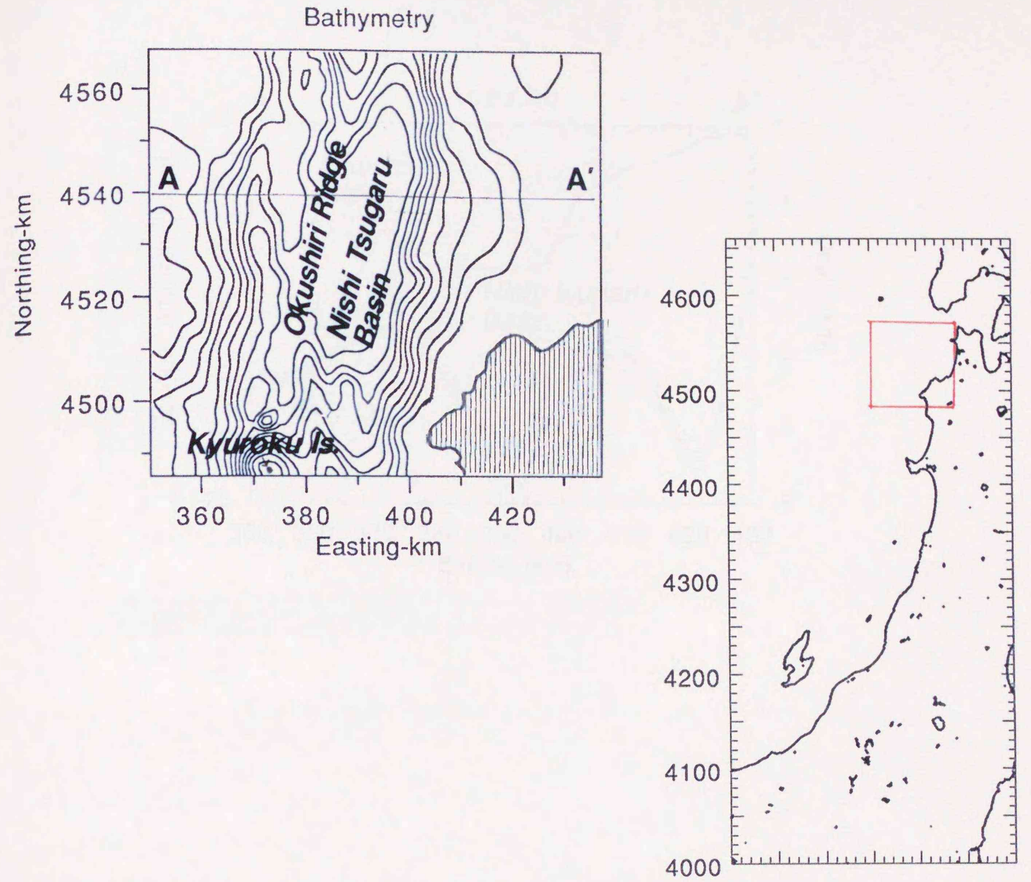

Fig.4-5-18

Bathymetry of Area-C. Line A-A' indicates the location of profiles shown in Fig.4-5-19. Contour interval was 200 m. Northing and Easting were UTM values origin Longitude was 141° E.

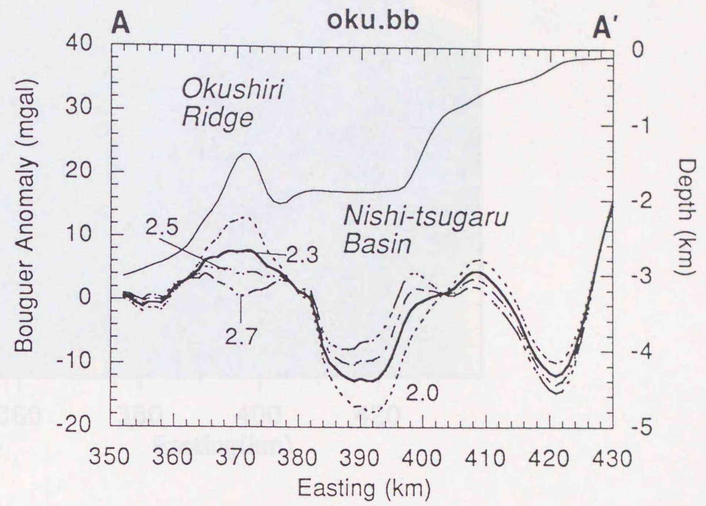

Fig.4-5-19

Relationship between assumed density and Bouguer anomalies removed the regional field. It shows E-W profile over Okushiri Ridge and Nishi-Tsugaru Basin. Gravity reductions have been performed using densities, 2.0g/cm^3, 2.3g/cm^3, 2.5g/cm^3, and 2.7g/cm^3 for both Bouguer and terrain corrections. Easting was UTM values origin Longitude was 141° E.

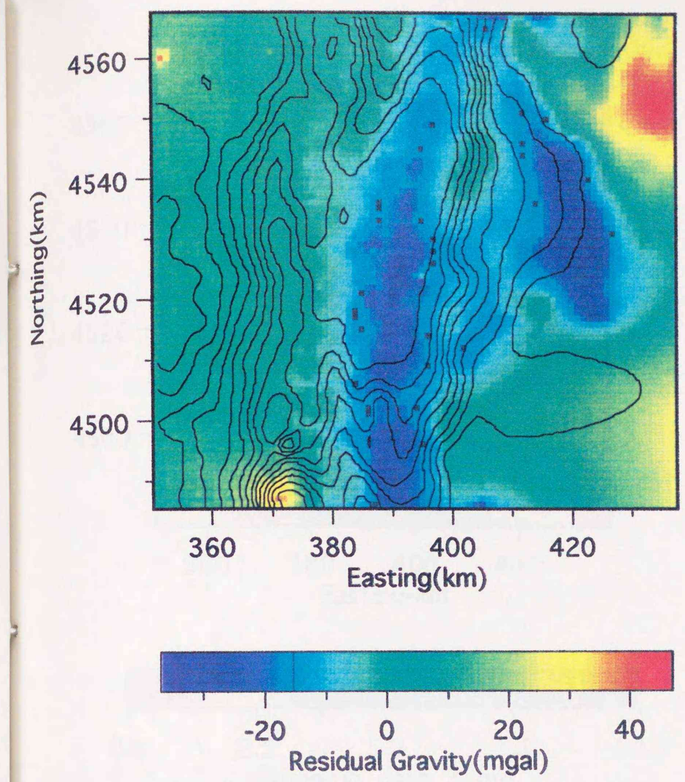

Fig.4-5-20

Residual Gravity anomalies around Okushiri Ridge and Nishi-Tsugaru Basin, the west of Tsugaru Peninsula. Data were subtracted linear trend from Bouguer gravity anomalies which assumed density was 2.3g/cm^3. The map was overlaid with bathymetric contour. Its interval was 200 m. Northing and Easting were UTM values origin Longitude was 141° E.

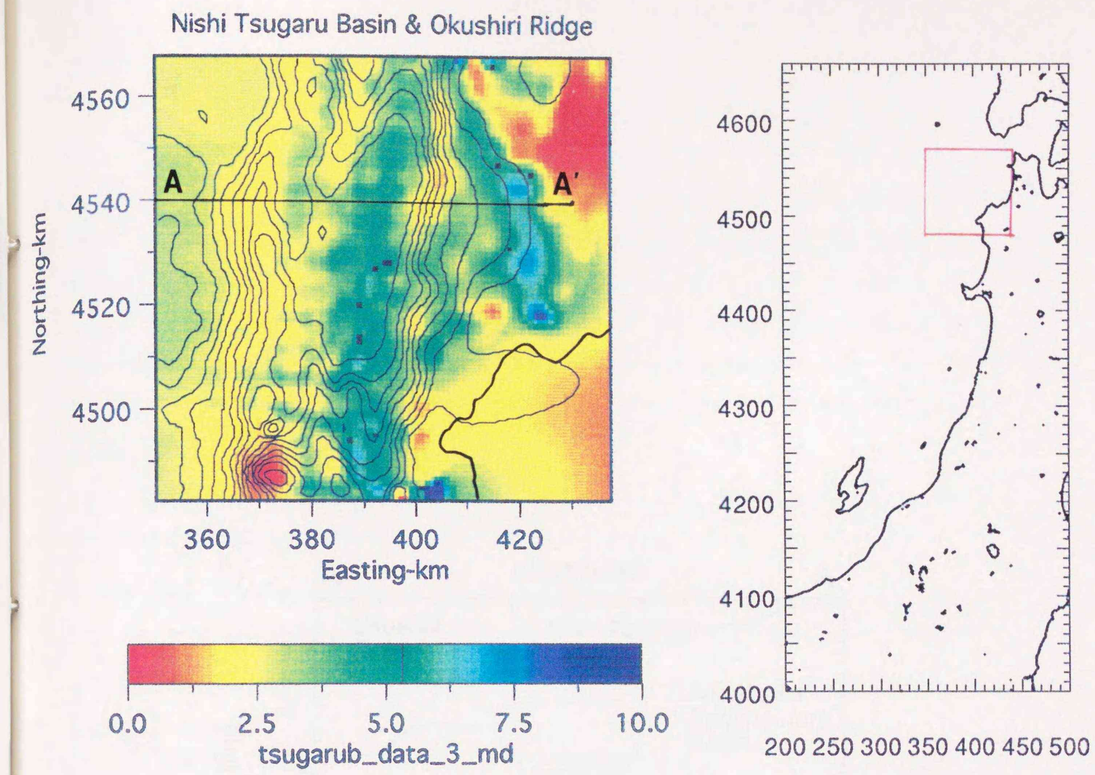

Fig.4-5-21

Gravity basement depth of Area-C. Basement depth were shown in color map. The map was overlaid with bathymetric contour which interval was 200 m. Density of sediment was assumed as 2.3 g/cm^3, and basement was assumed as 2.7 g/cm^3. Northing and Easting were UTM values origin Longitude was 141° E.

tsugarub_data_3_md vs. (row, col)

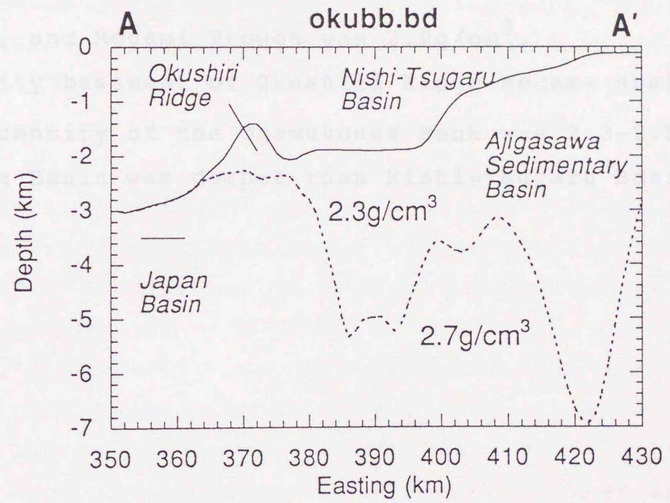

Fig.4-5-22

A E-W profile of gravity basement model over the Okushiri Ridge and Nishi-Tsugaru Basin. Location is shown in Fig.4-5-21 as A-A'. Solid line indicates bathymetry. Broken line indicates gravity basement depth. Easting was UTM values origin Longitude was 141° E.

4.6. *Conclusion*

The conclusions of gravity analysis are as follows:

(1) Bouguer gravity anomalies were calculated. Its assumed density was 2.3g/cm^3 for all of study area. Basement depth due to Bouguer gravity anomalies showed different pattern from bathymetry.

(2) The feature of gravity basement of Sado Ridge was that basement under the topographic high became deeper. In addition, assumed density of this area was estimated as 2.0g/cm^3.

(3) Gravity basement of Dewa Bank Chain became shallow. In addition, assumed density of the Ogamukouse Bank was 2.0-2.3g/cm^3, and Mogami Trough was 2.0g/cm^3.

(4) Gravity basement of Okushiri Ridge became shallow. Assumed density of the Ogamukouse Bank was 2.3-2.5g/cm^3. Ajigasawa Basin was deeper than Nishi-Tsugaru Basin.

5. Geomagnetic study

5.1. *Data processing for magnetic anomaly maps*

5.1.1. Cross-point magnetic control

The magnetic anomaly data suffered from diurnal variation, differences of each years of IGRF values, positioning error, ship's magnetization, and so on. If there are no errors, values on each line at a cross point are the same. However, data in cruise files made unnatural patterns in the contour map. Because crossover errors were caused by positioning errors, measuring errors, diurnal variation, and so on. When world wide marine magnetic anomaly data were compiled, each data files need to add offset values after calculation of DGRF residual (e.g. Verhof et al., 1991) to draw smooth contour lines. Because data were obtained by different measurement and positioning systems.

On the other hand, our data were measured with similar systems in comparatively narrow area and during only 4 years. However, the positioning system was changed in 1990 from LORAN-C to single-GPS. Moreover, the GPS system didn't work as good as usual in 1991.

In this study, only our IGRF residual data were used. They were edited on board during GH89-2, GH89-4, GH90, GH91, and GH92 cruises by R/V Hakurei-maru.

First, data in each cruise files were checked and error data were removed. The magnetic anomaly which amplitude was larger than 2,000nT or gradient was larger than 200nT/300m were regarded as error data. In addition, data were smoothed along each track lines with weighted running mean filter every seven data. However, contour maps using these data indicated unnatural patterns.

The cross-point control is quite useful for data correction. It is not perfect, but practical. Example maps

of data correction were shown in Fig.5-1-1. Some unnatural patterns were found in the uncorrected magnetic anomaly map. After the cross point control, such patterns were corrected.

Usually, diurnal variations need to be corrected. However, our data were observed during nighttime. The amplitude of diurnal variation in midnight was about 10-20nT, and accuracy of measurement was around 20nT, experimentally. Furthermore, if there were few measurement and positioning errors, crossover errors were mainly made by diurnal variations. For example, Nakatsuka (1994) showed that offset values of cross-point control were corresponding to diurnal variation (Fig.5-1-2). However, their aeromagnetic data were different from our sea borne data, i.e., observed positions were decided exactly by GPS and each survey lines continued several minutes. In comparison with it, crossover errors in our sea borne data were much larger than diurnal variations in nighttime. In Fig.5-1-3, a horizontal axis indicated time differences between cruises, and a vertical axis indicated crossover errors. These crossover errors looked not to correlate with observed time differences.

Actually, crossover errors were caused by complex reasons. Then it was not realistic way to correct one by one of several decades of thousands measurement points by every reasons (Morijiri and Yamazaki, 1994b). Here, the cross-point control was carried out as follow as Nakatsuka (1989). It gave offset values to each survey lines to distribute each crossover points. It was very useful to correct crossover error because offset values were calculated by least square means to minimize total of crossover errors and offset values.

The procedure was as follows;

(1) A magnetic anomaly changed more than ±200nT/minute (1 minute = about 300m) on the same line was considered as

noise and deleted. This threshold level depended on its water depth and gradient of magnetic anomalies.

(2) Weighted running mean filter (see Section 4.1) was worked with each seven data along time axis of each survey lines.

(3) Survey lines were divided into two groups by their directions. One was NNE-SSW, and another was ESE-WNW.

(4) Line numbers were attached each survey lines. Every survey lines had no time gap, i.e., data before time gap and after the gap were considered on different survey lines.

(5) Survey lines that were shorter than 5 minutes were deleted.

(6) Data were extracted of a map area.

(7) Locations of cross-points of NNE lines and ESE lines were investigated. In this case, cross-points were defined that there were inside a range of a radius 400m.

(8) Cross-points of each survey lines were listed.

(9) Survey lines that had only one cross-point were deleted.

(10) Offset values of each line were calculated to minimize square of crossover errors. At that time, totals of offset values were minimized, too.

(11) Offset values were added to observed data. In addition, adjusted magnetic anomalies were considered random data, and interpolated to mesh data with weighted hyperbolic surface fitting depending on distances.

Step (1)-(9) was foregoing process of cross-point control. In the case of aeromagnetic surveys, surveys were usually designed taking into the consideration of cross-point control. Then, these steps were contrived for our sea borne data. Because, our survey were not considered of cross-point control and restricted by insufficient ship time. Then, our survey lines arrangement was complicated.

In this method, offset values were calculated by least

square means. Then, crossover errors at some points were left when error values were large and survey lines arrangement was too complicated.

The study area was divided into three parts and processed respectively, they were off Akita (39° N-40° N), north of Sado Island(38° N-39° N), and northern part of Mogami Trough(40° N-41° 15'N). Data of each part were processed independently, then connection of each map was not considered. There were some cases of numerical offsets, though patterns were continuous. Some crossover errors were left because least square means was not perfect. Then it had to be considered including errors in magnetic anomalies when data were analyzed.

Histograms of crossover errors before and after cross-points control of Akita area(39° N-40° N) were shown in Fig.5-1-4. Corrected magnetic anomalies were shown in Fig.5-1-5.

Magnetic anomaly data in north of Sado Island area(38° N-39° N) were also processed in the similar way to off Akita area. A histogram of crossover errors of before and after cross-points control was shown in Fig.5-1-6, and a corrected magnetic anomaly map was shown in Fig.5-1-7.

There were less cross-points in northern part of Mogami Trough (40° N-41° 15'N) than those of off Akita and Niigata areas, because survey lines were rougher. A histogram of crossover errors of before and after cross-points control was shown in Fig.5-1-8, and a corrected magnetic anomaly map was shown in Fig.5-1-9.

Same color range was used for these magnetic anomaly maps to compare with them. The map of north of Sado Island seemed to be flat because amplitude of magnetic anomalies was smaller than other areas.

After cross points control, data were interpolated as 500m

mesh data. The method was the same for gravity data (See Section 4.1).

5.1.2. Survey design and structural models

It is very important to obtain dense survey lines for potential field, such as gravity and magnetic data. For example, Reid (1980) showed the ratio of altitude to line spacing needed to be less than 0.5 for total force aeromagnetic surveys. Figure 5-1-10 shows the expected percentage of aliases power from an aeromagnetic survey. Here, 'h' indicates average altitude and 'Δx' indicates survey lines interval.

Applied this condition to sea borne magnetic surveys, the smallest 'h' is the average water depth. In this study, Δx is set about 3km. Therefore, we can get the structure deeper than 1.5km below sea level. To show shallower structure requires denser surveys. However, it is difficult to arrange ideal survey lines, because the ship-time was limited and actual accuracy was not satisfied. Especially, because each cruise had many observation items including more than a hundred of sediment sampling points in limited ship time. Then some extra steps were required for magnetic data processing.

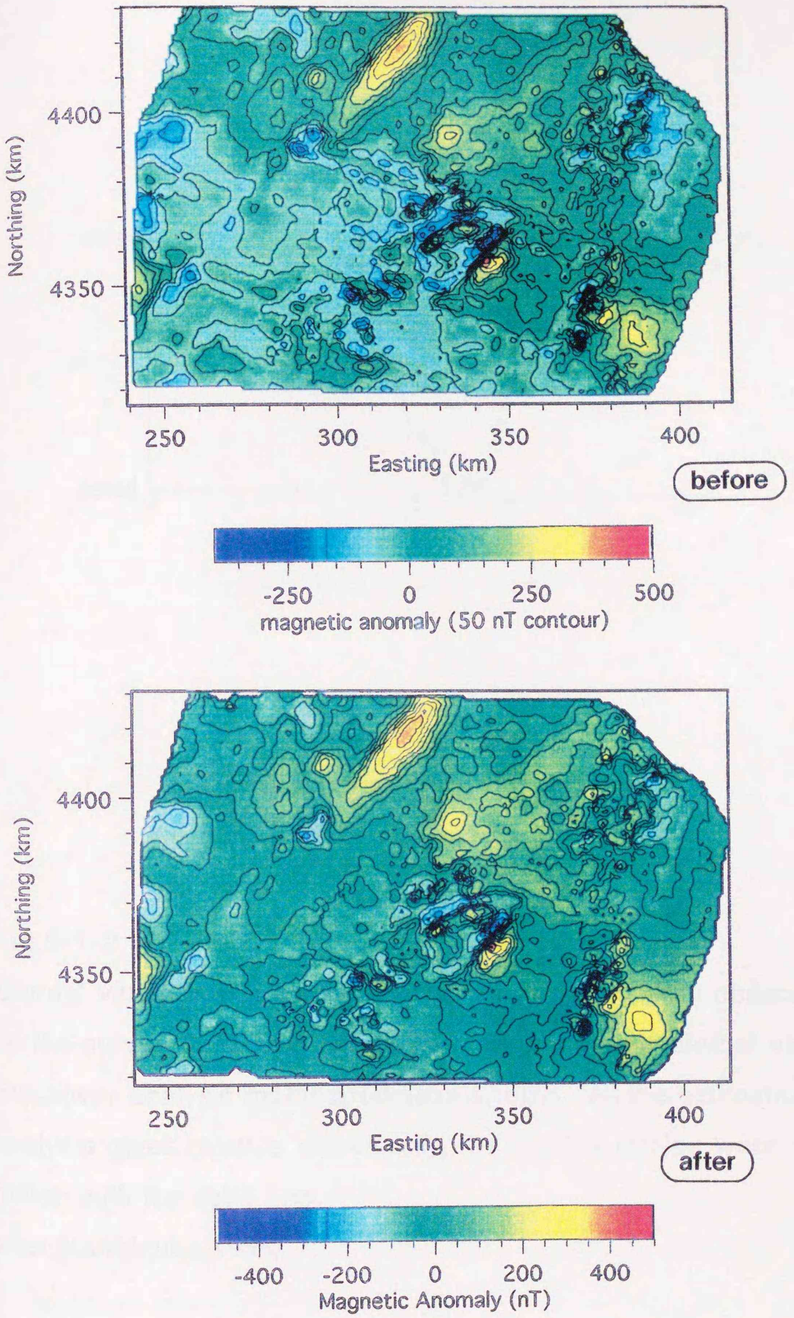

Fig.5-1-1

upper: Magnetic anomaly map using uncorrected data.

lower: Magnetic anomaly map using data after the editing and adjustment procedures.

Contour interval is 50 nT. Northing and Easting were UTM values origin Longitude was 141° E.

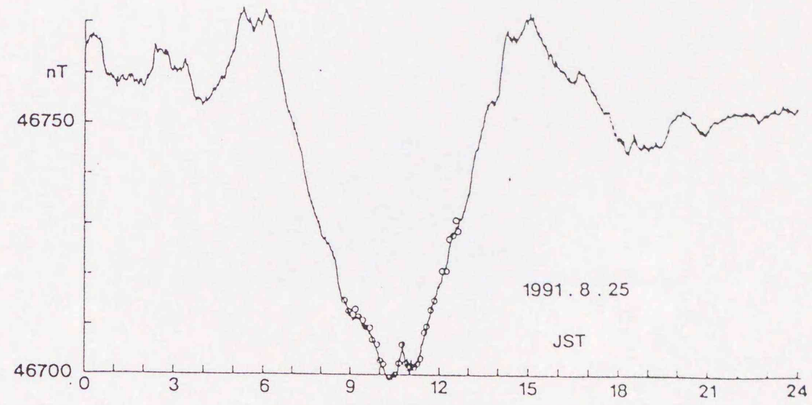

Fig.5-1-2

Diurnal variation of geomagnetic total force(solid line) observed at ASO on the survey date. The circles indicate estimated diurnal variation from crossover analysis method(Nakatsuka,1989). As the estimation by this analysis gives relative values only, the level of circles were shifted to match with the solid line.

after Nakatsuka(1994).

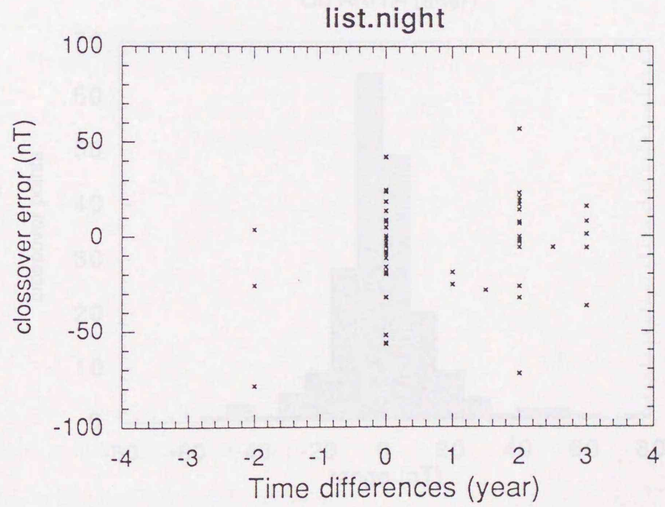

Fig.5-1-3

Time differences versus difference of magnetic anomaly at crossover points whose were observed from 22:00 to 03:00 JST. Magnetic and time differences are obtained that NNE lines minus ESE lines.

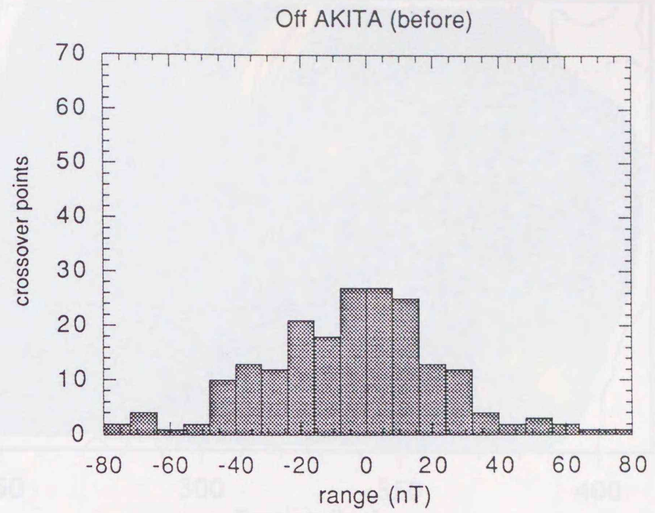

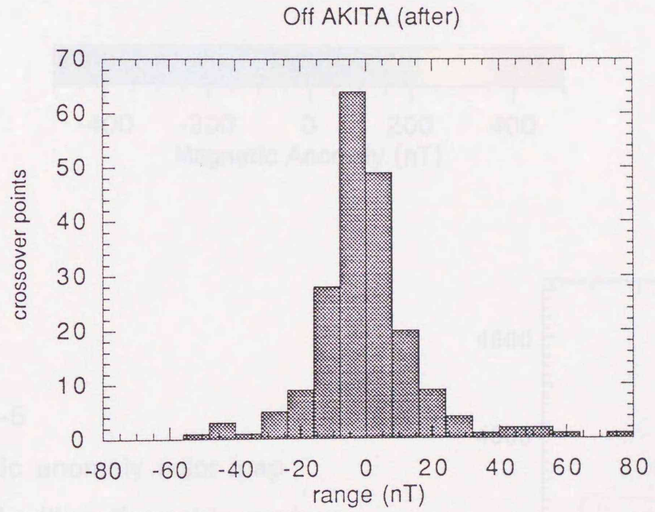

Fig.5-1-4

Histogram of the crossover errors in the off Akita area(39° N-40° N).

upper: uncorrected errors at crossover points.

lower: errors after cross-point control.

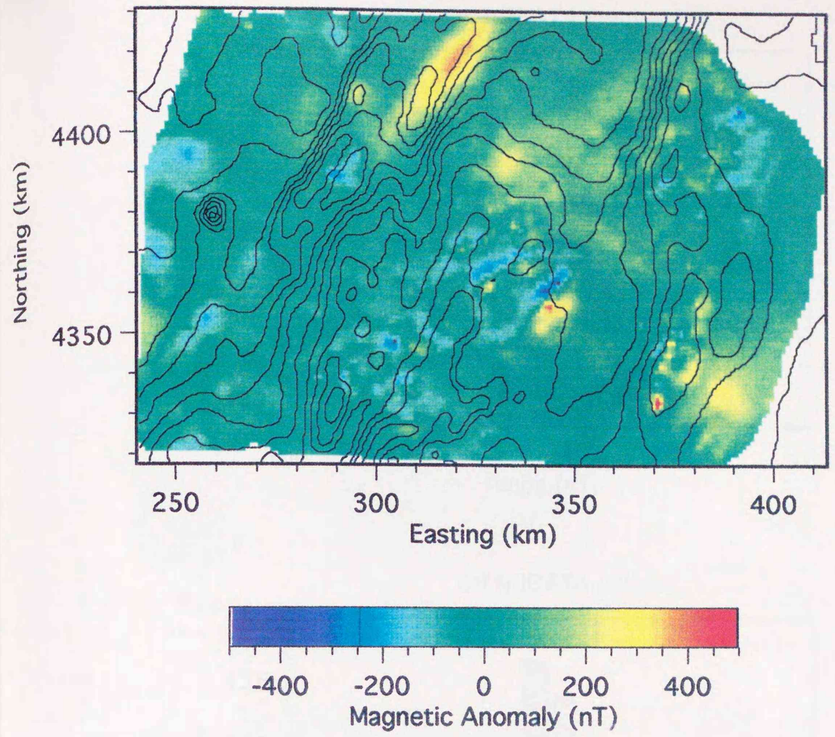

Fig.5-1-5
Magnetic anomaly color map overlaid with bathymetric contour of the off Akita area(39° N-40° N). Northing and Easting were UTM values origin Longitude was 141° E.

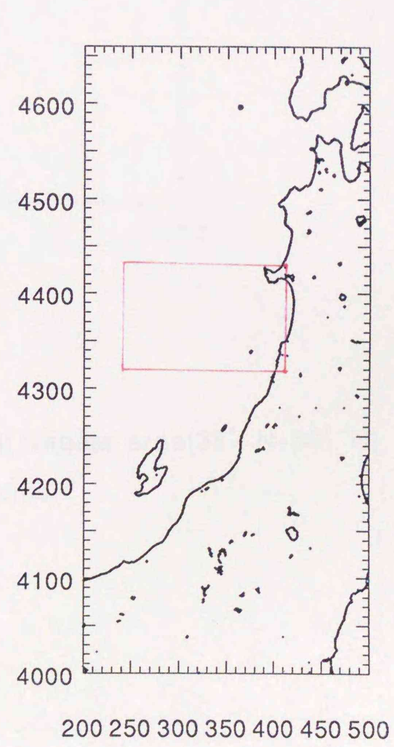

area_mag_poster_3 vs. (row, col)

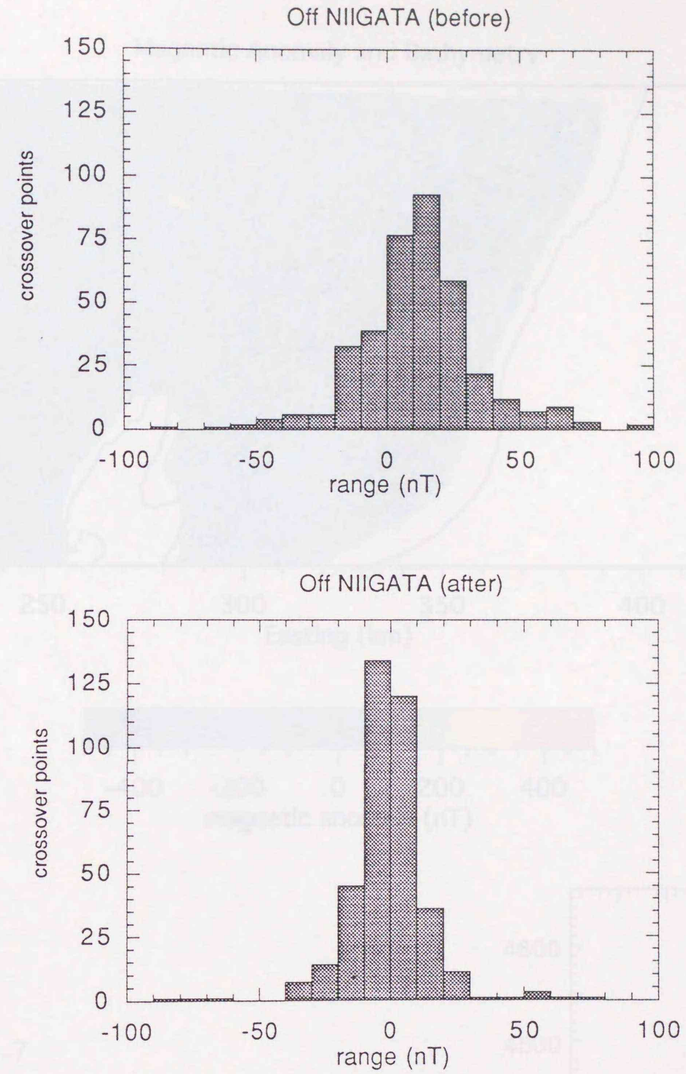

Fig.5-1-6

Histogram of the crossover errors in the off Niigata area(38° N-39° N).

upper: uncorrected errors at crossover points.

lower: errors after cross-point control.

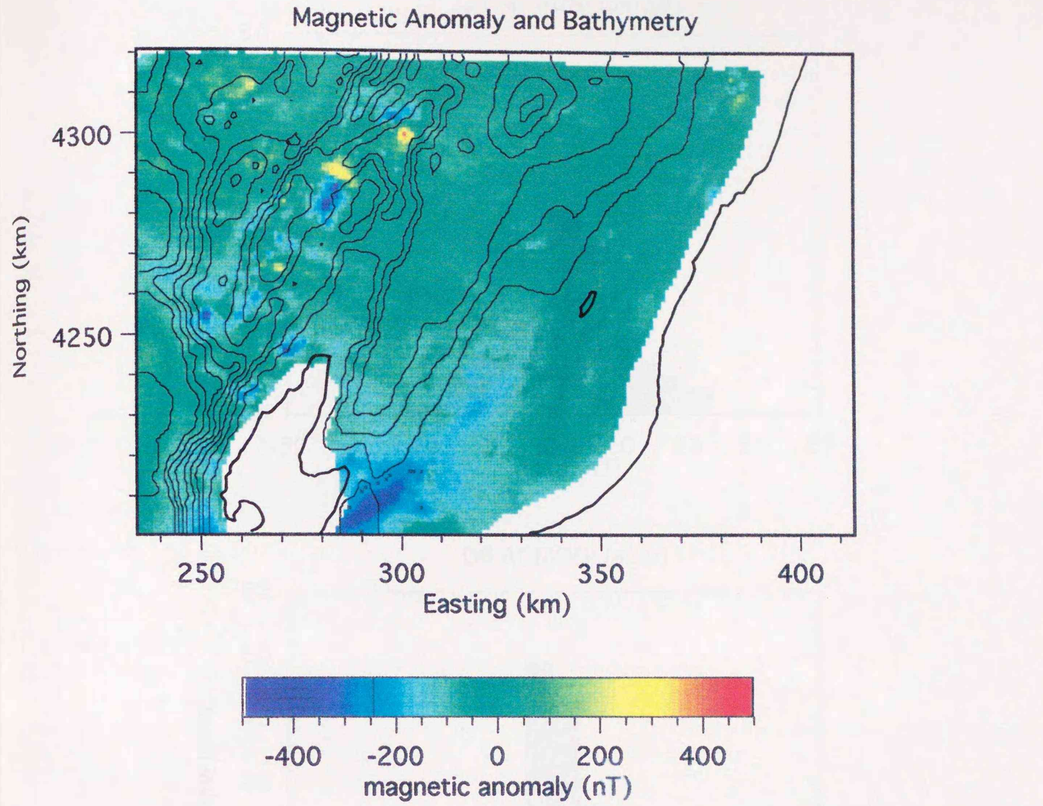

Fig.5-1-7
Magnetic anomaly color map overlaid with bathymetric contour of the off Niigata area(38° N-39° N). Northing and Easting were UTM values origin Longitude was 141° E.

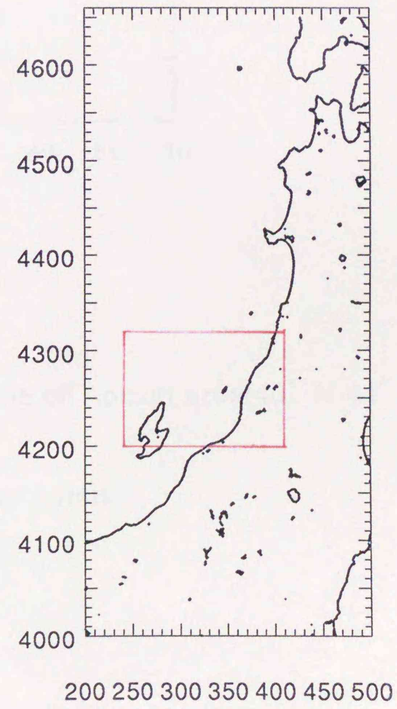

south_mag_1k_5 vs. (row, col)

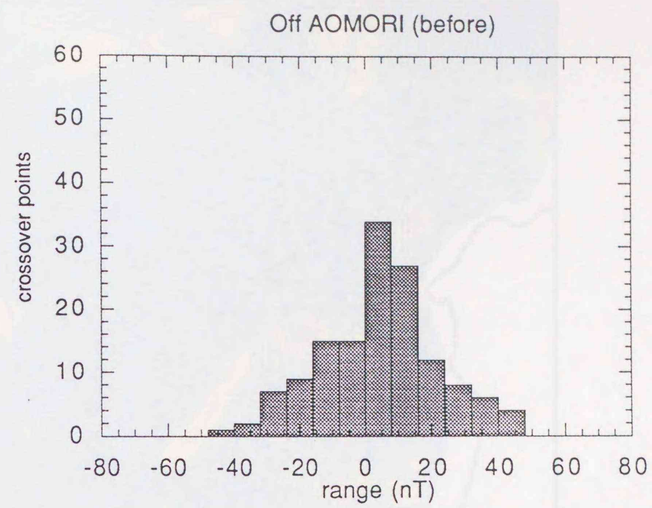

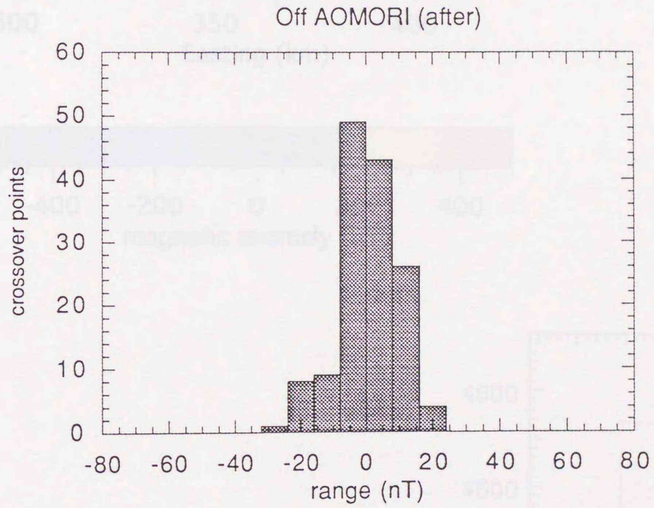

Fig.5-1-8

Histogram of the crossover errors in the off Aomori area(40° N-41° 15'N).

upper: uncorrected errors at crossover points.

lower: errors after cross-point control.

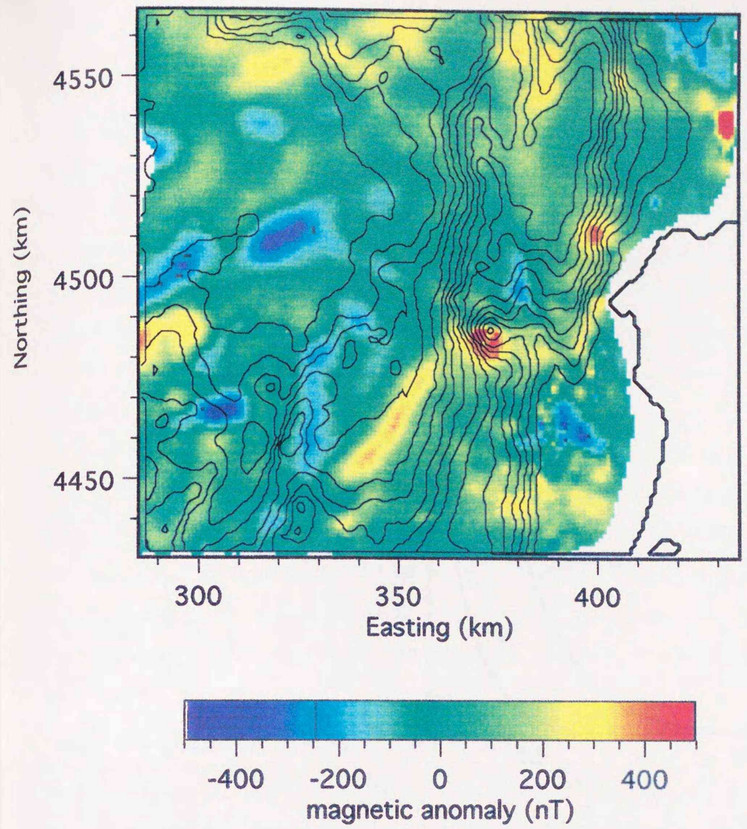

Fig.5-1-9
Magnetic anomaly color map overlaid with bathymetric contour of the off Aomori area(40° N-41° 15'N). Northing and Easting were UTM values origin Longitude was 141° E.

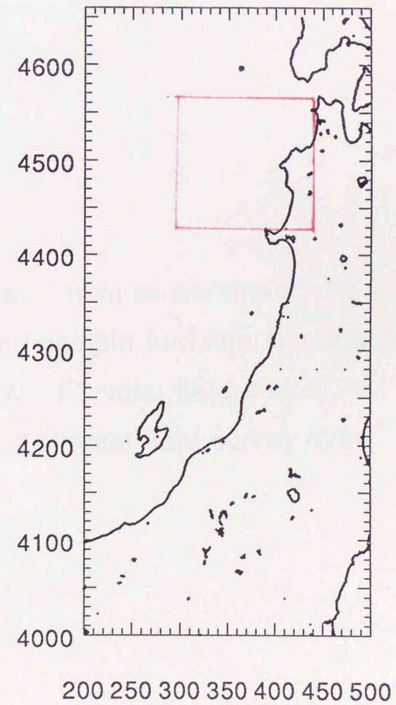

nnk_5 vs. (row, col)

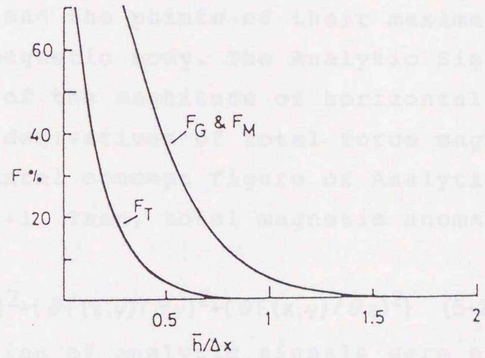

Fig.5-1-10

The expected percentage of aliased power F from an aeromagnetic survey, conducted at mean clearance h and sample and line spacing Δ x, versus the dimensionless parameter $h/\Delta x$. FT=total field survey, FG=vertical gradient(gradiometer) survey, FM=total field survey over isolated point dipole.

after Reid(1980).

5.2. *Approximating edges of source bodies from total force*

Blakely and Simpson (1986) showed that the steepest horizontal gradients of pseudo-gravity anomaly (Baranov, 1957) reflected abrupt lateral changes in magnetization and showed automatic mapping of maxima in the horizontal gradient. Makino (1997) showed that pseudo-gravity lost information when it was integrated and applied the same technique to the reduced to the pole anomaly to estimate magnetic boundaries. Similarly, Roest et al. (1992) showed the Analytic Signal and the points of their maxima reflected in a boundary of a magnetic body. The Analytic Signal was calculated as a sum of the magnitude of horizontal (east and north) and vertical derivatives of total force magnetic anomalies. A fundamental concept figure of Analytic Signal was shown in Fig.5-2-1. Then, total magnetic anomaly as F(x,y);

$$|A(x,y)|=\sqrt{\{(\partial F(x,y)/\partial x)^2+(\partial F(x,y)/\partial y)^2+(\partial F(x,y)/\partial z)^2\}} \quad (5\text{-}2\text{-}1)$$

Generally, the location of analytic signals were estimated discrepantly, when uniform magnetization was given to transformed to pseudo-gravity and reduced to the pole anomalies. Then, analytic signal was applied here, because it was less influenced by uniform magnetization than other transformations. However, the analytic signals suffered from discrepancy of locations of maxima, because they were fundamentally calculated from total force of magnetic anomalies (Roest and Pilkington, 1993).

Here, derivative calculations were applied with Fourier domain filters (Kato, 1987). As total force magnetic anomaly F(x,y,z) was transformed into Fourier domains;

$$F(x,y,z)=\Sigma\Sigma\,\delta_{mn}(a_{mn},b_{mn},c_{mn},d_{mn})\exp(p_{mn}z)||\Delta_{mn}||$$

$$||\Delta_{mn}||=\begin{pmatrix}\cos(mx)\cos(ny)\\ \sin(mx)\cos(ny)\\ \cos(mx)\sin(ny)\\ \sin(mx)\sin(ny)\end{pmatrix}$$

δ_{mn}=1/4 (m=n=Ø) or 1/2 (m≠Ø,n=Ø or m=Ø,n≠Ø) or 1 (m≠Ø,n≠Ø)

$b_{Øn}=c_{mØ}=d_{mØ}=d_{nØ}=Ø$ (5-2-2)

Where,

K,H : data number of x,y directions,

m,n : wave number of x,y directions,

and

$p_{mn}=\sqrt{(m^2+n^2)}$

Fourier coefficients, a_{mn}, b_{mn}, c_{mn}, and d_{mn} were requested by an inverse Fourier transform of equation (5-2-2).

Derivative with a direction υ whose direction cosines were (L,M,N) was;

$\partial F(x,y,z)/\partial\upsilon=L\partial F(x,y,z)/\partial x+M\partial F(x,y,z)/\partial y+N\partial F(x,y,z)/\partial z$ (5-2-3)

Fourier transform of the total force anomaly;

$$F'(x,y,z)=\Sigma\Sigma\,\delta_{mn}(a_{mn}',b_{mn}',c_{mn}',d_{mn}')\exp(p_{mn}z)||\Delta_{mn}|| \quad (5\text{-}2\text{-}4)$$

Where

$$||a_{mn}'||=T_{mn}(L,M,N)||a_{mn}|| \quad (5\text{-}2\text{-}5)$$

$||a_{mn}'||=(a_{mn}',b_{mn}',c_{mn}',d_{mn}')^T$,

$||a_{mn}||=(a_{mn},b_{mn},c_{mn},d_{mn})^T$,

$$T_{mn}(L,M,N)=\begin{pmatrix}p_{mn}N & mL & nM & Ø\\ -mL & p_{mn}N & Ø & nM\\ -nM & Ø & p_{mn}N & mL\\ Ø & -nM & -mL & p_{mn}N\end{pmatrix} \quad (5\text{-}2\text{-}6)$$

Tmn(L,M,N) was called as a derivative matrix.

The Analytic Signal was calculated with derivative x(1,0,0),

y(0,1,0), and z(0,0,1) respectively, and sum each squares like equation (5-2-1).

The maxima of Analytic Signals were scanned for four directions of N-S, E-W, NE-SW, and NW-SE similar way to Blakely and Simpson (1986). However, the threshold levels needed to set different values because gradients of magnetic anomalies became gentle as the surface depth of magnetic bodies. Here the threshold level of off Akita area(39° N-40 ° N) was given as linear as water depth. It was given as 30nT at 2km deeper and 100nT at sea surface. Magnetic anomalies of north of Sado Island area(38° N-39° N) were flatter, then the threshold level was given as linear as 30nT at 2km deeper and 50nT at sea surface. The threshold level of northern part of Mogami Trough area(40° N-41° 15'N) was set as 80nT at 3km deeper and 100nT at sea surface. Dots in Fig.5-2-2, Fig.5-2-3, and Fig.5-2-4 indicated the boundaries of magnetic structures.

The remarkable boundaries of magnetic structures appeared three lines in the off Akita area (Fig.5-2-2). They were corresponded to (1) from Oga peninsula to the Tobishima Island, (2) around a boundary of Sado Ridge and the Yamato Basin, (3) around the Mogamitai Bank in the northern part of the Sado Ridge.

Remarkable magnetic boundaries in the north of Sado Island area (Fig.5-2-3) were appeared only along Sado Ridge and they were not seen around Awashima Island. It was caused by gentle magnetic anomalies along the coast of Niigata. Moreover, magnetic boundaries were not corresponding to geological structures in both of Fig.5-2-2 and Fig.5-2-3. They could be considered as amplified crossover errors by derivation because they trended in the same direction of survey lines as N110° E.

The remarkable magnetic boundaries in Fig.5-2-4 trended in

SW and SE directions from west of the Kyuroku Jima Island. Especially, a magnetic boundary that trended in SW direction from the Kyuroku Jima Island looked to be extended to a magnetic boundary line in NNE direction that was shown in Fig.5-2-2. It was very interesting because here was corresponding to the epicenter area of Nihonkai-chubu earthquake (1983).

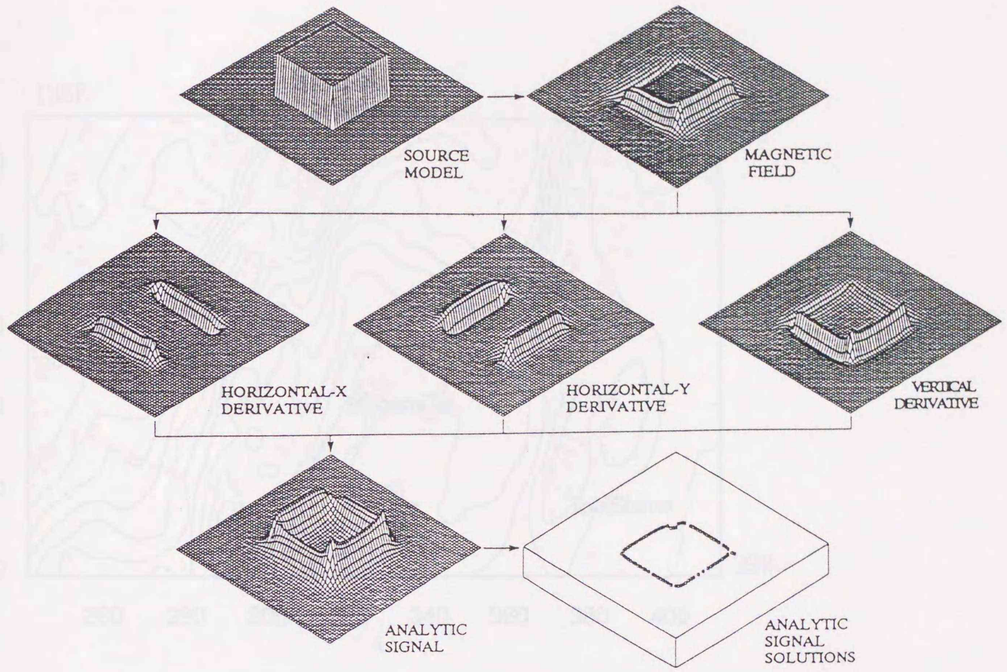

Fig.5-2-1
Schematic outline of the analytic signal method. Horizontal and vertical derivatives are calculated from the total field anomaly over a square prism and combined to yield the absolute value of the analytic signal. The location of the maxima and the shape of this signal can then be used to find body edges and corresponding depth estimates.
after Roest et al(1992).

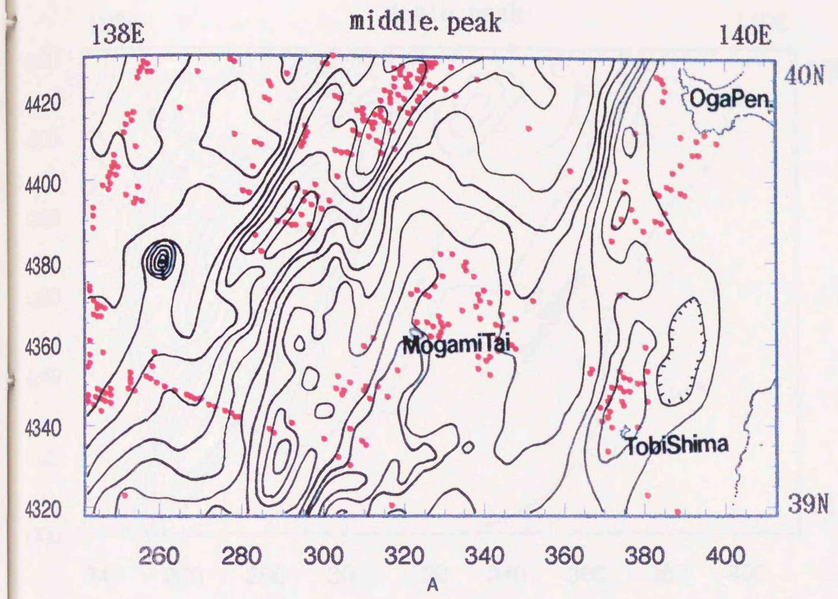

Fig.5-2-2

Distribution of the maxima of the analytic signals. solid circles indicate the maxima of the signals. off Akita area(39° N-40° N).

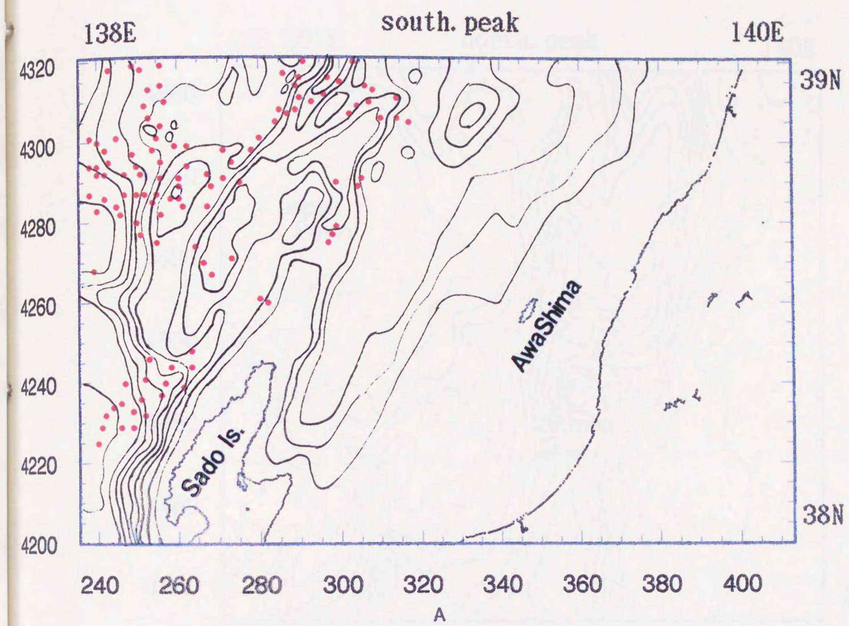

Fig.5-2-3

Distribution of the maxima of the analytic signals. solid circles indicate the maxima of the signals. off Niigata area(38° N-39° N).

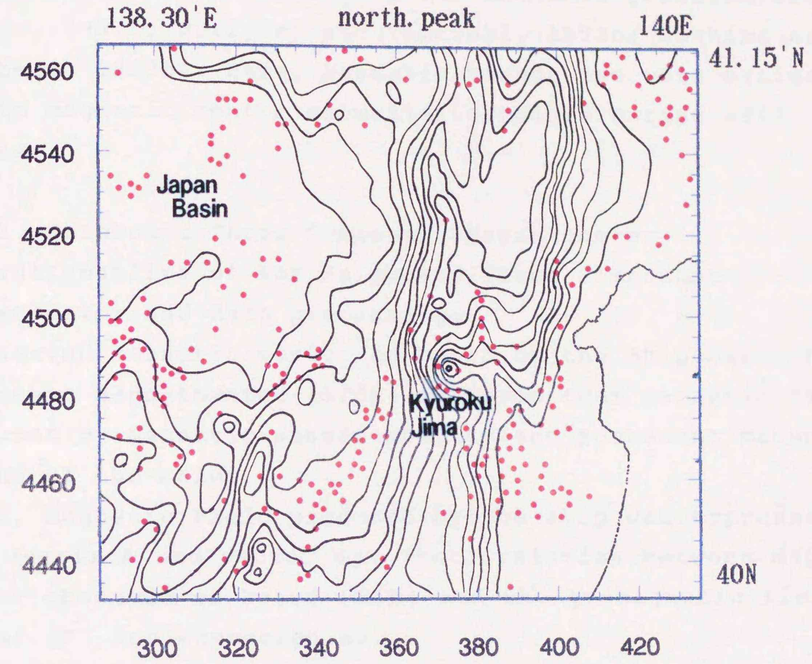

Fig.5-2-4

Distribution of the maxima of the analytic signals. solid circles indicate the maxima of the signals. off Aomori area(40° N-41° 15'N).

5.3. *Data processing for Shipboard Three Component Magnetometer*

Measurements of magnetic vector anomalies with the Shipboard Three Component Magnetometer (STCM) were carried out in three cruises, GH90, GH91, and GH92 (Joshima and Kikawa, 1991b; Morijiri and Yamazaki, 1992b; Joshima and Ishihara, 1993b). Here, magnetic boundaries were estimated due to magnetic vector anomalies obtained during GH91 cruise.

5.3.1. Shipboard Three Component Magnetometer

First, outline of the Shipboard Three Component Magnetometer and data processing.

Observed magnetic vector on board by the Shipboard Three Component Magnetometer (STCM) suffered from magnetic field produced by magnetic susceptibility and permanent magnetic moment of the ship.

Now, magnetic field produced by the ship was expressed as 3×3 matrix **A** and vector **Hp**. Then, relation between magnetic vector observed on board (**Hob**) and the geomagnetic field vector (**F**) was expressed as;

$$\mathbf{Hob} = \mathbf{ARPYF} + \mathbf{Hp} \qquad (5\text{-}3\text{-}1)$$

Where,

R, **P**, and **Y** were matrices of rotation due to roll, pitch, and yaw of a ship, respectively (Isezaki, 1986b).

Magnetic field (**Hob**) was observed on the right handed fixed coordinate on the ship with Heading (h), Starboard(s), and Downward (v). They were converted into the earth coordinates, Geographic North(x), East(y), and Down(z) using pitching(θp), rolling(θr), and yawing(θg). The relation between the fixed coordinate and the earth coordinate was shown in Fig.5-3-1. If twelve contents in **A** and **Hp** were known, the magnetic field **F** were obtained by measuring **R**,

P, **Y**, and **Hob**.

The twelve contents in **A** and **Hp** were calculated from variations of observed magnetic field with orientation of the ship were measured by "8-shaped ship's steering". Concretely, the ship was running along two circles which orientations were clockwise and anti-clockwise 360 ° of about 750m radius respectively, and ship's speed was about 10 knots. The ship's pitching (**P**), rolling(**R**), yawing (**Y**), and observed magnetic field (**Hob**) were measured. The geomagnetic field **F** was assumed to be uniform and given. The twelve contents in **A** and **Hp** were calculated by the least square means method. During the "8-shaped ship's steering", the ship was running on the sea surface. Then, it was not enough for calculation contents concerned in z component of magnetic field vector (v). Therefore, it was necessary to do "8-shaped ship's steering" at some places where z components of external magnetic field were different (Isezaki, 1986b). Experience showed it needed to do at least four times at places where z components were different.

Magnetic field **F**=(Fx,Fy,Fz) was represented by the 1990 version of the International Geomagnetic Reference Field(IGRF90: IAGA, Division V, Working Group 8,1991). The magnetic field along the figure '8' track was regarded to be uniform and it was given as the center point's value of figure '8' of the IGRF90. To obtain twelve contents, magnetic field was converted from earth coordinates of (x,y,z) to the ship's coordinates of (h,s,v) with matrices of rotation **R**, **P**, and **Y** due to rolling, pitching, and yawing.

$$F_{hsv} = RPYF_{xyz} \qquad (5\text{-}3\text{-}2)$$

Since every components were independent, Equation (5-3-1) was rewritten as follows, where observed magnetic field was **Hob**=(Hh,Hs,Hv), 3×3 matrix which represented magnetic

susceptibility of the ship was **A**=(aij), and magnetic field vector produced by permanent magnetic moment was **Hp**=(Hph,Hps,Hpv).

$$Hh_i = a_{11}*Fh_i + a_{12}*Fs_i + a_{13}*Fv_i + Hph$$
$$Hs_i = a_{21}*Fh_i + a_{22}*Fs_i + a_{23}*Fv_i + Hps$$
$$Hv_i = a_{31}*Fh_i + a_{32}*Fs_i + a_{33}*Fv_i + Hpv \qquad (5\text{-}3\text{-}3)$$

The twelve contents were determined by least square means (after Nakagawa and Koyanagi, 1982). Every component was calculated from all data obtained from several times, of "8-shaped ship's steering". Here, variance of solution for (a13, a23, a31, a32, a33) and (Hph,Hps,Hpv) were larger than those of other contents, and uniqueness of solution was unsatisfied. These contents were related to v-component of observed magnetic field. The variation of Hv was too small to determine constants, a13, a23, a31, a32, a33, Hph, Hps, and Hpv.

The location of "8-shaped ship's steering" during GH91 cruise was shown in Fig.5-3-2. During GH91 cruise, the "8-shaped ship's steering" were carried out only twice (gh91c1 and gh91c2), then seven times "8-shaped ship's steering" data obtained during NH91-1 cruise (Yamazaki, 1992) were added to determine the twelve contents. NH91-1 cruise finished just before GH91 cruise started. The twelve contents calculated from these nine times, "8-shaped ship's steering" data were shown in Table.5-3-1.

5.3.2. Present situation of measurement on the R/V Hakurei-maru

In order to check whether the twelve contents(3×3 matrix **A** and vector **Hp**) were calculate the most suitable or not, magnetic field data along gh91c1 which was one of "8-shaped ship's steering" during GH91 cruise were corrected using

these contents.

$$F'_{hsv}=A^{-1}(Hob-Hp) \qquad (5\text{-}3\text{-}4)$$

Where twelve contents in 3×3 matrix **A** and vector **Hp** were values shown in Table.5-3-1. The difference between corrected magnetic field (F'_{hsv}) and given field for calculation (F_{hsv}) was several 100nT. Moreover, the each component values of **F'-F** were plotted versus the direction of ship's heading during "8-shaped ship's steering" and shown in Fig.5-3-3. Errors were not constant and they correlated with the direction of ship's heading. It suggested that the twelve contents that were calculated here were not satisfied to correct magnetic field due to the ship's body. However, the calculation with least square means method was no problems because more than 20,000 data were used. Then, the equation (5-3-1) was not satisfied for measurement values in this case. As a cause of measurement errors, three reasons were thought, (1) the ship's attitude measurement, (2) assumption of standard magnetic field, and (3) viscous remaining magnetization. Then each reasons were checked using data obtained GH91 cruise and NH92-1 cruise (Morijiri, 1993) and cleared points of problems, though the reasons were complicated.

(1) Ship's attitude

At the beginning, as shown in Fig.5-3-3, errors of magnetic field were correlated with direction of the ship's heading. The resolution of gyrocompass system on R/V Hakurei-maru was regarded as unsatisfactory to determine twelve contents. Kitahara et al. (1992) compared corrected magnetic field using the different data sets of pitching, rolling and yawing of R/V Hakuho-maru cruise. One was measured by gyro compass which follow-up accuracy was 0.1° . Its resolution was similar to R/V Hakurei-maru. And another

data set was measured by high resolution gyro compass which follow-up accuracy was 0.01° . The result showed dispersion of corrected total magnetic anomalies **F'** became small when data of high-resolution gyrocompass were used for the calculation. Joshima and Komazawa (1996) showed that the correlation of variation of measured magnetic field and ship's attitude became better along some survey lines trended in North, when they used a higher resolution attitude sensor for observation during GH95 cruise. The follow-up accuracy of old sensor was 0.01° and new sensor was 0.0055° . However, there were still large differences of corrected magnetic field vector between actual and ideal data, though correction used high resolution sensors made data better.

Variation of observed magnetic field vector (Hh,Hs,Hv) along "8-shaped ship's steering" were caused by only variation of ship's attitude. Each measurement was satisfied with requirements for the calculation to determine twelve contents. The similar figure to Fig.5-3-3 was drawn for the check. Data obtained during "8-shaped ship's steering" gh91c1 were analyzed as a sample.

At first, magnetic field vector (Fx,Fy,Fz) was given as IGRF90 of the center of figure "8", and the vector was converted to ship's coordinate (Fh,Fs,Fv). Here, each second variation of H-component and S-component were compared, i.e., comparison (dHh,dHs) and (dFh,dFs). The profiles of dHh and dFh were shown in Fig.5-3-4a, and dHs and dFs were shown in Fig.5-3-4b. In these figures, data were from first two minutes of anti-clockwise part of "8-shaped ship's steering". They were randomly chosen. These profiles indicated that phase were not coincident. Then, measurement attitude data were not followed the real variation of ship's attitude. Data were sampled every 125 ms in the system on

the R/V Hakurei-maru. Profiles of each 125 ms variation were also compared, but these phases were not coincident. It indicated that phase coincident was not due to calculated 1 sec means.

Data measured with a set of gyrocompass, an attitude meter, and magnetic sensors were logged in the control unit (a personal computer) of this system every 125 ms. Each data were logged almost at the same time, but loggings were not synchronized strictly. For example, if the ship rolled 2° /sec, 50msec time delay made attitude error as 0.1° . Korenaga (1995) estimated that this attitude error made 40nT magnetic field error in the external field intensity was 25,000 nT. In addition, more, cycles of pitching, rolling, and yawing were mixed from a few seconds to a few minutes periods. Therefore, separation of signals and noise by periods was very difficult. It was difficult to calculate the ideal contents only by improvement of the ship's attitude measurements.

For the next, easy examples were calculated in order to estimate how much magnetic field error was caused by the ship's attitude error. Concretely, magnetic field vector (**Fo**), twelve contents of magnetic field due to the ship's body (**Ao,Hpo**), matrices of rotation (**RPY**) were given as "correct" data at first. Then, "ideal" observed magnetic field was calculated as **Hob'=Ao(RPY)Fo+Hpo** from "correct" magnetic field vector (**Fo**), twelve contents of magnetic field due to the ship's body(**Ao,Hpo**), and matrices of rotation(**RPY**). Here, ideal data of "8-shaped ship's steering" were made. Next, "error" matrices of rotation (**RPY**)' were made as added to random numbers. Yawing data were added random numbers from -1° to 1° , and pitching and rolling data were added to different series of random numbers from -0.1° to 0.1° . In the case of R/V Hakurei-

maru, the additional error was a little bit larger, because heading errors of R/V Hakurei-maru system were known experientially within ±1° . For the next, a new set of twelve contents (**A,Hp**) was calculated by least square means from "ideal" observed magnetic field (**Hob'**) and "error" matrices of rotation (**RPY**)'. Further more, corrected magnetic field vector,

$\mathbf{F}=\mathbf{A}^{-1}(\mathbf{Hob'}-\mathbf{Hp})$, were calculated from a new set of twelve contents (**A,Hp**), "ideal" observed magnetic field(**Hob'**) and "error" matrices of rotation(**RPY**)'. As compared this magnetic field(**F**) with the given magnetic field(**Fo**), difference in total intensities were only ±20nT, though each components had a several hundreds nT differences (Morijiri and Yamazaki,1994a). Total force of magnetic field did not suffered seriously from the ship's attitude errors. Therefore, it suggested that ship's attitude error did not caused a several hundreds nT difference in total force between IGRF at the center of figure "8" and corrected magnetic field from observed data.

(2) Magnetic anomaly at the "8-shaped ship's steering" point

Second problem was that magnetic field vector (**F**) was given as IGRF at the center of figure "8", because real magnetic field was different from IGRF. However, if the magnetic gradient of the place of "8-shaped ship's steering" was carried was gentle, magnetic field vector produced by permanent magnetic moments of ship's body (**Hp**) absorbed the value caused by magnetic anomaly there. Then, it did not become serious problem.

(3) Viscous Remanent Magnetization

Present way of analysis was according to equation (5-3-1) by Isezaki (1986b). It assumed the twelve contents were constant during the cruise and it didn't consider about

Viscous Remanent Magnetization (VRM). Actually, the ship's body was made by iron and it was in magnetic field long time, then the ship's body should get VRM. However, the VRM was considered as very small and it could be ignored. However, Yamazaki et al. (1994) suggested VRM was enough large because there were exponential trend of the difference between total force measured by the STCM and by the proton precession magnetometer, when the ship changed course.

There, Morijiri and Yamazaki (1997) estimated an influence of time variation of ship's magnetization using data obtained 14 times, of "8-shaped ship's steering" during NH92-1 cruise (Fig.5-3-5). Each observation was carried by a number order, and time difference of nh92c1 and nh92c14 was about 42 days. Experientially, data were required at least four times of "8-shaped ship's steering". Then we calculated five sets of the twelve contents of ship's magnetization in A and Hp using four kinds of combination of four times of "8-shaped ship's steering" data and all data (Table.5-3-2). Concretely, their combinations were
A(nh92c1+nh92c2+nh92c3+nh92c4),B(nh92c7+nh92c8+nh92c9+nh92c10), C(nh92c11+nh92c12+nh92c13+nh92c14), D(nh92c1+nh92c6+nh92c11+nh92c14),and E(all data).
To be easy comparison, total intensities of corrected magnetic field(Fx,Fy,Fz) were calculated from observed data(**Hob**) along a survey line trended in North measured just before nh92c7(blue arrow in Fig.5-3-5) using these 5 sets of twelve contents of ship's magnetization(**A**,**Hp**). These profiles were shown in Fig.5-3-6. The most suitable result for measurement data of the proton precession magnetometer(PPM) was correction using twelve contents that were calculated from data of "B set". The four "8-shaped ship's steering" which were combined into "B set" were located nearest from a sample survey line(almost the same as

nh92c7). For the opposite, the difference between total intensity of corrected magnetic field using twelve contents calculated from "A set" and total force by PPM was the largest. All of "8-shaped ship's steering" which were combined into "A set" was observed before a sample survey line. Then they were not influenced by VRM which sample data included. The result using "E set" was similar to using "A set", because "E set" combined all data. In addition, the result using "D set "was similar to the result using" B set, because half of data were influenced by VRM which sample data included. Therefore, it suggested that correction of magnetic field due to the ship's body was good for using twelve contents calculated from "A set" when data were obtained early half of NH92-1 cruise. Moreover, data obtained later half of the cruise were corrected using the twelve contents that were calculated using "B set or C set" in order that difference between magnetic field by STCM and by PPM became small. This example showed that when and where "8-shaped ship's steering" was carried during each cruise were very important factors to determine the twelve contents of magnetic field due to the ship's body.

5.3.3. Differences between total intensities by P.P.M. and S.T.C.M.

Errors of twelve contents of magnetic field due to the ship's body were estimated how much influence on magnetic field correction in this section. The total force of corrected magnetic field using twelve contents obtained from all "8-shaped ship's steering" data were compared total force measured by the proton precession magnetometer(PPM).

Average differences between total force measured by STCM (Tf) and by the PPM (Tp) of each survey line during GH91 cruise were shown in Fig.5-3-7. They were calculated as (Tf-

Tp). Actually, the ship moved very complicatedly during the cruise, though Fig.5-3-7 showed only magnetic survey lines. Then acquisition of VRM seemed to be too complicated to estimate value. The twelve contents of GH91 cruise were calculated from "8-shaped ship's steering" data. Moreover, they were not influenced by the VRM that was acquired during GH91 cruise. Because seven of nine "8-shaped ship's steering" data sets were obtained in NH91-1 cruise just before GH91 cruise.

Average differences between Tf and Tp of each survey lines were correlated with directions. As shown in Fig.5-3-7, though these values were different, 'Tf's were smaller than 'Tp's on lines trended in direction S, SSW, and ESE, and on the lines trended in the opposite, 'Tf's were larger than 'Tp's.

Now, 'Tf' and 'Tp' were compared along the line t112 trended in NNE (it was indicated with an arrow in Fig.5-3-7). Their profiles were shown versus the distance from starting point of line t112. The differences between 'Tf' and 'Tp' were caused by the error of the twelve contents of magnetic field by the ship's body. Then, the errors of the twelve contents were appeared as the different trend of each profile.

The errors of obtained magnetic vector anomaly, Fer=(Xer,Yer,Zer) was described as follows from equation (5-3-1);

magnetization line from equation (5-3-1),

$$Fer=-(RPY)^{-1}(A+dA)^{-1}(dARPYF+dHp) \qquad (5\text{-}3\text{-}5)$$

where, **dA**=(daij) was errors of matrix **A**, and **dHp**=(dHph,dHps,dHpv) was errors of the vector **Hp** (Seama et al.,1990). When survey lines were enough long, we could approximate as (**RP**)=**I** because average of pitching and

rolling were considered as enough small. Now, θ indicated yawing, and the equation (5-3-5) were described with each components;

$$Xer=-\{Ax*\sin\theta+Bx*\cos\theta+Cx+Dx*\sin2\theta+Ex*\cos2\theta\}*Fx$$
$$Yer=-\{Ay*\sin\theta+By*\cos\theta+Cy+Dy*\sin2\theta+Ey*\cos2\theta\}*Fy$$
$$Zer=-\{Az*\sin\theta+Bz*\cos\theta+Cz\}*Fz \qquad (5\text{-}3\text{-}6)$$

where,

$hh=dHph/Fx$, $hs=dHps/Fy$, $hv=dHpv/Fz$, $B_{ij}=(b_{ij})=(A+dA)^{-1}{}_{ij}$,

$dA1=da_{11}+da_{12}+da_{13}$, $dA2=da_{21}+da_{22}+da_{23}$, and $dA3=da_{31}+da_{32}+da_{33}$.

$$Ax=-(b_{21}*hh+b_{22}*hs+b_{23}*hv+b_{23}*dA3)$$
$$Bx=b_{11}*hh+b_{12}*hs+b_{13}*hv+b_{13}*dA3$$
$$Cx=\text{Ø}.5*(dA1*b_{11}+dA2*b_{12}-dA2*b_{21}+dA1*b_{22})$$
$$Dx=\text{Ø}.5*(dA2*b_{11}-dA1*b_{12}-dA1*b_{21}-dA2*b_{22})$$
$$Ex=\text{Ø}.5*(dA1*b_{11}+dA2*b_{12}+dA2*b_{21}-dA1*b_{22})$$
$$Ay=b_{11}*hh+b_{12}*hs+b_{13}*hv+b_{13}*dA3$$
$$By=b_{21}*hh+b_{22}*hs+b_{23}*hv+b_{23}*dA3$$
$$Cy=\text{Ø}.5*(dA1*b_{21}+dA2*b_{22}+dA2*b_{11}-dA1*b_{12})$$
$$Dy=\text{Ø}.5*(dA2*b_{11}-dA1*b_{12}-dA1*b_{21}-dA2*b_{22})$$
$$Ey=\text{Ø}.5*(dA1*b_{11}+dA2*b_{21}+dA2*b_{12}-dA1*b_{22})$$
$$Az=b_{31}*dA2-b_{32}*dA1$$
$$Bz=b_{31}*dA1+b_{32}*dA2$$
$$Cz=b_{31}*hh+b_{32}*hs+b_{33}*hv+dA3*b_{33} \qquad (5\text{-}3\text{-}7)$$

Yawing θ were considered to be equal along the each survey lines. Here, lines trended in North($\theta=0°$) or South($\theta=180°$) were considered as samples. Then, As and Ds in (5-3-6) were neglected, and only Bs changed their polarities when θ changed from 0° to 180°. Therefore, it needed that Bs were larger than As, Cs, Ds, and Es in order to change polarity depended on a direction θ as shown in

Fig.5-3-7.

Concrete the twelve contents in matrix A and vector Hp which were obtained from observed data during GH91 cruise were shown in Table.5-2-1. Covariance of solutions of a_{22}, a_{21}, a_{12}, and a_{11} were enough small, then errors, i.e., da_{22}, da_{21}, da_{12}, and da_{11}, were smaller than other terms. Now, dA1, dA2, b_{11}, b_{12}, b_{21}, and b_{22} were approximated as 0. Finally, equation (5-3-6) were supposed as,

$$Xer \fallingdotseq dHph,\ Yer \fallingdotseq dHps,\ Zer \fallingdotseq dHpv+da_{33}*Fz. \qquad (5\text{-}3\text{-}8)$$

The data along survey line t112 were shown versus latitude in Fig.5-3-8. Difference of profiles between 'Tf' and 'Tp' were appeared as different linear trends of them. If it could be supposed as $Zer \fallingdotseq dHpv+da_{33}*Fz$, error values were on the linear trend. In addition, Fz was depending on latitude, a difference of gradient of the linear trend was corresponding to da_{33}, and a difference of intercepts was corresponding to dHpv. In order to estimate actual values, other neglected terms had to be considered about their influence of errors. Then, only tendency in errors was discussed here.

In the case of GH91 cruise, errors of Z component were much larger than errors of other components, because Z component of magnetic field around Japan was the larger and correction of Z component was unsatisfactory. On the other hand, difference between 'Tf' and 'Tp' around the equator area(from 0° 30'N to 2° 30'N) along longitude 175° E was shown in Fig.5-3-9a. These data were obtained during NH92-1 cruise and the ship was going from South to North. In this area, 'Tf-Tp' became almost constant. In comparison with low latitudes area, middle latitudes area(from 38° 30'N to 40° 0'N) along longitude 175° E was shown in Fig.5-3-9b. Data

were obtained along the survey line from South to North on longitude 175° E during NH93-1 cruise. Each gradients of linear trend of 'Tf' and 'Tp' were different similarly to the Japan Sea area. Therefore, the reason that 'Tf-Tp' became almost constant in low latitudes area was suggested that Z component was small in this area and X component became large relatively. Moreover, X component error (dHph) became major of errors in low latitudes area. On the other hand, as Z component became large, errors of $dHpv+da_{33}*Fz$ became major in middle latitudes area. Then 'Tf-Tp' became differences of linear trends.

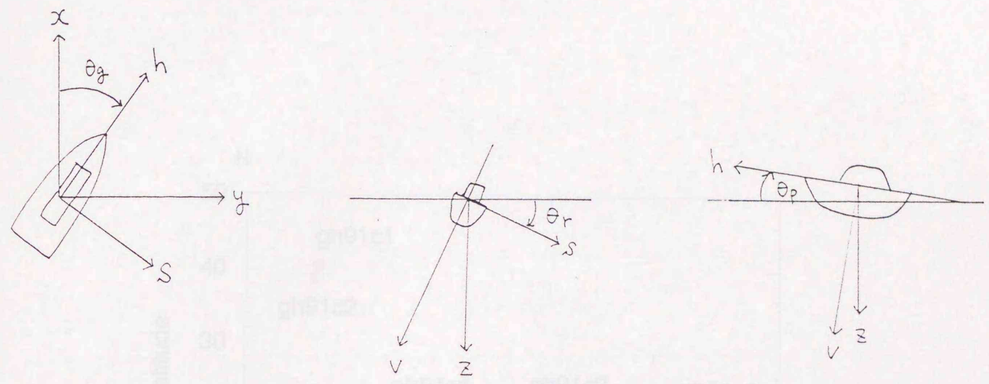

Fig.5-3-1

The fixed earth coordinate system(x,y,z) and the fixed ship coordinate system(h,s,v). θ g, θ p, and θ r are yaw, pitch, and roll angles, respectively.

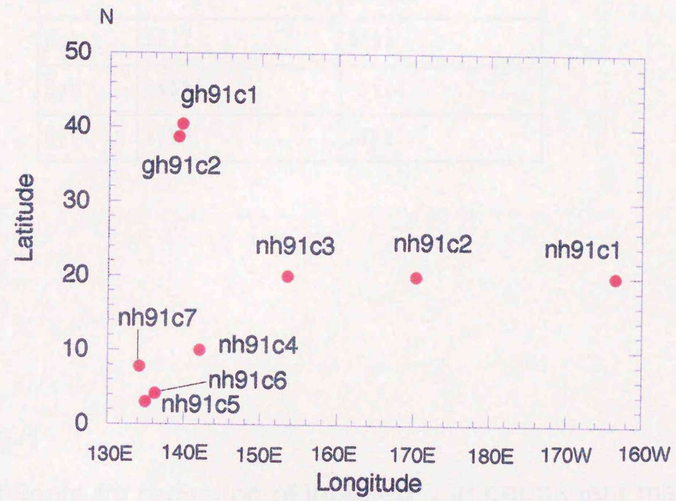

Fig.5-3-2

Location of 'figure 8' showing ship's steerings during GH91 and NH91-1 cruises.

	GH91	NH91-1
a11	0.9957	0.9960
a12	-0.0224	-0.0227
a13	0.0848	0.0738
a21	0.0130	0.0117
a22	0.7297	0.7292
a23	0.0048	0.0117
a31	0.0686	0.0669
a32	-0.0146	-0.0129
a33	1.0373	1.0300
Hph	3912	3945
Hps	-5380	-5414
Hpv	1793	1754

Table.5-3-1

12-Coefficients for reduction of induced and permanent magnetizations of the ship's body.

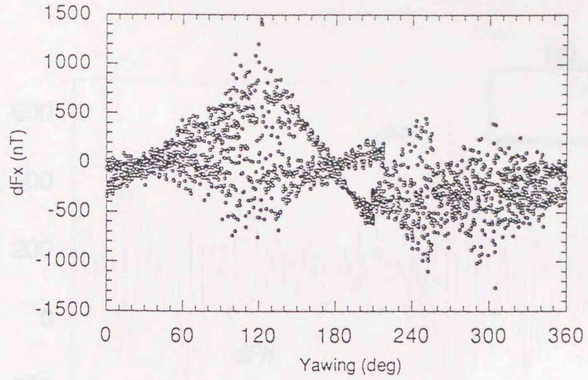

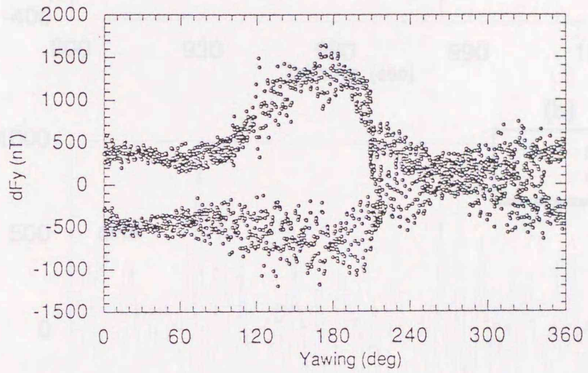

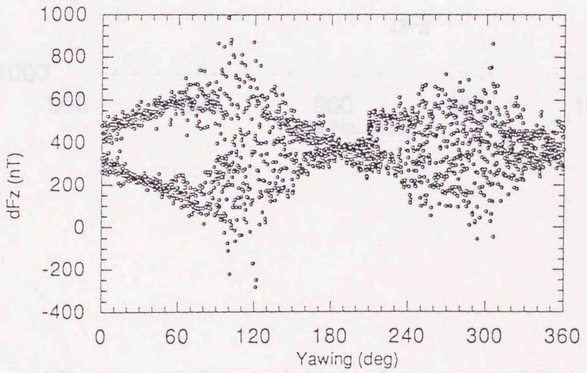

Fig.5-3-3

Differences between IGRF and geomagnetic vector after 'figure 8' compensation. Horizontal axis indicates yawing angle. dFx, dFy, and dFz indicate north, east and down components, respectively. upper:X-component, middle:Y-component, lower:Z-component.

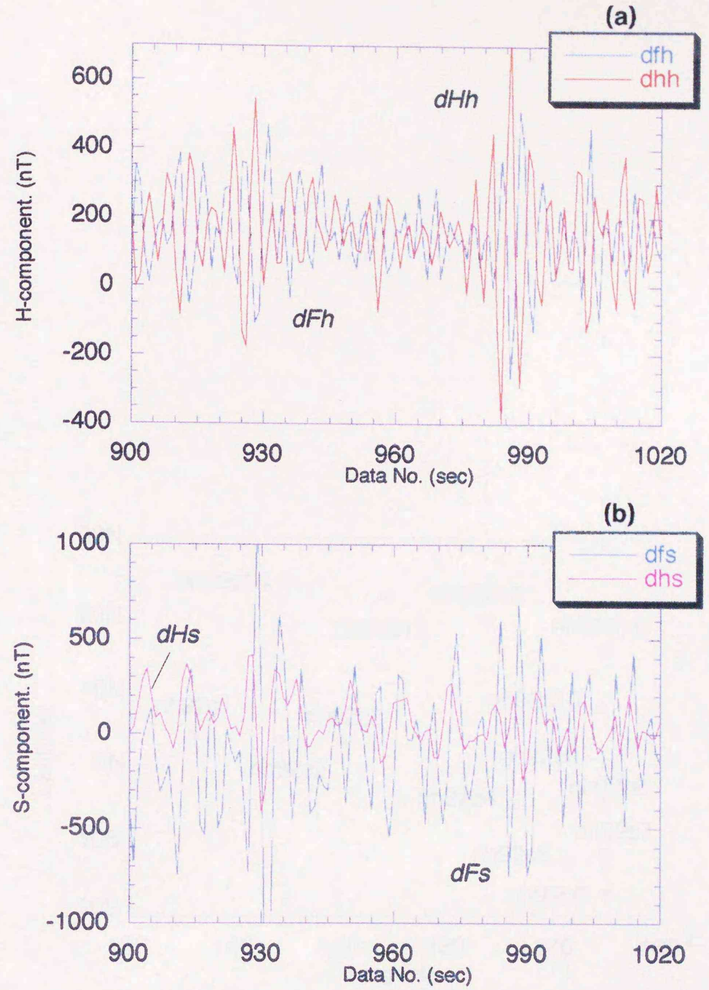

Fig.5-3-4

Comparison of the magnetic variation of measured field (dHh, dHs) with calculated field (dFh, dFs) by attitude of the ship.

a:H-component, Red line indicates dFh and blue line indicates dHh.

b:S-component, Red line indicates dFs and blue line indicates dHs.

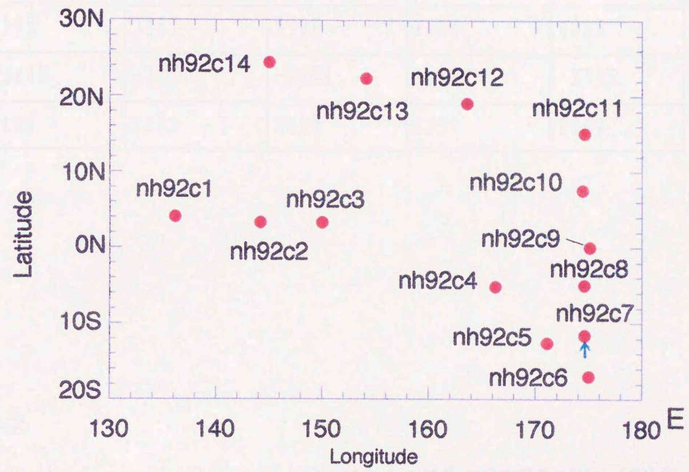

Fig.5-3-5

Location of 'figure 8' showing ship's steerings during NH92-1 cruises.

The blue arrow indicates location of sample data.

	A	B	C	D	E
a11	0.9942	0.9931	0.9935	0.9906	0.9925
a12	-0.0125	-0.0119	-0.0113	-0.0120	-0.0122
a13	0.0596	0.0776	0.0764	0.0750	0.0723
a21	0.0036	0.0029	0.0017	0.0035	0.0020
a22	0.7279	0.7296	0.7295	0.7266	0.7276
a23	-0.0331	0.0084	-0.0666	-0.0000	-0.0080
a31	0.0728	0.0744	0.0737	0.0736	0.0750
a32	-0.0228	-0.0239	-0.0245	-0.0243	-0.0234
a33	1.0557	1.0222	1.0253	1.0468	1.0478
Hph	4189	3987	3990	4040	4086
Hps	-3440	-3277	-2494	-3497	-3395
Hpv	2490	2112	2613	2397	2249

Table.5-3-2

12-Coefficients for reduction of induced and permanent magnetizations of the ship's body.

A:nh91c1+nh91c2+nh91c3+nh91c4

B:nh91c7+nh91c8+nh91c9+nh91c10

C:nh91c11+nh91c12+nh91c13+nh91c14

D:nh91c1+nh91c6+nh91c11+nh91c14

E:all

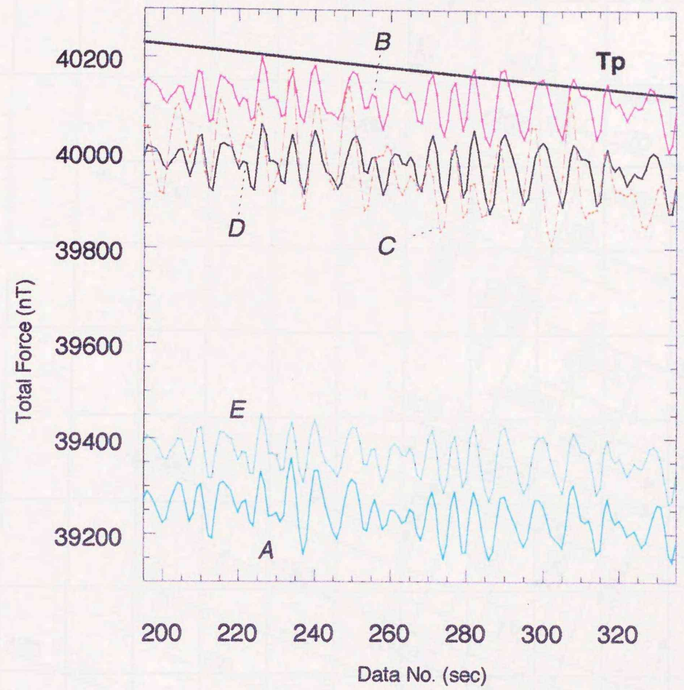

Fig.5-3-6

Differences between total force calculated from geomagnetic vector using 12 constants obtained from 4 'figure 8' ship's steerings.

The straight line indicates the value observed by Proton Precession Magnetometer.

Profiles;

A:nh91c1+nh91c2+nh91c3+nh91c4

B:nh91c7+nh91c8+nh91c9+nh91c10

C:nh91c11+nh91c12+nh91c13+nh91c14

D:nh91c1+nh91c6+nh91c11+nh91c14

E:all

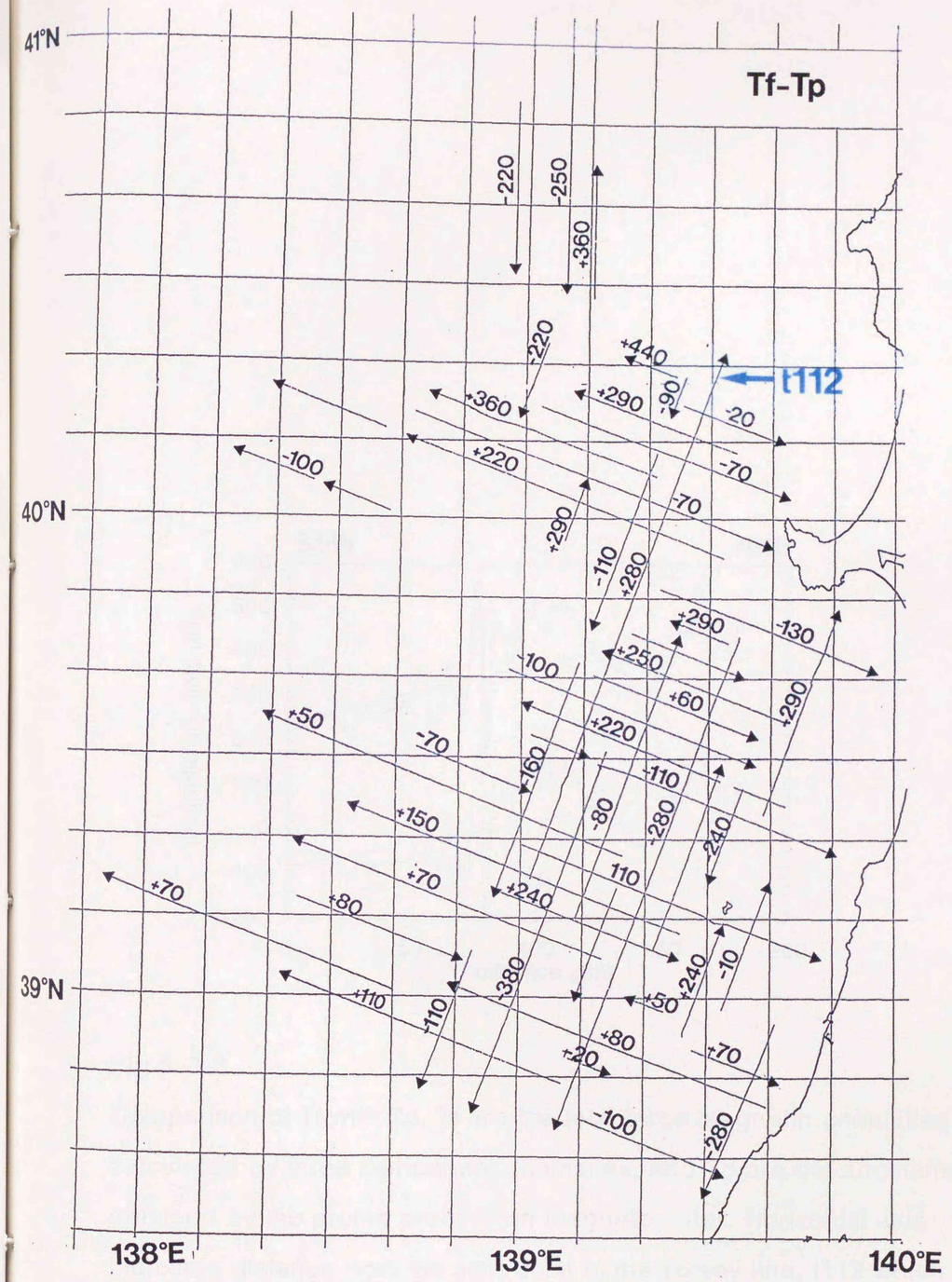

Fig.5-3-7

The differences between the total intensity calculated from the three component magnetic fields (Tf) and that measured by the proton precession magnetometer (Tp).

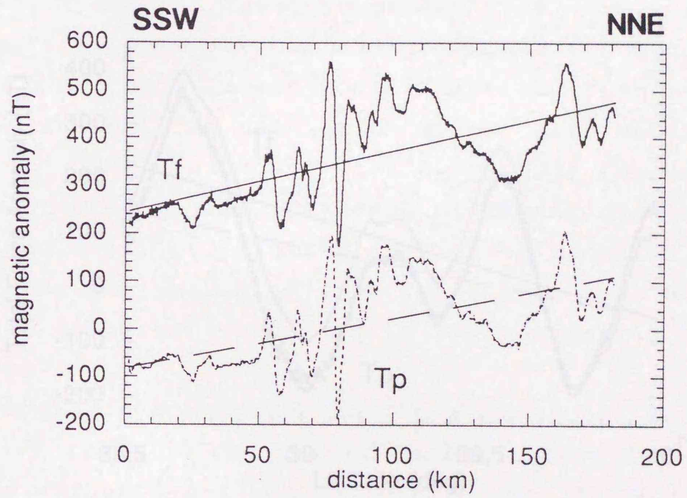

Fig.5-3-8

Comparison of Tf with Tp. Tf are the total force magnetic anomalies calculated by three component anomalies, and Tp are the anomalies obtained by the proton precession magnetometer. Horizontal axis indicates distance from the start point of the survey line, t112 which is located in Fig.5-3-7.

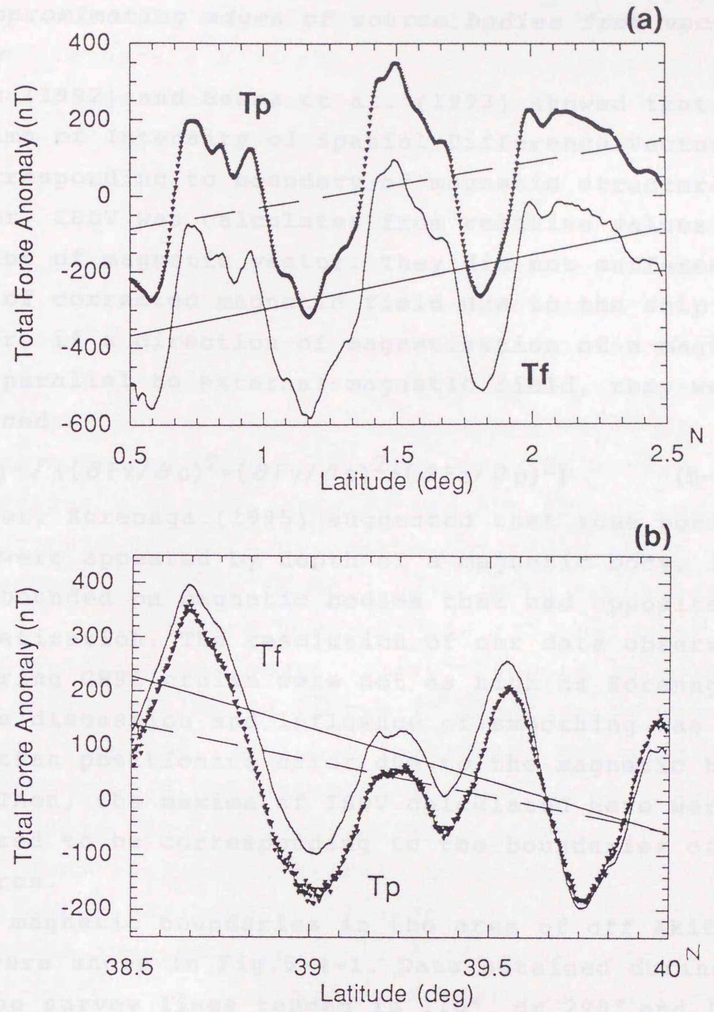

Fig.5-3-9

Total force magnetic anomaly profiles along 175° E. Tf is the anomaly calculated by three component anomalies, and Tp is the anomaly obtained by proton precession magnetometer. Horizontal axis indicates latitude.

a: 0.5° N - 2.5° N,

b: 38.5° N - 40.0° N

5.4. *Approximating edges of source bodies from vector anomaly*

Seama (1992) and Seama et al. (1993) showed that location of maxima of Intensity of Spatial Difference Vector (ISDV) was corresponding to boundary of magnetic structure. Moreover, ISDV was calculated from relative values of three component of magnetic vector. They did not suffered from errors of corrected magnetic field due to the ship's body. Moreover, if a direction of magnetization of a magnetic body wasn't parallel to external magnetic field, they were not influenced.

$$|\partial F/\partial p| = \sqrt{\{(\partial Fx/\partial p)^2+(\partial Fy/\partial p)^2+(\partial Fz/\partial p)^2\}} \quad (5\text{-}4\text{-}1)$$

However, Korenaga (1995) suggested that some position errors were appeared by depth of a magnetic body, if they didn't bounded on magnetic bodies that had opposite polarity of magnetization. The resolution of our data observed by STCM during GH91 cruise were not as high as Korenaga (1995)'s discussion and influence of smoothing was larger rather than positioning error due to the magnetic body's depth. Then, the maxima of ISDV calculated here were considered to be corresponding to the boundaries of magnetic structures.

Here, magnetic boundaries in the area of off Akita(39° N-40° N) were shown in Fig.5-4-1. Data obtained during GH91 along the survey lines tended in 110° or 290° and line length were more than 36km (2 hours) were used for this calculation. Their threshold level was set as 100nT/km basically, but influences of measurement error depended on peak patterns and water depth were considered when I judged whether the maxima was due to the magnetic boundary or other reasons.

Every ISDV profiles along each survey lines were shown

from North to South (Fig.5-4-2 to Fig.5-4-17). The horizontal axis in each figure indicated distance from starting point of survey lines. Every figure was drawn as the right side was east. The peak shown in Fig.5-4-1 were indicated with '*' in each figures. It should be suitable to the Analytic Signal shown in Fig.5-2-2.

One of advantages of using ISDV data to estimate magnetic boundaries was that rough data could also estimate magnetic boundaries. However, as horizontally, ISDV data were of doubtful accuracy, then it was very difficult to determine the threshold level and pick up signals due to magnetic boundaries. As this study, total force of magnetic anomalies were obtained enough and the survey lines were arranged like a lattice, there wasn't an advantage of using magnetic vector measured by STCM. Then, total forces of magnetic anomalies were used for all of later analysis.

If accuracy of magnetic vector anomalies measured by STCM become better to estimate direction of magnetization, they will contribute for structural modeling. However, total force magnetic anomaly profiles resembled Z component of magnetic vector anomaly profiles around Japan area. Therefore, ISDV profiles had larger inflection than differential calculus of total force magnetic anomaly profiles (dt/dp), when the horizontal component changed large. This was a standard to the most.

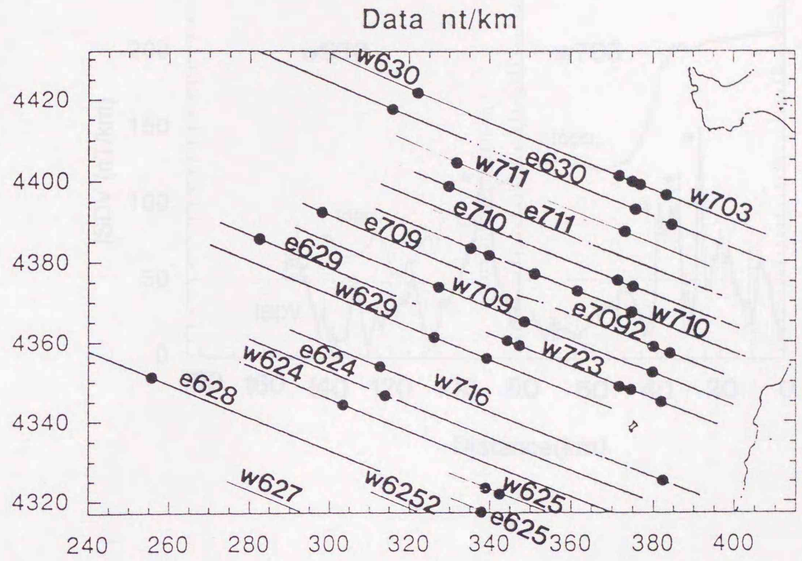

Fig.5-4-1

Solid circles indicate the maxima of the Intensity of Spatial Difference Vector(ISDV) on each survey lines.

Fig.5-4-1

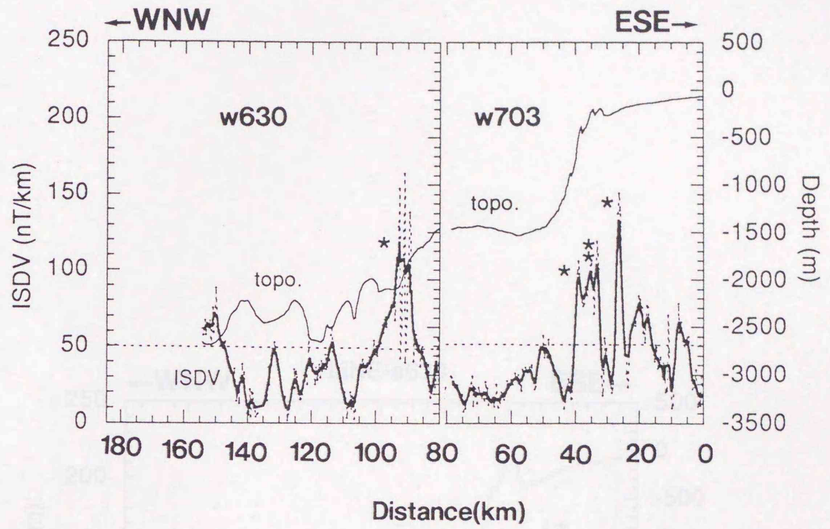

Fig.5-4-2

ISDV and bathymetry profiles on Line w630 and w703. Location of each lines are shown in Fig.5-4-1. Straight broken line indicates the threshold level. Broken curve indicates the original profile of ISDV. Thick solid curve imdicates the smoothed profiles by 5 data running mean method. Star marks(*) indicate the ISDV peaks shown in Fig.5-4-1.

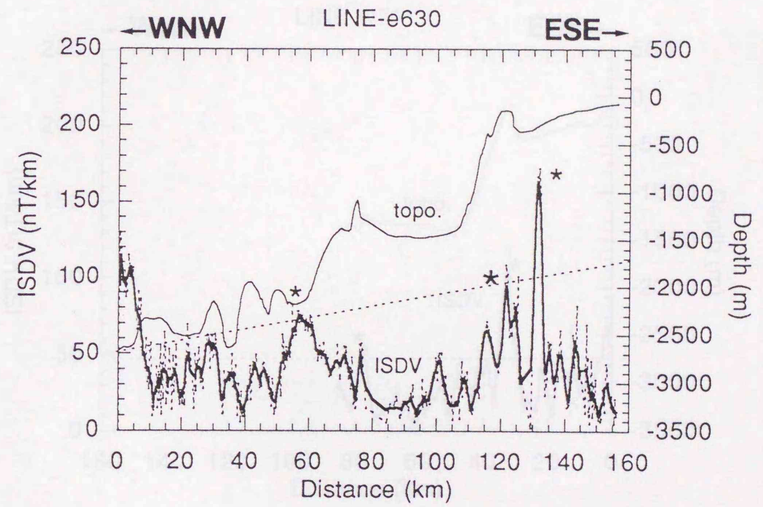

Fig.5-4-3

ISDV and bathymetry profiles on Line e630. Location of the line is shown in Fig.5-4-1. Straight broken line indicates the threshold level. Broken curve indicates the original profile of ISDV. Thick solid curve imdicates the smoothed profiles by 5 data running mean method. Star marks(*) indicate the ISDV peaks shown in Fig.5-4-1.

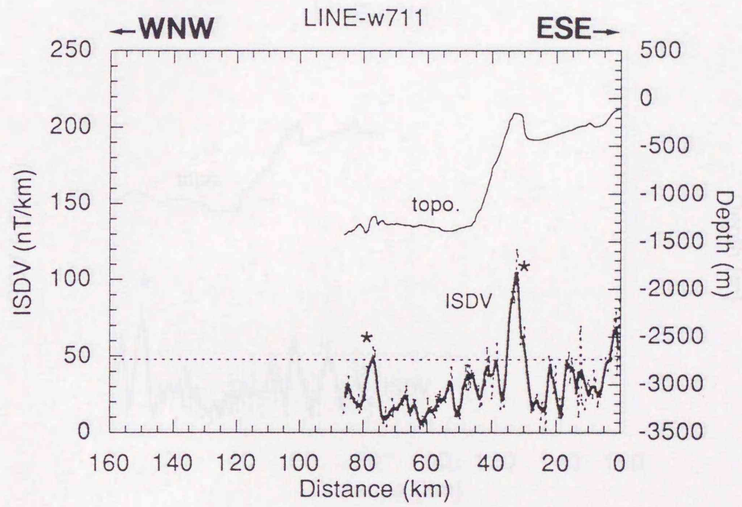

Fig.5-4-4

ISDV and bathymetry profiles on Line w711. Location of the line is shown in Fig.5-4-1. Straight broken line indicates the threshold level. Broken curve indicates the original profile of ISDV. Thick solid curve imdicates the smoothed profiles by 5 data running mean method. Star marks(*) indicate the ISDV peaks shown in Fig.5-4-1.

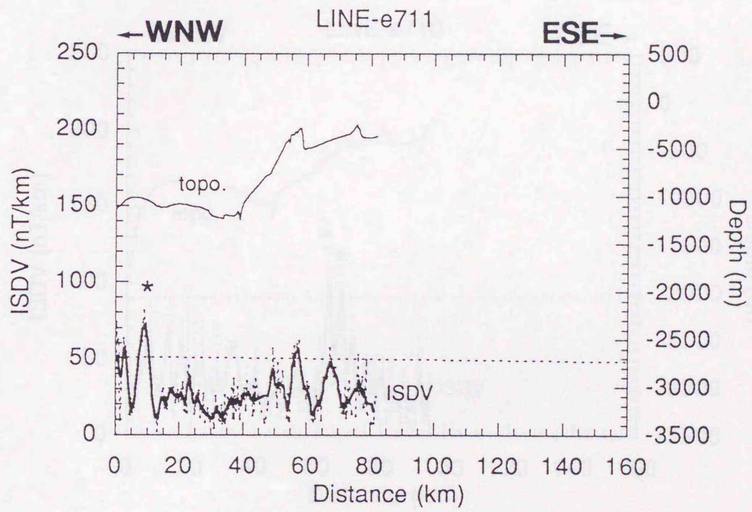

Fig.5-4-5

ISDV and bathymetry profiles on Line e711. Location of the line is shown in Fig.5-4-1. Straight broken line indicates the threshold level. Broken curve indicates the original profile of ISDV. Thick solid curve imdicates the smoothed profiles by 5 data running mean method. Star marks(*) indicate the ISDV peaks shown in Fig.5-4-1.

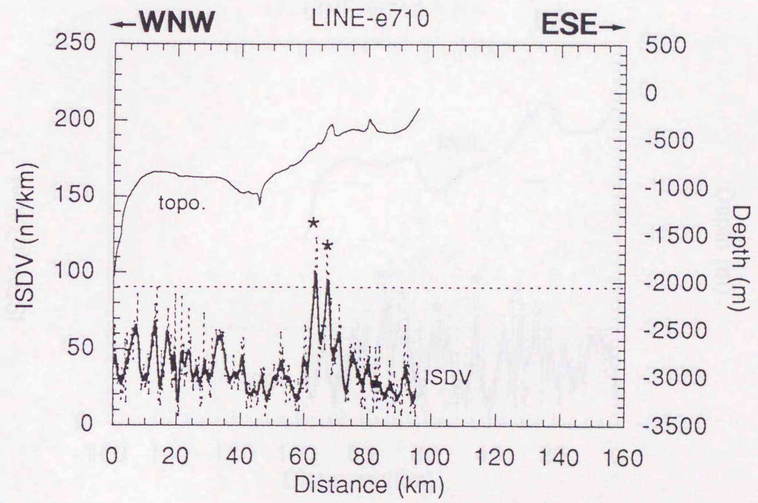

Fig.5-4-6

ISDV and bathymetry profiles on Line e710. Location of the line is shown in Fig.5-4-1. Straight broken line indicates the threshold level. Broken curve indicates the original profile of ISDV. Thick solid curve imdicates the smoothed profiles by 5 data running mean method. Star marks(*) indicate the ISDV peaks shown in Fig.5-4-1.

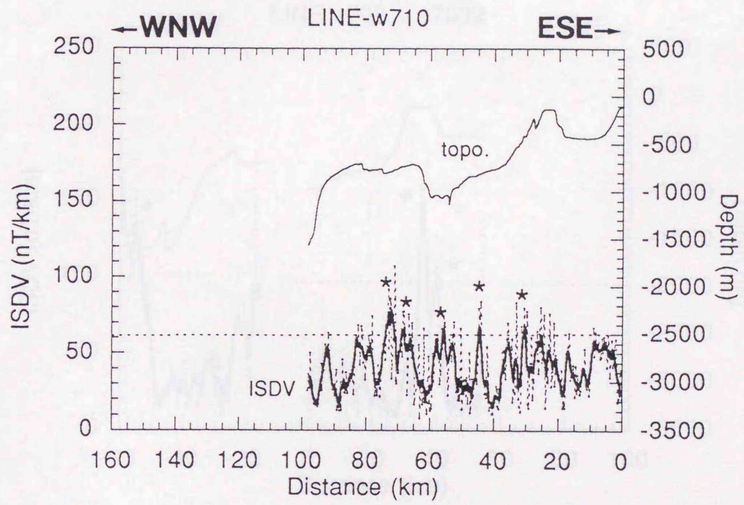

Fig.5-4-7

ISDV and bathymetry profiles on Line w710. Location of the line is shown in Fig.5-4-1. Straight broken line indicates the threshold level. Broken curve indicates the original profile of ISDV. Thick solid curve imdicates the smoothed profiles by 5 data running mean method. Star marks(*) indicate the ISDV peaks shown in Fig.5-4-1.

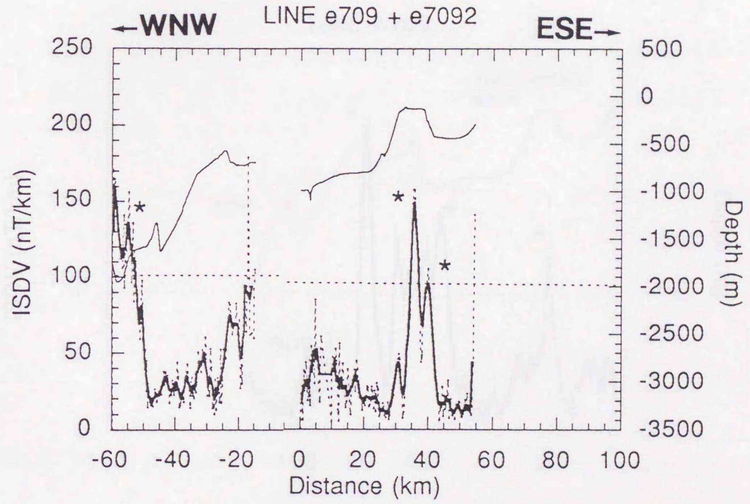

Fig.5-4-8

ISDV and bathymetry profiles on Line e709 and e7092. Location of each lines are shown in Fig.5-4-1. Straight broken line indicates the threshold level. Broken curve indicates the original profile of ISDV. Thick solid curve imdicates the smoothed profiles by 5 data running mean method. Star marks(*) indicate the ISDV peaks shown in Fig.5-4-1.

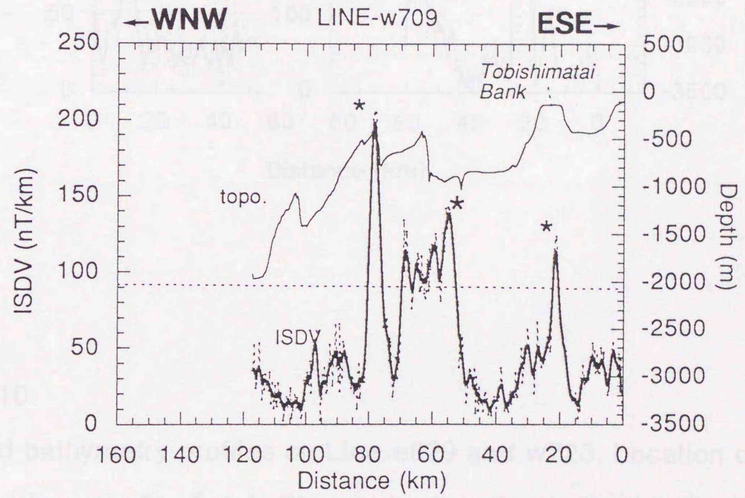

Fig.5-4-9

ISDV and bathymetry profiles on Line w709. Location of the line is shown in Fig.5-4-1. Straight broken line indicates the threshold level. Broken curve indicates the original profile of ISDV. Thick solid curve imdicates the smoothed profiles by 5 data running mean method. Star marks(*) indicate the ISDV peaks shown in Fig.5-4-1.

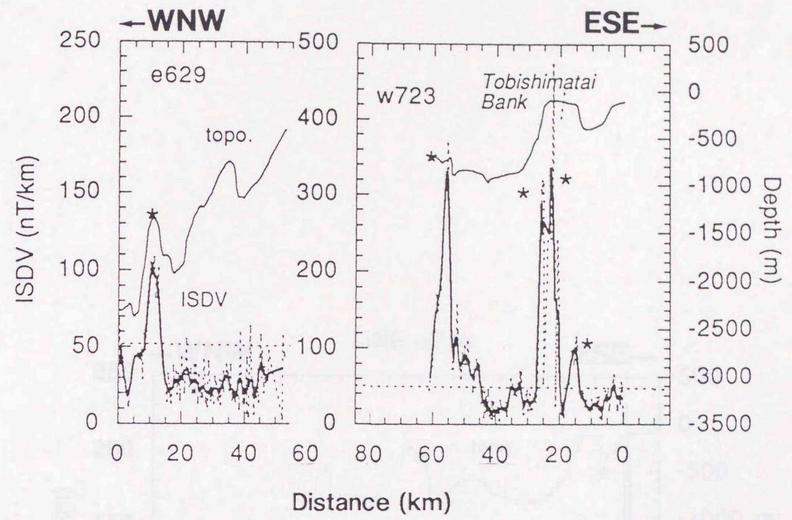

Fig.5-4-10

ISDV and bathymetry profiles on Line e629 and w723. Location of each lines are shown in Fig.5-4-1. Straight broken line indicates the threshold level. Broken curve indicates the original profile of ISDV. Thick solid curve imdicates the smoothed profiles by 5 data running mean method. Star marks(*) indicate the ISDV peaks shown in Fig.5-4-1.

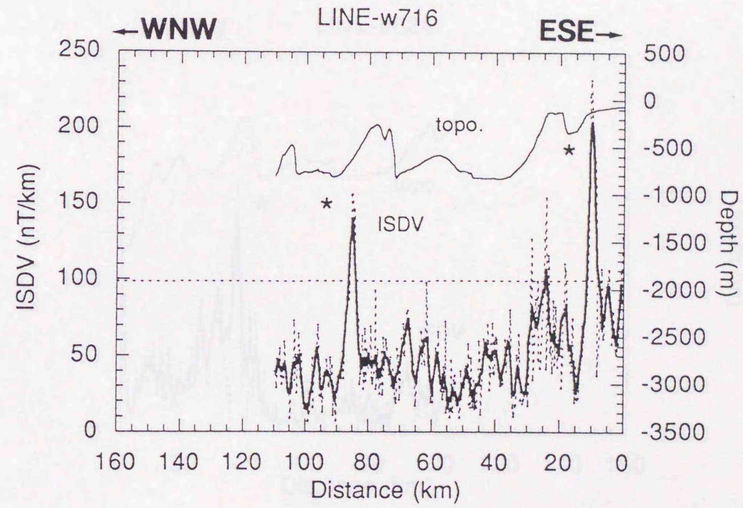

Fig.5-4-11

ISDV and bathymetry profiles on Line w716. Location of the line is shown in Fig.5-4-1. Straight broken line indicates the threshold level. Broken curve indicates the original profile of ISDV. Thick solid curve imdicates the smoothed profiles by 5 data running mean method. Star marks(*) indicate the ISDV peaks shown in Fig.5-4-1.

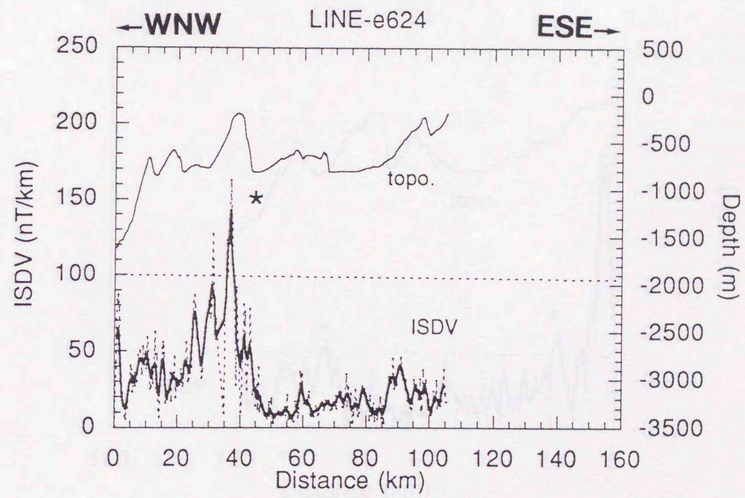

Fig.5-4-12

ISDV and bathymetry profiles on Line e624. Location of the line is shown in Fig.5-4-1. Straight broken line indicates the threshold level. Broken curve indicates the original profile of ISDV. Thick solid curve imdicates the smoothed profiles by 5 data running mean method. Star marks(*) indicate the ISDV peaks shown in Fig.5-4-1.

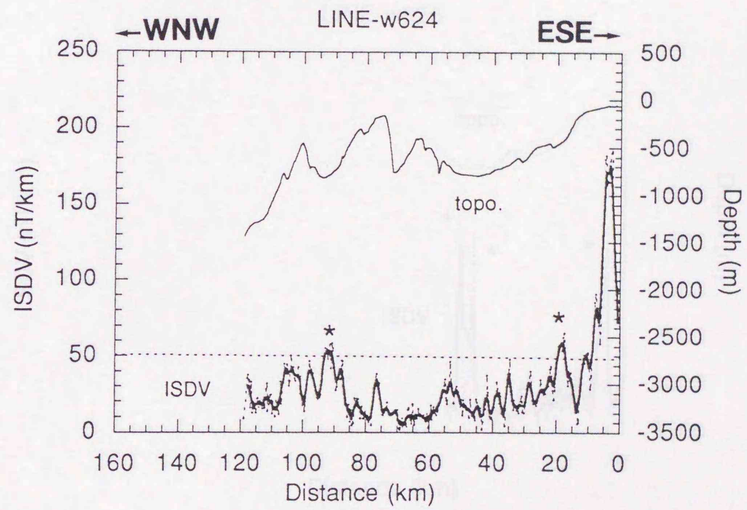

Fig.5-4-13

ISDV and bathymetry profiles on Line w624. Location of the line is shown in Fig.5-4-1. Straight broken line indicates the threshold level. Broken curve indicates the original profile of ISDV. Thick solid curve imdicates the smoothed profiles by 5 data running mean method. Star marks(*) indicate the ISDV peaks shown in Fig.5-4-1.

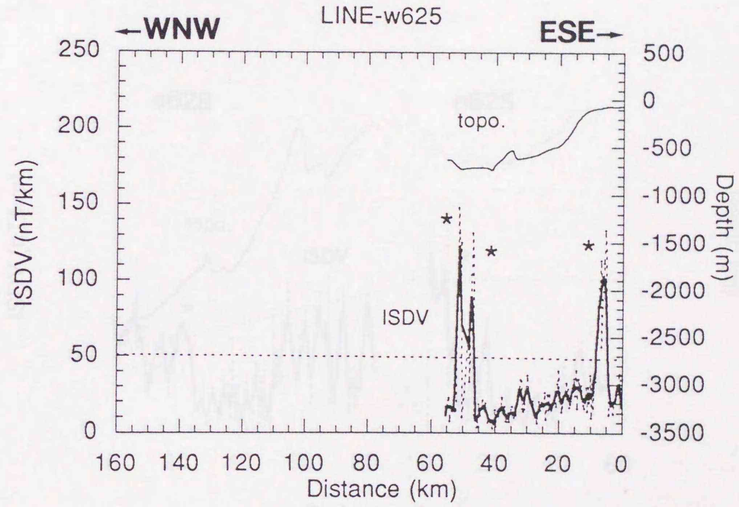

Fig.5-4-14

ISDV and bathymetry profiles on Line w625. Location of the line is shown in Fig.5-4-1. Straight broken line indicates the threshold level. Broken curve indicates the original profile of ISDV. Thick solid curve imdicates the smoothed profiles by 5 data running mean method. Star marks(*) indicate the ISDV peaks shown in Fig.5-4-1.

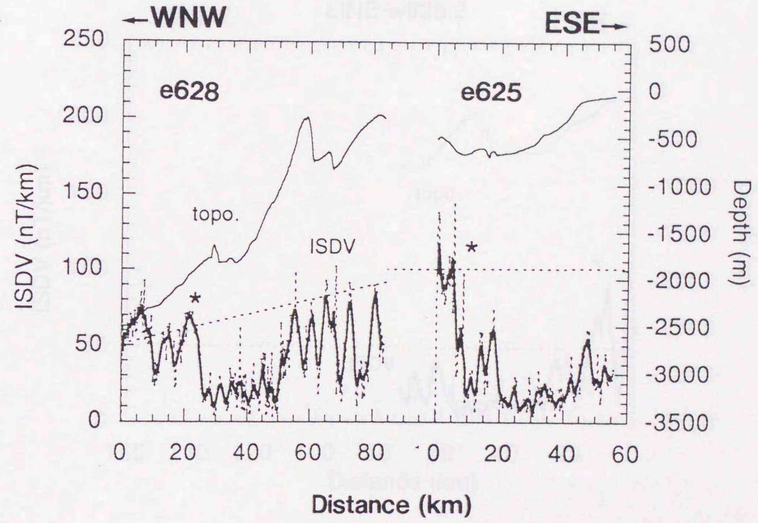

Fig.5-4-15

ISDV and bathymetry profiles on Line e628 and e625. Location of each lines are shown in Fig.5-4-1. Straight broken line indicates the threshold level. Broken curve indicates the original profile of ISDV. Thick solid curve imdicates the smoothed profiles by 5 data running mean method. Star marks(*) indicate the ISDV peaks shown in Fig.5-4-1.

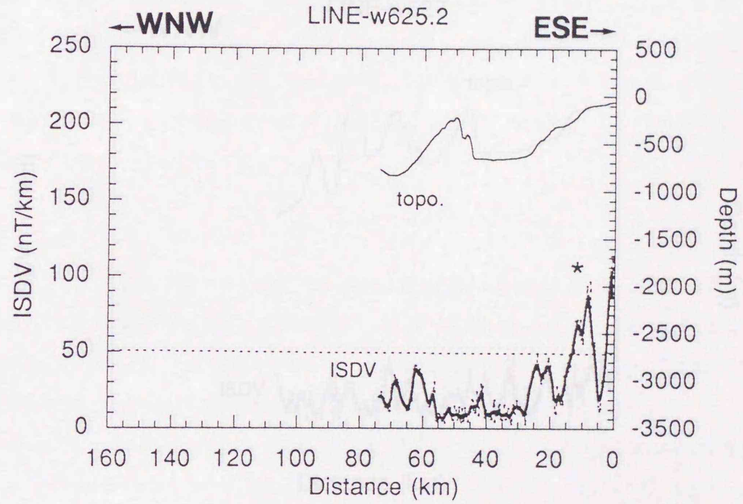

Fig.5-4-16

ISDV and bathymetry profiles on Line w6252. Location of the line is shown in Fig.5-4-1. Straight broken line indicates the threshold level. Broken curve indicates the original profile of ISDV. Thick solid curve imdicates the smoothed profiles by 5 data running mean method. Star marks(*) indicate the ISDV peaks shown in Fig.5-4-1.

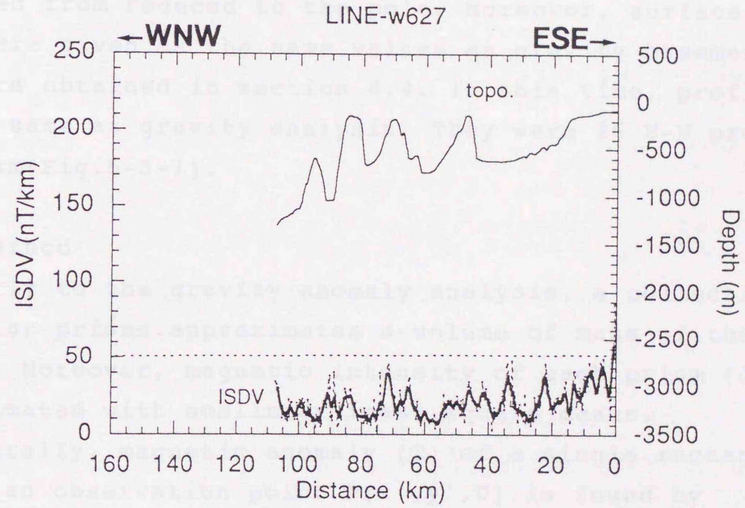

Fig.5-4-17

ISDV and bathymetry profiles on Line w627. Location of the line is shown in Fig.5-4-1. Straight broken line indicates the threshold level. Broken curve indicates the original profile of ISDV. Thick solid curve imdicates the smoothed profiles by 5 data running mean method. There were no ISDV peaks shown in Fig.5-4-1.

5.5. *Estimation of magnetic intensity distribution, 2.5-dimensional modeling*

Generally, not all parameters of each magnetic body were determined uniquely from measured magnetic anomalies. Especially, structural parameters (location, width, length, shape, and depth) and magnetization parameters (direction and intensity of magnetization vector) were not determined both. Therefore, we often gave location, magnetic body size (width, length), shape, and direction of magnetization beforehand. Moreover, the surface depth of magnetic bodies or intensity of magnetization was often set as parameters. Here, the distribution of magnetic intensities was calculated from reduced to the pole. Moreover, surface depths were given as the same values as gravity basement, which were obtained in section 4.4. In this time, profiles were the same as gravity analysis. They were 26 E-W profiles every 10km(Fig.5-5-1).

5.5.1. Method

Similarly to the gravity anomaly analysis, a collection of rectangular prisms approximates a volume of mass of the basement. Moreover, magnetic intensity of each prism (J) were estimated with nonlinear least square means.

In generally, magnetic anomaly (T) of a single rectangular prism at an observation point P(x',y',0) is found by equation 5-5-1 by Bhattacharryya (1964). It is on the right hand coordinate system that considers +z as downward (See Fig.4-4-1).

$$T(x',y')=-kJF(p,q,z)p=p1,p2|q=q1,q2|z=h+d,h$$

$$F(p,q,z)=c_{yz}\{\log((R-p)/(R+p))\}+c_{zx}\{\log((R-q)/(R+q))\}$$
$$+c_{xy}\{\log((Rz)/(R+z))\}+c_x\{\tan^{-1}((qz)/(Rp))\}$$
$$+c_y\{\tan^{-1}((pz)/(Rq))\}+c_z\{\tan^{-1}((pq)/(Rz))\} \quad (5\text{-}5\text{-}1)$$

where,

$R=\sqrt{(p^2+q^2+z^2)}$, $c_i=e_ip_i$ $(i=x,y,z)$,

$c_{ij}=(e_ip_j+e_jp_i)/2$ $((i,j)=(x,y),(y,z),(z,x))$

And, k is given as 1 in emu system, and $1/4\pi$ in SI system, (p_x,p_y,p_z) is a direction cosine of a magnetization, (e_x,e_y,e_z) is a direction cosine of an external magnetic field, and J is magnetic intensity. And, surface depth as h, thickness as d, center of a prism surface as (x_0,y_0,h), a prism with dimensions described by the limits;

$-a<x<a$, $-b<y<b$, and $h<z<h+d$.

Here,

$x=x'-x_\emptyset$, $y=y'-y_\emptyset$, $p1=-x+a$, $p2=-x-a$, $q1=-y+b$, and $q2=-y-b$.

Here, 2.5-D analysis applied least square means was described. The same as gravity analysis, the centerlines of prisms were parallel to Y-axis, length of each prism for direction of X-axis was given enough long against surface depth. Moreover, assumed observed points were set along the Y-axis.

As considering a position of a magnetic body for y, and an observation point for i, a magnetic anomaly at an observation point y was;

$$T_y = \Sigma\ J_i w_{iy} \quad (y=1,2,,) \qquad (5\text{-}5\text{-}2)$$

w_{iy} was a structural factor of magnetic anomaly at an observation point y due to a magnetic body at point i, and J_i was a magnetic intensity of a magnetic body at point i.

Here, a distribution of magnetic intensity, J_i was calculated. Then, the most suitable J_i made minimum squares of residual between observed data (F_y) and calculated data (T_y).

$$R=\Sigma\ (F_y-T_y)^2 \rightarrow \text{minimum}. \qquad (5\text{-}5\text{-}3)$$

Where a position of magnetic body was given as k,

$$\partial R/\partial Jk=(\partial/\partial J_k)\{\Sigma\ (F_y-T_y)^2\}$$
$$=-2\Sigma\ (F_y-T_y)w_{ky}$$
$$=2\{\Sigma\ (\Sigma\ w_{iy}w_{ky})J_i-\Sigma\ F_yw_{ky}\}$$
$$=\emptyset \qquad (5\text{-}5\text{-}4)$$

Solve it.

In generally, if the magnetization and external fields are vertical, positive magnetic anomaly is located over a magnetic body. Therefore, measured total force of magnetic field were transformed into 'reduced to the pole'. The transformation used a double Fourier transform filter (Kato, 1987).

The Poisson's relation was shown as;

$$V=(J/\rho G)(\partial U/\partial p) \qquad (5\text{-}5\text{-}5)$$

where, Gravity potential for U, magnetic potential for V, density for ρ, Newton's gravitational constant for G, magnetization direction for p, and magnetization intensity for J.

Pseudo-gravity and reduced to the pole were transformed from total force magnetic field depended on the relation. Where, pseudo-gravity anomaly for G(x,y,z), reduced to the pole anomaly for P(x,y,z), and pseudo-gravitational potential for UG(x,y,z);

$$G(x,y,z)=(\partial/\partial z)UG(x,y,z) \qquad (5\text{-}5\text{-}6)$$

$$P(x,y,z)=(\partial^2/\partial z^2)UG(x,y,z) \qquad (5\text{-}5\text{-}7)$$

On the other hand, magnetic potential, V(x,y,z), total force magnetic anomaly, T(x,y,z), and direction of magnetization, p, and external field, e, were shown as;

$$V(x,y,z)=-(\partial/\partial p)UG(x,y,z) \quad (5\text{-}5\text{-}8)$$

$$T(x,y,z)=-(\partial/\partial e)V(x,y,z) \quad (5\text{-}5\text{-}9)$$

Here, a transformation of total force magnetic anomaly into reduced to the pole was as follows; to integrate to direction of external field(inclination 50° , declination N8 ° W), to integrate again to direction of magnetization(here the same as external field), to differentiate to vertical twice. The relationships of transformation were shown in Fig.5-5-2.

5.5.2. Modeling

Similarly to a gravity anomaly analysis from 38° N to 40° 20'N in the eastern margin of the Japan Sea, the 26 E-W direction profiles every 10km were taken for magnetic intensity analysis. The same as gravity analysis, observed points were set along the Y-axis, and length of each prisms for direction of X-axis were given enough long against surface depth. First, the surface depths of prisms were estimated from gravity anomalies. The analysis was assumed two layers model which Bouguer correction density was 2.3g/cm^3 and density contrast between sediment and basement layers was 0.4g/cm^3. Next, the depth of gravity basement was regarded as the same as the magnetic basement, and calculated intensities of magnetization from reduced to the pole anomalies.

If depths of "magnetic basement" are calculated from reduced to the pole anomalies, it is very difficult to give a magnetic intensity. For example, the profiles across the Torimiguri Bank were shown in Fig.5-5-3. Upper one showed

basement depth profiles calculated from Bouguer anomalies. The profile B was calculated with density contrast 0.3g/cm^3, C was 0.4g/cm^3, and D was 0.5g/cm^3. They looked to be similar. On the other hand, middle one showed basement depth profiles calculated from magnetic anomalies. The profile E was calculated with magnetic intensity 0.1A/m, F was 0.3A/m, and G was 0.5A/m. They were different. Moreover, lower one showed the profile C and F. The shape and depth of gravity basement and magnetic basement were quite different. Moreover, the seismic profile looked to be similar to the profile C. It suggested that magnetic anomalies were affected by distribution of magnetized intensities more than basement shapes.

The locations of 26 profiles were shown in Fig.5-5-1. Each attached numbers were values on N-S axis of UTM coordinate system which an origin of longitude was 141° E and an origin of latitude was the equators.

Magnetic anomalies calculated from magnetic bodies as a uniform magnetization were not conformed to observed magnetic anomalies. It showed that a variation of magnetization was large. Moreover, any other constraint conditions were not given in the calculation except that all prisms became deeper than water depth. Then, the intensities obtained from the calculation were relative values.

Apparent magnetic intensities were shown in Fig.5-5-4. The negative values mean that their intensities were very weak. They didn't mean negative magnetization.

It clearly showed two borderlines between the strong area and the weak area. One was between profile No.4450 and No.4460. Magnetic intensities along the profile No.4460 became stronger than other southern profiles. The profile No.4460 was located around a clear geological boundary that

Sado Ridge disappeared here and Okushiri Ridge appeared. Another boundary was corresponding to the line from Sakata to Japan Basin, which direction was NW-SE.

Each results of modeling along these profiles were shown in these figures from Fig.5-5-5 to Fig.5-5-13. They were arranged from the north (No.4460) to south (No.4210). Profiles No.4460 to No.4440 (in Fig.5-5-5) showed that their western part had very thin sedimentary layers and they were deep. Thick sedimentary layers appeared around the profile No.4430 (in Fig.5-5-6).

For example, on the profile No.4380 (in Fig.5-5-7) at Easting 320km along Horizontal-axis, gravity basement deepened steeply. It was interpreted as a fault. Because a fracture zone close to a fault should become low-density zone. Distribution of such a ditches (steeply deepened zone) were corresponding to faults shown by Okamura,et al. (1995b). These faults were shown in Fig.5-5-1. Moreover, the zones which magnetization became strong were corresponding to the ditch zones interpreted as faults. The profiles trended in E-W directions, then data did not suffered seriously from transformation errors by influence that direction of magnetization were given as average values of external field. The strong intensity of magnetization zone was interpreted as volcanic rocks intruded into fracture zone along faults, if basement ditches were regarded as faults.

Furthermore, a basement deep zone in the Mogami Trough continued from profile No.4240 to profile No.4230 (in Fig.5-5-12).

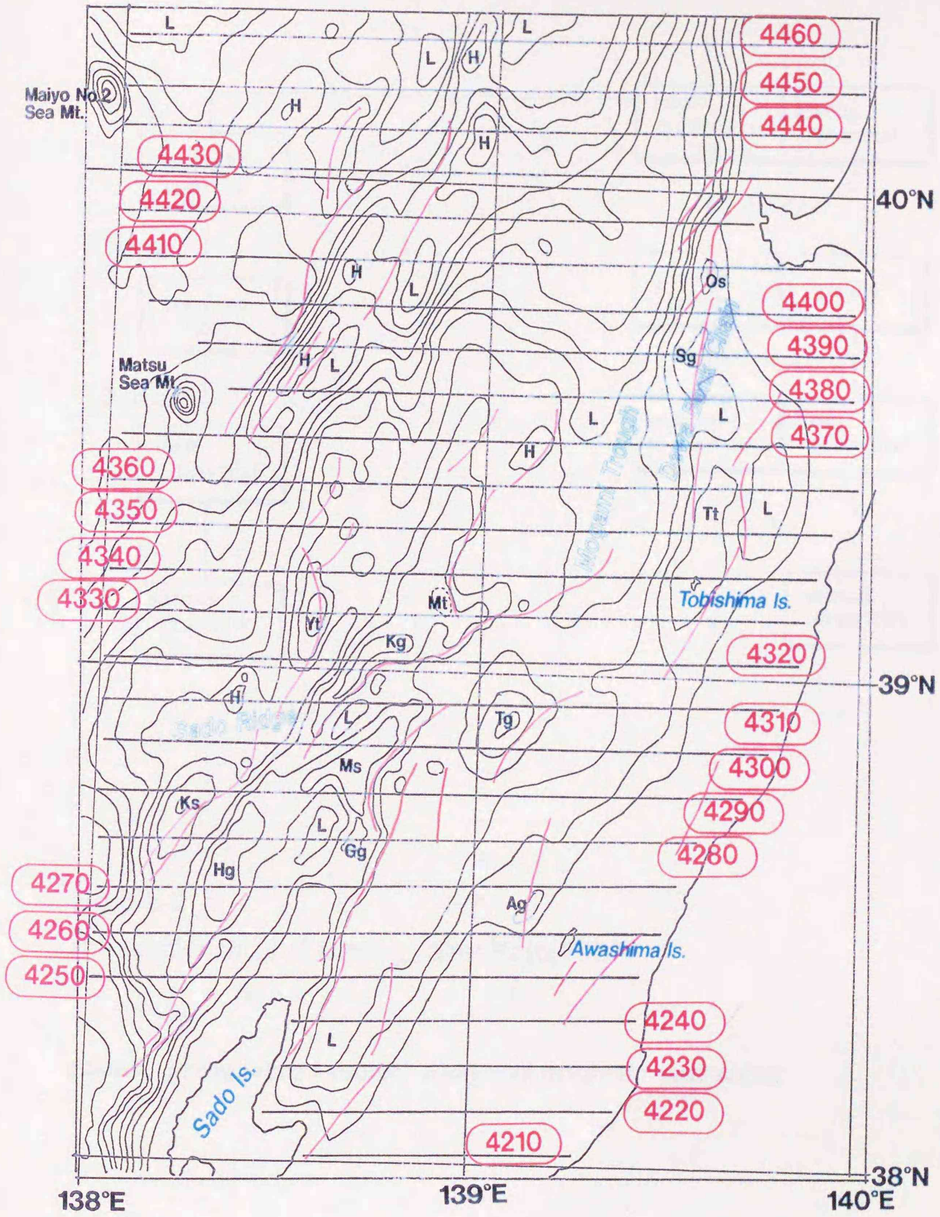

Fig.5-5-1

Index map of E-W profiles. Contour indicate bathymetry and its interval is 200m. Red lines show the distribution of reactivated reverse fault after Okamura et al(1995b).

H means topographic high and L means topographic low.

Os:Ogamukouse Bank, Sg:Shinguri Bank, Tt:Tobishimatai Bank, Ag:Awashimaguri Bank, Gg:Gassanguri Bank, Hg:Hyotanguri Bank, Ks:Koshijisho Bank, Ms:Mukouse Bank, Kg:Kamaguri Bank, Yt:Yahikotai Bank, Tg:Torimiguri Bank, Mt:Mogamitai Bank.

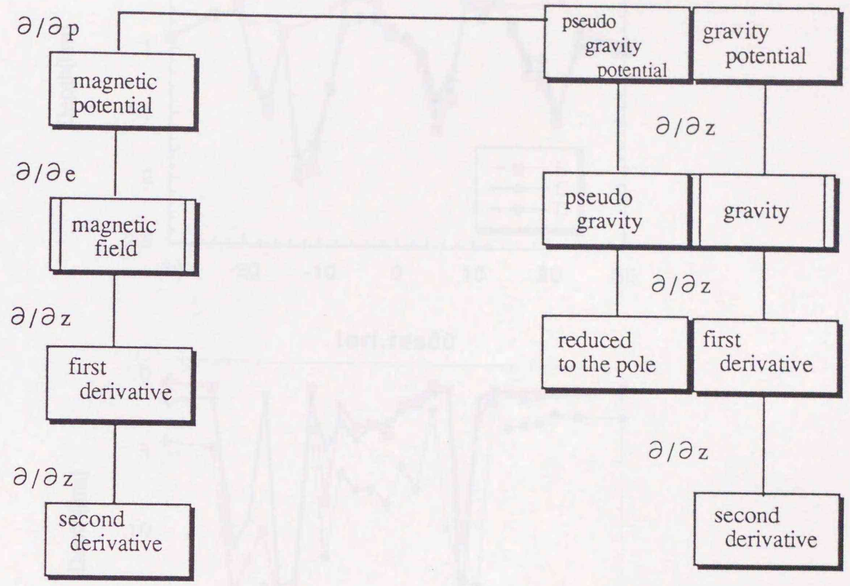

Fig.5-5-2
The relationships of filtering. after Kato(1987)

z:down, p:magnetized vector, e:external magnetic field vector

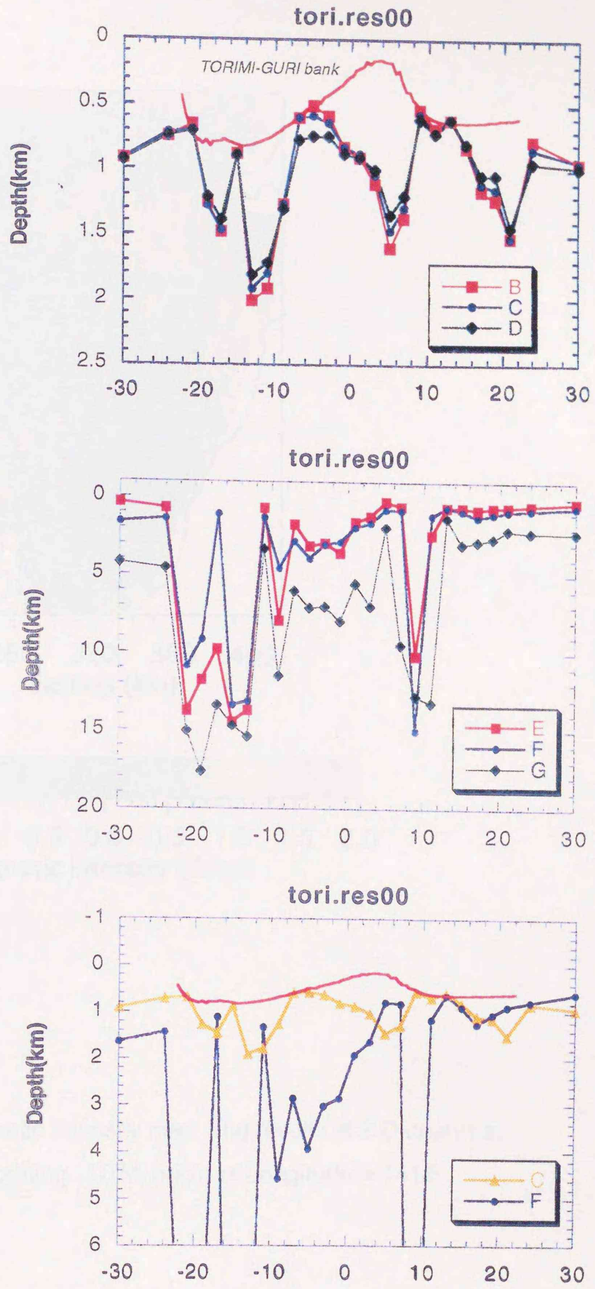

Fig.5-5-3

The profiles across the Torimiguri Bank.

Upper : Basement depth calculated from Bouguer anomalies. Density contrast B; 0.3g/cm^3, C; 0.4 g/cm^3, D; 0.5 g/cm^3 *Middle*: Basement depth profiles calculated from magnetic anomalies. Magnetic intensity E; 0.1 A/m, F; 0.5 A/m, G; 1.0 A/m. *Lower* : C; gravity basement (density contrast 0.4 g/cm^3) F; magnetic basement (magnetic intensity 0.5 A/m)

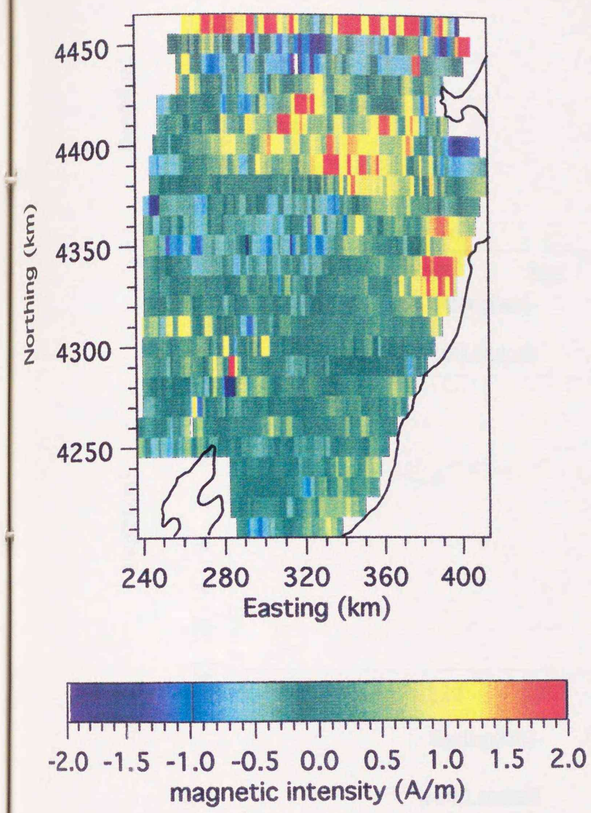

Fig.5-5-4

Apparent magnetic intensity map. The results of 2-D analysis.

Easting and Northing : UTM, origin of Longitude = 141E

spy_dat_6 vs. (row, col)

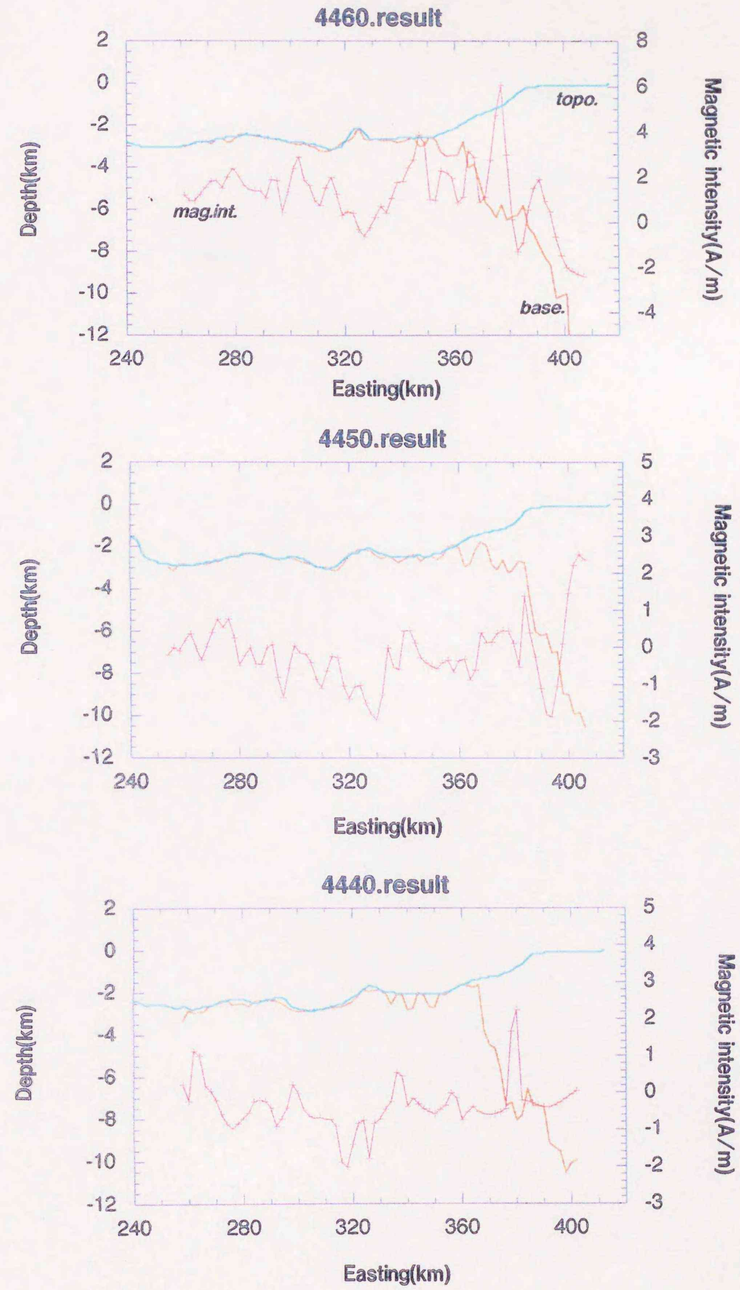

Fig.5-5-5

Line 4460, 4450, 4440

Bathymetry(blue), gravity basement depth(orange), and apparent magnetic intensity(red) profiles along E-W lines. Location of profiles are shown in Fig.5-5-1. Easting means UTM value whose origin longitude is 141° E.

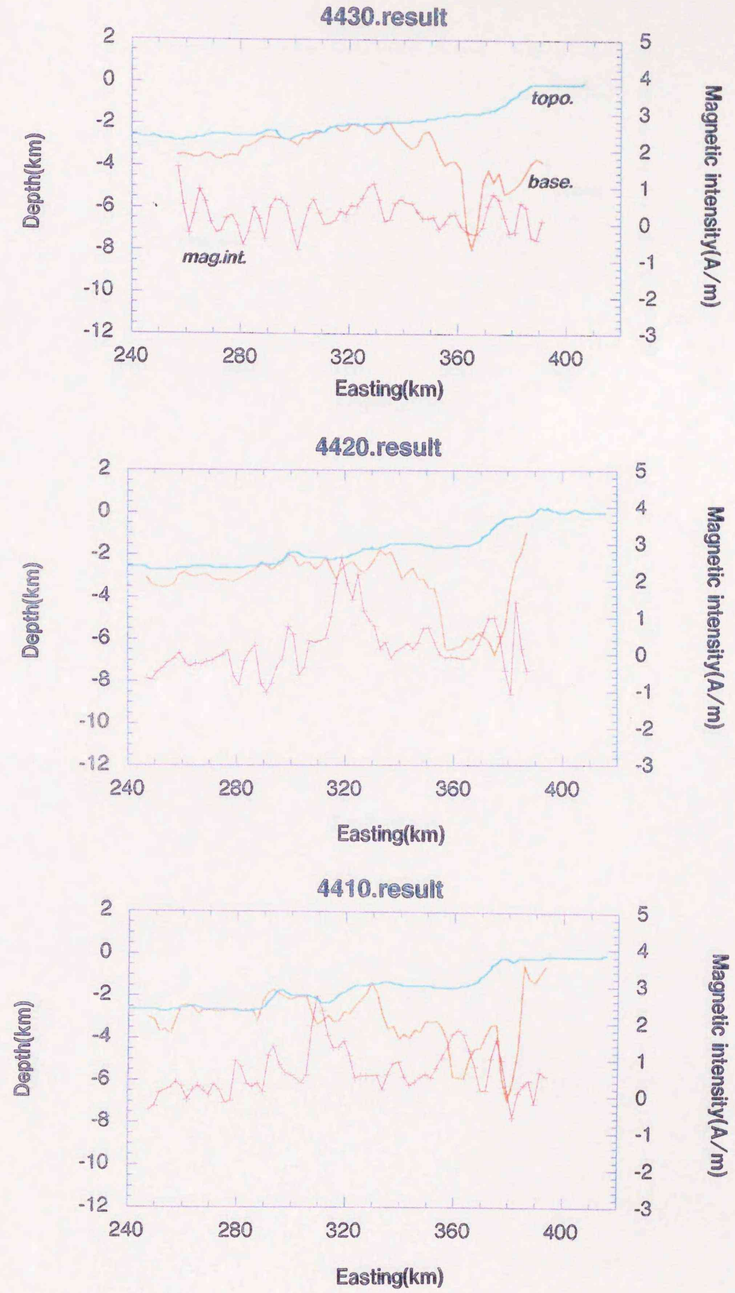

Fig.5-5-6

Line 4430, 4420, 4410 : Off Oga Pen.

Bathymetry(blue), gravity basement depth(orange), and apparent magnetic intensity(red) profiles along E-W lines. Location of profiles are shown in Fig.5-5-1. Easting means UTM value whose origin longitude is 141° E.

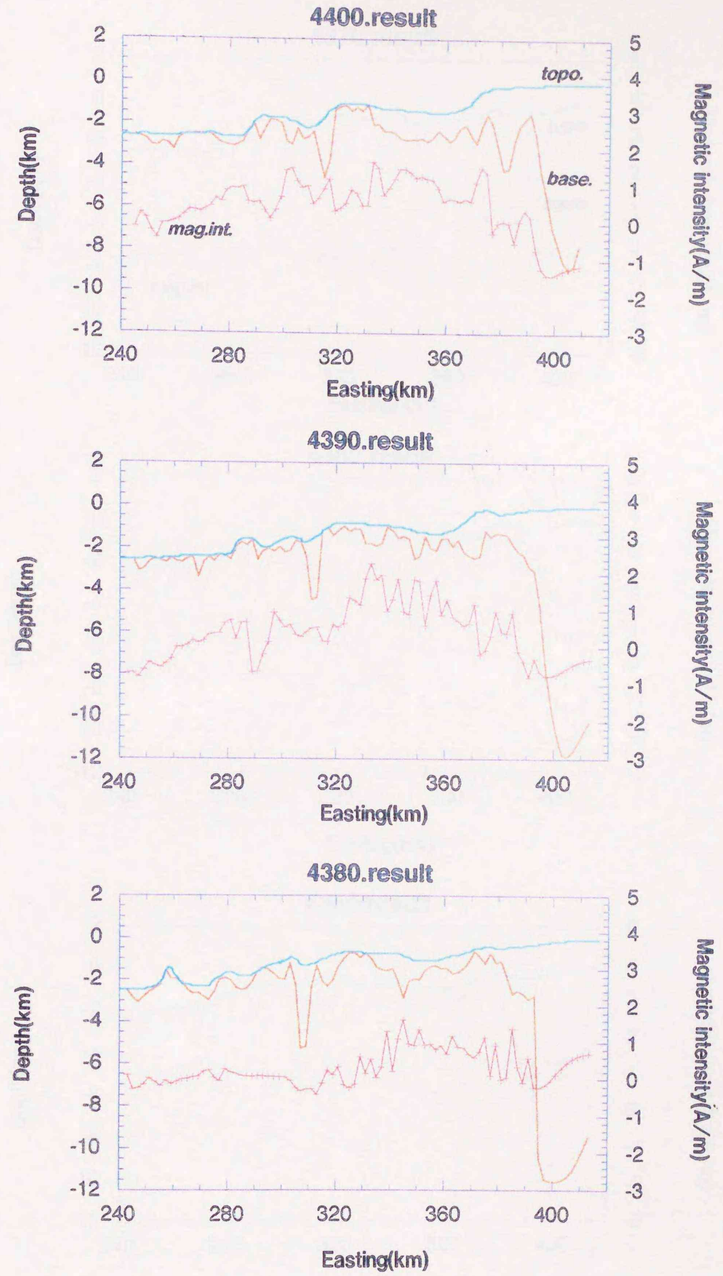

Fig.5-5-7

Line 4400, 4390, 4380 : Dewa Bank Chain

Bathymetry(blue), gravity basement depth(orange), and apparent magnetic intensity(red) profiles along E-W lines. Location of profiles are shown in Fig.5-5-1. Easting means UTM value whose origin longitude is 141° E.

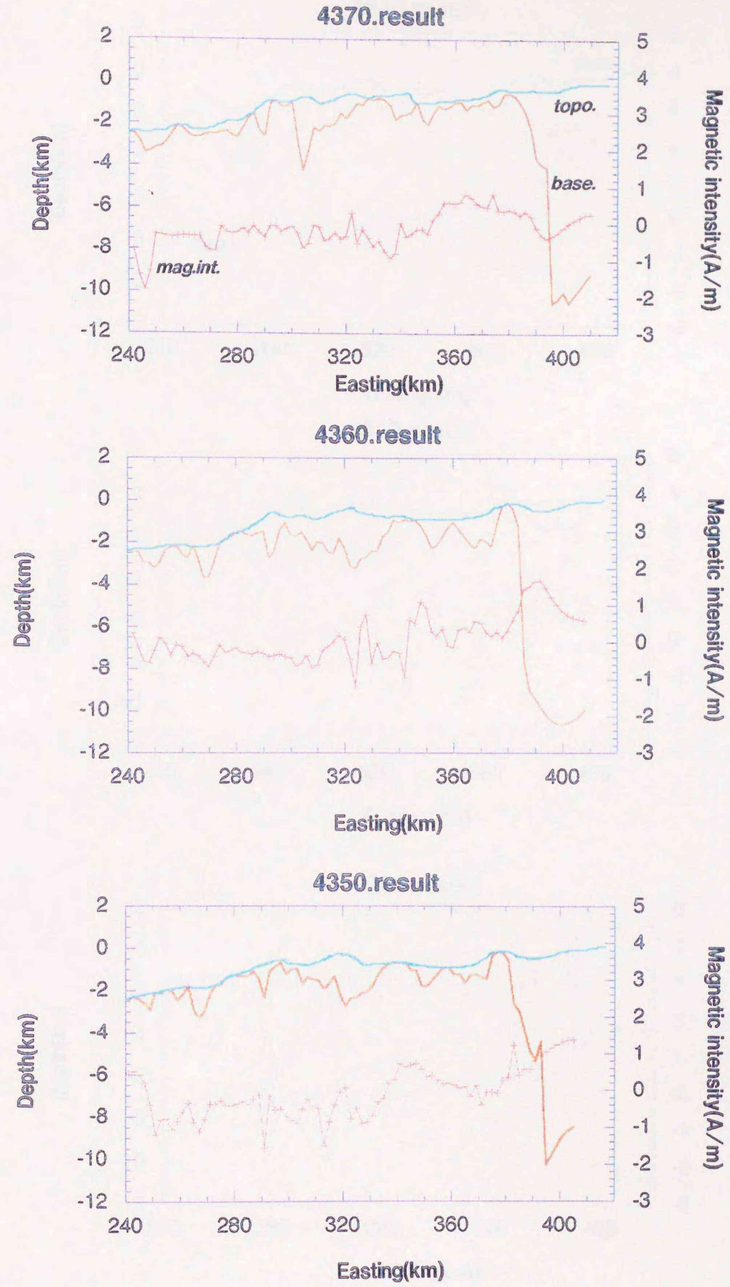

Fig.5-5-8

Line 4370, 4360, 4350 : Akita Basin

Bathymetry(blue), gravity basement depth(orange), and apparent magnetic intensity(red) profiles along E-W lines. Location of profiles are shown in Fig.5-5-1. Easting means UTM value whose origin longitude is 141° E.

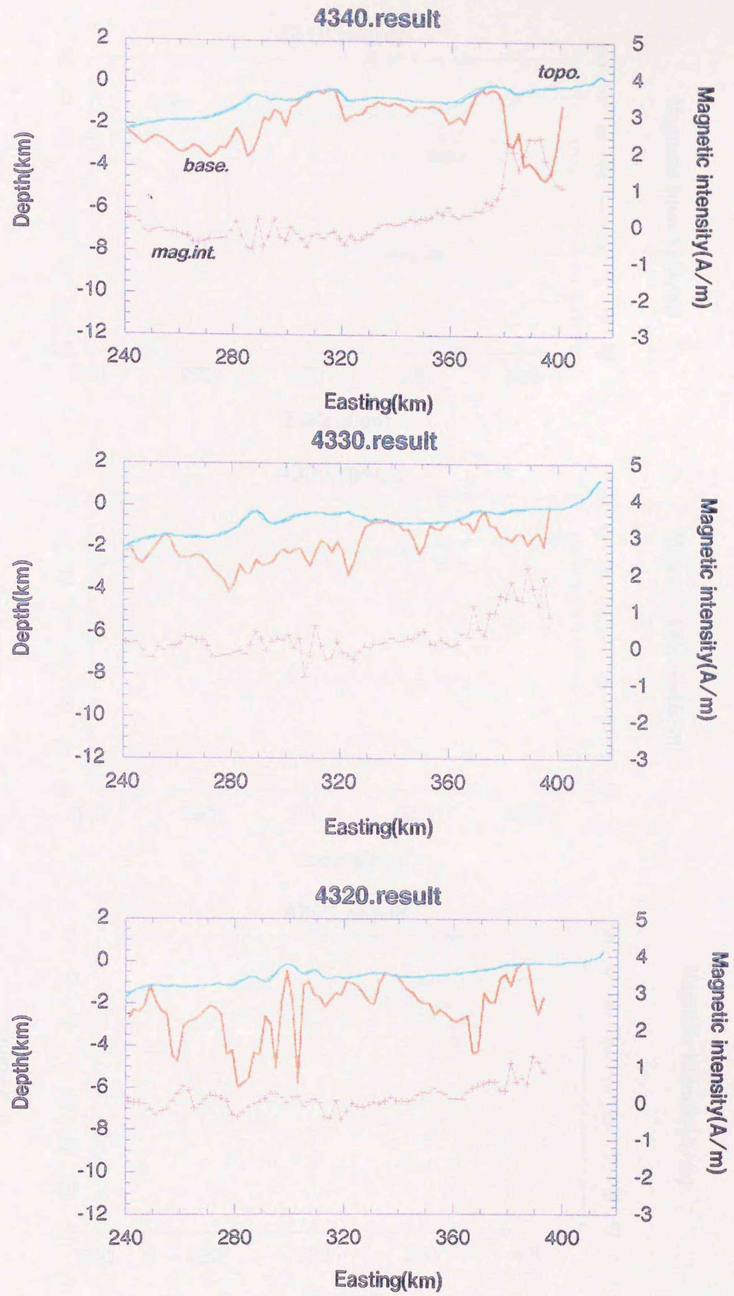

Fig.5-5-9

Line 4340, 4330, 4320 : Mogamitai, Yahikotai, Kamaguri Banks

Bathymetry(blue), gravity basement depth(orange), and apparent magnetic intensity(red) profiles along E-W lines. Location of profiles are shown in Fig.5-5-1. Easting means UTM value whose origin longitude is 141° E.

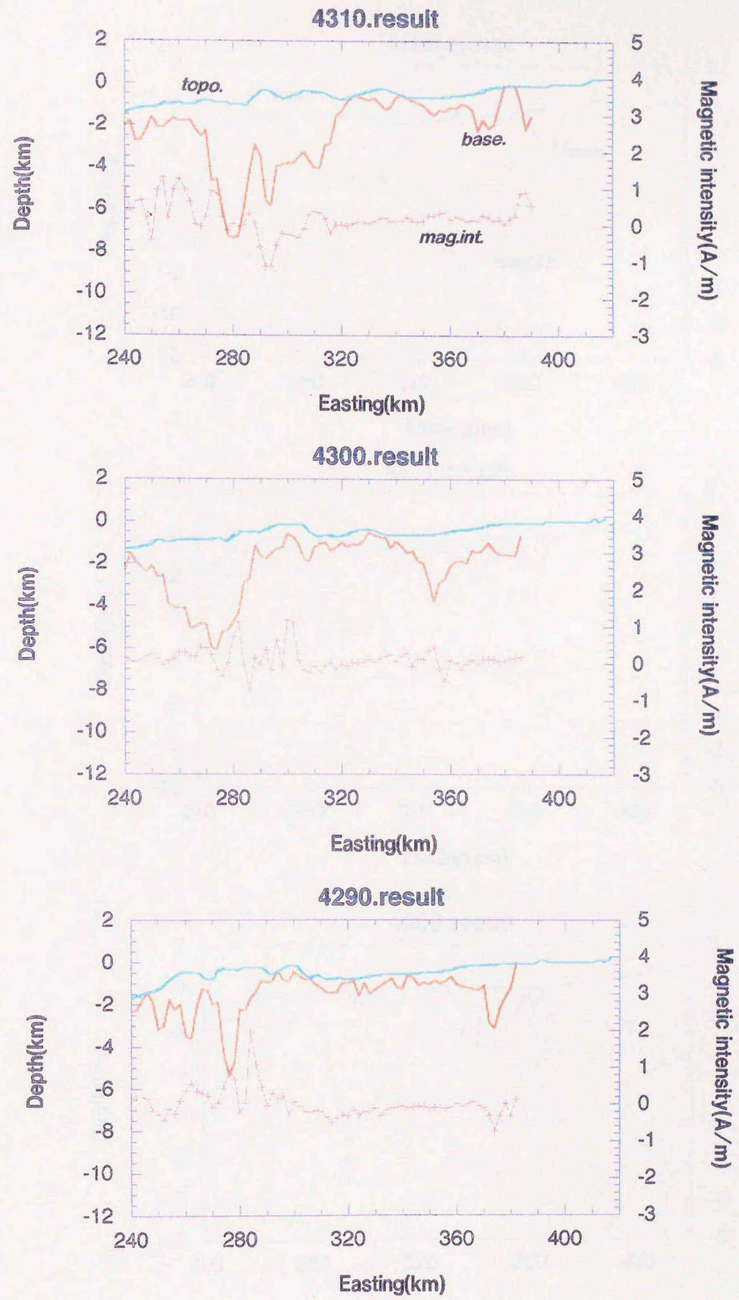

Fig.5-5-10

Line 4310, 4300, 4290 : Torimiguri Bank

Bathymetry(blue), gravity basement depth(orange), and apparent magnetic intensity(red) profiles along E-W lines. Location of profiles are shown in Fig.5-5-1. Easting means UTM value whose origin longitude is 141° E.

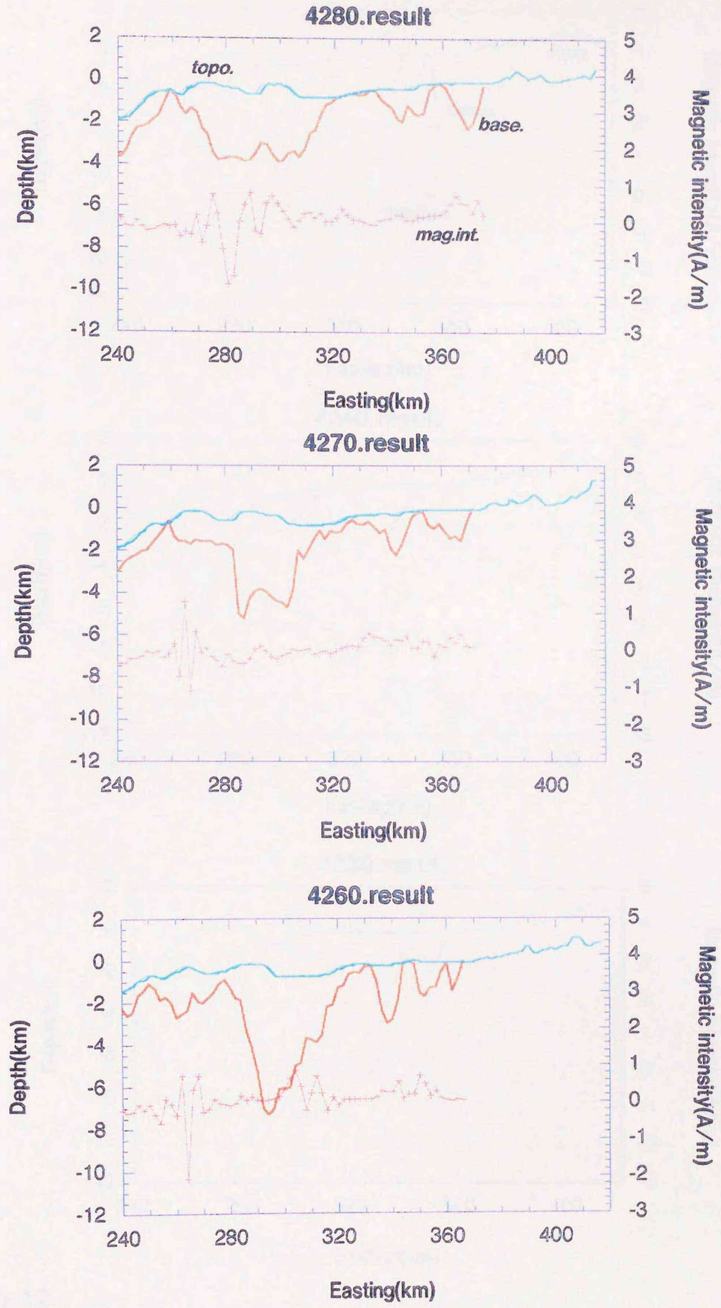

Fig.5-5-11

Line 4280, 4270, 4260 : Hyotanguri, Awashimaguri Banks

Bathymetry(blue), gravity basement depth(orange), and apparent magnetic intensity(red) profiles along E-W lines. Location of profiles are shown in Fig.5-5-1. Easting means UTM value whose origin longitude is 141° E.

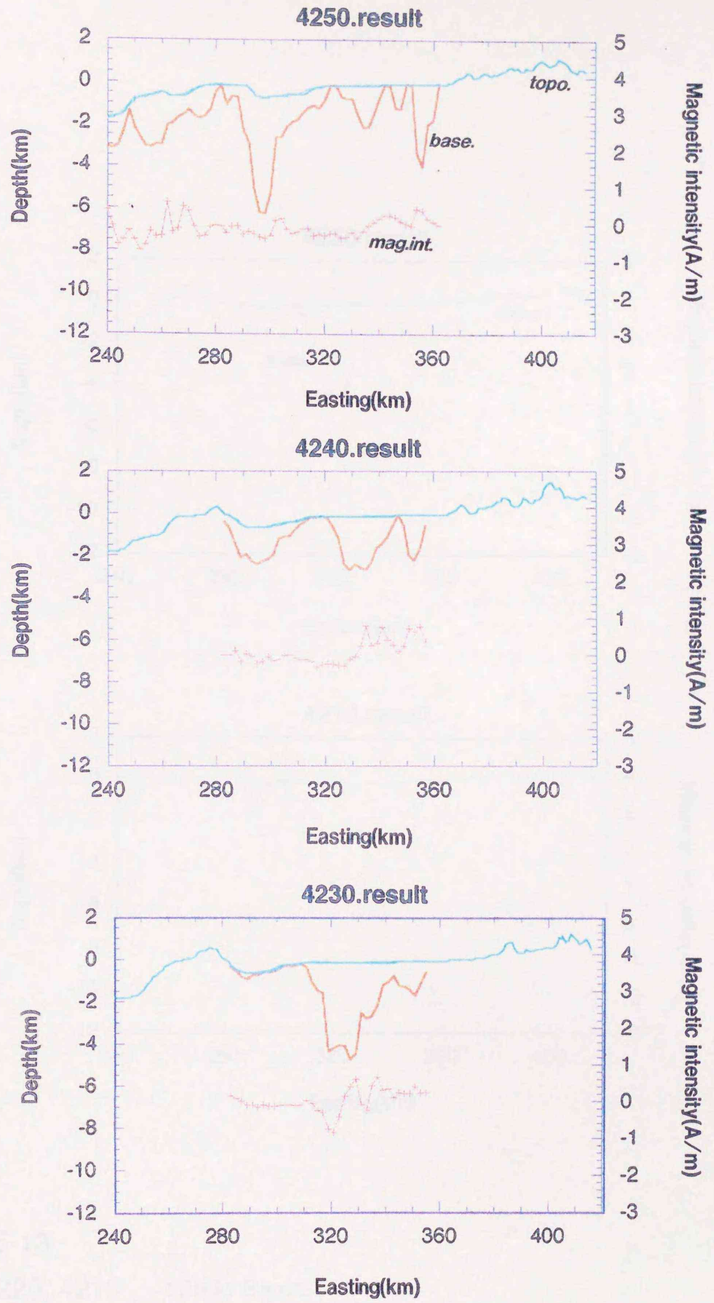

Fig.5-5-12

Line 4250, 4240, 4230 : North of Sado Island

Bathymetry(blue), gravity basement depth(orange), and apparent magnetic intensity(red) profiles along E-W lines. Location of profiles are shown in Fig.5-5-1. Easting means UTM value whose origin longitude is 141° E.

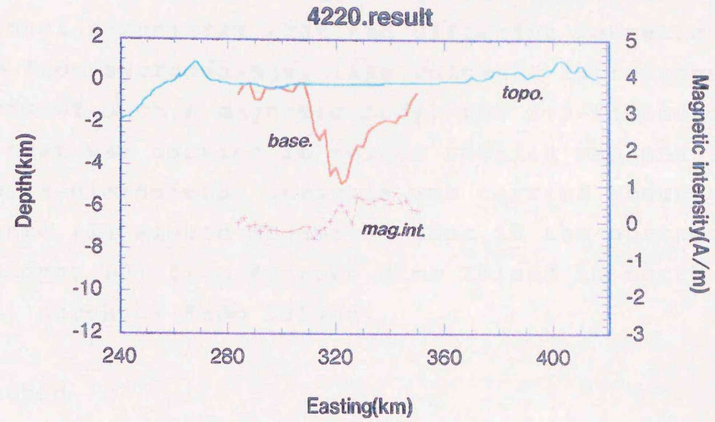

Fig.5-5-13

Line 4220, 4210 : Sado Basin

Bathymetry(blue), gravity basement depth(orange), and apparent magnetic intensity(red) profiles along E-W lines. Location of profiles are shown in Fig.5-5-1. Easting means UTM value whose origin longitude is 141° E.

5.6. *Estimation of magnetic intensity distribution, 3-dimensional modeling*

There were many magnetic boundaries around Sado Ridge, which were estimated by distribution of maxima of Analytic Signals. These boundaries suggested that they were caused by 3-dimensional structures that had different magnetic intensity from surroundings, like volcanic intrusions. For an analysis of such a magnetic body, the 2.5-dimensional analysis that was carried in former section was unsuitable. Therefore, 3-dimensional analysis was carried about three areas, where (1) around Mogamitai Bank in the northern part of Sado Ridge, (2) from Kyuroku Jima Island to north of Sado Ridge, (3) north of Sado Island.

5.6.1. Method

The method to estimate a magnetic intensity distribution was followed after Okuma et al. (1994). As described in Section 5.5.1, considering a position of a magnetic body for x, and an observation point for i, a magnetic anomaly at an observation point x was;

$$T_x = \sum J_i w_{ix} \quad (x=1,2,,) \qquad (5\text{-}6\text{-}1)$$

w_{ix} was a structural factor of magnetic anomaly at an observation point x due to a magnetic body at point i, and J_i was a magnetic intensity of a magnetic body at point i.

Here, a distribution of magnetic intensity, J_i was calculated. Then, the most suitable J_i made minimum squares of residual between observed data(F_x) and calculated data(T_x).

$$R=\sum (F_x-T_x)^2 \rightarrow \text{minimum}. \qquad (5\text{-}6\text{-}2)$$

Where a position of magnetic body was given as k,

$$\partial R/\partial J_k=(\partial/\partial J_k)\{\Sigma (F_x-T_x)^2\}$$
$$=-2\Sigma (F_x-T_x)w_{kx}$$
$$=2\{\Sigma (\Sigma w_{ix}w_{kx})Ji-\Sigma F_x w_{xy}\}$$
$$=\emptyset \qquad (5\text{-}6\text{-}3)$$

Solve it.

However, it was difficult to solve linear equation, $\partial R/\partial J_k=0$, because a dimension of i and k of equation (5-6-3) became too large in fact. There,

$$D_i=\Sigma (F_x-T_x)w_{ix} \quad (i=1,2,,,) \qquad (5\text{-}6\text{-}4)$$

Equation (5-6-3) became

$$\partial R/\partial J_k=-2D_i \qquad (5\text{-}6\text{-}5)$$

The equation showed, an inclination vector of R at spatial $J_i(i=1,2,,,)$ trended toward opposite of vector $\{D_i\}$, and R decreased for a direction of vector $\{D_i\}$ locally. For a unit vector $\{s_i\}$ of the vector $\{D_i\}$ was,

$$s_i=D_i/\sqrt{(\Sigma D_i^2)} \qquad (5\text{-}6\text{-}6)$$

As given the most suitable magnetic intensity ΔJ, considered J_i as

$$\Delta J_i=s_i \Delta J.$$

Consequently,

$$J_i^{(n+1)}=J_i^{(n)}+\Delta J_i^{(n)} \qquad (5\text{-}6\text{-}7)$$

Revisions were repeated.

Here, the most suitable magnetic intensity ΔJ was decided as follows. After (n) times of revisions, a revision value $\Delta J_i^{(n)}$ was decided, for equation (5-6-2) became

$$R^{(n+1)}=\Sigma (F_x-T^{(n)}{}_x-\Delta J^{(n)}\Sigma s_i^{(n)}w_{ix})^2 \qquad (5\text{-}6\text{-}8)$$

The most suitable value of $\Delta J^{(n)}$ made $R^{(n+1)}$ minimized, and it was satisfied

$$\partial R^{(n+1)}/\partial \Delta J=\emptyset.$$

Then,

$$\Delta J^{(n)}=\Sigma \{(F_x-T^{(n)}{}_x)\Sigma s_i^{(n)}w_{ix}\}/\Sigma (\Sigma s_i w_{ix})^2 \qquad (5\text{-}6\text{-}9)$$

As considered as equations (5-6-6) and (5-6-9), the most suitable revision quantity of J_i became $\Delta J_i=s_i \Delta J$,

$$\Delta J^{(n)}=D_i^{(n)}\Sigma \{(F_x-T^{(n)}{}_x)\Sigma D_i^{(n)}w_{ix}\}/\Sigma (\Sigma D_i^{(n)}w_{ix})^2 \qquad (5\text{-}6\text{-}10)$$

These relations were rewritten as 2-dimensional expression,

$$J_{ij}^{(n+1)}=J_{ij}^{(n)}+\Delta J_{ij}^{(n)} \qquad (5\text{-}6\text{-}11)$$

$$\Delta J_{ij}^{(n)}=D_{ij}^{(n)}\Sigma \{(F(x,y)-T^{(n)}(x,y))E^{(n)}(x,y)\}/\Sigma (\Sigma E^{(n)}(x,y))^2 \qquad (5\text{-}6\text{-}12)$$

$$E^{(n)}(x,y)=\Sigma \Sigma D_{ij}^{(n)}w_{ij}(x,y) \qquad (5\text{-}6\text{-}13)$$

$$D_{ij}^{(n)}(x,y)=\Sigma \Sigma \{(F(x,y)-T^{(n)}(x,y))w_{ij}(x,y)\} \qquad (5\text{-}6\text{-}14)$$

From equation (5-6-11) to equation (5-6-14), an approximate calculation depending on repeated revisions in order to estimate the most suitable magnetic intensity distribution. To shorten calculation time, the calculation area was divided into some windows.

5.6.2. Northern part of the Sado Ridge -off Akita area-

1) Regional-residual separation

Observed magnetic anomalies were strongly influenced by regional magnetic field, then in order to isolate the residual anomalies due to local magnetic structures. The regional field was removed using the upward continuation transforms (Gupta and Ramani, 1980). To estimate the most suitable altitude for the upward continuation transforms, the mean depth of basement was calculated from the gradient to power spectrum of magnetic anomalies. Here, observed magnetic anomalies were transformed into Fourier domain, and

natural logarithm of power spectrum ($\log_e P$) was plotted versus frequency (f) for a horizontal axis. Then, an average depth (D) was estimated from the gradient of equation as $\log_e P = c - 4\pi Df$.

First, the mean depth of magnetic layer of off Akita area(39° N-40° N) was estimated from a gradient of a power spectrum(Fig.5-6-1). The result was 0.9km. This mean depth (=0.9km) was too shallow in comparison with the water depth. It was expected that some locally strong magnetizations made mean depth became too shallow. Therefore, as similar method of Section 4.5, depths of gravity basement were calculated. Assumed density was 2.0g/cm^3, and density contrast between sediment and basement layers was 0.4g/cm^3. The gravity basement depths were calculated around 2-3km below sea surface. Then, magnetic anomalies were transformed to the 4km (above sea surface) upward continuation as regional magnetic field. Moreover, the 0.5km upward continuation filter was used for removing high frequency anomalies as noise. Accordingly, observed magnetic anomalies were transformed to 0.5km upward continuation data. Next, the regional anomalies were calculated by 4km upward continuation. Then, the regional anomalies were subtracted from 0.5km upward continuation data. The residual magnetic anomalies were given as signal.

An N-S profile was shown in Fig.5-6-2 as a sample of this calculation. The location of the profile was shown in Fig.5-6-3 as line A-A'. The profiles indicated that 4km upward continuation data were suitable to the regional field.

The residual magnetic anomaly map was shown in Fig.5-6-3.

2) Initial setting

First, gravity basement was calculated. The surface density was assumed as 2.0g/cm^3, and basement density was 2.4g/cm^3. The linear trend of Bouguer anomalies was separated. Basement depth was calculated due to the residual gravity anomalies. The result was shown in Fig.5-6-4. Then, magnetic basement was regarded as the same of gravity basement. Moreover, the basement density (2.4g/cm^3) was suitable value for basement. Tertiary green-tuff layer was thought as basement.

Here, magnetic anomalies at sea surface were calculated from a combination of prism models which each size was 1km×1km×4km. Surface depths of each prism were given as gravity basement depth. Where, magnetizations of each prism were given as unique. Their direction was parallel to external magnetic field(inclination; 50° , declination; N8° W), and intensity was 1.0A/m. The calculated anomalies due to undulations of the gravity basement were shown in Fig.5-6-5. Moreover, residual magnetic anomalies separated from regional magnetic anomalies were also shown in Fig.5-6-6. For easy comparing, the same N-S profile of Fig.5-6-2 was shown in Fig.5-6-7. The solid line (obs) indicated the residual magnetic anomalies, and broken line (base) indicated the calculated magnetic anomalies due to undulations of the gravity basement. A, B, and C indicated shallow gravity basement rises. Positive peaks of residual magnetic anomalies; a and b became larger than calculated anomalies. They were looked to correlate with basement rise B. It showed that magnetic intensity of rise B should be stronger than 1.0A/m. And negative peak which was a pair of positive anomaly, a, looked to be shifted to south. The reason was surmised that anomaly 'b' interfered anomaly 'a'. On the other hand, remarkable magnetic anomalies were not

correlated with the rise A. This was suggested that a magnetization corresponding to the rise A was not so strong.

Then, it was difficult to recognize volcanic intrusions by gravity anomalies, because the density contrast between the basement and volcanic intrusions assumed to be small. Therefore, magnetic anomalies were quite useful.

3) Apparent magnetization intensity

For this calculation, the direction of magnetization was assumed to be parallel to external magnetic field, and surface depth of magnetic bodies were given the same as those of gravity basement.

A calculation method was the same way as Okuma et al. (1994). The result was shown in Fig.5-6-8. It was overlaid with gravity basement contours. Where, the calculated magnetic intensities were relative, and color pattern was significant.

The strong parts of magnetic intensity were suitable to volcanic intrusions, and they were located around structural boundaries of gravity basement or deepened zones. On the other hand, there were two reasons to explain the weak parts of magnetic intensity. One was that magnetic intensity was weak in structural, another was that deep negative anomalies were made by interference surrounding strong magnetic intensities, then magnetic intensities were calculated weak apparently.

A difference of a basement rise A and B (white characters in Fig.5-6-8) was explained as a part of rise B was considered as a volcanic intrusive rock. Probably magnetic anomaly patterns around the Mogamitai Bank was caused by mounds of volcanic rocks or volcanic intrusive rocks which were buried in sediments similarly to the north of Mogami Trough.

5.6.3. North of Sado Island -off Niigata Area-

A similar analysis of north of Sado Island area(38° N - 39 ° N) was carried out. Total forces of magnetic anomalies were shown in Fig.5-6-9, and a gravity basement calculated from Bouguer gravity anomalies were in Fig.5-6-10. The gravity basement was calculated with surface density were 2.0g/cm^3, and basement density was 2.4g/cm^3. In addition, Bouguer anomalies were separated from linear trend.

The mean depth of magnetic basement was estimated from the gradient of power spectrum of total force magnetic anomalies (Fig.5-6-11). In addition, it was calculated about 1.3km. Then the altitude for upward continuation was given as 3km. The altitude was corresponded to be little deeper than mean depth of gravity basement, too. The transformed magnetic anomalies were regard as regional field. The residual magnetic anomalies were shown in Fig.5-6-12. It was separated from regional anomalies using subtraction. Apparent magnetization intensities were calculated from the residual magnetic anomalies (Fig.5-6-13). The distribution of intensities was estimated on the surface of gravity basement. Further more, the direction of magnetization was assumed to be parallel to external field. They were transformed to reduced to the pole with the direction.

Here, strong parts of magnetic intensities were regarded as volcanic intrusions. Moreover, they were located around boundaries and deepened area of gravity basement. On the other hand, there were some remarkable weak parts of magnetic intensities. One reason was that magnetic intensity was weak in structural, and another one was that deep negative anomalies were made by interference surrounding strong magnetic intensities, then magnetic intensities were calculated weak apparently.

5.6.4. Northern part of Mogami Trough -off Aomori Area-

A distribution of magnetic intensities in the northern part of the Mogami Trough was calculated with similar way to other areas. The mean depth of magnetic basement was estimated from the gradient of power spectrum of total force magnetic anomalies (Fig.5-6-14). It was about 1.4km. The mean depth of gravity basement was also calculated about 1.4km. Then, the separation of residual magnetic anomalies from regional field was not carried out. Total forces of magnetic anomalies were shown in Fig.5-6-15, and a gravity basement map was shown in Fig.5-6-16. The gravity basements were calculated from residual Bouguer anomalies. The surface density was 2.3g/cm^3, and basement density was 2.7g/cm^3. Residual anomalies were separated from linear trend. Apparent magnetic intensities on the gravity basement were shown in Fig.5-6-17. Where, the direction of magnetization was assumed as parallel to external field, and anomalies were transformed to reduced to the pole.

Here a remarkable strong magnetic intensity zone was trended in about SW directions from the Kyuroku Jima Island. It located along the gravity basement boundary where Mogami Trough was burying into Japan Basin. On the other hand, magnetic intensities looked to be especially weak on the end of the Sado Ridge. Some faults were recognized around here by seismic profiling. It was thought that faults made such weak zone of magnetic intensities.

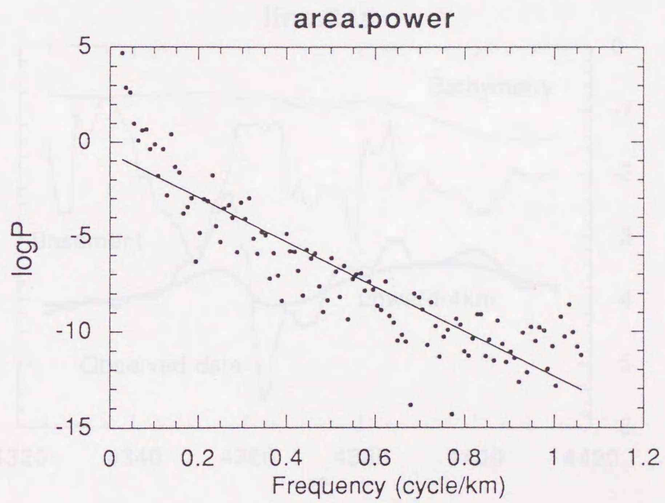

Fig.5-6-1
Power spectrum of magnetic anomalies off Akita area.

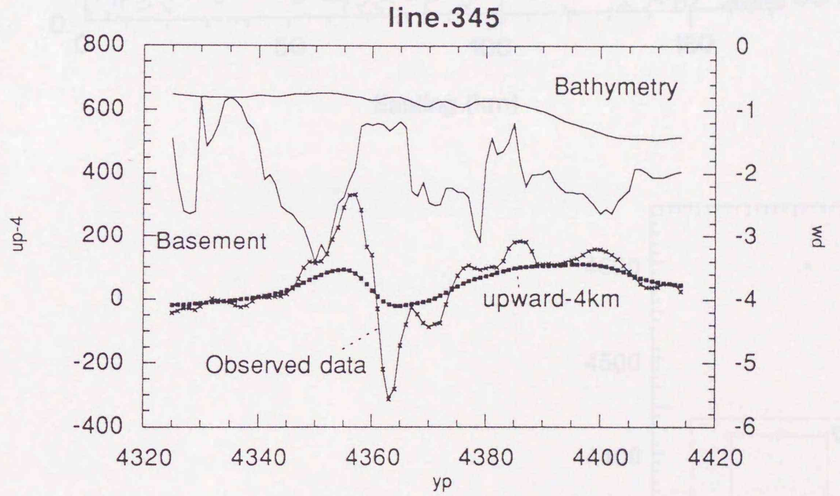

Fig.5-6-2
A N-S profile of the bathymetry, gravity basement, observed magnetic anomaly, and 4km upward filtered anomaly. The location is shown in Fig.5-6-3 as A-A'.

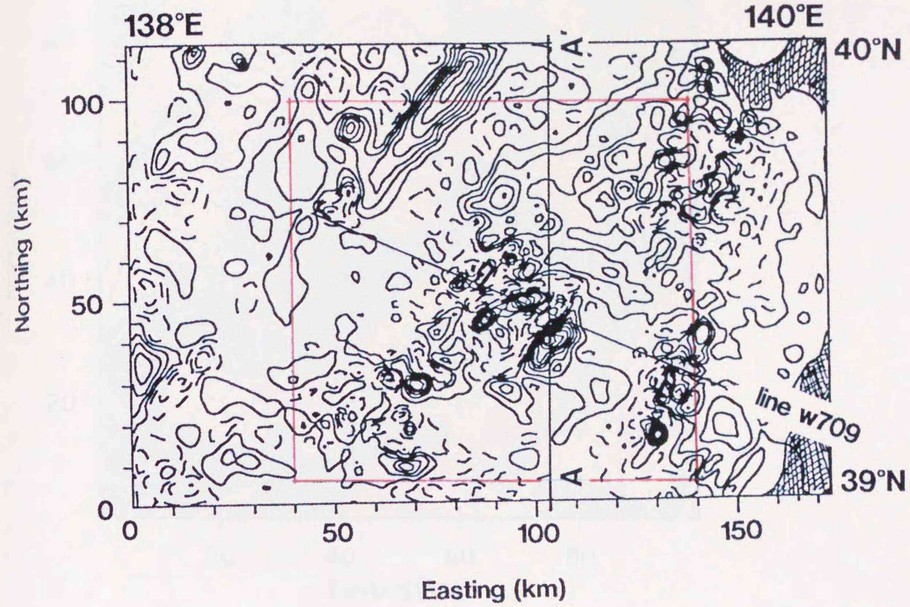

Fig.5-6-3

Residual magnetic anomalies off Akita area.

The box indicates analysed area shown

from Fig.5-6-4 to Fig.5-6-8. Contour interval is 25nT.

A-A' indicates the location of N-S profile

shown in Fig.5-6-2 and Fig.5-6-7.

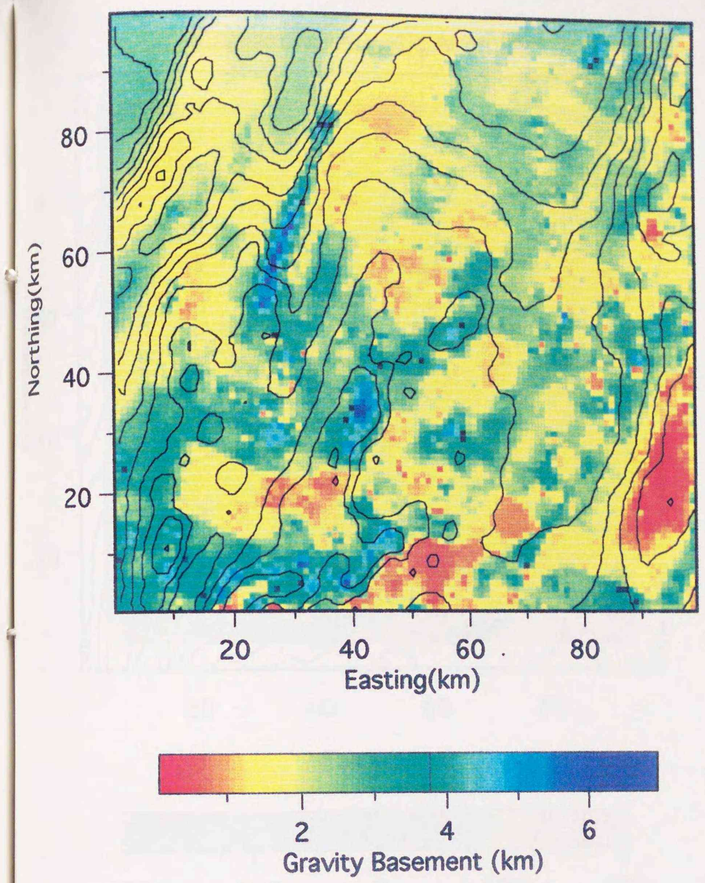

Fig.5-6-4

Gravity basement depth around Mogamitai Bank, northern part of Sado Ridge. Density : surface=2.0g/cm^3 , basement=2.4g/cm^3 . Bathymetry contour interval is 200 m.

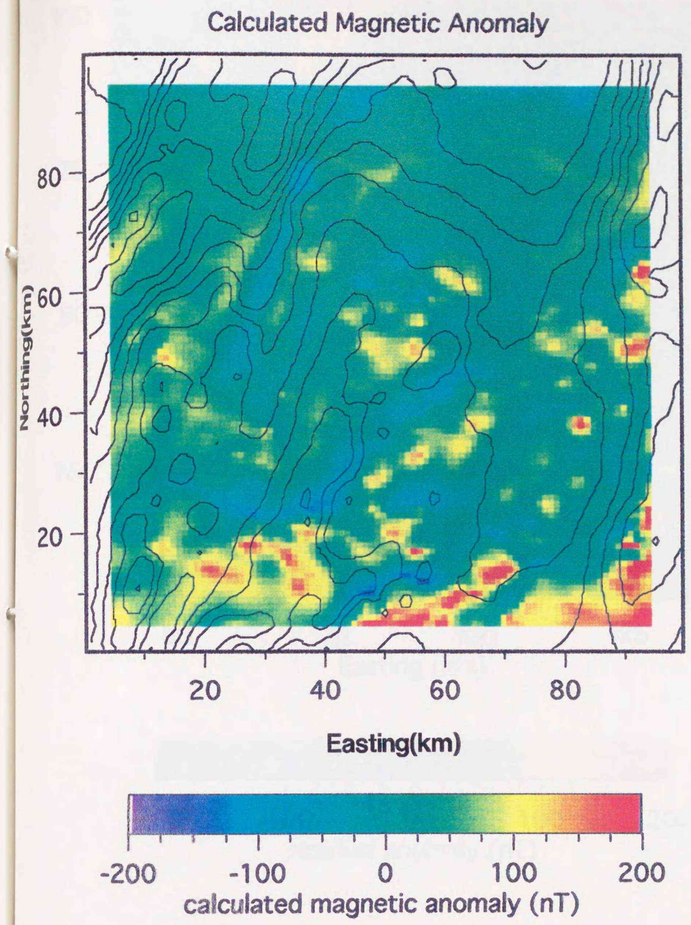

Fig.5-6-5
Calculated magnetic anomalies around Mogamitai Bank northern part of Sado Ridge. Magnetic anomalies were calculated due to the gravity basement. (Magnetization : Dec=-8° , Inc=50° , J=1.0A/m.) Bathymetry contour interval is 200 m.

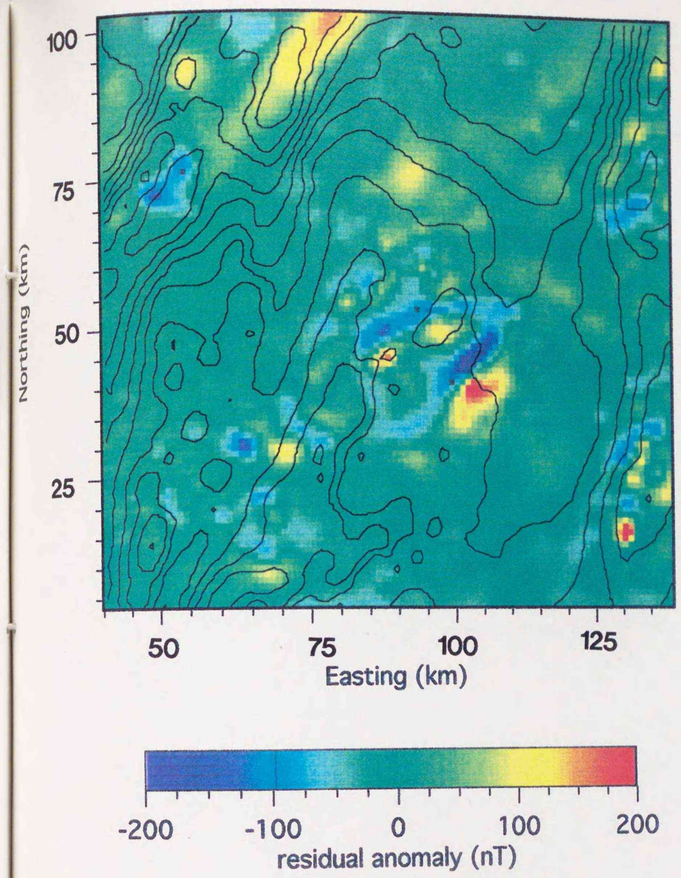

Fig.5-6-6

Residual magnetic anomalies around Mogamitai Bank northern part of Sado Ridge. Bathymetry contour interval is 200 m.

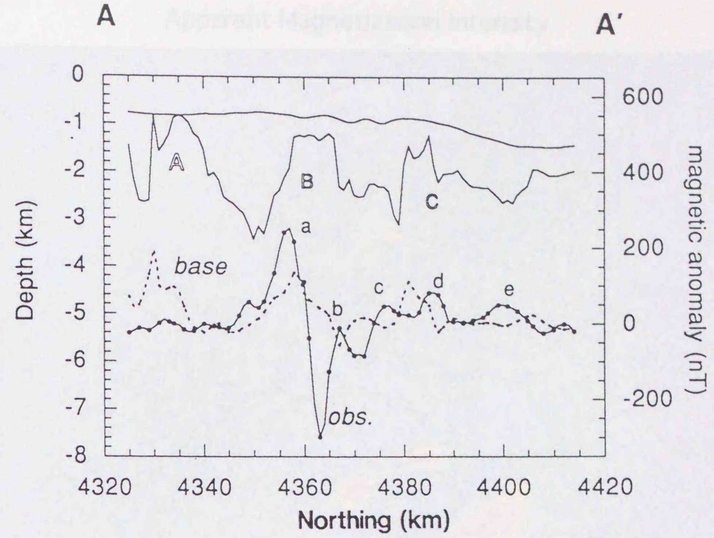

Fig.5-6-7

A N-S profile of the bathymetry, gravity basement, residual magnetic anomaly, and calculated magnetic anomaly due to the gravity basement. The location is shown in Fig.5-6-3 as A-A'.

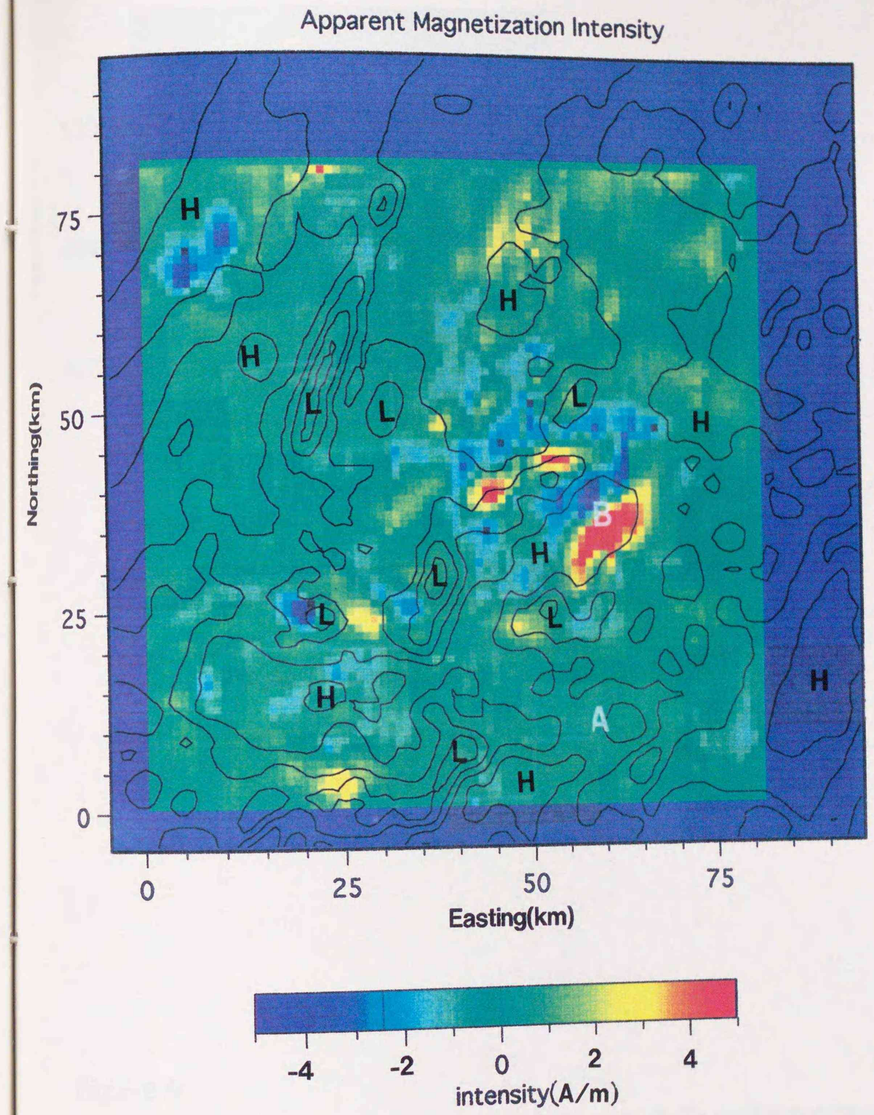

Fig.5-6-8

Apparent magnetization intensity of around Mogamitai Bank northern part of Sado Ridge. Gravity basement depth contour interval is 1 km.

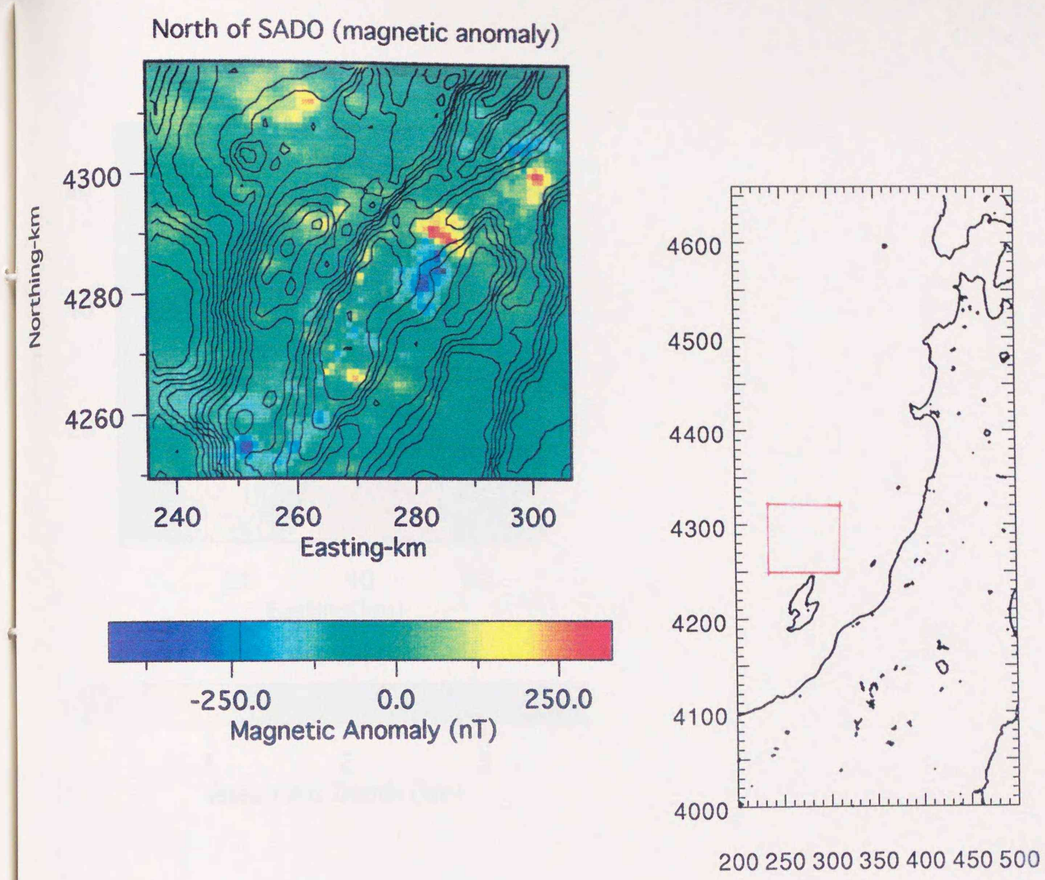

Fig.5-6-9
Magnetic anomalies of the north of Sado Island. Bathymetry contour interval is 200 m.

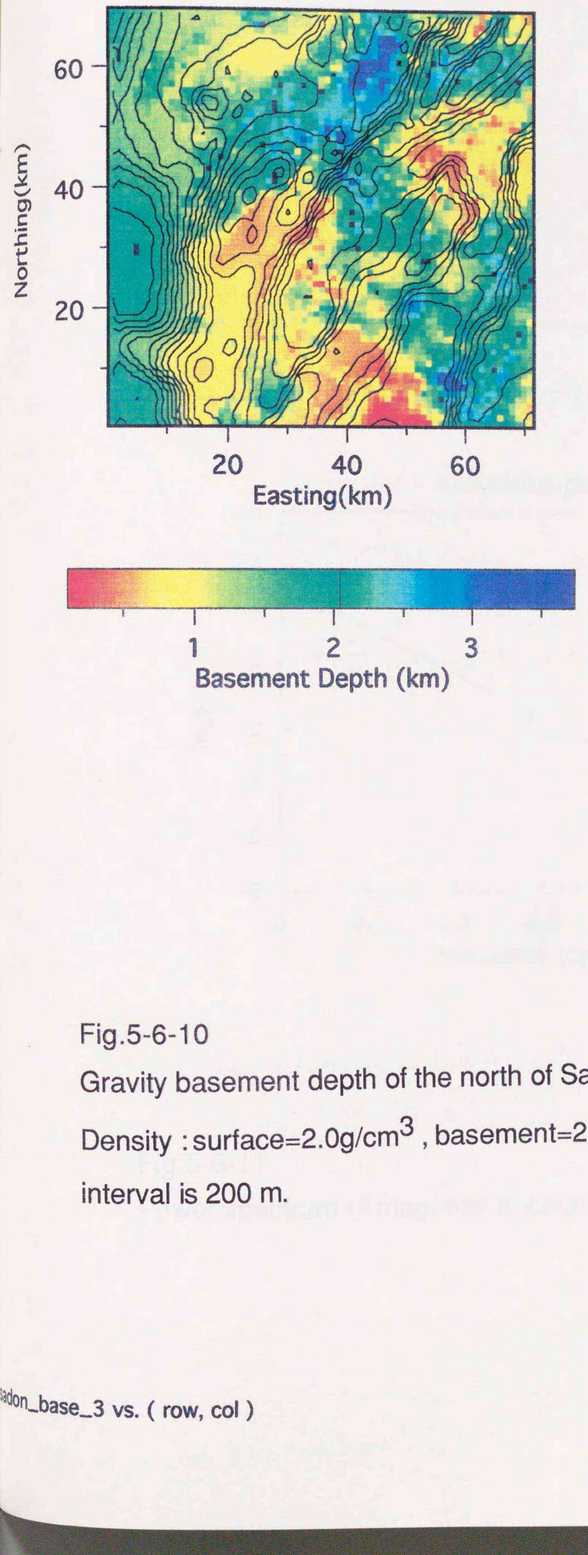

Fig.5-6-10

Gravity basement depth of the north of Sado Island.

Density : surface=2.0g/cm^3 , basement=2.4g/cm^3 . Bathymetry contour interval is 200 m.

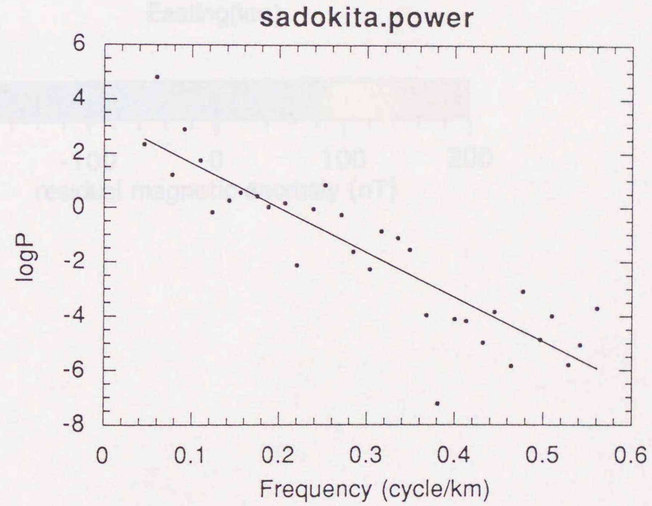

Fig.5-6-11

Power spectrum of magnetic anomalies of the north of Sado Island.

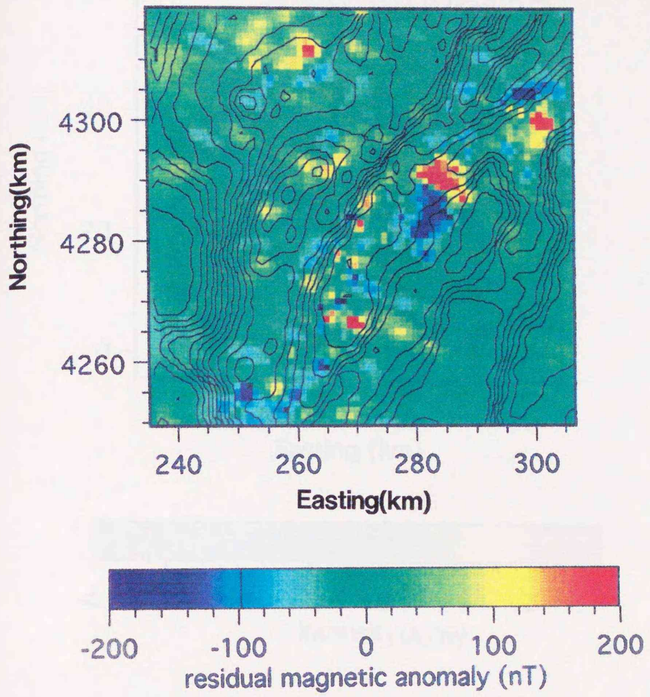

Fig.5-6-12
Residual magnetic anomalies of the north of Sado Island. Bathymetry contour interval is 200 m.

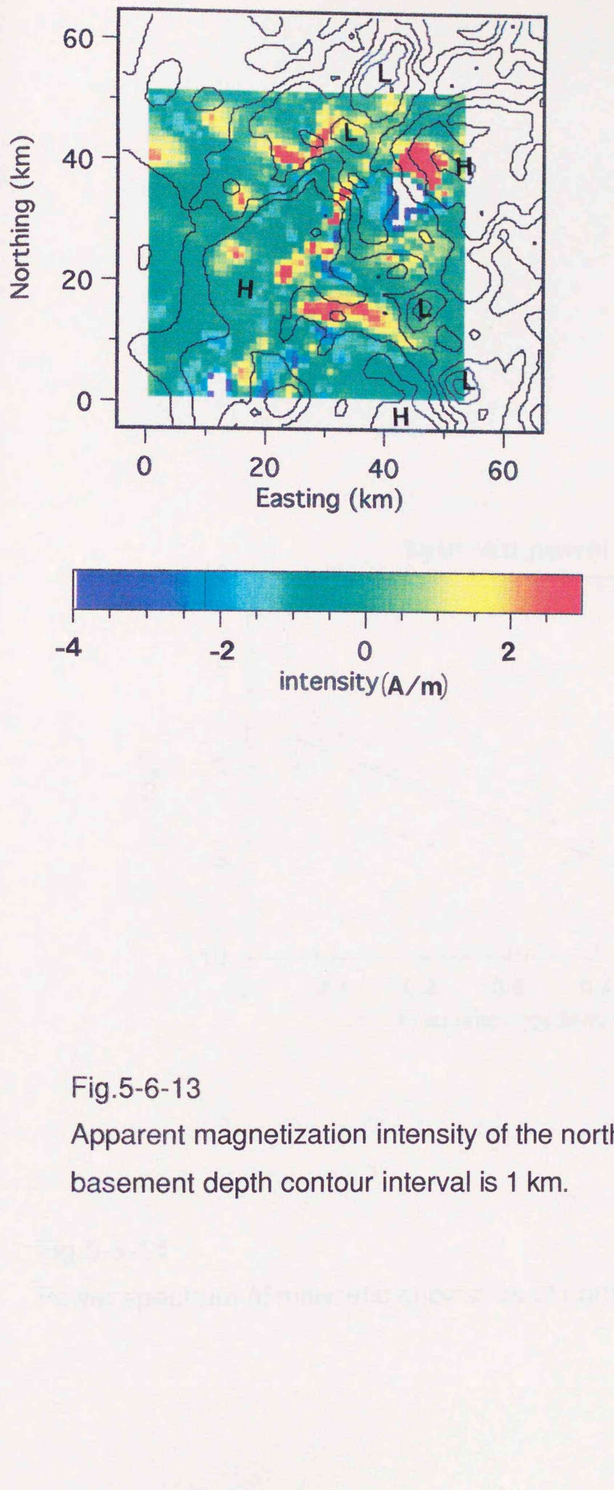

Fig.5-6-13
Apparent magnetization intensity of the north of Sado Island. Gravity basement depth contour interval is 1 km.

sadon_intensity_3 vs. (row, col)

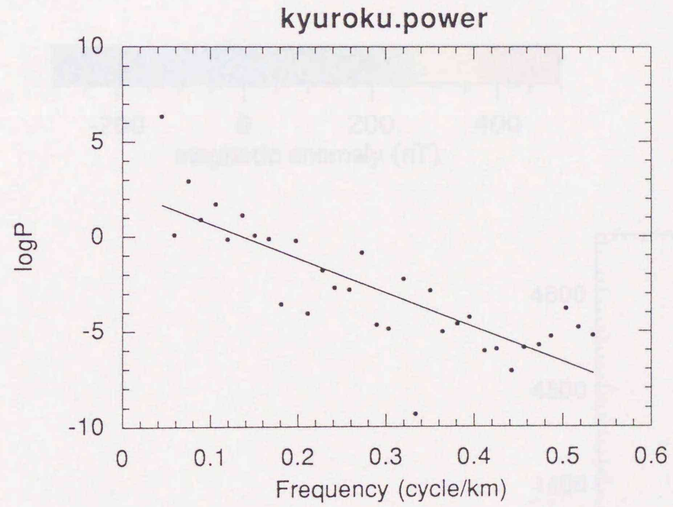

Fig.5-6-14

Power spectrum of magnetic anomalies of northern part of Mogami Trough.

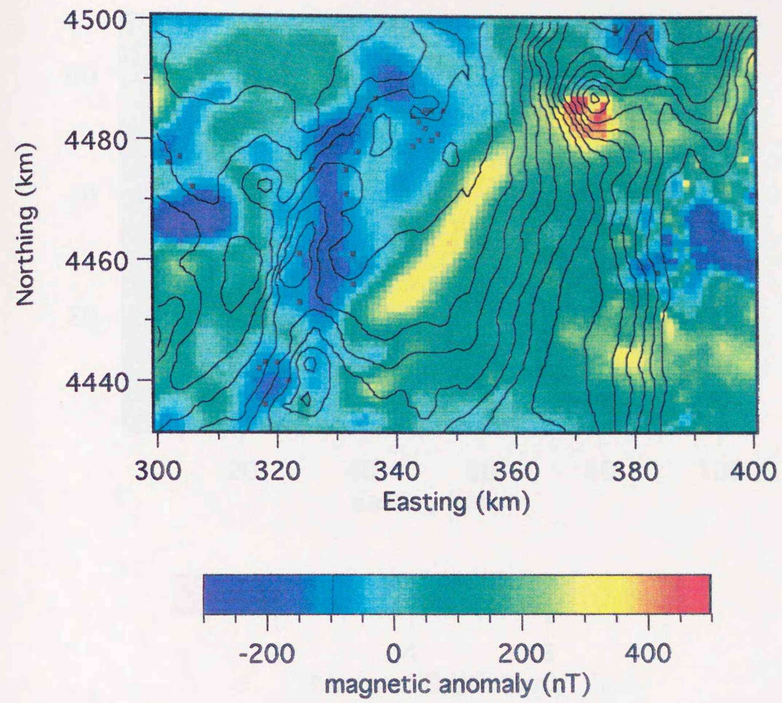

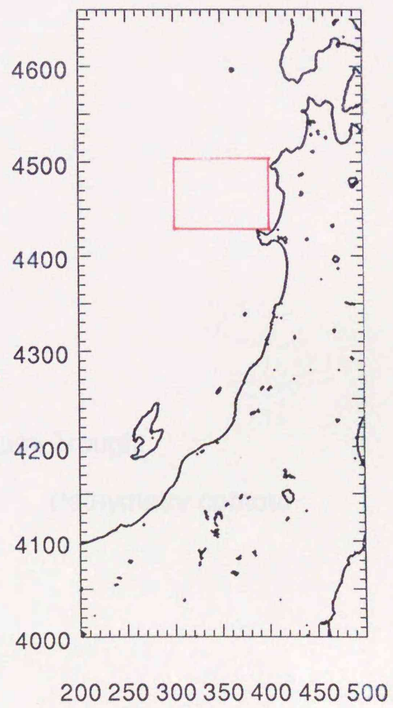

Fig.5-6-15
Magnetic anomalies of northern part of Mogami Trough.
Bathymetry contour interval is 200 m.

kyuroku_mag_5 vs. (row, col)

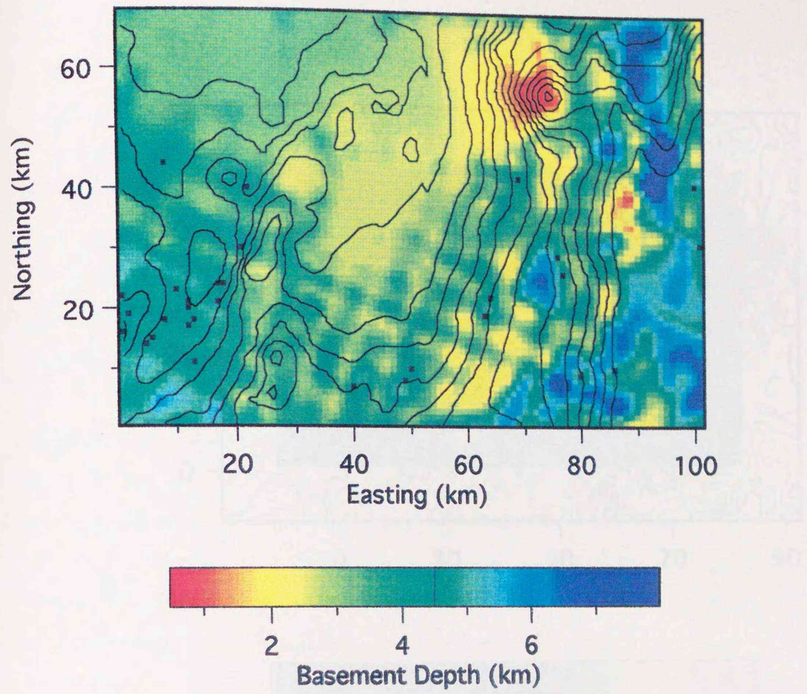

Fig.5-6-16

Gravity basement depth of northern part of Mogami Trough.

Density : surface=2.3g/cm^3 , basement=2.7g/cm^3 . Bathymetry contour interval is 200 m.

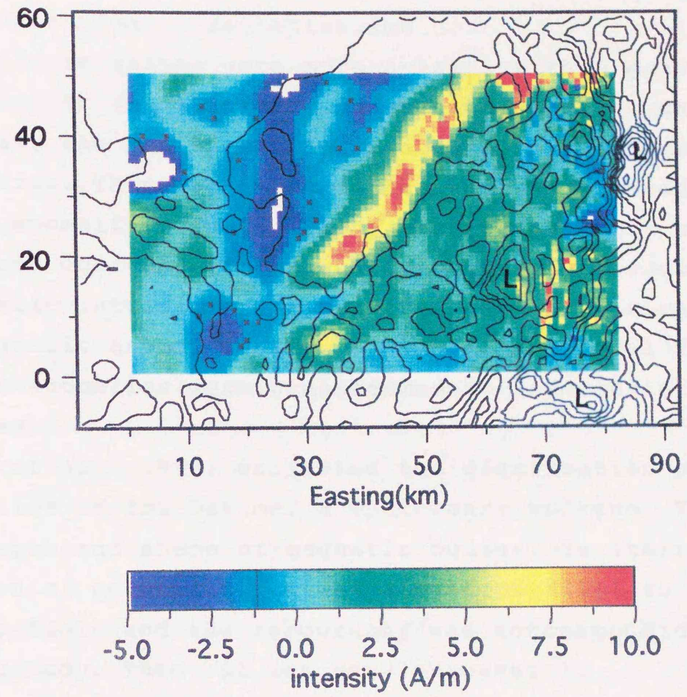

Fig.5-6-17

Apparent magnetization intensity of northern part of Mogami Trough. Gravity basement depth contour interval is 1 km.

5.7. *Discussions*

5.7.1. Direction of magnetization

Magnetic anomalies were more sensitive than gravity anomalies. If we calculated basement depth from magnetic anomalies, the result was influenced by assumed magnetic intensities. Then, basement depths were calculated from gravity anomalies. In addition, gravity basement was considered equivalent to magnetic basement. The distribution of magnetic intensities on gravity basement was calculated from magnetic anomalies. To be simplified, total force of magnetic anomalies were transformed to reduced to the pole anomalies.

Okuma et al. (1994) estimated the distribution of magnetic intensities of Izu Oshima, a Quaternary volcano. They gave fixed depth and shape of magnetic bodies. In their case, direction of magnetization was almost parallel to external magnetic field and the topography was corresponding to magnetic body. Then, it was very successful.

However, if the remanent magnetization was strong, it was difficult to give direction of magnetization as unique and parallel to external field. An isolated magnetized body shows the direction of magnetization. Because, the direction of a pair of positive and negative magnetic anomaly peak shows a direction of sum of magnetization vector and external magnetic field vector (Fig.5-7-1). The distance between positive and negative peaks is roughly suited to a width of the magnetic body, though it is depending on surface depth of a magnetic body. Therefore, if the survey line spacing is wider than magnetic bodies, the observed data are not possible to pick up true pairs of positive and negative peaks. For example, the magnetic anomaly map of off Akita area(Fig.5-6-3), survey lines spacing was about 3km in

direction of N110° E, and 7km in direction of N20° E. They were arranged on a lattice form. From this, in consideration of water depth of the area, magnetic bodies needed to be much wider than line spacing to pick up the pair of peaks exactly. Alternatively, remanent magnetization needed to be quite strong to be observed positive and negative anomaly peaks on survey lines. Accordingly, if magnetization trended in east, the pair of peaks were observed on N20° E survey lines, though the declination of external field was about N8 ° W. Similar to this, remanent magnetization trended in west in order that pairs of peaks were observed on N110° E survey lines. Then, some positive and negative magnetic anomaly peaks in the map are probably unreal pairs. If we could obtain exact magnetic vector anomalies with STCM, direction of magnetization should be obtained. Unfortunately, as shown in Section 5.3, accuracy of data were unsatisfactory to obtain magnetization vector have isolated magnetic bodies like volcanic intrusions. Then it was difficult to specify direction of magnetization directly. Now, as an example, three components of magnetic vector anomalies were calculated (Fig.5-7-2). The inclination of magnetization of the isolated prism shaped body was given as 15° or 60° . The shapes of profiles were dependent on location of assumed survey lines. Then it was difficult to know magnetization vector of a magnetized body from total force anomalies on survey lines.

After all, the direction of magnetization was assumed to parallel to external magnetic field. It was convenience and satisfactory to estimate approximate magnetic structures when we could not obtain exact directions.

5.7.2. Magnetic structure

The directions of magnetization were estimated to be

parallel to external magnetic field, because we didn't have any information about magnetization vector. However, our data have advantages that gravity and magnetic anomalies were observed along the same dense survey lines.

Peaks of analytic signal showed boundaries of magnetic structure. Yellow lines in Fig.5-7-3 indicated the magnetic structural boundaries. There were three remarkable boundaries in the study area. First one was going along edges of sedimentary basins like Akita Basin. Second one was on the extension of the boundary between Sado Ridge and Yamato Basin. Third one was on southern part of Sado Ridge. First one was corresponding to the East Japan Sea Tectonic line proposed by Suzuki (1989). The orange line indicated plate boundary proposed by Nakamura (1983). In addition, green lines enclosed the quiet magnetic anomaly area. The quiet area located between Akita Basin and Niigata Basin. It was corresponding to a blank of sedimentary basins. Then, between Sakata and Niigata, there should be remarkable structural boundaries.

Apparent magnetization intensities on the gravity basement were estimated. First they were calculated by 2.5-dimensional analysis along E-W profiles every 10km. Next, they were calculated by 3-dimensional analysis in three areas, northern and southern parts of Sado Ridge, and southern part of Okushiri Ridge (blue boxes in Fig.5-7-3). The results of 2.5-dimensional analysis showed that strong intensity parts appeared slopes of gravity basement and steeply deepened areas of basement. They should be corresponding to faults. Therefore, the strong intensity parts should be corresponding to volcanic intrusions, because volcanic intrusions often appear along structural boundaries. Moreover, remarkable strong parts of magnetic intensities appeared around the Mogamitai Bank(Mo) in

northern part of Sado Ridge, Hyotanguri Bank(Hy) in southern part of Sado Ridge, and north end of Mogami Trough (red marks in Fig.5-7-3).

The south of Hyotanguri Bank was a strong magnetic intensity part of south of the Sado Ridge. It was corresponding to deepened zone of gravity basement. On the other hand, the area between Hyotanguri Bank and Koshijisho Bank (Ko) also had strong magnetic intensities. However, their gravity basements were shallow, though it located in topographic valley. Okamura et al. (1995b) suggested Koshijisho Bank was formed by typical "Basin Inversion". Then, basement under the top of bank was deepened steeply corresponding to a reactivated reverse fault trended in ENE direction. And the area between Hyotanguri and Koshijisho Banks were suggested that volcanic rocks had intruded into weak zone of basement, then gravity basement became shallow and magnetic intensity was strong.

Kato et al. (1986) reported that there were small-scale volcanic mounds on the fan where between Kyuroku Spur and Sado Ridge and Mogami Trough was burying into Japan Basin. However, these mound's diameters were less than 1km, then isolated magnetic anomaly patterns were difficult to recognize in magnetic anomaly map based on sea-borne magnetic surveys. In addition, Okamura et al. (1996) found the similar volcanic mounds buried in sediment layers in northern parts of Sado Ridge based on seismic profiling. They should be larger than volcanic mounds around the Kyuroku Spar.

However, isolated magnetic anomalies caused by these mounds were not appeared. Then they suggested that their magnetization were small.

It was very interesting that size of volcanic rocks in Mogami Trough became larger as going south. If they were

formed by similar tectonic process, it suggested something relations with previous rifting.

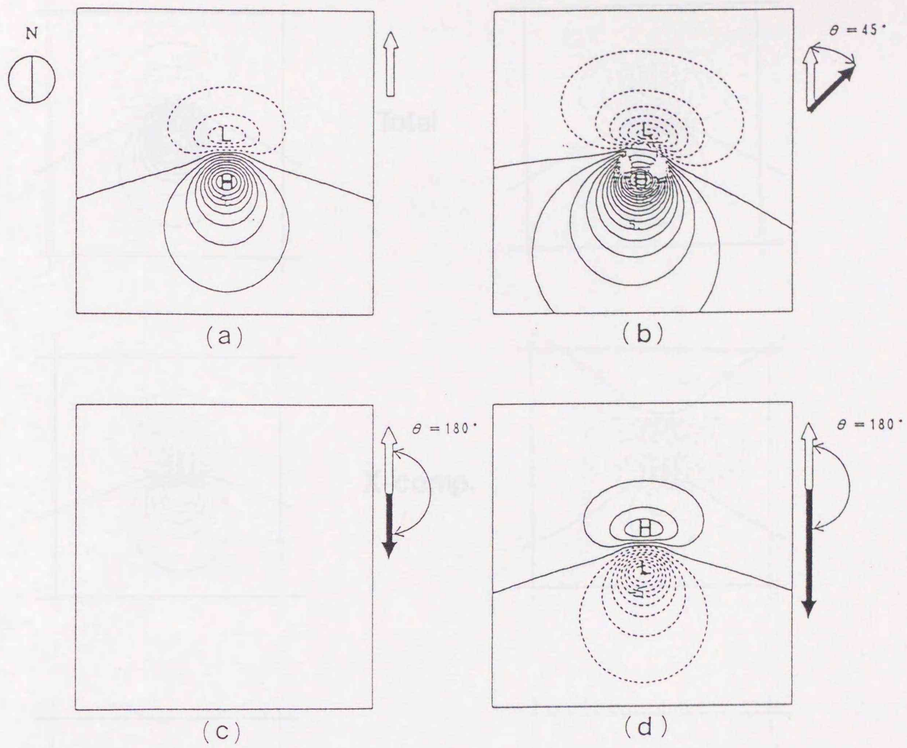

Fig.5-7-1

Samples of total magnetic anomaly patterns due to a 3-dimensional prism shaped model. Prism has remanent magnetization vector from the external magnetic field. Solid lines indicate positive values and broken lines indicate negative values. Black arrow(R) indicate remanent magnetization. White arrow(I) indicate induced magnetization. θ indicates the angle between I and R.

(a):$|I|>0$, $|R|=0$, (b):$|R|=|I|$, $\theta=45^{\circ}$, (c):$|R|=|I|$, $\theta=180^{\circ}$, (d):$|R|=2|I|$, $\theta=180^{\circ}$

after Okuma et al.(1995)

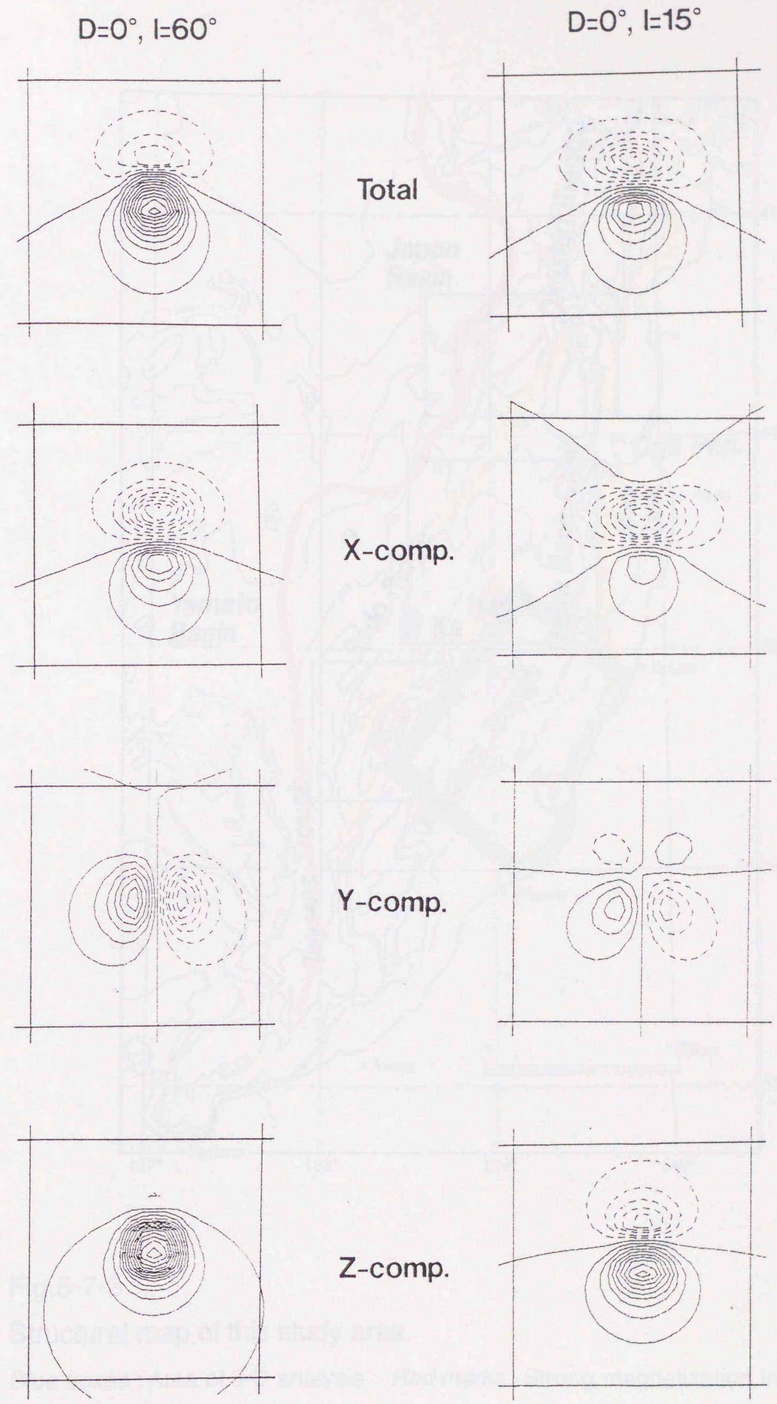

Fig.5-7-2
Samples of total, x-component, y-component, and z-component anomalies due to a 3-dimensional prism shaped model.

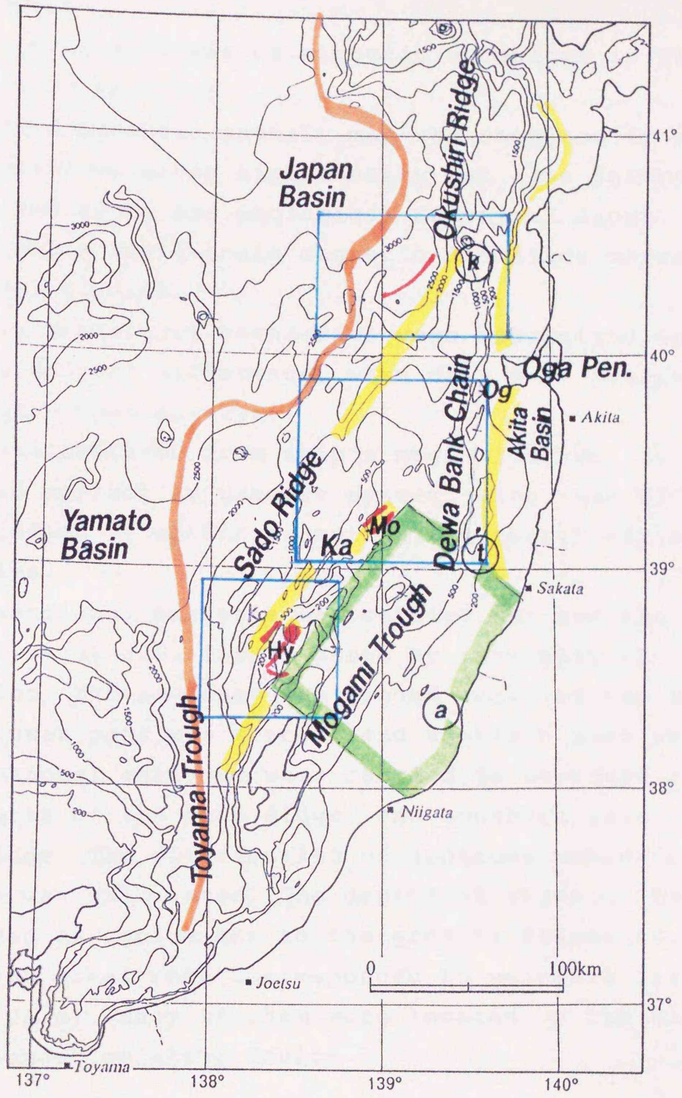

Fig.5-7-3

Structural map of this study area.

Blue boxes : Area of 3-D analysis , *Red marks* : Strong magnetization intensity parts, *Orange line* : Plate boundary by Nakamura(1983), *Yellow lines* : magnetic structural boundaries

k: Kyurokujima Island, t: Tobishima Island, a: Awashima Island, Og: Ogamukouse Bank
Mo: Mogamitai Bank, Ka: Kamaguri Bank, Hy: Hyotanguri Bank, Ko: Koshijisho Bank

5.8. *Conclusion*

The results of analysis of magnetic anomalies in this chapter were as follows;

(1) A detailed magnetic anomaly map was obtained from data that were observed along high-density (at line intervals of about 3km) survey by the Geological Survey of Japan. Then, we can recognize small-scale magnetic anomalies corresponded to geological studies.

(2) Magnetic structural boundaries were recognized easily by calculating spatial difference, when data were observed by 2-dimensional dense surveys.

(3) STCM data suffered from ship's magnetization. It may be difficult to correct by present system. Then, our STCM data were unsatisfied to obtain magnetization vector of isolated source bodies.

(4) 2.5-dimensional analysis was carried out and the result divided the study area into 2 parts by intensity of magnetization. The boundary was around north of the Sado Ridge. Northern part was strong, and southern part was weak.

(5) 3-dimensional analyses were carried in northern and southern parts of the Sado Ridge, and southern part of the Okushiri Ridge. The distribution of apparent magnetic intensities was calculated. The depths of magnetic basements were regarded as equivalent to the gravity basements. Strong magnetization areas were corresponded to volcanic intrusions (more than 2A/m). Many of them were located on the slope of gravity basement or along faults.

6. Discussion

A technology of Positioning is progressing year by year, then high-density surveys became possible recently. Detailed magnetic and gravity anomaly maps were obtained from dense survey data. Basement structures were revealed due to gravity and magnetic anomalies. Single-channel seismic profilings hardly show basement structures in this study area. The advantages of this study were that gravity and magnetic anomalies were obtained on the same dense survey lines. The restriction condition was possible to be added to a structural model.

6.1. *Basin Inversion*

Okamura et al. (1995b) suggested that Sado Ridge and Dewa Bank Chain were formed by "Basin Inversion" inferred from single-channel seismic profiling and other geological studies. In this time, basement undulation was revealed due to gravity anomalies, though it was difficult to be shown horizontally by geologic studies.

Bathymetry map was shown in Fig.6-1-1 for the index of names of banks. The basement undulation calculated from gravity anomalies showed quite different pattern from topography in the southern part of Sado Ridge and central part of Mogami Trough areas. Especially, in Kamaguri Bank (R8) and Torimiguri Bank (R6) area, basement showed typical structure formed by "Basin Inversion". The basement deepened under the top of mountain bodies. This result supported to the geological study. In contrast to that, the basement of Dewa Bank Chain became shallow under the top of mountain bodies, though they were also formed by "Basin Inversion" inferred from geologic studies. The basement undulation was similar to topography and sediment layers were thinner than Sado Ridge area.

The distribution of faults were shown in Fig.6-1-2 (after Okamura et al., 1994; 1995a; 1996a; 1996b; Okamura and Kuramoto, 1996). Okamura et al. (1995b) showed that the arrangement of reactivated reverse faults had two different directions. One was NNE and another was ENE. They proposed that direction of reverse faults influenced on structure of small ridges. Concretely, E-W compressional stress worked more effectively for the NNE trending faults than ENE trending faults. Then, NNE trending faults, for example the fault along Ogamukouse Bank (R12), displaced more than ENE trending faults. In contrast, ENE trending faults, for example the fault along Kamaguri Bank (R8) or Torimiguri Bank (R6), displaced less. Then basement became deep under the top of the mountains.

However, only differences of fault trending could not explain about difference of sediment thickness. For example Yahikotai Bank (R9) located west side of Kamaguri Bank (R8) was along a NNE trending fault. The basement seemed to be shallow under the top of the mountain relatively. However, the sediment thickness was about 2km. It was similar to Kamaguri Bank (R8) and Torimiguri Bank (R6) that faults trended to ENE. It was considered that scale of half graben formed in extensional stress field was larger around Sado Ridge than Dewa Bank Chain.

Okamura et al. (1995b) discussed about two models for the origin of NNE and ENE trending normal faults and rifts (Fig.6-1-3). One was WNW-ESE extension, and another was NNW-SSE extension. Former model supported to the double door opens model (Otofuji et al., 1985), and later models supported to the hypothesis by Jolivet and Tamaki (1992).

If WNW-ESE model can be supported, Dewa Bank Chain and Sado Ridge become the rift zone. Then, their mountain bodies consisted of sediments in rifts. Moreover, Dewa Bank Chain

located edge of Akita Basin. Basins along the coast were proposed to be developed from the large rift zone (Suzuki, 1989). It was a suitable suggestion that there was rift zone around Sado Ridge but it was not developed to a sedimentary basin.

On the other hand, if NNW-SSE model can be supported, Sado Ridge and Dewa Bank Chain areas was transtensional zone and the rift zone crossed into Mogami Trough. It is good to explain basement under the top of banks along ENE trending fault were deep. However, southern part of Sado Ridge was suitable to have had been rift zones to explain the thickness of sediments.

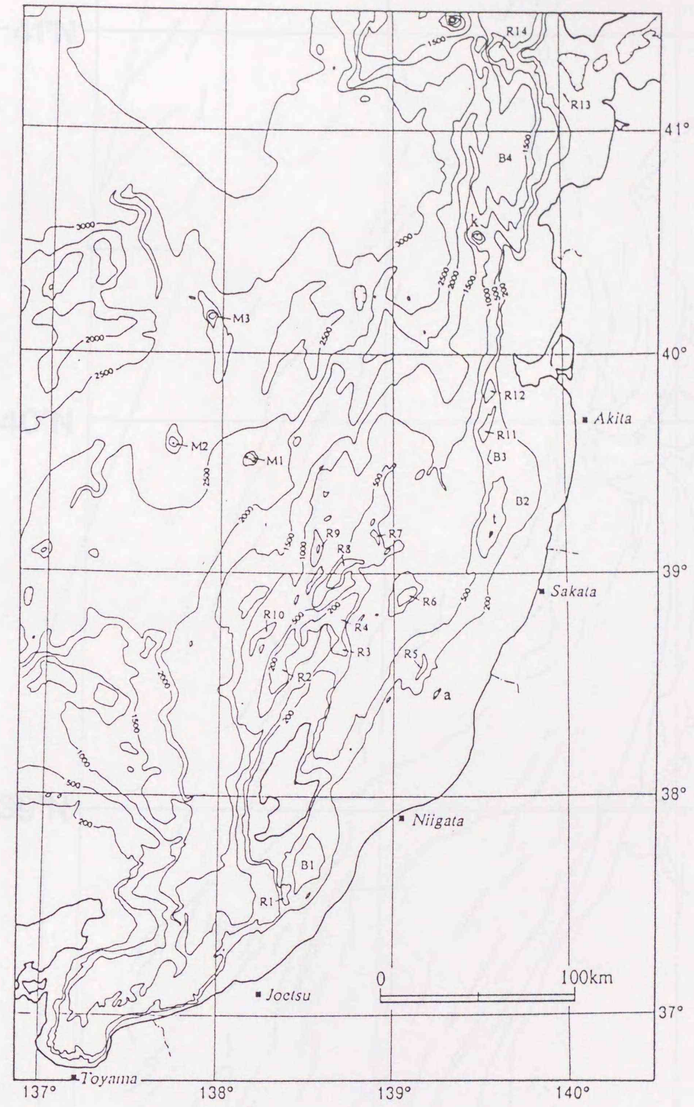

Fig.6-1-1 (the same as Fig.2-1-1)

Bathymetric map of the study area.

a:Awashima Island, k:Kyurokujima Island, t:Tobishima Island,
B1:Sado Basin, B2:Tobishima Basin, B3:Oga Basin, B4:Nishi-Tsugaru Basin, M1:Matsu Seamount, M2:Maiyo No.2 Seamount, M3:Maiyo No.3 Seamount, R1:Sado Bank, R2:Hyotanguri Bank, R3:Gassanguri Bank, R4:Mukouse Bank, R5:Awashimaguri Bank, R6:Torimiguri Bank, R7:Mogamitai Bank, R8:Kamaguri Bank, R9:Yahikotai Bank, R10:Koshijisho Bank, R11:Shinguri Bank, R12:Ogamukouse Bank, R13:Nishi-Tsugarutai Bank, R14:Kojimatai Bank

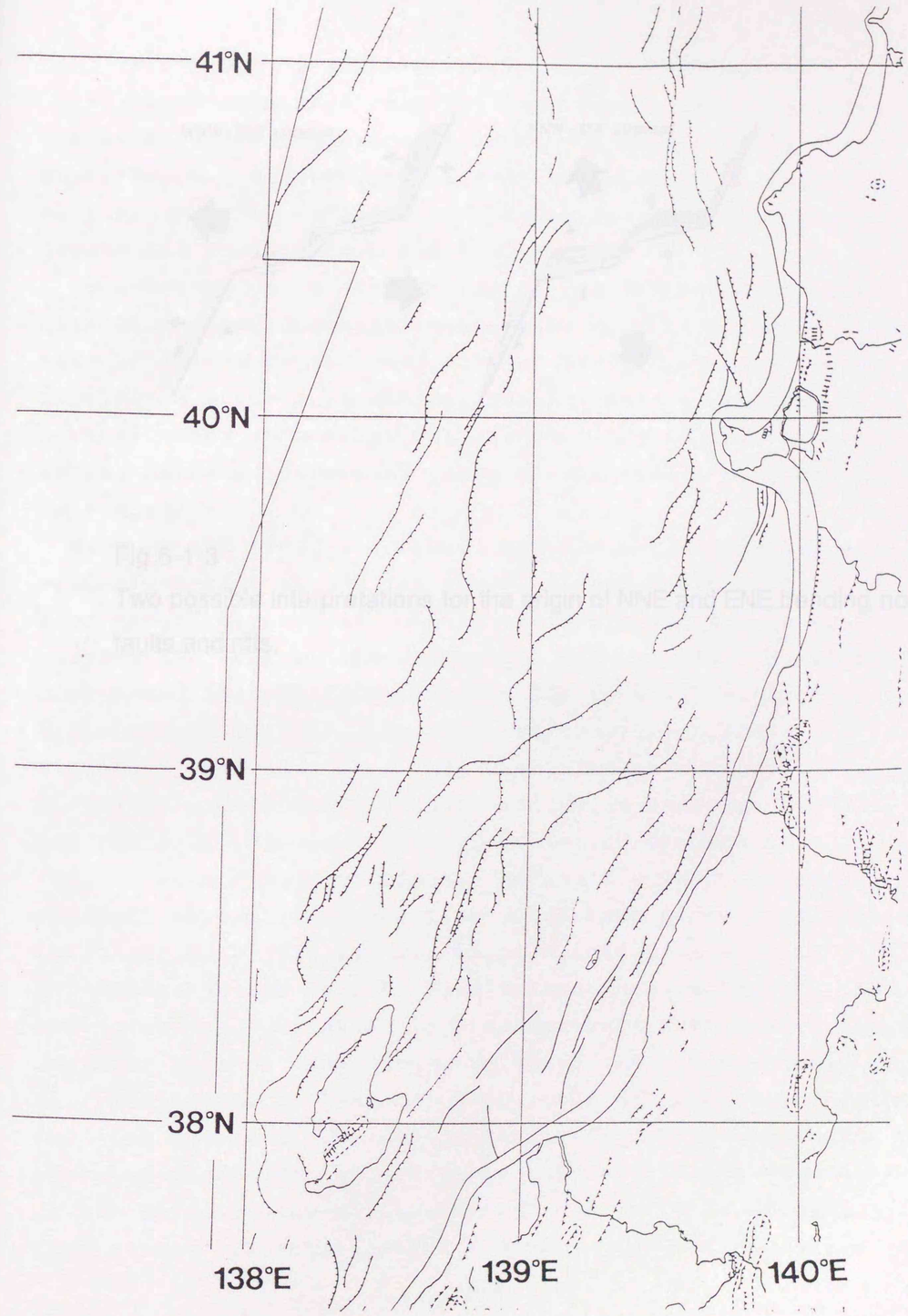

Fig.6-1-2
Structural map of the study area.

after Okamura et al.(1994, 1995a, 1996a, 1996b) and Okamura and Kuramoto(1996)

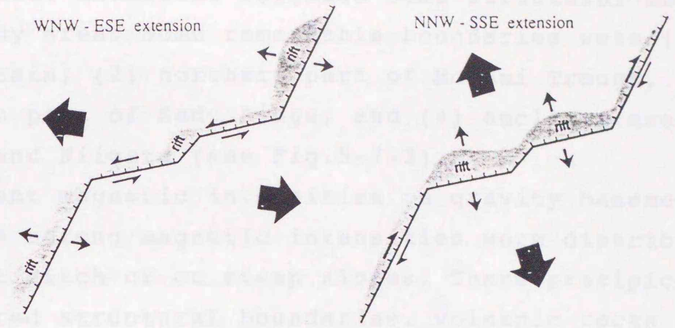

Fig.6-1-3
Two possible interpretations for the origin of NNE and ENE trending normal faults and rifts.

6.2. *Structural boundaries*

Magnetic anomalies revealed some structural boundaries in the study area. Some remarkable boundaries were (1) along Akita Basin, (2) northern part of Mogami Trough, (3) southern part of Sado Ridge, and (4) enclosed area between Sakata and Niigata (see Fig.5-7-3).

Apparent magnetic intensities on gravity basement showed that the strong magnetic intensities were distributed along basement ditch or on steep slopes. These precipices were considered structural boundaries. Volcanic rocks often intrude along structural weak lines, like faults. Therefore, strong magnetic intensity parts should indicate volcanic intrusions.

Kato et al. (1986) reported that there were small-scale volcanic mounds on the fan where between Kyuroku Spur and Sado Ridge (Fig.6-2-1). Around there, Mogami Trough was burying into Japan Basin. However, the volcanic mounds were discovered for the first time by Sea Beam surveys around Kyuroku Jima Island. They were very small and their diameters were less than 1km. Then, isolated magnetic anomalies were difficult to recognize in magnetic anomaly map based on sea-borne magnetic surveys. Okamura et al. (1996b) also found the similar volcanic mounds buried in sediment layers in northern parts of Sado Ridge from seismic profiling data (Fig.6-2-2). These mounds were much larger than those around Kyuroku Jima Island were. Moreover, the strong areas of magnetic intensities were distributed around southern part of Sado Ridge. Volcanic intrusions should be distributed there. However, there were not recognized such volcanic mounds in seismic profiling data from center to south of Mogami Trough. If these intrusive rocks were buried in the basement layer, it was very difficult to recognize from seismic profiling data. However, magnetic anomalies

showed clearly existence of magnetic bodies, even if they were enough large.

It was very interesting that size of volcanic rocks became larger as going south in Mogami Trough. If they were formed by similar tectonic process, it suggested something relations with previous rifting.

The quiet magnetic anomaly area located between Akita Basin and Niigata Basin. It was corresponding to a blank of sedimentary basins. Then, between Sakata and Niigata, there should be remarkable structural boundaries. There are active folds instead of faults, and sediments in this area was thick (Okamura et al., 1995a). The reason why magnetic anomalies were low frequency was thought that magnetic basement was deep and volcanic intrusions couldn't appear near sea floor.

Suzuki (1989) considered the quiet area as the Yamagata Basin (or Mogamigawa-oki Basin). However, it was much smaller than other sedimentary basins. Then it was proposed that the area had not developed to be a sedimentary basin by something-tectonic conditions.

The basement structure of Okushiri Ridge was different from Sado Ridge and Dewa Bank Chain. Geological studies suggested that it be formed by anticline not by "Basin Inversion". The basement structure was suitable to topography and magnetic intensity was strong. Okushiri Ridge was recognized from the north of 40° 20'N clearly in topography, but the anticline appeared from around Oga peninsula. North of Oga Peninsula should be a clear structural boundary. In generally, north of Oga Peninsula, magnetization intensities became strong. Moreover, it became the boundary between "Basin Inversion" area and anticline area, too. Anyway, it was an important boundary for tectonics in the eastern margin of Japan Sea.

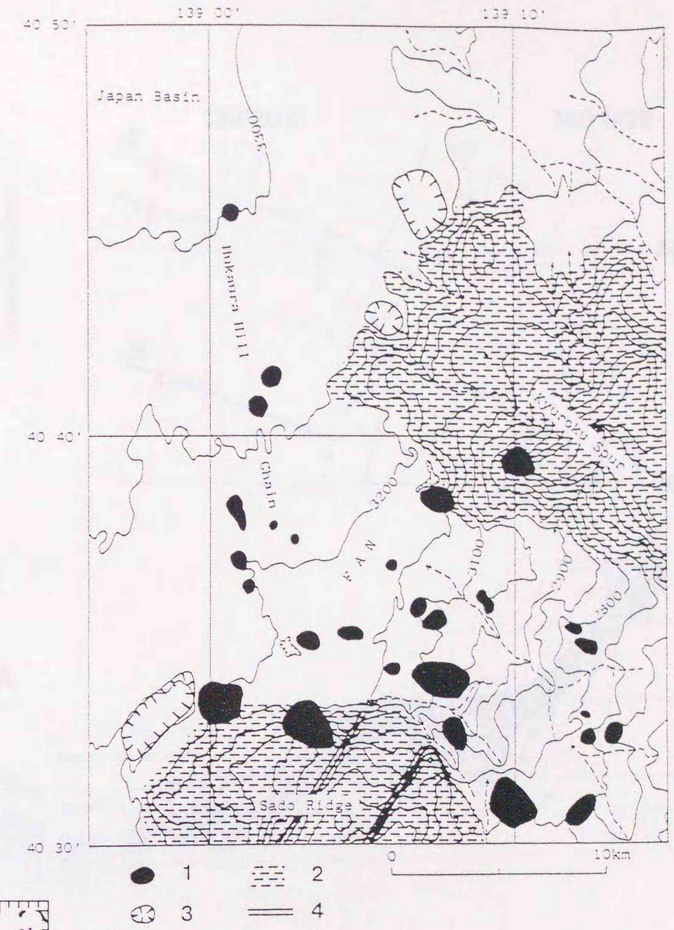

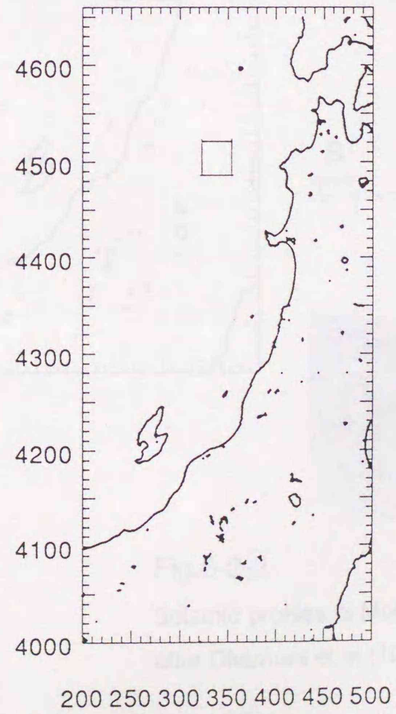

Fig.6-2-1

Morphological characteristics of the area.

1: Knoll or small hill, 2: Ridge or Spur,

3: Shallow depression along the border of Japan Basin

4: Linearment on Sado Ridge

after Kato et al.(1986)

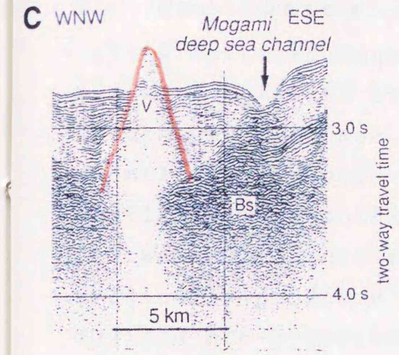

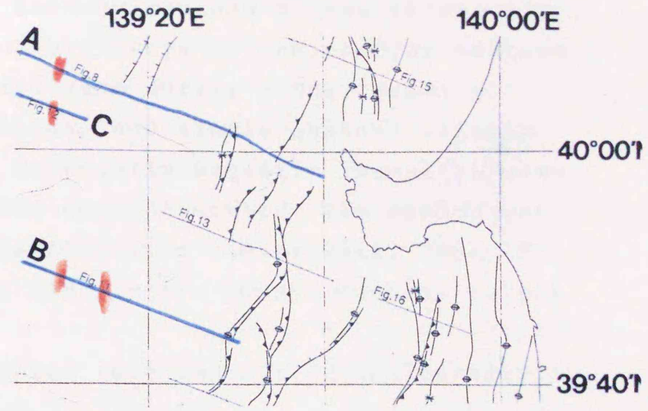

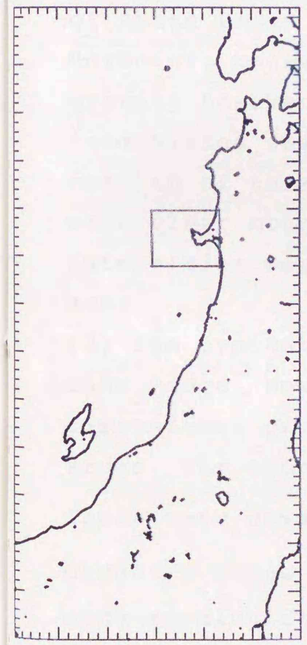

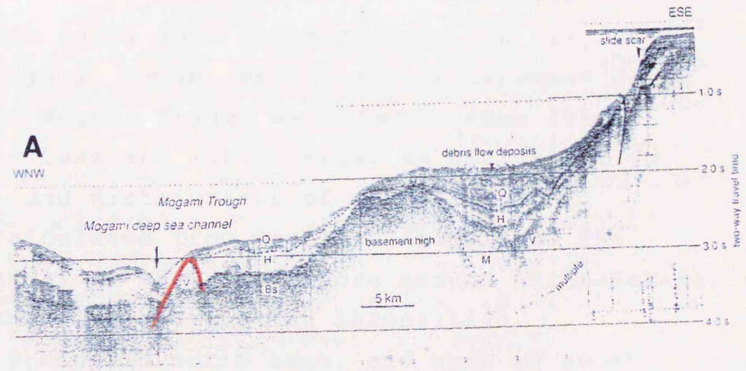

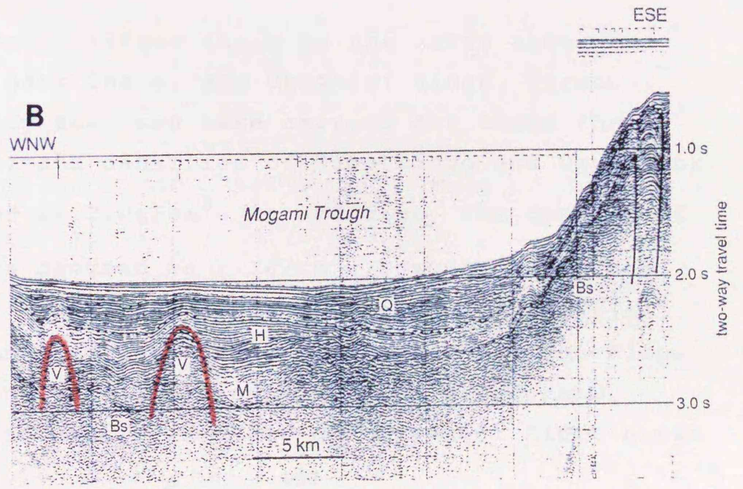

Fig.6-2-2

Seismic profiles of Mogami Trough. Red marks indicate volcanic mounds.

after Okamura et al.(1996b)

7. Conclusion

(1) A detailed magnetic anomaly map and a gravity anomaly map were obtained from dense surveys in the central eastern margin of Japan Sea. On the same survey lines, gravity anomalies, magnetic anomalies, and single-channel seismic profiling were obtained. Especially magnetic anomalies were processed with cross-points control method. The method was originally produced for aeromagnetic survey data. Then, I devised pre-processing to apply cross points control to our sea borne data.

(2) Bouguer gravity anomalies were calculated and density was assumed 2.3g/cm^3. E-W profiles for 2.5-dimensional analysis were taken every 10km automatically. In all, 26 profiles were analyzed. These results showed basement depth of Akita Basin and Mogami Trough were deeper than 10km. Moreover, magnetic basement was regarded as equivalent to gravity basement, and distribution of magnetization intensities was calculated from magnetic anomalies. The results of this analysis showed offshore around Akita-Sakata were clear boundary of magnetization intensities. Intensities were strong in north area, and weak in south area.

(3) The typical small ridges chain in the study area were Sado Ridge, Dewa Bank Chain, and Okushiri Ridge. Three-dimensional gravity analyses were carried out these three areas. The approximate densities of Sado Ridge and Dewa Bank Chain were assumed as 2.0g/cm^3. In addition, the density of Okushiri Ridge was assumed as 2.3g/cm^3. Bouguer anomalies were recalculated each area using these assumed densities. The gravity basement pattern of southern part of Sado Ridge was quite different from topography. On the other hand, gravity basement of Dewa Bank Chain and Okushiri Ridge areas

were suitable for their topographic patterns.
(4) Analytic signals were calculated with pseudo three components of magnetic anomalies by double-Fourier transform. Boundaries of magnetic structure were revealed by distribution of analytic signal peaks. Their magnetization vectors were assumed to parallel to external magnetic field. The assumption was realistic, though it was not correct. We also observed three components of magnetic field vector on board. However, these data suffered seriously from the ship's magnetization and the correction system has not been perfect yet. Then, they were not good for analysis in this study area.
(5) A peak distribution of Analytic Signal revealed magnetic structural boundaries. Some groups of small scale isolated magnetic bodies seemed to be buried around Mogamitai Bank in the northern part of Mogami Trough and Hyotanguri Bank in the southern part of Sado Ridge. Moreover, larger scale boundaries were appeared between northern part of Sado Ridge and Japan Basin or Yamato Basin, along rims of Akita Basin and Noshiro Basin. On the other hand, such boundaries were not appeared around Awashima Island, off Niigata.
(6) Basement structures and apparent magnetic intensities were calculated around Mogamitai Bank, northern part of Mogami Trough, Hyotanguri Bank, southern part of Sado Ridge, and south of Kyuroku Jima Island, southern part of Okushiri Ridge. Surface depth undulations of basement were calculated from Bouguer gravity anomalies. Their assumed densities were $2.0g/cm^3$, $2.0g/cm^3$, and $2.3g/cm^3$, respectively. The parts which have strong magnetic intensities (more than 2A/m) were considered to volcanic intrusions. Moreover, they appeared along structural boundaries of basement. If they were similar volcanic mounds that intruded around Kyuroku Spar,

the distribution of such volcanic intrusions should show active boundaries.
(7) Geological studies suggested that Sado Ridge be formed by "Basin Inversion". Moreover, gravity basement structure of this study supported the suggestion. The structural differences between Sado Ridge and Dewa Bank Chain were shown clearly by the basement structures. Okamura et al. (1995b) discussed the reason of these differences. They thought the effect of compressional stress field was different with directions of faults. The basement structure of this study added the differences in scale of rifts to their discussion. In other words, the gravity basement showed the scale of past rift in southern part of Sado Ridge was larger than the past rift of Dewa Bank Chain.
(8) Magnetic anomalies between Akita Basin and Niigata Basin were quieter than other areas. The gravity basement bottom of Mogami Trough appeared in west of the topographic bottom, and the depth was similar to other sedimentary basins located on the coast. Therefore, the area was possible to be stopped developing into a sedimentary basin.

Reference

Asada,A., S.Kato, and S.Kasuga, 1989, Tectonic landform and geological structure survey in the Toyama Trough. *Rep.Hydrogr.Res.*, **25**, 93-122.

Baranov,V., 1957, A new method for interpretation of aeromagnetic maps: pseudo-gravimetric anomalies. *Geophysics*, **22**, 359-383.

Bhattacharrya,B.K., 1964, Magnetic anomalies due to prism-shaped bodies with arbitrary polarization. *Geophysics*, **29**, 517-531.

Blakely,R.J., and R.W.Simpson, 1986, Approximating edges of source bodies from magnetic or gravity anomalies. *Geophysics*, **51**, 1494-1498.

Blakely,R.J., 1995, Potential Theory in Gravity and Magnetic Applications. *Cambridge University Press*, 441p., London.

Gupta,V., and Ramani, 1980, A new variable-magnetization terrain correction method for aeromagnetic data. *Geophysics*, **52**, 1, 94-107.

Hotta,H.,1967, The structure of sedimentary layer in the Japan Sea. *Geophys.Bull.Hokkaido Univ.*, **18**, 111-131.

IAGA, Division I, Working Group 1,1987, International geomagnetic reference field revision 1987, *J.Geomag.Geoelectr.*, **39**, 773-799.

IAGA, Division V, Working Group 8,1991, International geomagnetic reference field revision 1991, *J.Geomag.Geoelectr.*, **43**, 1007-1012.

Ishihara,T., 1994, Magnetic Anomaly Map of East Asia. *Miscellaneous Map Series.*, **32**, Geol.Surv.Japan.

Isezaki,N., and S.Uyeda, 1973, Geomagnetic anomaly pattern of the Japan Sea. *Marine Geophys.Res.*, **2**, 51-59.

Isezaki,N., 1986a, A Magnetic Anomaly Map of Japan Sea. *J.Geomag.Geoelectr.*, **38**, 403-410.

Isezaki,N., 1986b, A new shipboard three component magnetometer. *Geophysics*, **51**,.1992-1998.
Iwabuchi Y., 1968, Submarine geology of the southeastern part of the Japan Sea. *Contributions from Inst.Geol.Paleontology*, Tohoku Univ., **66**, 1-76.
Japan Natural Gas Association and Japan Offshore Petroleum Development Association, 1982, Petroleum and Natural Gas Resorces of Japan. 455p., Tokyo
Jolivet,L., and K.Tamaki, 1992, Neogene kinematics in the Japan Sea region and volcanic activity of the northeast Japan Arc. *Proceedings of ODP, Scientific Results*, eds. Tamaki,K., K.Suyehiro, J.Allan, M.McWilliams, et al., **127/128**, 1311-1331., College Station, TX.
Jolivet,L., K.Tamaki, and M.Fournier, 1994, Japan Sea, opening history and mechanism: A synthesis. *J.Geophys.Res.*, 99, **B11**, 22,237-22,259.
Joshima,M.,Y.Yamazaki, and E.Kikawa, 1990a, Gravity anomalies. Geological Investigation of the continental shelf in central eastern margin of Japan Sea -off Aomori to Niigata prefecture-, *Preliminary rept. of Hakurei Maru cruise GH89-2 and GH89-4*, 17-20, Geol.Surv.Japan
Joshima,M.,Y.Yamazaki, and E.Kikawa, 1990b, Magnetic anomalies. Geological Investigation of the continental shelf in central eastern margin of Japan Sea -off Aomori to Niigata prefecture-, *Preliminary rept. of Hakurei Maru cruise GH89-2 and GH89-4*, 21-24, Geol.Surv.Japan
Joshima,M. and E.Kikawa, 1991a, Gravity anomalies. Geological Investigation of the continental shelf in central eastern margin of Japan Sea -off Niigata prefecture-, *Preliminary rept. of Hakurei Maru cruise GH90*, 11-16, Geol.Surv.Japan
Joshima,M. and E.Kikawa, 1991b, Magnetic anomalies. Geological Investigation of the continental shelf in central

eastern margin of Japan Sea -off Niigata prefecture-, *Preliminary rept. Hakurei Maru cruise GH90*, 17-20, Geol.Surv.Japan
Joshima,M. and T.Ishihara, 1993a, Gravity anomalies. Geological Investigation of the continental shelf in central eastern margin of Japan Sea -off Niigata prefecture-, *Preliminary rept. of Hakurei Maru cruise GH92*, 11-18, Geol.Surv.Japan
Joshima,M. and T.Ishihara, 1993b, Magnetic anomalies. Geological Investigation of the continental shelf in central eastern margin of Japan Sea -off Niigata prefecture-, *Preliminary rept. of Hakurei Maru cruise GH92*, 19-24, Geol.Surv.Japan
Joshima,M., and M.Komazawa, 1996, Magnetic, Gravimetric, and Three Component Magnetic anomaly surveys. Geological and environmental Investigation of the west of Hokkaido, *Preliminary rept. of Hakurei Maru cruise GH95*, 13-29, Geol.Surv.Japan
Kano,K.,H.Kato,Y.Yanagisawa, and S.Yoshida, 1991, Stratigraphy and geologic history of the Cenozoic of Japan. *Report*, **274**, Geol.Surv.Japan, 114p.
Kato,M., 1987, 2-Dimensional Fourier Transformations for Gravity and Magnetic Applications. *Lattice*, 263p., Tokyo.
Kato,S., T.Katsura, A.Asada, and S.Kasuga, 1986, Submarine topography and geology in the source region of the 1983 Nihonkai-Chubu earthquake. *Rep.Hydrogr.Res.*, **21**,.1-20.
Kato,S., A.Asada, and S.Kasuga, 1990, Tectonic landform and geological structure in the Toyama Trough, southeast margin of Japan Sea. *J.Geography*, 99, **1**, 3-12.
Kawai,N.,T.Nakajima, and K.Hirooka, 1971, The evolution of the island arc of Japan and the formation of granites in the circum-Pacific belt. *J.Geomag.Geoelectr.*, **23**, 267-293.
Kearey,P., and M.Brooks, 1984, An Introduction to

Geophysical Exploration. *Blackwell*, 296p., Oxford.
Kisimoto,K., T.Ishihara, and K.Tamaki, 1984, Marine Geophysical Data Processing at Geological Survey of Japan, *Proceedings of Marine Surveys.*, **4**, 34-45, Soc.Marine Surv.Tech.
Kitahara,A., K.Sayanagi, and N.Isezaki, 1992, Measurement of geomagnetic three component anomalies in the southwestern part of the Kuril Trench, *Preliminary rept. of Hakuho Maru cruise KH92-3*, Ocean Res.Inst., Univ.Tokyo.
Kobayashi,Y., 1983, On the initiation of subduction of plates, *The Earth Monthly*, **5**, 510-514.
Komazawa,M., 1980, The Three-Dimensional Gravity Analysis by using Finite Harmonic Series, *Butsuri-Tanko (Geophys.Explor.)*, 33, **3**, 1-9.
Komazawa,M., 1984, On the Quantitative Gravimetric Analysis in the Hokuroku District, *Butsuri-Tanko(Geophys.Explor.)*, 37, **3**, 19-30.
Komazawa,M., 1988, A Gravimetric Terrain Correction Method by Assuming Annular Prism Model, *J.Geodetic Soc.Japan.*, 34, **1**, 11-23.
Komazawa,M., 1989, Bouguer Anomaly below Sea Level, *J.Geodetic Soc.Japan.*, 35, **3**, 349-351.
Komazawa,M., 1995, Gravimetric Analysis of Aso Volcano and its Interpretation, *J.Geodetic Soc.Japan.*, 41, **1**, 17-45.
Komazawa,M., and K.Kisimoto, 1995, Bathymetric data file around Japan (1km grid). *Seis.Soc.Japan News Letter*, 7, **4**, 3-4.
Korenaga,J., 1995, Comprehensive analysis of marine magnetic vector anomalies, *J.Geophys.Res.*, 100, **B1**, 365-378.
Lallemand,S., and L.Jolivet, 1986, Japan Sea: A pull-apart basin, *Earth.Planet.Sci.Letters*, **76**, 375-389.
Makino,M.,Y.Okubo, and T.Nakatsuka, 1992, Magnetic map of Japanese Islands and their explanatory notes, *1:2,000,000 Map Series*, **23**, Geol.Surv.Japan
Miyazaki,J. and M.Sato, 1992, Bathymetry. Geological Investigation of the continental shelf in central eastern margin of Japan Sea -from off Yamagata prefecture to Akita prefecture-, *Preliminary rept of Hakurei Maru cruise GH91*, 10-20, Geol.Surv.Japan
Mogi,A. and T.Sato, 1957, Bathymetry and Geology around Mogamitai Bank, Japan Sea. *Rep.Hydrogr.Res.*, **55**, 1-46.
Morijiri,R. and T.Yamazaki, 1992a, Gravity and Magnetic anomalies. Geological Investigation of the continental shelf in central eastern margin of Japan Sea -from off Yamagata prefecture to Akita prefecture-, *Preliminary rept.Hakurei Maru cruise GH91*, 21-25, Geol.Surv.Japan
Morijiri,R. and T.Yamazaki, 1992b, Magnetic vector anomaly survey. Geological Investigation of the continental shelf in central eastern margin of Japan Sea -from off Yamagata prefecture to Akita prefecture-, *Preliminary rept.Hakurei Maru cruise GH91*, 26-31, Geol.Surv.Japan
Morijiri,R., 1993, Gravity, Magnetic total force, and magnetic vector anomalies along 175° E in the west central Pacific ocean. Marine Geological Study on Element Cycles in the Ocean, *Preliminary rept.Hakurei Maru cruise NH92-1*, 63-90, Geol.Surv.Japan
Morijiri,R. and T.Yamazaki, 1994a, Magnetic and Gravity anomalies along 175° E. Marine Geological Study on Element Cycles in the Ocean, *Preliminary rept.Hakurei Maru cruise NH93-1*, 47-67, Geol.Surv.Japan
Morijiri,R. and T.Yamazaki, 1994b, Processing of Magnetic Anomaly Map in the Central Part of the Eastern Margin of the Japan Sea with the Cross-Point Control Method. *J.Marine Surv.Tech.*, 6, **1**, 1-10.
Morijiri,R., 1996, Subsurface structure of the southeastern margin of the Japan Sea inferred from Bouguer gravity

anomalies, *Zisin(J.Seis.Soc.Japan)*, 49, **2**, 403-416.
Morijiri,R. and T.Yamazaki, 1997, The present state of measurement Vector Geomagnetic Anomaly on the R/V Hakurei-Maru, *Bull.Geol.Surv.Japan*, 48, **2**,65-77.
Nakamura,K., 1983, Possible nascent trench along the eastern Japan Sea as the convergent boundary between Eurasian and North American Plates. *Bull.Earthq.Res.Inst.*, **58**, 711-722.
Nakatsuka,T., 1989, Systematization of Aeromagnetic Survey (II) -Data Processing Software-. *Bull.Geol.Surv.Japan*, 40, **2**, 99-111.
Nakatsuka,T., 1994, Aeromagnetic Anomalies over the Area of Unzendake Volcano. *J.Geomag.Geoelectr.*, **46**, 529-540.
Nakagawa,T., and Y.Koyanagi, 1982, Data analysis using least square means, *Univ.Tokyo Press*, 206p.
Netteleton,L.L., 1971, Elementary Gravity and Magnetics for Geologists and Seismologists. Society of Exploration geophysicists, Tulsa. *Monograph Series* no.1.
Nishizawa,A., A.Asada, T.Matsumoto, K.Hirata, and S.Kuramoto, 1996, Seismic structure off Akita, eastern margin of the Japan Sea. *Abstracts of the Seis.Soc.Japan*, **2**, B32.
Okamura,Y., M.Sato, M.Watanabe, and H.Yamamoto, 1992, Inversion Tectonics in the southeastern part of the Japan Sea, *J.Tectonic Res.Group.Japan*, **38**, 47-58.
Okamura,Y., and M.Sato 1993, Geological structure from the west of Oga Peninsula to Tsugaru Peninsula, eastern margin of Japan Sea. Geological Investigation of the continental shelf in central eastern margin of Japan Sea, *Preliminary rept.Hakurei Maru cruise GH92*, 48-56, Geol.Surv.Japan
Okamura,Y.,K.Takeuchi, M.Joshima, and M.Sato, 1994, Marine Geological Maps of south of Sado Island and their explanatory notes, *Marine Geology Map Series*, **43**, Geol.Surv.Japan

Okamura,Y.,K.Takeuchi, M.Joshima, and M.Sato, 1995a, Marine Geologcal Maps of north of Sado Island and their explanatory notes, *Marine Geology Map Series*, **46**, Geol.Surv.Japan
Okamura,Y.,M.Watanabe, R.Morijiri, and M.Sato, 1995b, Rifting and basin inversion in the eastern margin of the Japan Sea, *The Island Arc*, 4, 166-181.
Okamura,Y.,R.Morijiri, N.Tsuchiya, and M.Sato, 1996a, Marine Geological Maps of the vicinity of Awashima and their explanatory notes, *Marine Geology Map Series*, **47**, Geol.Surv.Japan
Okamura,Y.,R.Morijiri, and M.Sato, 1996b, Marine Geologcal Maps of west of Akita and their explanatory notes. *Marine Geology Map Series*, **48**, Geol.Surv.Japan
Okamura,Y., and S.Kuramoto, 1996, Geological structure of the west of Tsugaru Peninsula, southern margin of Japan Basin, and Yamato Basin -Single Channel Seismic Reflection Surveys-. Geological Investigation of the continental shelf in central eastern margin of Japan Sea, *Preliminary rept.Hakurei Maru cruise GH93*, 42-60, Geol.Surv.Japan
Okuma,S., M.Makino, and T.Nakatsuka, 1994, Magnetization Intensity Mapping in and around Izu-Oshima Volcano, Japan. *J.Geomag.Geoelectr.*, **46**, 541-556.
Oshima,S., T.Kondo, T.Tsukamoto, and K.Onodera, 1975, Magnetic anomalies at Sea around the northern part of Japan. *Rep.Hydrogr.Res.*, **10**, 39-44.
Oshima,S., T.Tozaki, and K.Onodera, 1980, Magnetic anomalies at Sea around the south-west Japan. *Rep.Hydrogr.Res.*, **15**, 33-54.
Otofuji,Y., T.Matsuda, and S.Nohda, 1985, Paleomagnetic evidence from the Miocene counter-clockwise rotation of Northeast Japan - rifting process of the Japan Arc. *Earth Planet.Sci.Letters*, **75**, 265-277.
Rasmussen,R., and L.B.Pedersen, 1979, End corrections in

potential field modeling. *Geophys.Prospect.*, **27**, 749-760.
Reid,A.B., 1980, Aeromagnetic survey design. *Geophysics*, 45, **5**, 973-976.
Roest,W.R., J.Verhoef, and M.Pilkington, 1992, Magnetic interpretation using the 3-D analytic signal. *Geophysics*, 57, **1**, 116-125.
Roest,W.R., and M.Pilkington, 1993, Identifying remnant magnetization effects in magnetic data. *Geophysics*, 58, **5**, 653-659.
Sakurai,M., and T.Sato, 1971, Submarine geological structures and history of the Mogami Trough. *J.Geol.Soc.Japan*, 77, **8**, 489-496.
Sato,H., 1992, Late Cenozoic tectonic evolution of the central part of Northern Honshu, Japan. *Bull.Geol.Surv.Japan*, 43, **1/2**, 119-139.
Sato,H., 1994, The relationship between late Cenozoic tectonic events and stress field and basin development in northeast Japan. *J.Geophys.Res.*, 99, **B11**, 22,261-22,274.
Sato,T., 1971, Sea Bottom Survey in westward of the Northeast Japan. *J.Geography*, 80, **5**, 1-17.
Savitzky,A., and M.J.E.Golay, 1964, Smoothing and Differentiation of Data by Simplified Least Squares Procedures. *Analytical Chemistry*, 36, **8**, 1,627-1,639.
Seama,N., and N.Isezaki, 1990, Sea-floor magnetization in the eastern part of the Japan Basin and its tectonic implications. *Tectonophysics*, **181**, 285-297.
Seama,N., T.Ichikita, and N.Isezaki, 1990, Measurement of Three Component Geomagnetic Field by STCM. *Preliminary Rept.Hakuho Maru Cruise KH-89-1*, 50-57, Ocean Res.Inst., Univ.Tokyo.
Seama,N, 1992, Studies of Vector Geomagnetic Anomalies in the Oceans. *J.Japan Soc.Marine Surv.Tech.*, 4, **2**, 41-49.
Seama,N.,Y.Nogi, and N.Isezaki, 1993, A new method for

precise determination of the position and strike of magnetic boundaries using vector data of the geomagnetic anomaly field. *Geophys.Jour.International*, **113**, 155-164.
Suzuki,U., 1989, Geology of Neogene Basins in the eastern part of the Sea of Japan, In Kitamura N., Otsuki,K., and Ohguchi,T. eds. *Mem.Geol.Soc.Japan*, **32**, 143-183.
Tamaki,K.,E.Honza,M.Yuasa,K.Nishimura, and F.Murakami, 1981, Marine Geological Maps of central part of Japan Sea. *Marine Geology Map Series*, **15**, Geol.Surv.Japan
Tamaki,K.,1988, Geological structure of the Japan Sea and its tectonic implications. *Bull.Geol.Surv.Japan*, 39, 269-365.
Tamaki,K., K.Suyehiro,J.Allan,J.C.Ingle, and K.A.Pisciotto, 1992, Tectonic synthesis and implications of Japan Sea drilling. *Proceedings of ODP*, Scientific Results, **127/128**, 1,333-1,348, College Station, TX(Ocean Drilling Program).
Verhof,J.,B.J.Collete, J.J.Danoitia, H.A.Roser, and W.R.Roest, 1991, Magnetic Anomalies Off West-Africa (20° -38 ° S). *Marine Geophys.Res.*, 13, 81-103.
Watanabe,M.,Y. Okamura, and M.Sato, 1994, Diatom fossil and geologic structure of the southeastern margin (off Tohoku) of the Japan Sea, *Bull.Geol.Surv.Japan*, 45, **7**, 405-436.
Williams, G. D., C.M.Powell, and M.A.Cooper, 1989, Geometry and kinematics of inversion tectonics, in "Inversion tectonics", ed. by M.A.Cooper and G.D.Williams, *Geol.Soc.London Special Publication*, **44**, 3-15.
Yamazaki,T., and E.Kikawa, 1991, Magnetic vector measurement in the Philippine Sea and the West Caroline Basin. Marine Geological Study on Element Cycles in the Ocean, *Preliminary rept.Hakurei Maru cruise NH90-1*, 79-86, Geol.Surv.Japan
Yamazaki,T., 1992, Gravity, magnetic total force, and magnetic vector measurement along 20° N line from the West of Hawaii to the east of Mariana Trough. Marine Geological

Study on Element Cycles in the Ocean, *Preliminary rept.Hakurei Maru cruise NH91-1*, 41-50, Geol.Surv.Japan

Yamazaki,T.,E.Kikawa,H.Yamamoto, and F.Murakami, 1994, Spreading Mode of the West Caroline Basin Deduced from Magnetic Vector Anomalies., *J.Geomag.Geoelectr.*, **46**,443-453

Yasui,M., Y.Hashimoto, and S.Uyeda, 1967, Geomagnetic Studies of the Japan Sea -Anomaly pattern in the Japan Sea-, *Oceanogr.Mag.*, **19**,221-231

